Contaminant Flux through Capped and Uncapped Sediments

BY

PRISCILLA Z. VIANA
B.S., State University of Campinas, Brazil, 2001
M.S., Federal University of Rio de Janeiro, Brazil, 2004

THESIS

Submitted in partial fulfillment of the requirement
for the degree of Doctor of Philosophy in Civil Engineering
in the Graduate College of
the University of Illinois at Chicago, 2012

Chicago, Illinois

Defense Committee:

Karl J. Rockne, Chair and Advisor
Amid Khodadoust
Thomas L. Theis
Jill A. Kostel, The Wetlands Initiative
Joseph W. Schulenberg, U.S. Army Corps of Engineers

This thesis is dedicated to my father, Paulo Lopes Viana. I am eternally grateful for your support during my studies.

ACKNOWLEDGEMENTS

It has been a long journey, and I have been helped by many along the way. I would like to take this opportunity to thank some of them.

I wish to gratefully and sincerely thank my advisor Dr. Karl Rockne for his unwavering support and assistance. This dissertation would not have been possible without his guidance. He encouraged me not only to grow as an environmental engineer, but also as an independent thinker.

I thank my thesis committee members Professors Amid Khodadoust and Thomas Theis from the University of Illinois at Chicago (UIC), Dr. Jill Kostel from The Wetlands Initiative, and Joseph Schulenberg from the U.S. Army Corps of Engineers for their willingness to serve on the committee, and for their constructive suggestions and help.

I would like to acknowledge my fellow lab student Ke Yin for his full assistance and involvement with my work. His help came from multiple aspects, including as friend. Deep thanks are also given to my fellow lab students Kelly Granberg, Saikrishnan Ramamurthy, Solidea Bonina, Srinivasa Varadhan and Xiuhong Zhao, who have become great friends. I extend many thanks to my colleagues and friends at the Environmental Laboratories in the Civil and Materials Engineering Department at UIC: Azivy Che Aziz, Menka Mittal, Jayashree Jayaraj, Burcu Uyusur, Itzel Godinez, Janardhanan Gangathulsasi, Raja Kaliappan, Ravikumar Srirangam, Pratibha, Dorin Bogdan, and Narendrakumar. I am also grateful to the Metropolitan Water Reclamation District of Greater Chicago and the crew who assisted us during field work.

I am grateful to Fulbright, The Brazilian Federal Agency for the Support and Evaluation of Graduate Education (*CAPES*), and the American Association of University Women (AAUW) for

providing financial support during my PhD. I also owe a great debt to the National Oceanic and Atmospheric Administration (NOAA) Sea Grant Knauss Marine Policy Fellowship, who provided me with the wonderful opportunity of working at the National Science Foundation (NSF). At NSF, I had the privilege of learning more about this outstanding agency's mission and of working with Phillip Taylor, David Garison, Matthew Hawkins and Ian Ridley, who deserve special thanks for their guidance, friendship and encouragement during my work at NSF. This study was also partially supported by the grant BES-0348512 from the National Science Foundation.

Last but not least, I would like to thank my husband and family. I am fortunate to have such unquestioning love and support from my husband. I would not have made it without him. My father has unwaveringly encouraged me to keep going when I faltered, and given me the confidence I often lacked. My mother has been unfailingly supportive in every way, and has always listened to my troubles, big and small. My sister and my brother have been an oasis of friendship and affection.

PZV

TABLE OF CONTENTS

TABLE OF CONTENTS (continued)

TABLE OF CONTENTS (continued)

TABLE OF CONTENTS (continued)

LIST OF TABLES

LIST OF TABLES (continued)

LIST OF FIGURES

LIST OF FIGURES (continued)

LIST OF FIGURES (continued)

LIST OF FIGURES (continued)

LIST OF FIGURES (continued)

LIST OF FIGURES (continued)

LIST OF FIGURES (continued)

LIST OF ABBREVIATIONS

AET……...…Apparent Effects Threshold
AP……...……..……..Apatite
ATSDR…….....Agency for Toxic Substances and Disease Registry
AVS……...…….Acid Volatile Sulfide
BDL……..…… Below Detection Limit
BET……..Brunaur, Emmett, Teller Isotherm Model
BJH…….Barett, Joyner and Halenda Model
BOD…….….Biological Oxygen Demand
CAM…….California Assessment Manual
CCC…….....….Criterion of Continuous Concentration
CDM…….Camp, Dresser & McKee Engineering
CEC……...…..Cation Exchange Capacity
CI……Confidence Interval
CL……...……..…….Confidence Level
CMC……..……Criterion of Maximum Concentration
CN……..……...……Cyanide
CPM……..Chloropyromorphite
CSO…….……Combined Sewage Outfall
DDT……..Dichlorodiphenyltrichloroethane
D_{mol}…….…….Molecular Diffusivity
DOM……...…..Dissolved Organic Matter
D_s……...Depth of Scour
E……..…….Elevated
ERDC……..……...…Engineering Research and Development Center
EX……..Extremely Elevated
FOG……..Fats, Oil and Grease
GAC…….……...Granular Activated Carbon
GC-ECD…….…….Gas Chromatography-Electron Capture Detector
HE……...…….Highly Elevated
HOC…….……..Hydrophobic Organic Carbon
IEPA……...……Illinois Environmental Protection Agency
K_d……..Partitioning Coefficient
K_{sp}…….....Solubility Product Constant
L_{bio}……...……Depth of Bioturbation
MWRD-GC……..Metropolitan Water Reclamation District of Greater Chicago
NELAP…….…….. National Environmental Laboratory Accreditation Program
NOAA……..National Oceanic and Atmospheric Administration
OC……..……...……..Organoclay
OM……..……..……Organic Matter
PAHs…….Polycyclic Aromatic Hydrocarbons
PCBs…….……...Polychlorinated Biphenyls
PDF…….…….Probability Density Function
PEL……...…….Probable Effects Level
PMF…….…….....Probability Mass Function

LIST OF ABBREVIATIONS (continued)

RAPS……..……..…….Racine Avenue Pumping Station
SEM……Simultaneously Extracted Metal
SG…….……..…..Surface Grab
OM…….....……..……..Soil-sediment Organic Matter
TEL……..……Threshold Effects Level
TS……...……..……Total Solid
TSS……...…….……Total Suspended Solid
u_{cr}……...Critical Vertically Average Velocity for the Initiation of Sediment Movement
UET……..……..Upper Effects Threshold
USACE…….…...US Army Corps of Engineering
USEPA……..US Environmental Protection Agency
USGS….…….…...……....US Geological Survey
VGPR…….Volumetric Gas Production Rate

SUMMARY

This study contributes to the state of the science of contaminant flux through capped and uncapped sediments. Cd, Cr, Pb, Ag, As, Ba, Hg, CH_3Hg and CN transport through sand (25 cm), granular activated carbon (GAC, 2 cm), organoclay (2 cm), shredded tires (10 cm) and apatite (2 cm) caps was modeled by deterministic and Monte Carlo methods. Sand caps performed best under diffusion due to the greater diffusive path length. Apatite had the best advective performance for Cd, Cr and Pb. Organoclay performed best for Ag, As, Ba, CH_3Hg and CN. Organoclay and apatite were equally effective for Hg. Monte Carlo analysis was used to determine output sensitivity. Sand was effective under diffusion for Cr within the 50% confidence interval (CI), for Cd and Pb (75% CI) and for As, Hg and CH_3Hg (95% CI). Under diffusion and advection, apatite was effective for Cd, Pb and Hg (75% CI) and organoclay for Hg and CH_3Hg (50% CI). GAC and shredded tires performed relatively poorly. Although no single cap is a panacea, apatite and organoclay have the broadest range of effectiveness. Cap performance is most sensitive to the partitioning coefficient (K_d) and hydraulic conductivity, indicating the importance of accurate site-specific measurement for these parameters.

Important cap and contaminant parameters were measured through isotherm and column studies with the goal of re-performing model simulations with measured parameters and of comparing results to literature-derived model simulations. Although none of the caps exhibited a high sorption capacity for As, organoclay and apatite performed clearly better than sand and activated carbon. Surprisingly, organoclay exhibited a significantly higher sorption capacity than apatite for Cd based on the isotherm study results. On the other hand, based on the column study, apatite performed very well for Cd in the column study, as expected. Surprisingly, sand did not

exhibit such a poor sorption capacity as expected for Cd. Based on the column experiment results, activated carbon performed poorly for both As and Cd. The K_d results indicate close agreement between the experimental and literature K_d values with the exception of As and Cd with apatite.

This study also quantified the magnitude of organic and metal contaminant facilitated transport due to gas ebullition at numerous urban waterway sites with wide variation in physical, chemical, and contamination characteristics. The magnitude of the ebullition-facilitated measured fluxes indicates that gas ebullition is an important pathway for release of both polycyclic aromatic hydrocarbons (PAHs) and heavy metals from buried sediments in urban freshwater systems. Measured benthic contaminant fluxes were compared to ebullition-facilitated contaminant fluxes at the same sites with the goal of understanding the role of these contaminant transport mechanisms on total contaminant transport. Comparison of direct benthic release rates to ebullition facilitated rates suggests that total PAHs are released at significantly greater rates by biogenic gas production. Although the increase in release rate is not as great for metals, ebullition facilitated release rates are frequently greater than benthic release. Mechanistic and empirical models developed in this study may be used to predict *in situ* gas ebullition flux and ebullition-facilitated contaminant flux. Results from both multivariate regression analyses and a mechanistic model suggest that metal transport likely is due to sediment particle re-suspension, while PAH transport is due to both contaminant partitioning to gas bubbles and to sediment re-suspension.

CHAPTER I. INTRODUCTION

Prior to the enactment of the Resource Conservation and Recovery Act in 1976 and the Comprehensive Environmental Response, Compensation and Liability Act in 1980, indiscriminant releases of contaminants to the air, water and soil were largely unregulated and led to substantial pollution of the environment. Contaminants like polycyclic aromatic hydrocarbons (PAHs), polychlorinated biphenyls (PCBs) and heavy metal contaminants accumulated on the bottom of rivers and lakes due to chemical interactions and transformations and due to their relatively long environmental persistence. Increased incidences of fish disease and decreased species biodiversity in pollution-impacted benthic/aquatic environments have been proposed as possible signals of the costs to ecological and human health posed by these contaminants *(1-2)*. According to the United States Environmental Protection Agency (USEPA) *(2)*, approximately ten percent of the sediments underlying US surface waters are contaminated with toxic pollutants. This represents some 2 billion m^3 of contaminated sediment based upon estimates of the total surface sediments in the upper (20 cm) bioactive zone.

Concentration gradients at the sediment-water interface result in the transport of sediment porewater contaminants to and from the overlying water by diffusion, but for most contaminants, advection is the most important contaminant transport process. Gas bubbles produced in sediments with a high organic matter content may also frequently result in the release of contaminants to the water column *(3-4)*. Moreover, even though pollutants in the deeper sediments are generally not directly bioavailable, dredging, navigation, storms and high flow events frequently disturb the sediments and thus increase contaminant availability to the bioactive zone and water column. In addition, benthic animals can consume and/or uptake these

persistent pollutants through bioturbative activities, and subsequently release them to the water phase, contributing to accumulation in the food chain.

Standard contaminated sediment remedial alternatives include dredging and *in situ* capping with sand or clean sediment *(5-7)*. Each of these technologies has advantages and disadvantages. Dredging may re-suspend and release contaminants to the water column if effective containment is not maintained. In addition, dredging may be cost-prohibitive in large contaminated areas. Capping is susceptible to contaminant migration, scouring in high energy environments and may not be applicable for shallow navigable areas.

A relatively recent innovation in the field of contaminated sediment remediation is active capping. Active capping both isolates contaminated sediments from the water phase while offering degradation and/or sequestration of contaminants by the active materials *(8-9)*. Like normal capping, active capping is also subject to contaminant migration through the cap. However, selection of appropriate active materials and cap thicknesses can minimize contaminant flux to the water column at levels that are not significant from a risk standpoint; even with significant advective sediment-to-water-column porewater flow. A detailed evaluation of *in situ* processes that might compromise cap effectiveness is vital to guarantee cap effectiveness.

Several capping projects have recently been implemented for remediation of contaminated sediments as an alternative to dredging, including the Anacostia River in Washington, DC *(10)*, the McCormick and Baxter Creosote Superfund Site in Portland, OR *(11)*, the Grasse River in Massena, NY *(12)*, and Stryker Bay in Duluth, MN *(13)*. Although it has been demonstrated that capping is effective at minimizing release of contaminants to the water column *(14-16)*, no studies have yet been published comparing the effectiveness of both a wide variety of cap

materials and contaminants. Because many contaminated sediment sites have a mixture of both metal and organic contaminants, active media may be required to sequester both metals and organics. Additionally, gas bubble migration may cause cap damage and a pathway for contaminant release *(10, 17)*.

Recent research suggests that gas ebullition due primarily to methanogenic activity in sediments is an important mechanism of contaminant transport in sediments *(3-4, 17-19)*. As observed by Reible and others *(10)*, gas bubbles may damage the cap layer, opening preferential holes in the cap or even rupture the cap. Additionally, as gas bubbles are hydrophobic and tend to accumulate hydrophobic contaminants and sediment particles on their surface, they may transport contaminants by enhancing sediment re-suspension *(3)*. Ebullition-facilitated sediment re-suspension may be as or a more significant mechanism of contaminant transport than bubble-porewater contaminant partitioning *(3, 19)*.

Although contaminant transport from sediments by diffusion and advection has been extensively investigated, comparatively less is known about contaminant transport due to gas ebullition. Understanding and quantifying this contaminant transport mechanism is key to enable prediction of the total contaminant transport from sediments to the water column. However, there are a limited number of studies investigating organic contaminant transport to the water surface due to gas ebullition *(3, 19-21)* and almost no studies have investigated the role ebullition plays in facilitating metal release from sediments. Moreover, no studies to date, up to my knowledge, have compared the magnitude of organic and metal contaminant fluxes due to gas ebullition to direct benthic contaminant fluxes.

Thus, the overall objective of this study is to contribute to the state of the science of contaminant flux through capped and uncapped sediments focusing on questions that are not yet well understood. With this broad objective, the specific goals of this study are to:

A) Compile model parameter data for a range of cap materials and for a range of contaminants from the scientific literature with the goal of modeling the transport of Cd, Cr, Pb, Ag, As, Ba, Hg, CH_3Hg and CN through different capping configurations using stochastic methods to evaluate how sensitive model results are to uncertainty in model parameters;

B) Measure important cap and contaminant parameters through isotherm and column studies with the goal of re-performing model simulations with measured parameters and of comparing results to literature-derived model simulations. Breakthrough column studies with anionic and cationic metals with multiple cap materials were also performed to evaluate cap performance and compare the experimental results with the output from the model;

C) Prepare a pre-remedial site characterization in Bubbly Creek, Chicago River. A demonstration active capping project will potentially be implemented in Bubbly Creek;

D) Quantify the magnitude of organic and metal contaminant facilitated transport due to gas ebullition at numerous urban waterway sites with wide variation in physical, chemical, and contamination characteristics. Models were also developed to predict ebullition-facilitated contaminant release and compare these predictions to literature values.

E) Quantify benthic organic and metal contaminant fluxes at the sediment-water interface in urban waterway sites with wide variation in physical, chemical, and contamination characteristics. The measured benthic contaminant fluxes were compared to ebullition-

facilitated contaminant fluxes at the same sites with the goal of understanding the role of these contaminant transport mechanisms on total contaminant transport.

CHAPTER II. LITERATURE REVIEW

Active capping is implemented to minimize sediment metal and organic contaminant release to the water column. This study focused on the performance of cap materials that have been (or proposed to be) used to minimize sediment metal contaminant release, and on contaminant transport mechanisms affecting cap or uncapped sediments.

Thus, the first section of the literature review describes some biogeochemical characteristics of the heavy metal and organometal contaminants that are the focus of this research, and explores their fate in the sediment environment. This task is necessary to understand the importance of minimizing environmental and human exposure to each of these metal contaminants and to understand how metal speciation and sediment composition can affect metal solubility and bioavailability.

The second section of the literature review focuses on mechanisms of contaminant transport (diffusion, advection, gas ebullition, bioturbation and consolidation) in addition to factors affecting cap performance. Literature studies evaluating capping effectiveness to minimize metal contaminant release to the water column are reviewed.

2.1. Heavy Metals and Organometals

Heavy metals represent a subset of the group of elements with metallic properties and with a specific gravity of greater than 4. They include the transition metals, some metalloids (such as As), lanthanides (atomic number 57 through 71) and actinides (atomic number 89 through 103). These elements pose a threat to the environment due to their high toxicity, persistence and widespread anthropogenic source. Sediments tend to act as reservoirs for most metals as the vast

majority tend to sorb to particles with high sedimentation propensity (with important exceptions like Hg). However, changing environmental conditions may affect metal behavior and increase bioavailability once in the benthic environment.

The focus of this work is on Cd, Cr, Pb, Ag, As, Hg, CH_3Hg and CN due to their importance as sediment contaminants based upon frequency of observation and risk. Cd, Cr, Pb, Ag, As and Hg comprise seven of the Resource Conservation and Recovery Act (RCRA) metals. Although CH_3Hg and CN are not strictly considered heavy metals, CH_3Hg is associated with Hg, and sites contaminated with heavy metals are frequently also contaminated with CN due to complex formation with heavy metals and their high solubility and/or toxicity.

Although total metal concentration is typically not sufficient to evaluate the impact of metals on organisms or on the environment due to the well known role speciation plays on activity *(22)*, it is not without utility to investigate transport relative to guidelines which are typically based on total metal concentration. This is because measuring the true metal speciation in situ for analysis can be difficult due to the complexity of matrices like soil and sediment, difficulties for sample preservation during sampling and analysis (particularly for redox-sensitive metals), and the presence of very low concentrations of different metal species. Additionally, assuming that metal speciation is invariant with time may lead to incorrect assessment of risk because metal species concentrations can change rapidly due to changing environmental conditions.

Metal speciation is affected by many factors, including pH, oxidation-reduction potential, organic matter (in particular dissolved organic matter - DOM), and presence of solid precipitating phases and other catalysts of heterogeneous reactivity (e.g. iron and manganese-oxides and sulfur). For example, Cd and Pb precipitate at increasing pH, which can be caused by interaction of acid waters with carbonates or silicate rocks *(23)*. These complexities can make

any conclusions difficult to make without positing some system constraints. Thus, the primary metric of effectiveness used in this work will be the total metal concentration referenced to sediment quality guidelines which are themselves based on total metal levels. That being said, the importance of speciation on toxicity and mobility are addressed in the literature review. Site-specific sediment, porewater, and water column characteristics are vital to assess metal speciation.

A large fraction of contaminated sediments in the USA underlie ports. Although many ports are in marine and estuarine locations, ports in the Laurentian Great Lakes and the myriad river systems result in extensive freshwater sediment issues. Thus, understanding metal behavior in both marine and freshwater is important; particularly given the great differences in dissolved solids and resultant effects on metal reactivity (Table 2.1).

Table 2.1. Typical marine and freshwater concentrations of the eight most prevalent ions[a]

	Seawater		Freshwater	
Constituent	mg L^{-1}	mM	mg L^{-1}	mM
Na^+	10,000	500	10	0.3
Mg^{2+}	1,000	60	10	0.3
Ca^{2+}	400	10	40	0.9
K^+	400	10	1	0.03
Cl^-	20,000	500	20	0.5
SO_4^{2-}	3,000	30	20	0.2
HCO_3^-	200	2	100	1
Br^-	70	0.8		
Total dissolved solids	35,000		200	
Ionic strength		700		4
pH (unitless)	7.5 – 8.5		6.5 - 8	
Conductivity (µS cm^{-1})	30,000		400	

[a] Sources: *(24-28)*

2.2. Criteria for Heavy Metal Contaminants in Water and Sediments

The USEPA has compiled extensive studies of the toxicity of most metals to aquatic organisms to establish acute and chronic exposure criteria protective to sensitive organisms. USEPA uses the criterion for maximum concentration (CMC) and the criterion for continuous concentration (CCC) for metals in freshwater and saltwater (Table 2.2). The CMC criterion is defined as the "highest concentration of a material in surface water to which an aquatic community can be exposed briefly without resulting in an unacceptable effect", thus representing an acute criterion. The criterion for continuous concentration (CCC) is an estimate of the "highest concentration of a material in surface water to which an aquatic community can be exposed indefinitely (i.e. chronic exposure) without resulting in an unacceptable effect" *(29)*.

Table 2.2. USEPA CMC and CCC for metals in freshwater and saltwater[a]

Pollutant	CAS Registry Number	Freshwater		Saltwater	
		CMC ($\mu g\ L^{-1}$)	CCC ($\mu g\ L^{-1}$)	CMC ($\mu g\ L^{-1}$)	CCC ($\mu g\ L^{-1}$)
Cd	7440439	2.0	0.25	40	8.8
Cr (III)	16065831	570	74		
Cr (VI)	18540299	16	11	1,100	50
Pb	7439921	65	2.5	210	8.1
Ag	7440224	3.2		1.9	
As	7440382	340	150	69	36
Hg	7439976	1.4	0.77	1.8	0.94
CH_3Hg *	22967926	1.4	0.77	1.8	0.94
CN	57125	22	5.2	1	1

[a] Source: *(29)*. * According to USEPA, if a substantial portion of the mercury in the water column is methyl mercury, this criterion will probably be under protective.

The nature of toxicological response is clear in these values. Chronic exposure criteria are much lower than acute criteria as exposure time is related to total dose. These values are in greatly simplified systems with organism exposure resulting directly through the aqueous pathway. However, in the sediment environment, the presence of a solid phase results in

complex partitioning behavior that makes exposure difficult to predict. Guidelines have been developed by several agencies that are typically designed to be protective in most sediments given an average exposure scenario. Table 2.3 shows two sets of guidelines for metal contaminant concentration in sediments developed by the Illinois EPA (IEPA) and the National Oceanic and Atmospheric Administration (NOAA). The IEPA classification of Illinois stream sediments was performed based on one, two, four and eight standard deviations. The sediment contaminant concentration was classified as elevated (E), highly elevated (HE) and extremely elevated (EX) *(30)*. The NOAA guideline values are for preliminary screening purposes and do not constitute clean-up levels. The threshold effects level (TEL) is defined by the "concentration below which adverse effects are expected to occur only rarely", while the probable effects level (PEL) is the "level above which adverse effects are frequently expected." The apparent effects threshold (AET) and the upper effects threshold (UET)) are the "concentration above which adverse biological impacts would always be expected by that biological indicator" *(31)*. EX values from IEPA classification are much higher for Cd and As than UET values from NOAA, while UET values are higher than EX for Cr, Pb and Hg. It is important to remember that the IEPA classification is actually a statistical classification of Illinois stream sediment concentrations from 94 sites comparing stream sediments across the state while the NOAA guideline reports values related with probabilities of adverse biological effects.

When comparing marine and freshwater values, it is important to consider the different porewater composition and pH. Salinity affects the speciation of metals in the water and the physiology of organisms and marine water usually has a pH around 7.5 – 8.5, while freshwater has a pH around 6.5 – 8.0. Considering only the pH effect, Pb is usually more toxic at lower pH as Pb speciation is usually dominated by free Pb^{2+} at lower pH, which results in an increase in Pb

bioavailability and toxicity *(32-33)*. This may help explain the more restrictive criteria for Pb in freshwater and in freshwater sediment (Tables 2.2 and 2.3). Cd criteria for marine water and marine sediment can be less restrictive than for freshwater due to strong Cd-Cl complexation in seawater. The fraction of uncomplexed Cd^{2+} ion decreases from 92.2% in freshwater to 4.4% in seawater at pH 8 *(34)*, which in general decreases its bioavailability. This is true for TEL and PEL, but not for UET versus AET.

Table 2.3. IEPA classification of Illinois stream sediments and NOAA guideline for freshwater and marine sediments[a]

Pollutant	IEPA classification (mg kg^{-1})			NOAA screening reference table (mg kg^{-1})					
				Freshwater sediment			Marine sediment		
	E	HE	EX	TEL	PEL	UET	TEL	PEL	AET
Cd	>1.0	≥2.0	≥20	0.60	3.5	3.0	0.68	4.2	3.0
Cr	≥23	≥38	≥60	37.3	90	95	52.3	160	62
Pb	≥38	≥60	≥100	35	91	127	30	112	400
Ag						4.5	0.73	1.8	3.1
As	≥11	≥17	≥28	5.9	17	17	7.2	42	35
Hg	≥0.10	≥0.17	≥0.30	0.17	0.49	0.56	0.13	0.70	0.41

[a] Sources: *(30-31)*. These criteria do not mention CH_3Hg and CN levels.

2.3. Importance of Redox Potential on Heavy Metal Speciation

Oxygen is the most energetic biological electron acceptor, with energy yields many times those of anaerobic electron acceptors like sulfate. However, oxygen has very low solubility and thus it is typically limited or absent from high organic content aqueous systems. When oxygen is available, Fe^{2+} and Mn^{2+} may be oxidized biologically or inorganically to Fe^{3+} (low solubility, mostly in particulate form) and Mn^{4+} (low solubility) via reactions 2.1 and 2.2. Surprisingly, Fe^{2+} oxidation is statistically significantly more correlated with pH than with dissolved oxygen and very slow Fe^{2+} oxidation kinetics may delay reaching equilibrium for Fe redox couples *(35)*.

$$Mn^{2+} + \frac{1}{2}O_2 + 2HCO_3^- \rightarrow MnO_2 + 2CO_2 + H_2O \quad (2.1)$$

$$Fe^{2+} + \frac{1}{4}O_2 + 2HCO_3^- + \frac{1}{2}H_2O \rightarrow Fe(OH)_3 + 2CO_2 \quad (2.2)$$

In general for organic-rich sediments, which are typically found in contaminated sites, after a few millimeters to centimeters beneath the sediment-water interface, oxygen is unavailable and a gradient of terminal electron acceptors exists (Figure 2.1). Strict redox conditions affect contaminant fate and transport and its study is needed to understand contaminant attenuation processes *(36)*. At a specific oxidation/reduction potential, one electron acceptor is favored. Some electron acceptors involved in anaerobic respiration according to their thermodynamic energy yield are NO_3^-, Mn^{+4}, Fe^{3+}, SO_4^{2-} and CO_2. Methanogenesis, which is the conversion of methanogenic substrates such as acetate, hydrogen and carbon dioxide into methane and carbon dioxide, occurs when the other electron acceptors have been used up, although competition may occur between sulfate reducers and methanogens *(37)*.

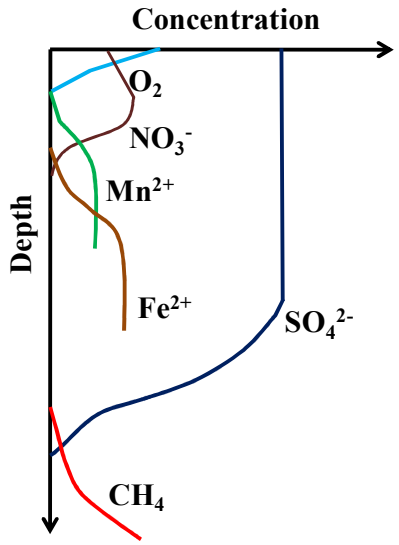

Figure 2.1. Generalized sediment porewater profile of electron acceptors in an organic rich sediment system resulting in complete utilization of all electron acceptors through methanogenesis. Depth is shown below the sediment-water interface. Adapted from Rockne *(38)*.

Oxide reduction occurs (reactions 2.3 - 2.7), forming again the soluble forms of iron, Fe^{2+}, and manganese, Mn^{2+}, which are thermodynamically stable only under anaerobic conditions *(39)*.

$$MnO_2 + 4H^+ + 2e^- \rightarrow Mn^{2+} + 2H_2O \quad (2.3)$$

$$Fe(OH)_3 + 3H^+ + e^- \rightarrow Fe^{2+} + 3H_2O \quad (2.4)$$

$$Fe(OH)_3 + 2H^+ + HCO_3^- + e^- \rightarrow FeCO_3 + 3H_2O \quad (2.5)$$

$$\gamma FeOOH + 3H^+ + e^- \rightarrow Fe^{2+} + 2H_2O \quad (2.6)$$

$$\gamma Fe_2O_3 + 3H^+ + e^- \rightarrow Fe^{2+} + {}^3/_2\, H_2O \quad (2.7)$$

When sulfate is available, sulfate-reducing bacteria (such as those in the genera *Desulfovibrionacaea*, *Desulfobacteracaea* and *Desulfotomaculum*) use electron donors, such as H_2, lactate and pyruvate, and reduce SO_4^{2-} to H_2S (eq. 2.8). Sulfide is highly reactive with divalent metal cations forming compounds with very low solubility products (eq. 2.9) *(40)*. Sulfide also reacts with Fe^{2+} forming pyrite (FeS_2) and troilite (FeS) (eq. 2.10 - 12) *(41-42)*. The prevalence of this reaction is demonstrated by the fact that the black color seen in many polluted sediments is due primarily to the high levels of FeS and other metal-S compounds.

The solubility of FeS increases greatly with decreasing pH. According to Huerta-Diaz *(43)*, trace metals may precipitate and/or adsorb on Fe sulfides, may form metal sulfides which precipitate due to very low solubility, or they may displace Fe from the FeS, and form new metal sulfides. These metals may become bioavailable if sediments are disturbed by storms, navigation, gas production, bioturbation, etc., causing sediment re-suspension and subsequent exposure to oxygen. The fraction of the sulfide complexes that are readily dissolved in acid are termed acid-volatile sulfides (AVS). AVS is an important parameter that controls cationic metal

activity and metal-induced toxicity as AVS binds with cationic metals forming sulfide compounds which are usually not highly bioavailable *(44)*.

$$2CH_2O + SO_4^{2-} \rightarrow H_2S + 2HCO_3^- \quad (2.8)$$

$$M^{2+} + S^{2-} \xrightarrow{abiotic} MS_{[s]} \quad (2.9)$$

$$Fe^{2+} + H_2S \rightarrow FeS + 2H^+ \quad (2.10)$$

$$H^+ + FeS \rightarrow Fe^{2+} + HS^- \quad (2.11)$$

$$FeS + S_0 \rightarrow FeS_2 \quad (2.12)$$

2.4. Mechanisms of Interaction between Particles and Metals

Sorption describes the attachment and release of compounds between the aqueous and particulate phases. Sorption of metals may occur through adsorption and/or absorption. In many instances, due to the difficulty to distinguish between adsorption and absorption, the more general term, sorption, is used as it embraces both phenomena and usually neither adsorption nor absorption alone represents the whole picture of the accumulation phenomena *(45)*. Adsorption is the accumulation of constituents at the interface of two phases (in this case the solid-water interface). It may be a physical process when it happens on the external surface of a particulate and involves only the weaker intermolecular forces (i.e., van der Waals interactions or hydrogen bonding) with no significant change in the electronic orbital states of the interacting species *(46)*. It is a chemical process when there is the formation of chemical associations between ions or molecules from solution and the particle surface with significant chemical bonds being formed at the interfacial region. These bonds change the electronic orbital states of the interacting species *(46)*. Adsorption mechanisms include electric interactions at surfaces, hydrophobic expulsion

(for hydrophobic compounds) and surface complexation *(22, 47)*. Absorption occurs when sorbates diffuse or partition into the bulk phase of the solid phase (i.e. enters within the intra-particle pore network of a porous solid).

There are a multitude of mechanistic and empirical models to describe the solid-liquid sorption process. At equilibrium, these are frequently referred to as isotherms as their measurements are performed at constant temperature. Mechanistic models include the Langmuir and Brunaur, Emmett, Teller (BET) isotherms, and empirical or semi-mechanistic models include the Freundlich and linear equilibrium partitioning isotherms. The latter is the simplest model as the partitioning is a direct linear function of concentration (i.e. the partitioning parameter does not change as a function of concentration). Such a formulation lends itself to modeling as it greatly simplifies incorporation within ordinary and partial differential equations. The partitioning coefficient (K_d) is the ratio of concentrations of a compound in the two phases of a mixture of two immiscible phases at equilibrium. More specifically in our case it is the ratio of sorbed metal concentration on the solid matrix (mg kg^{-1} of sorbing material) to dissolved metal concentration in the aqueous phase (mg L^{-1} of solution) at equilibrium.

Limitations of assuming a linear mathematical model consist in not imposing a limit to the amount of pollutant that can be sorbed on the solid matrix, and a limited dataset may lead to the conclusion that the relation is linear when it is actually not. For the non-linear sorption, the partitioning is a function of concentration. Freundlich and Langmuir models are most often used to represent such adsorption isotherms (eqs. 2.13 – 2.14).

$$C_{sorb} = K_d C_w^f \tag{2.13}$$

$$C_{sorb} = \frac{M_s K_d C_w}{1 + K_d C_w} \tag{2.14}$$

Where C_{sorb} (mg kg of sorbent^{-1}) is the contaminant equilibrium concentration on the sorbent phase; C_w (mg L^{-1}) is the contaminant equilibrium concentration in the liquid phase; K_d is the partitioning coefficient (L kg^{-1}) and M_s is the maximum mass of contaminant that the adsorptive material can hold (mg kg of sorbent^{-1}). For the Freundlich model, when $f = 1/N = 1$, the relationship is linear; when $0<f<1$ (or $N>1$) there is a high affinity of the contaminant for the sorbent at low concentrations; when $f>1$ (or $0<N<1$), there is a low affinity of the contaminant for the solution (Figure 2.2). The Langmuir model describes the high affinity of the contaminant for the sorbent at low aqueous concentration with low or invariant affinity at higher contaminant aqueous concentrations *(47)*.

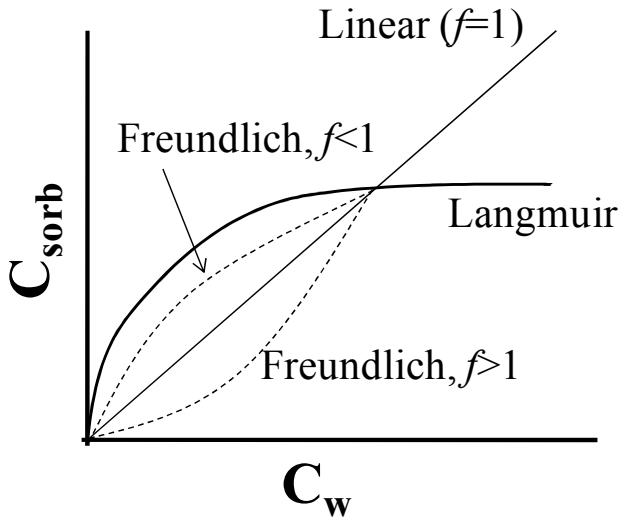

Figure 2.2. Isotherm models (adapted from Alvarez and Illman *(47)*).

In my specific case, I am interested in the partitioning of contaminant between the cap material solid phase and the aqueous porewater phase. The partition coefficient for organic contaminants is a measure of the degree of hydrophilicity or hydrophobicity of the chemical of interest. Hydrophobic compounds (high partition coefficients) partition preferentially to

hydrophobic materials, while hydrophilic compounds partition preferentially to the water phase. Compilations of K_d values for many organic contaminants of concern have been performed, and there are many free energy relationships used to predict unknown K_d for compounds, perhaps most famously by the well known Karickhoff equation *(48)*. The situation is not as simple for heavy metal contaminants, as K_d values are also a function of geochemical characteristics of the solid matrix and the porewater composition, pH and nature and concentration of sorbents *(49)*. Despite these difficulties, attempts have been made to compile K_d data for some metals *(49-51)*.

Buergisser et al. *(52)* developed a method to obtain nonlinear isotherms based on breakthrough curves obtained from column experiments (flow-through reactors). The authors argue that equilibrium isotherms produced from batch experiments are subject to errors, such as particle morphological changes (e.g. shearing and milling) that occur during shaking that affect sorption capacity. One of the advantages of their method consists on the facility of identifying the shape of the isotherm based on the appearance of the breakthrough curve. The isotherm is linear if the adsorption and desorption front have exactly the same shape, convex if there is a substantial tailing in the desorption front or concave if the adsorption front is diffuse while the desorption front is sharp. The disadvantage of this method is the difficulty in reaching local equilibrium in the column. The method involves interpolating the data points of the breakthrough curve using a least-squares spline fit. The interpolated function is then numerically integrated using equation 2.15 to obtain the adsorption isotherm.

$$c_{sorb} = \frac{1}{\rho}\int_0^c \left(\frac{t(c')}{t_0} - 1\right) dc' \tag{2.15}$$

c_{sorb} is the concentration of the sorbed species on the sorbate, ρ is mass of sorbent per unit pore volume ($\rho=\rho_s(1-\theta)/\theta$), ρ_s is the density of the sorbent matrix, θ is the porosity and *t(c)* is the concentration in the solution at the column outlet at time t.

2.5. Factors Affecting Metal Biogeochemistry

Some of the factors affecting heavy metal biogeochemistry include redox potential, pH, salinity, sulfate/sulfide concentration, iron concentration and organic matter (OM) content. Each of these factors affects metal speciation in a different way. For example, increased salinity does not affect Cd(II) in the same way it affects Cr(VI), as Cr(VI) is not subjected to Cl complexation *(33)*. For Cd, increased salinity increases Cd-Cl complexation and reduces the proportion of free ion concentration, decreasing its bioavailability *(53-54)*.

An increase in alkalinity affects differently sorption mechanisms for each metal, affecting metal mobility differently. In general, sorption increases with pH for all cationic metals (such as Cd, Cr(III), and Pb) while it decreases with pH for anionic metals (such as Cr(VI) as CrO_4^{2-} and As as $AsO_3^{3-}$and AsO_4^{3-}). This can be explained by many sorption sites in sediments being pH dependent, such as Fe and Mn oxides, carbonates and the edges of clay minerals. The number of sites for cation sorption diminishes as the pH becomes more acidic while the number of sites for anion sorption increases. Additionally, metal cations face competition for available charged sites occupied by other metals, such as Al^{3+}, H^+ and Ca^{2+}. Fe and Mn oxides usually dissolve below pH 6, releasing sorbed metal ions to solution. However, DOM can affect this behavior due to formation of metal complexes with DOM, which can either increase or decrease metal mobility *(55-56)*. DOM generally reduces metal bioavailability by metal complexation *(57)*. However,

DOM may enhance metal transport through the water column and DOM-bound metals might be more mobile than dissolved uncomplexed metal ions.

Some metals have more than one important oxidation state normally found in the environment and thus are substantially affected by the redox potential of the sediment *(42, 56, 58-61)*. Oxidizing conditions in general favor retention of metals while reducing conditions favor mobility *(55, 60-61)*. For example, As (III) is predominant in reduced conditions and its species have higher solubility than As(V) species. However, care should be taken when making this consideration. For example, Cr(VI) is substantially more toxic than Cr(III) and usually more soluble, but it is usually not present in sediments when AVS is in excess. Cr(VI) is in general reduced to Cr(III) by excess AVS and the risk of Cr exposure to organisms should be low under reduced conditions as Cr(III) will be the major environment species under anoxic conditions *(62-63)*, and it is less toxic and usually less mobile than Cr(VI).

The factors affecting metal biochemistry are discussed in more detail for Cd, Cr, Pb, Ag, As, Hg and CN in the next items.

2.6. Cadmium in the Environment

Cd is classified as a class B1 carcinogen by USEPA (i.e., probably human carcinogen with sufficient evidence from animal bioassay data, but limited human evidence). Human response to Cd exposure includes diarrhea, anemia, bone disorders, liver, kidney and lung damage, and even death in acute exposures *(64)*. The most serious event involving Cd occurred in Japan, when rice was grown with irrigation from water contaminated with Cd from a Zn mining and smelting operation downstream. Hundreds of people contracted a degenerative bone disease, mostly older woman, due to a Cd intake around 600 μg d^{-1}. Primary anthropogenic sources of Cd to the environment include metal plating, smelting and mining industries, nickel-cadmium rechargeable

batteries, phosphate fertilizers, and paints *(64)*. Natural sources include volcanic action, forest fires and release of metal-enriched particles from terrestrial vegetation *(61)*.

The primary oxidation state of Cd in aqueous environments is +II. The solubility curve for Cd (and Zn) is shown in Figure 2.3 in equilibrium with carbon dioxide concentrations normally found in inland waters (10^{-2} – 10^{-3} moles CO_2 dissolved L^{-1}) *(23)*. Cd is substantially soluble in water. However, when sulfide ions are present, Cd has very low solubility, precipitating as CdS *(65)*. In general, more mobile Cd species are formed when pH decreases (i.e., increase in H^+ ion concentration) from near neutral to a moderately acid and oxidizing environment *(23)*. Solubility values of some Cd species are shown in Table 2.4 and it can be observed that CdS has very low solubility, followed by $Cd(OH)_2$.

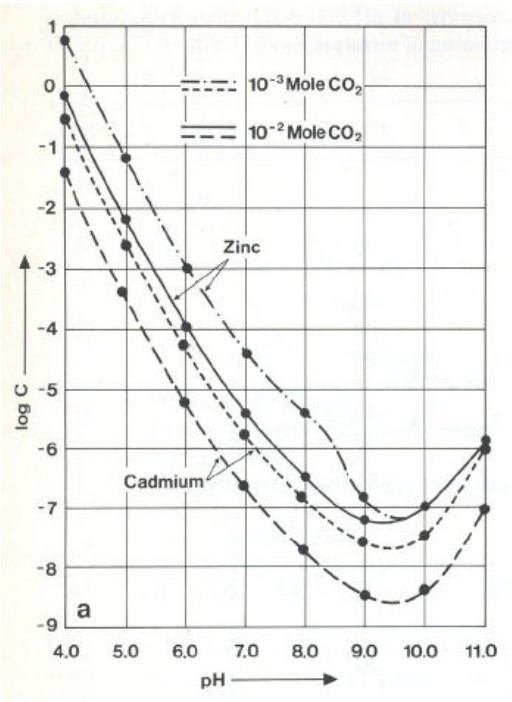

Figure 2.3. Solubility of Cd and Zn as a function of pH *(23)*.

Cd in freshwater sediments is mainly bounded to iron and manganese oxides, but it is also substantially bounded to OM and sulfides *(66-67)*. A smaller fraction can be found as the free ion. Cd in its ionic form seems to be more readily absorbed by fish *(68)*.

Table 2.4. Literature reported solubility of different Cd species in water

Compound	Name	Solubility (mg L^{-1})
CdS	cadmium sulfide	$1.6\ 10^{-5}$ – 0.01
$CdSO_3$	cadmium sulfite	248
CdO	cadmium oxide	4.2
$Cd(OH)_2$	cadmium hydroxide	1.2

[a] Sources: *(69-71)*

At pH less than five and low sulfide concentrations, Cd solubility rises with decrease in sulfide concentrations due to formation of Cd^{2+}, $CdCl_2$, and Cd-DOC complexes (Figure 2.4). At pH higher than 5, solubility increases due to formation of anionic $CdOHS^-$. Considering only Cd-S species, which have low solubility, at high total sulfide concentrations (regardless of pH), solubility rises because of formation of the anions $Cd(HS)_4^{2-}$ and $Cd(HS)_3^-$. Sulfide levels can vary substantially for different sites and with temperature due to sediment microbial activity and with sediment depth. Typical total hydrogen sulfide concentrations in porewater from freshwater and marine sediments are on the order of 10^{-5} M and 10^{-2} M *(72)*, respectively. Moreover, typical acid volatile sulfide (AVS) concentrations in unpolluted freshwater and marine water sediments are on the order of 0.01 and 0.06 mol S kg^{-1} dry wt *(73)*, respectively. Thus, at marine water with pH usually around 8 and sulfide concentrations on the order of 10^{-2} M, Cd concentrations could be higher than 0.1 μg L^{-1} at the Cl concentration of 0.1 M (which is considered low for marine waters).

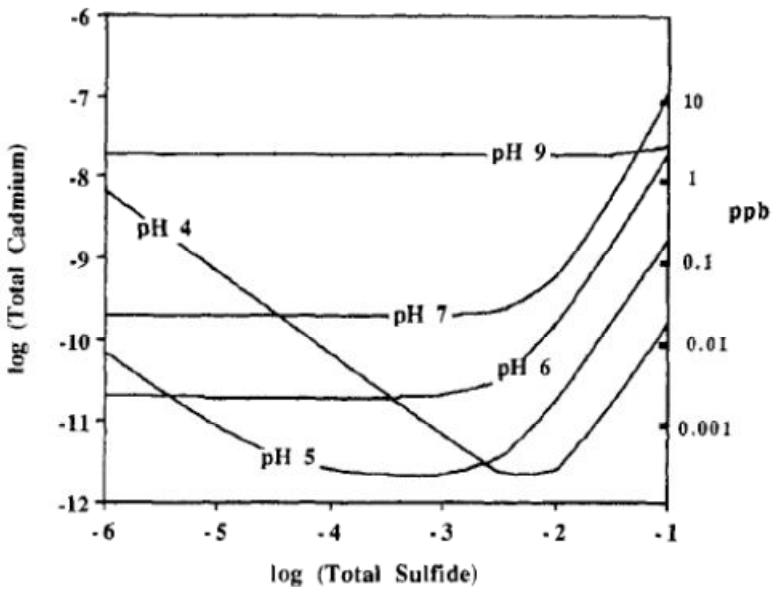

Figure 2.4. Cd solubility as a function of total S^{2-} concentration at different pH values. Total [Cl^-] = 0.1 M; *T* = 25 °C *(69)*.

Due to strong Cl complexation in seawater, the fraction of uncomplexed Cd^{2+} ion decreases from 92.2% in freshwater to 4.4% in seawater at pH 8 *(34)*. Thus, increased salinity increases Cl complexation and reduces the proportion of free ion concentration, reducing metal availability and decreasing metal uptake from solution. Cd as free Cd^{2+} concentration increases by 20-30 times with decreasing salinity from 35 parts per thousand to 0 and this corresponds to a 20-30 times higher uptake in freshwater fish than in marine fish *(33)*. Although Cd complexation with Cl ligands may dominate Cd speciation, there is substantial complexation of dissolved Cd to organic ligands *(74)*.

2.7. Lead in the Environment

The USEPA has adopted a Maximum Contaminant Level Goal (MCLG) of zero for Pb in drinking water because Pb is classified as a Class B2 carcinogen (i.e., probably human carcinogen with sufficient evidence from animal bioassay data, but with little or no human data)

(75). Lead exposure is associated with children reduced stature, retarded postnatal growth, anemia, kidney injury, fatal childhood Pb encephalopathy, severe damage to brain, and ultimately death *(76-77)*. Pb is highly toxic especially for children. Pb exposure for children in the USA is usually through lead paint. After Pb was banned for use in paints in 1978, children became less likely to be exposed to Pb poisoning. Nevertheless, old houses still present high risk for children lead poisoning. Pb also causes restricted development of IQ and increased blood pressure in adults. Lead is a bluish-gray metal and it occurs naturally in the environment. It can be found in minerals like galena (PbS), anglesite ($PbSO_4$) and cerussite ($PbCO_3$). Anthropogenic sources of Pb to the environment include burning of fossil fuels (including post lead amendment to gasoline to increase octane), mining, batteries, ammunition, metal production, deteriorating pipes, solders and paints, waste incineration, coal burning, drinking water, and lead arsenate use in agriculture *(65, 77)*. Pb has four stable isotopes, ^{204}Pb, ^{206}Pb, ^{207}Pb and ^{208}Pb.

According to Rendberg et al. *(78)*, the first traces of Pb pollution in Sweden sediment can be traced back to 3500 years ago. It is interesting that the authors observed that at least 50% of the cumulative anthropogenic load of atmospheric Pb is from pre-industrial time. Pb was used in the Roman period in water ducts and for cooking vessels and its production increased during the medieval period. Brannvall et al. *(79)*, concluded in a study in northern European that atmospheric Pb deposition did not increase substantially with the Industrial Revolution, but did increase significantly during 1950 – 1970 due to the extensive use of leaded gasoline. After the 1970s, there was a reduction in Pb emissions *(80)*, although this pattern was not followed worldwide *(81)*, as developing countries have not controlled emissions and leaded gasoline is sometimes still used *(82)*.

Pb can be found in the +II and +IV oxidation states. The most common species found in freshwater are Pb^{2+}, $PbOH^{+}$, $Pb(OH)_2$, $Pb(OH)_3^{-}$, $PbCO_3(aq)$, $Pb(CO_3)_2^{2-}$, $PbSO_4$, PbCl, $PbCl_2$, $PbCl_3$, $PbCl_4$, PbS and Pb(DOM) *(22, 83)*. Solubility values of some of these compounds can be found in Table 2.5. PbS has the lowest solubility value in the table, followed by $PbCO_3$, which is usually the dominant species for pH higher than 7 (Table 2.6) based on a study by Smolyakov et al. *(83)* with a reservoir water. The researchers observed that at higher pH, $PbCO_3(aq)$ and $Pb(OH)_2$ (in a smaller scale) concentration increases, while Pb^{2+} and Pb(DOM) concentrations decreases. Pb is usually less toxic at high pH as decrease in the proportion of free ion concentration usually suggests a decrease in metal bioavailability and thus decrease in metal uptake by organisms and toxicity. $PbSO_4(aq)$ and $PbCl^{+}$ concentrations also decrease with pH increase *(22)*.

Table 2.5. Literature reported solubility of different Pb species in water

Compound	Name	Solubility (mg L^{-1})
$PbCl_2.PbO$	lead chloride.oxide	41
PbS	lead sulfide	0.19
$PbSO_4.PbO$	lead sulfate oxide	5.3
$PbSO_3$	lead sulfite	1.7
PbO	lead oxide	63
$PbCO_3$	lead carbonate	1.3

[a] Sources: *(70-71)*

Table 2.6. Pb species (%) in a reservoir water at different pH[a]

pH	Pb^{2+}	$PbOH^{+}$	$Pb(OH)_2$	$PbCO_3$	Pb(DOM)
6	61.1	0.6	0.01	11.3	27.1
7	12.8	1.3	0.1	61.1	24.8
8	1.4	1.5	0.7	79.8	16.5
9	0.1	1.7	7.6	83.9	6.7

[a] Source: *(83)*

Pb in sediments is mainly found bounded to iron and manganese oxides or as the free ion species. A smaller fraction of Pb in sediments can be found bounded to carbonates *(67)*. Fe and Mn oxides are thermodynamically unstable under anoxic conditions and thus Pb may be released under low redox potential, while the fraction bounded to carbonates is pH sensitive *(84)*.

2.8. Chromium in the Environment

Cr(VI) is classified as a Class A carcinogen (i.e., known human carcinogen) by the inhalation route of exposure. Breathing Cr(VI) may cause ulcers and holes in the nasal septum. Cr (VI) swallow in high doses may lead to lung cancer, asthma attacks, ulcers, convulsions, kidney and liver damage, and even death *(59)*. Cr is the 21st most abundant element on Earth. The mean concentration of Cr in U.S. soils is 40 mg kg^{-1} *(42)*. Cr is used primarily in stainless steel, chromate production, chrome plating, leather and wood preservation, ferrochrome industry, chrome pigments and leather tanning. Painters, welders, battery makers, candle makers, rubber and dye makers and cement workers face possible workplace exposure to Cr.

Cr can be found in the oxidation states from –II to +VI, while the divalent, trivalent and hexavalent states are the most prevalent in the environment. Cr(III) is the most stable state and is usually found in combination with iron or other metal oxides. This form has very low solubility (with the exception of acetate, hexahydrate of chloride and nitrate salts, Table 2.7) and low reactivity resulting in low mobility in the environment and relatively low toxicity to organisms *(42, 59)*. Cr(VI) is much more toxic than Cr(III) and usually more soluble, thus representing a significantly increased risk from both a dose and exposure standpoint. Cr(VI) usually exists as chromate (CrO_4^{2-}, pH>6.4), bichromate ($HCrO_4^-$, 1<pH<6.4) and dichromate ($Cr_2O_7^{2-}$, pH<3) *(85)*. Cr solubility in water at pH 7 increases from species $FeO.Cr_2O_3 < Cr_2O_3 < Cr(OH)_3 < CrPO_4 < PbCrO_4 < CrAsO_4 \sim BaCrO_4 < CaCrO_4 < CrCl_3 \sim Cr_2(SO_4)_3$ *(85)*.

Table 2.7. Cr solubility for different Cr species

Compound	Name	Solubility (mg L^{-1})
$CrSO_4$	chromium(II) sulfate	38,649
$PbCrO_4$	lead chromate (VI)	0.016
$FeO\text{-}Cr_2O_3$	ferrochromite (III)	insoluble
Cr_2O_3	chromium (III) oxide	insoluble
Ag_2CrO_4	silver chromate (VI)	4.1
$BaCrO_4$	barium chromate (VI)	2.1
$CaCrO_4$	calcium chromate (VI)	7,400
CrO_3	chromium (VI) trioxide	Very soluble
$CrCl_3.6H_2O$	chromium (III) chloride, hexahydrate	114,000

[a] Sources: *(59, 70)*

In natural waters, Cr can be found as both Cr(III) and Cr(VI). Normally, Cr(III) is mainly found in anaerobic conditions and Cr(VI) in aerobic environment. pH is also an important factor as under basic pH Cr(III) tends to precipitate out and under acidic pH it tends to solubilize. Also, DOM affects Cr speciation and may increase Cr(III) concentration in oxygenated surface *(55)*.

Cr(VI) can be reduced to Cr(III) in the presence of oxidizable OM, zerovalent metals, Fe^{2+} and sulfides *(59, 85-86)*; all of which are frequently found in polluted sediments. Cr(III) can be oxidized to Cr(VI) by O_2 and Mn oxides *(87)*. Schlautman and Han *(86)* verified that Cr(VI) reduction rates increase with pH increase within the pH range of 3.5 to 7. Further, Graham et al. *(63)* observed that Cr(VI) is usually not present in sediments when AVS (mostly represented by FeS) is in excess. The researchers noticed that in this case all Cr(VI) should be reduced to Cr(III) by excess AVS and the risk of Cr exposure to organisms should be low as Cr(III) precipitates or is sorbed onto the sediment. However, the authors mentioned that sediment re-suspension or increase in dissolved oxygen in bottom waters may change the sediment redox buffering capacity leading to oxidation of Cr(III) to Cr(VI). In experiments performed by Patterson et al. *(88)*, all

added Cr(VI) was removed from solution by FeS, forming for example $[Cr_{0.25}, Fe_{0.75}](OH)_3$. Thus, a potential un-intended benefit of sediment pollution is that Cr is more likely to be found in the Cr(III) state, particularly in higher pH marine systems.

$$Cr(VI)_{aq} + 3Fe(II)_{aq} \rightarrow Cr(III)_{aq} + 3Fe(III)_{aq} \quad (2.16)$$

2.9. Silver in the Environment

Ag may cause argyria (sickness where skin and other body tissues turn gray in a permanent state), kidney problems (more studies are necessary to prove this effect), lung and throat irritation and stomach pain (usually through silver nitrate and silver oxide). Even though Ag may cause harmful health effects, it does present some helpful uses, such as use in salves for burn victims, and some water treatment methods use it to kill bacteria *(89)*. On the other hand, Ag is considered one of the most toxic metals to fish *(90)*. Ag^{+1} is highly toxic to fish due to its toxic effects on the Na^+ and Cl^- transport across the gills and the intestine, resulting in failure to maintain constant Na^+ and Cl^- concentrations in the blood plasma *(91)*. $AgNO_3$ is more toxic than AgCl and silver thiosulfate ($Ag_2S_2O_3$) *(92)*. Rodgers et al. *(92)* also reported that free ionic Ag is substantially more acutely toxic than complexed and sorbed Ag species. Silver sulfide and silver chloride are not highly toxic *(93)*.

Ag is used to make jewelry, silverware, electronic equipment, photographs and dental fillings. It occurs in metal form, but also in powdery white (silver nitrate and silver chloride) or dark-gray to black compounds (silver sulfide and silver oxide). Ag is released in the environment through mining activity, photo-processing and dental effluents, natural wearing down of silver-bearing rocks and soil by the wind and rain, and other sources *(89-90)*. The most common oxidation states are 0 and +I, but other possible states are +II and +III.

Ag in freshwater is usually found as AgBr, AgCl and AgI under oxidizing conditions and as free metal and Ag_2S under reducing conditions *(93)*. It can also be found in combination with HCO_3^- and SO_4^{2-}. Ag is frequently found adsorbed onto manganese and ferric oxides and clay minerals, to which it has a high affinity. Howe and Dobson *(93)* reported that Ag is usually less toxic to freshwater aquatic organisms under low dissolved Ag^+ concentration and under high pH, hardness, sulfide and dissolved and particulate organic loadings. Highly contaminated waters or waters with elevated OM content may contain silver thiolate ($AgSC_nH_{2n+1}$) as the dominant dissolved species *(93)*. Solubility values for some Ag species can be found in Table 2.8 with Ag_2S being the least soluble species and $AgNO_3$ the most soluble one.

Table 2.8. Ag solubility for different Ag species

Compound	Name	Solubility (mg L^{-1})
Ag_2O	silver (II) oxide	48
$AgNO_3$	silver nitrate	$1.5\ 10^6$
Ag_2SO_3	silver sulfite	2.2
AgCl	silver chloride	1.4
Ag_2S	silver sulfide	0.12
Ag_2CO_3	silver carbonate	23
Ag_3PO_4	silver phosphate	4.9
$AgC_2H_3O_2$	silver acetate	4,732
Ag_2SO_4	silver sulfate	5,743

[a] Sources: *(70-71, 89, 92)*

Reduced redox conditions and pH greater than 7 usually favor immobilization of Ag in sediments decreasing percentage of Ag^+, although there are other sediment characteristics that may affect Ag speciation more strongly, such as AVS *(92)*. Thus, interactions of different sediment characteristics determine Ag bioavailability and toxicity. For example, in marine unpolluted waters, Ag speciation is dominated by inorganic chloride complexes and dissolved

Ag is present at very low concentrations, resulting in lower bioavailability of Ag with marine organisms *(93-94)*.

2.10. Arsenic in the Environment

The US Department of Health and Human Services (DHHS), the International Agency for Research on Cancer (IARC) and the USEPA all have determined that inorganic As is a Class A carcinogen. Inorganic As is a human poison and in large oral doses can cause death. It may cause irritation of stomach and intestines, diarrhea, liver and kidney damage, nervous system disorders, anemia, skin changes and cancer, and it increases the risk of cancer in liver, bladder and lungs. There is comparatively less information available on the effects of organo-arsenic compounds in humans, but some studies suggest they are less toxic than the inorganic forms *(60)*.

As is the 20th most abundant element in nature *(85)*. As is typically present in one of these three oxidation states: -III, 0, +III and +V. A variety of arsenate ions (AsO_4^{3-} with As in the oxidation state +V) and arsenite ions (AsO_3^{3-} with As in the oxidation state +III) occur in the water, air, soil and food. Arsenites tend to be more toxic and mobile than arsenates *(95)*, while arsine (AsH_3) is the most highly toxic. AsH_3 can be formed under very reducing conditions (Eh < -500mV at pH 7).

As (V) is the major dissolved As species under oxic conditions and its solubility is lower, while As (III) is predominant in reduced conditions and is more soluble. When As (III) is released to oxic waters, it is transformed in As (V) with a timescale of days *(61)*. Under moderately reduced conditions, As solubility is mostly controlled by dissolution of iron oxyhydroxides, such as goethite (α-FeOOH), lepidocrocite (γ-FeOOH) and hematite (Fe_2O_3).

There are several methyl and phenyl derivatives of As that are widely used in agriculture. Common sources are nonferrous metal mining and smelting, pesticide application, coal combustion, wood preservative, and waste incineration. It is also released from natural sources, like wind-blown soil and volcanoes. It can also be found in drinking water from private wells *(60)*. 20 countries have reported problems with As groundwater contamination *(85)*. Aquifers may naturally have high immobilized As concentrations. However, anthropogenic changes to the environment mobilize As in groundwater. For example, excessive depletion of aquifer level may lead to oxidation of naturally occurring As complexes, such as the As-sulfide mineral arsenopyrite (FeAsS), mobilizing As. Also, oxyanionic As species may be adsorbed on surfaces of Fe and Mn oxyhydroxides, which have pH-dependent surface charges. At increased alkalinity, the oxide surfaces become zero charged and release As oxyanions by desorption. In reduced environments, dissolution of Fe oxyhydroxides results in release of Fe and As into the water. Also, aquifers rich in OM appear to provide a reducing environment due to rapid depletion of O_2, resulting in As(V) being reduced to the more soluble form of As (As(III) species) and to methylated arsenicals *(96-97)*.

As speciation and solubility is also strongly affected by pH (Figure 2.5). According to Masscheleyn et al. *(95)*, under oxidized conditions and high pH (when arsenate is dominant), As concentrations in soil were three time higher than at lower pH. Decreasing positive surface charge of oxides with increasing pH facilitates desorption of arsenate.

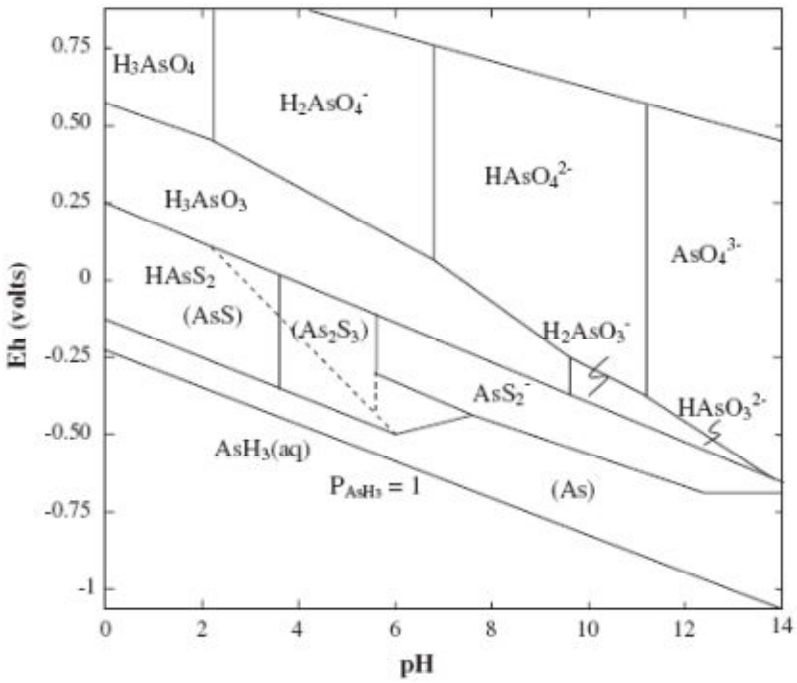

Figure 2.5. The Eh-pH diagram for As at 25° C and 101kPa *(98)*.

Under reduced conditions, As_2S_3 and FeAsS are dominant sinks. Jay and others *(99)* reported that in sulfidic sediments at high Fe/S ratios, As usually precipitates as AsS and at low Fe/S ratios As_2S_3 is usually formed. As may occur also preferentially as arsenopyrite (FeAsS). Arsenite adsorption reactions on ZnS and PbS are also important sinks. However, As-containing minerals may dissolve, releasing both adsorbed As and As bounded in the mineral structure. Floroiu et al. *(100)* observed that arsenic sulfide dissolution rates increase with an increase in pH and with high concentrations of sulfide. However under acidic and neutral conditions, As_2S_3 solubility (Table 2.9) is independent of pH. According to the authors, that is probably due to hydroxide ions adsorption onto As surface sites at basic pH, creating charge on the surface and weakening the interstitial bonds through bond polarization. As species will does dissolve from the As_2S_3.

Table 2.9. As solubility for some As species

Compound	Name	Solubility (mg L^{-1})
As_2O_3	arsenic (III) trioxide	11,322
As_2S_3	arsenic (III) trisulfide	0.32
As_2S_5	arsenic (V) pentasulfide	0.43
Ag_3AsO_3	silver arsenite (III)	1.9

[a] Source: *(70)*

2.11. Mercury and Methyl Mercury in the Environment

High Hg exposure may lead to lung, stomach, kidney, brain and intestinal damage and cause death. It also causes tremor, deafness, vomiting, diarrhea, adverse effects on the developing fetus and increases the number of spontaneous abortions *(58)*. The CH_3Hg species is the most toxic one, with well-publicized poisoning cases such as the Minamata Bay, Japan environmental disaster where thousands of people were poisoned by consuming fish contaminated with as high as 100 mg kg^{-1} CH_3Hg concentrations, resulting in high frequency of teratogenesis in the exposed populations. The North American recommended Hg limit in fish is 0.5 ppm *(65)*.

Hg can be found as metallic or elemental mercury Hg^0, inorganic mercury as Hg^{2+} and Hg^{1+}, and organic mercury (normally found as methyl mercury). Metallic mercury is a shiny, silver-white metal that is a liquid at room temperature and it has a high tendency to evaporate as gas. Mercuric (Hg^{2+}) mercury is the predominant form of Hg in surface waters and it is present as complexes with chloride and hydroxide ions and chelates (complex formation with metals) with ligands. DOM strongly affects Hg speciation. Most inorganic Hg in waters is associated with DOM (around 95%) with a small fraction (<5%) occurring in dissolved inorganic, potentially reactive, forms *(101)*.The most common forms of organo-mercury compounds are methyl mercury and dimethyl mercury *(58)*. CH_3Hg is soluble, mobile, and quickly enters the aquatic food chain, where it is frequently biomagnified in top predators. CH_3Hg is predominant over $Hg(CH_3)_2$ under neutral and acidic conditions *(65)*.

Hg is used to produce chlorine gas and caustic soda, to extract gold from ore or articles that contain gold and as a fungicide. It is also used in thermometers, fluorescent light bulbs, barometers, batteries, electrical switches and in dental fillings. According to ATSDR *(58)*, around 80% of the Hg released from human activities is elemental Hg released to the air from fossil fuel combustion, mining, smelting and from solid waste incineration.

CH_3Hg is mainly formed by microorganisms such as sulfate reducing bacteria and it is usually the form of Hg that bioaccumulates in the food chain as it is the most easily absorbed Hg form through the gastrointestinal tract *(58)*. Methylation is faster at lower pH due to the higher bioavailability of the neutral Hg-sulfides from which CH_3Hg is formed *(65)*. Sulfate-reducing bacteria (SRB) *Desulfovibrioacaea*, *Desulfotomaculum*, and the *Dsulfobacteracaea* in particular play the key role in this process *(102)*. High sulfate concentrations are necessary so that SRB activity is not limited. However, very high sulfide concentrations produced by SRB inhibits methylation by precipitation of HgS *(103)*. Therefore, there is an ideal sulfate and sulfide concentration range in which methylation occurs *(104)*.

The Hg cycle is shown in Figure 2.6. At a pH range of 4 to 9 and typical sulfide concentration, Hg forms HgS, which is relatively insoluble in aqueous solution ($11\ 10^{-17}$ μg L^{-1}) and precipitates, removing mercury ions from the water and reducing their availability to fish *(58, 105)*. Typical total H_2S concentrations in porewater from freshwater and marine sediments are on the order of 10^{-5} M and 10^{-2} M, respectively *(72)*. Typical concentration of mercury in bottom sediments is 10 – 200 ng g^{-1} of dry mass. Typical CH_3Hg concentration in bottom sediments is 1 – 1.5% of total mercury *(106-107)*.

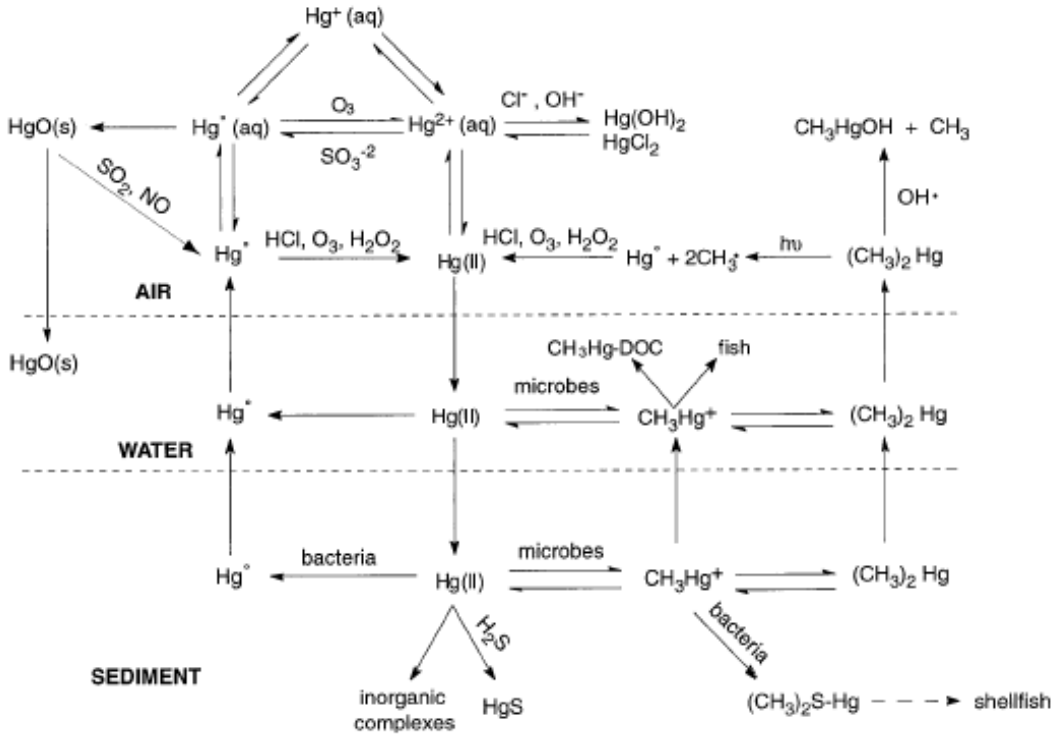

Figure 2.6. Simplified aquatic Hg cycle showing inter-species transformations. Dashed lines represent the boundary between environmental compartments where the processes are most prevalent. Figure from ATSDR *(58)*.

The solubility of some Hg species can be found in Table 2.10 with Hg_2SO_3 being the lowest soluble, followed by HgS. $HgCl_2$ and $Hg(CN)_2$ are highly soluble. Hg-S complexes are abundant in anoxic marine waters, with HgS solubility increasing with an increase in redox levels. Hg in aquatic systems is mostly immobilized in the sediments. However, changes in environmental conditions can remobilize Hg to the water column due to sulfide oxidation or CH_3Hg formation through biotic and abiotic transformations *(108)*. $HgCl_2$ species are the main species in very oxic sediments, which is not a common characteristic in sediments *(105)*.

Table 2.10. Hg solubility for some Hg species

Compound	Name	Solubility (mg L^{-1})
Hg_2SO_3	mercury (I) sulfite	$3.0\ 10^{-6}$
$Hg(OH)_2$	mercury(II) hydroxide	50
HgO	mercury(II) oxide	48
$HgCl_2$	mercury(II) chloride	49,965
Hg_2Cl_2	mercury (I) chloride	slightly soluble
$Hg(CN)_2$	mercury(II) cyanide	73,855
HgS	mercury(II) sulfide	0.011
Hg_2SO_4	mercury(I) sulfate	315
$HgC_2H_3O_2$	mercury(I) acetate	5,795
CH_3Hg	methyl mercury	100

[a] Sources: *(70-71, 109-110)*

2.12. Cyanide in the Environment

CN may cause shortness of breath, brain and heart damage, and can cause coma and death. According to ATSDR *(111)*, breathing 546 ppm of HCN causes death after a 10 min exposure and a 110 ppm concentration is life-threatening after a 1 hr exposure.

CN is found in low amounts in plants and fruits, mainly in pits and seeds of apricots, apples and peaches *(111)*. CN is a strong solvent for metals that solubilizes many substances and it is frequently used in gold and other mining industries. CN also enters the environment through discharges from organic chemical industries, iron and steel plants or manufacturers, wastewater treatment facilities, vehicle exhaust, burning of waste, cyanide-containing pesticides, photographic developing and the manufacture of plastics. The most common forms of CN in the environment are HCN, NaCN and KCN. HCN is a colorless gas while NaCN and KCN are both white solids. HCN is highly toxic and it was used in gas-chamber executions and as a war gas agent *(111)*.

Free cyanide (HCN, CN^-) is the most reactive and toxic form, readily forming compounds with lower solubility. At pH less than 8, more than 93% of the free cyanide in water will exist as

non-dissociated HCN, with a pk_a of 9.2 at 25° C. In sediments and soil, CN may occur as HCN, alkali metal salts or as low solubility metallocyanide complexes *(111)*. NaCN, KCN and $Ca(CN)_2$ are highly soluble in water and rapidly dissolve to form free cyanide. Weak metal-cyanide complexes (like AgCN, $HgCN_2$ and $CdCN_2$) can dissociate under weak acid conditions, while strong metal-cyanide complexes (e.g. $Fe(CN)_6^{4-}$) only dissociate under strong acid conditions in the dark or easily decompose when exposed to light *(112)*. The solubility of Fe-CN complexes generally increases with an increase in pH *(113)* as adsorption on OM surface and precipitation are important processes affecting dissolved Fe-CN concentrations and they decrease as pH increases *(114)*. Solubility values for some CN species can be found in Table 2.11.

Volatilization is an important process affecting the fate of CN. Other important processes are CN complexation with metals and biodegradation. Biodegradation of CN occurs aerobically and anaerobically, Under aerobic conditions, CN compounds are converted into ammonia and under anaerobic conditions, into ammonia and methane *(112, 115)*. Upper limits of 200 and 2 mg kg^{-1} CN^-, respectively, may inhibit aerobic and anaerobic biodegradation of cyanide in soil *(116)*.

Table 2.11. CN solubility for some CN species

Compound	Name	Solubility (mg L^{-1})
HCN	hydrogen cyanide	slightly soluble
NaCN	sodium cyanide	highly soluble
KCN	potassium cyanide	highly soluble
AgCN	silver cyanide	highly soluble
$Cd(CN)_2$	cadmium cyanide	0.78
$Ba(CN)_2$	barium cyanide	121,965
$Hg(CN)_2$	mercury(II) cyanide	19,145

[a] Sources: *(70, 117)*

2.13. Bioavailability and Toxicity

In its most general definition, bioavailability refers to the rate or extent that a compound of interest comes into contact with the organism of interest in a form that can be brought within the cell. Being able to distinguish between the available and non-available fractions of metals to biological systems is an important task that cannot be accomplished by total metal measurements *(118)*. Bioavailability can be assessed in many different ways: by measuring contaminant accumulation into tissues of organisms; by using metal-specific bacterial sensors; by performing toxicity tests with fishes, worms and crustaceans; by measuring the ratio of concentration of simultaneously extracted metal (SEM) and AVS (SEM/AVS); etc *(44, 118-119)*.

Some factors affecting bioavailability are the rate of transfer of the contaminant from the media to the cell and the rate of uptake and metabolism of the cell, which means that its value differs for different organisms and different contaminants. Sorption to surfaces within the nano- and micropores in the solid phase may protect contaminants from attack by microorganisms. The affinity to the various solid-phase fractions is very important. During desorption of solid-bound organic contaminants to the liquid phase, adsorbents in contact with the solid phase will preferentially intercept and adsorb the contaminants before they become bioavailable to organisms. The sorption capacity is enhanced when the particle size of the adsorbent is very small due to the greater contact area between solid phase and carbon particles and because of the greater carbon surface areas per unit mass of carbon *(120)*.

Although there have been attempts to correlate metal bioavailability with aqueous metal concentrations as a proxy to assess the much less easily measured bioavailability, uptake is greatly affected by sediment characteristics such as organic carbon content, pH, redox potential and AVS. According to Ankley et al. *(121)*, different studies have shown that total metal concentrations in sediments are not good predictors of bioavailability, while metal concentrations

in interstitial porewater are better predictors for biological effects. The authors consider that assessment of AVS concentrations and measurement of interstitial porewater metal concentrations are the most useful parameters to predict metal bioavailability.

Liao and others *(118)* successfully used bacteria that are genetically engineered to emit a measurable signal when in contact with bioavailable metal ions. They used a green fluorescent protein-based bacterial biosensor and measured cell growth and the fluorescence of cells grown in the medium containing a range of different metal ions.

USEPA *(44)* reported that uptake of metals is more correlated to free metal activity and not with total metal concentration as other forms of metal may become unavailable to organisms by binding to dissolved organic carbon (DOC) and other ligand-complexed fractions. Thus, even part of the dissolved metal compounds may not be bioavailable. Campbell *(53)* reported that the biological response to a dissolved metal is usually related to the free-metal ion concentration. Factors affecting this are passive diffusion of neutral lipophilic species, accidental metal transport with low molecular weight metabolites and presence of OM. Janes and Playle *(90)* reported that DOC may decrease the free-ion concentration and thus bioavailability. It is also hard to assay metal bioavailability due to the ephemeral nature of environmental conditions in sediment; particularly at the sediment-water interface. For example, OM degradation in sediments by sulfate reducers increases bicarbonate concentrations, increasing concentration of metal-carbonate complexes, which affects metal bioavailability *(44)*. Even when heavy metals form minerals, some minerals are more easily dissolved than others and changes in pH may affect which mineral will be formed. For example, cerrusite ($PbCO_3$) presents higher risk of re-mobilization due to changing environmental conditions than pyromorphite [$Pb_{10}(PO_4)_6$(OH, F,

$Cl)_2$]. Pyromorphite is much less bioavailable than cerrusite under a variety of existing geochemical conditions *(122)*.

The metal species that is present in the sediment is very important to assess metal bioavailability and toxicity. Thus, the following paragraphs are a summary of main metal species found in sediments and their most toxic forms. However, it is important to mention that these are the typical species found in sediments, but sediment re-suspension, increase in dissolved oxygen in bottom waters, wastewater discharge and other environmental changes may modify metal speciation and thus affect metal toxicity. Additionally, metal speciation is dependent upon concentration of chemicals in sediments such as Cl^-, CO_3^{2-} and S^{2-}.

Cd in freshwater sediments is mainly bounded to iron and manganese oxides, which are pH and redox sensitive and considered as relatively mobile forms. It is also substantially bounded to OM and sulfides *(66-67)*. A smaller fraction can be found as the free ion. The described speciation is highly dependent of chemicals concentration, such as Fe, Mn, Cl and S. Cd in its ionic form seems to be more readily absorbed by fish *(68)*. In marine water sediment, the fraction of uncomplexed Cd^{2+} ion decreases due to strong chloride complexation in seawater *(34)*. Thus, increased salinity increases chloride complexation and reduces the proportion of free ion concentration, reducing metal availability and decreasing metal uptake from solution.

Pb in sediments is mainly found bounded to iron and manganese oxides or as the free ion species. A smaller fraction of Pb in sediments can be found bounded to carbonates *(67)*. Fe and Mn oxides are thermodynamically unstable under anoxic conditions, and thus Pb may be released under low redox potential, while the fraction bounded to carbonates is pH sensitive *(84)*.

Cr(VI) is usually not present in sediments when AVS (mostly represented by FeS) is in excess. Graham et al. *(63)* observed that in this case all Cr(VI) should be reduced to Cr(III) by

excess AVS and the risk of Cr exposure to organisms should be low as Cr(III) is less toxic than Cr(VI). Cr(III) is usually found in sediments in combination with iron or other metal oxides. This form has very low solubility (with the exception of acetate, hexahydrate of chloride and nitrate salts) and low reactivity resulting in low mobility in the environment and relatively low toxicity to organisms *(42, 59)*. Cr(VI) is much more toxic than Cr(III) and usually more soluble, thus representing a significantly increased risk from both a dose and exposure standpoint. Cr(VI) can be reduced to Cr(III) in the presence of oxidizable OM, zerovalent metals, Fe^{2+} and sulfides *(59, 85-86)*. This occurs particularly in marine waters, which usually have higher sulfide concentrations. Typical total hydrogen sulfide concentrations in porewater from freshwater and marine sediments are on the order of 10^{-5} M and 10^{-2} M *(72)*, respectively.

Reduced redox conditions and pH greater than 7 usually favor immobilization of Ag in sediments decreasing percentage of Ag^{+}, although there are other sediment characteristics that may affect Ag speciation more strongly, such as AVS *(92)*. For example, in marine unpolluted waters, Ag speciation is dominated by inorganic chloride complexes and dissolved Ag is present at very low concentrations, decreasing Ag toxicity with marine organisms *(93-94)*.

As (III) is predominant in reduced conditions and its species have higher solubility than As(V) species. Under reduced conditions, As_2S_3 and FeAsS are dominant sinks. Jay and others *(99)* reported that in sulfidic sediments at high Fe/S ratios, As usually precipitates as AsS; and at low Fe/S, ratios As_2S_3 is usually formed. As may occur also preferentially as pyrite (FeAsS). Under moderately reduced conditions, As solubility is mostly controlled by dissolution of iron oxyhydroxides, such as goethite (α-FeOOH), lepidocrocite (γ-FeOOH) and hematite (Fe_2O_3). In reduced environments, dissolution of Fe oxyhydroxides results in release of Fe and As into the water. Also, oxyanionic As species may be adsorbed on surfaces of Fe and Mn oxyhydroxides,

which have pH-dependent surface charges. At increased alkalinity, the oxide surfaces become zero charged and releases As oxyanions by desorption. Arsenites (As in the oxidation state +III) tend to be more toxic and mobile than arsenates (As in the oxidation state +V) *(95)*.

Hg-S complexes are abundant in anoxic marine waters, with HgS solubility increasing with an increase in redox levels. However, changes in environmental conditions can remobilize Hg to the water column due to sulfide oxidation or CH_3Hg formation through biotic and abiotic transformations *(108)*. The CH_3Hg species is the most toxic one and it is soluble, mobile, and quickly enters the aquatic food chain, where it is frequently biomagnified in top predators.

In sediments and soil, CN may occur as HCN, alkali metal salts or as low solubility metallocyanide complexes *(111)*. NaCN, KCN and $Ca(CN)_2$ are highly soluble in water and rapidly dissolve to form free cyanide. Free cyanide (HCN, CN^-) is the most reactive and toxic form, readily forming compounds with lower solubility.

2.14. Technologies for Remediation of Metal Contaminated Sediments

In the past, it was a common consideration to dump waste in the rivers and oceans, treating the sediments as a sink for pollutants. Nowadays, it is clear that waste disposal in the oceans and rivers is not an alternative. Even though contaminant sorption to the sediment OM occurs, sediments can act as a continual source of contamination to aquatic ecosystems and to the water column. Some factors that affect contaminant release from the sediments to the water column are natural diffusive and advective contaminant transport, gas ebullition due to OM degradation, storms, ships and benthic organisms revolving the sediments.

The two most common technologies to reduce exposure to sediment contaminants are in situ capping using either inert or reactive barriers and dredging with subsequent disposal *(5-7, 123)*. Dredging can lead to re-suspension and re-mobilization of contaminants. In addition, the large

amount of entrained water during dredging necessitates extensive dewatering periods, which may lead to release of volatile contaminants *(124)*. Conventional capping works as a physical barrier to isolate the contaminated sediments from the overlying water and minimize flux. Some advantages of this technology compared to dredging are: reduction of worker exposure to contaminants during the remediation project; it is typically less expensive than dredging and it minimizes ecosystem disturbance *(125)*. Although caps are frequently cited as being more effective from a short term risk standpoint, they do not result in contaminant removal or destruction and they are limited to sites where water depth limitations are not an issue. Capped sediment can also represent a future risk if the confinement structure is compromised due to gas ebullition, cap scouring or changes in environmental conditions; or by excessive contaminant breakthrough due to diffusion and/or advection. Conditions for an appropriate benthic organism habitat creation on the top of the cap may also be an important consideration, with installation of irregularly shaped rock islands if benthic habitat creation is desired *(126)* or selection of a capping design that discourages colonization by native deep-burrowing organisms to limit possibility of contaminant release due to bioturbation *(127)*.

2.15. Active Capping

Active capping consists in the addition of layers of materials over contaminated sediments to promote sequestration, enhanced retardation and/or chemical or biological degradation of contaminants in the underlying sediment to increase efficacy. These modes of action can be classified as bioaugmentation (addition of benthic animals or microorganisms), biostimulation (addition of nutrients, electron acceptors or donors, or other agents to stimulate benthic organisms), contaminant sequestration (addition of granular activated carbon (GAC), apatite or

other agents to bind pollutants) and hydraulic sequestration (addition of water-expanding clay or other agents to decrease hydraulic conductivity) *(10, 14-15, 128-130)*.

Many biostimulation and bioaugmentation studies have been performed in groundwater systems for chlorinated solvent remediation, the main contaminants in groundwater *(131-133)* and for PCB and PAH remediation *(134-135)*, but to date comparatively few have been performed in sediment systems. Biostimulation and bioaugmentation for metal contaminant degradation is not possible *(136)* as microbes cannot destroy metals, they can only change the redox state of many metals. As demonstrated in the above review, changes in oxidation state greatly affect metal speciation, solubility and mobility. For example, sulfate-reducing bacteria have been used to transform soluble and mobile U(VI) to its lower soluble form U(IV) *(137)*. Microorganisms, such as sulfate-reducing bacteria, can reduce Cr(VI) to Cr(III) and As(V) reduction can be catalyzed by biotic and abiotic processes forming As(III), which is more toxic and mobile.

Cap modifications with the ability to sequester contaminants by sorption and/or low hydraulic conductivity have been the most frequently mode of action applied. Active materials can provide over 1000 yr of isolation time for some pollutants, even under moderate porewater seepage through different mechanisms *(14-15)*. For example, apatite binds some metals into insoluble phases that are extremely stable by replacing Ca^{2+}, PO_4^{3-} and OH^- ions by metal ions *(138-139)*, and it can act as geosorbent for other metals with binding strength affected by solution pH *(125, 140)*. Organoclay (OC) and GAC have been applied to minimize transport of hydrophobic compounds through different sorption mechanisms. Other advantages of active capping application is that active capping minimizes contaminant release to the water column

over a long time, allowing natural recovery processes to occur in the sediments. In addition, deposition of clean sediment over the cap also contributes to increase cap reliability.

One of the difficulties in using generally high-cost active cap amendments is the need to ensure adequate uniform coverage to prevent localized cap failure. Several methods have been used to respond to this need, and many vendors now offer technical solutions. For example, a reactive core mat has been applied to some sites due to difficulties in placing a thin layer over submerged contaminated sediments *(141)*. Mats filled with coke were placed in 2004 in the Anacostia River, Washington, D.C., where an overlain sand layer was also used to help sink the mat readily and to protect cap integrity from benthic organism activity.

AquaBlok™ is an example of hydraulic barrier that has been applied in active capping *(10)*. It is formed of bentonite clay with polymer additives covering a small aggregate core. It was also applied in the Anacostia River project. It was delivered by flatbed trailer in 2 ton capacity SuperSacks. Aquablok™ bags were placed in a material barge and a tugboat was used to move it beside a crane barge. The crane barge was used to construct the caps and it was secured by anchor cable lines attached to anchors deployed outside the capping area to avoid impacts on the cap being placed. A clamshell bucket was used on the crane boom to release the material above the water surface. A version of the Offshore Positioning Software (WINOPS) system was used to assist the crane operator to properly release the material envisioning consistent coverage and proper cap thickness. Silt curtains were used to reduce cap material migration and sediment re-suspension downstream *(142)*. Some other examples of active capping projects can be seen in Table 2.12.

Table 2.12. Selected capping projects installed in USA as of spring 2009

Cap material	Purpose	Location
15 cm apatite/15 cm sand; 2.5 cm coke reactive mat/15 cm sand; 10 cm AquaBlock™/15 cm sand; 30 cm sand	metal and organic sequestration; permeability control	Anacostia River, Washington, D. C. *(10)*
60 cm–1.5 m sand/600 tons of organoclay/ armoring	prevent breakthrough of NAPL through the cap	McCormick and Baxter Creosoting Superfund Site, Portland, OR *(11)*
30 cm sand/topsoil; 30 cm granular bentonite/sand/topsoil; 30 cm AquaBlock™/sand/topsoil	prevent breakthrough of PCBs through the cap	Grasse River, Massena, NY *(12)*
30 - 90 cm of sand	heavy metals and PCBs (1^{st} capping project, 1984)	Duwamish Waterway, Seattle, WA *(143)*
120 – 600 cm of sand	prevent breakthrough of many contaminants	St. Paul Waterway (Simpson Tacoma Kraft superfund site), Tacoma, WA *(144)*
30 – 450 cm of sand	prevent breakthrough of PAH and Hg	East Eagle Harbor (Wyckoff, superfund site), WA *(144-145)*
90 – 180 cm of clean sand and 120 – 210 cm of armor stone	prevent breakthrough of PCBs	Lower Fox River and Green Bay superfund site, WI *(146)*
clay cap, 60 cm of limestone, 720 cm of clean soil	prevent breakthrough of Cd, Ni, Co and Zn	Marathon Battery superfund site, East Foundry, Cove Marsh, Cold Spring, NY *(147)*
geotextile/360 cm of sand and cement-stabilized cap	prevent breakthrough of PAHs, pentachorophenol, Cu, Cr, As	Koppers superfund site, Charleston, SC *(148)*
15 cm sand/activated carbon mat (total thickness of 11 mm and 2 kg m^{-2} activated carbon loading)/75 cm sand	prevent breakthrough of PAH	Stryker Bay, St. Louis River/Interlake/ Duluth Tar superfund site, Duluth, MN *(13)*

2.16. Apatite for Remediation of Metal Contaminated Sediment Remediation

Apatite $Ca_5(PO_4)_3(OH, F, Cl)$ is found in mineral form, in teeth, and also bones. The chemical form $Ca_5(PO_4)_3OH$ is called hydroxyapatite, $Ca_5(PO_4)_3F$ is known as fluorapatite and $Ca_5(PO_4)_3Cl$ as chlorapatite. Apatite has two modes of action: it binds some metals into insoluble

phases that are extremely stable by replacing Ca^{2+}, PO_4^{3-} and OH^- ions by metal ions *(138-139)* and it can act as geosorbent for other metals with binding strength affected by solution pH *(125, 140)*. Ca is usually replaced by Sr, Ba, Cd or Pb; P may be replaced by As, Mn or Cr; and OH, F, Cl can be replaced by Br. Some examples are chloropyromorphite (CPM) ($Pb_5(PO_4)_3Cl$) and hydroypyromorphite ($Pb_5(PO_4)_3OH$), with dissolution of the more soluble mineral $Ca_5(PO_4)_3OH$ supplying the compounds necessary for formation and precipitation of pyromorphites (Pb-apatite), which are mostly insoluble.

The mechanisms for metal immobilization by apatite include: 1) isomorphous substitutions and diffusion, which are more likely to occur for cations with ionic radii close to that of Ca^{2+}, as well as for cations with high electronegativity like Cd^{2+} and Pb^{2+}, while Ba^{2+} and Mg^{2+} are only sparingly removed due to their larger radii and low electronegativity; 2) adsorption, which likely occurs at the surface of apatite via the formation of inner sphere complexes; 3) formation of insoluble compounds via dissolution–precipitation processes *(149)*.

According to Crannel et al. *(138)*, apatite has the potential to be a more reliable cap for metals than one utilizing clays or clay-like materials due to possible metal dissociation from clay layers with change in porewater ionic strength. Metals immobilized in apatite caps are geochemically stable over a broad range of pH and redox conditions. The authors showed that apatite reduced Pb diffusivity by 67%, Zn by 50%, but Cu diffusivity remained unchanged. Bostick et al. *(150)* concluded that biogenic apatite has the potential to successfully retard migration of U, Pb, Cd, Cu and Hg, but was less effective for As, Se, Ba and Cr.

Kaplan and Knox *(125)* concluded that apatite significantly ($p \leq 0.05$) reduced Cd, Co, Hg, Pb and U porewater concentrations. However, it enhanced desorption of As, Se and Th. According to the authors, As and Se were not released directly from the mineral or from the

DOM; they result from phosphate competition for sorption sites. The porewater concentration increased only under oxidized conditions and probably due to the increase in desorbed organic C under oxidized conditions. The researchers concluded that the DOC did not originate from apatite, but it desorbed from the sediment probably as a result of pH increase, which resulted in a more ionic OM, reducing its hydrophobicity and promoting its repulsion from the sediment negative charge. Additionally, aqueous phosphate may have competitively exchanged anionic OM from mineral sorption sites. Others have found that adding zero-valent iron particles with apatite reduced enhanced desorption of As, Se and Th *(151)*. Some possible mechanisms include: (1) dissolved Fe(0) may have converted the phosphate into a complex that would not desorb OM and thus would not exchange with the sorbed As and Se; (2) spontaneously adsorption and co-precipitation of As(III) may have occurred with Fe(II) and Fe(III) oxides/hydroxides, which formed during Fe(0) oxidation; (3) Fe(0) may have donated electrons for sulfate reducers to transform sulfate in hydrogen sulfide, where the H was replaced by a metal, and the metal sulfide precipitated (K_{sp}=10^{-24} – 10^{-53}). As FeS has a higher K_{sp} than heavy metal sulfides, Fe^{2+} do not outcompete with precipitation of heavy metals.

In a column study investigating metal transport through hydroxyapatite, zeolite, OC and OC/anthracite blend columns, Alther et al. *(152)* observed that hydroxyapatite was the only sorbent to retain its sorption capacity in hard water. Matusik et al. *(153)* observed that Cd removal by different forms of phosphates is highly affected by pH. Highly insoluble and thermodynamically stable Cd products formed for different forms of phosphate for pH 6.8 to 9. However at pH smaller than 5, Cd reduction was less effective, and varied from 28 to less than 80%, according to phosphate form used.

Lang and Kaupenjohann *(154)* discussed the effects of pH and OM content on heavy metal mobility. Lead-phosphate minerals have very low solubility product, with CPM K_{sp} varying from 10^{-84} *(155)* to 10^{-167} *(156)*. Experiments performed by the researchers showed that CPM mass precipitated is not affected by presence of OM at pH 5 – 7. However, at pH 3 – 4, OM presence strongly inhibited CPM precipitation and OM presence under all pH ranges affected particle size, suggesting that OM blocked the surfaces of crystal seeds and impaired crystal growth, thus favoring the formation of mobile colloids (diameter of 0.001 to 1 μm). Pb may not only be adsorbed to colloids, which facilitate metal transport due to their mobility and comparable large surface area, but may also form colloids itself.

Scheckel and Ryan *(157)* argue that the use of selective sequential extraction procedures and scanning electron microscopy coupled with energy dispersive X-ray spectroscopy may lead to erroneous speciation results. The authors suggest the use of statistical analysis by linear combination fitting applied to X-ray absorption fine structure spectroscopy (XAFS) to generate more reliable results. Their technique was used to assess Pb speciation in soils amended with P. The non-amended control soil Pb speciation results included 0% of pyromorphite, 53% of Pb-sulfur species, 45% of adsorbed Pb and 2% of Pb-carbonate species. Amended soils with P resulted in increased pyromorphite concentration (up to 45%) with increased P concentrations. As pyromorphite has much lower solubility than the other Pb-compounds, P addition clearly increased Pb immobilization, at least around neutral pH (the experiment was performed with pH varying from 6.9 to 7.2).

Some studies have also tested phytate (a natural organophosphorus compound) for metal contaminant immobilization, which removes contaminants through the same mechanism as apatite *(50, 158)*. Phytate can be used in a soluble form and thus immobilize metals throughout

the sediment layer. Efficiency limitations include applied phytate form, adequate concentration and its capacity to sorb to hydrous oxides, limiting its capacity to reach the contaminant zone of interest. For example, Ca-phytate precipitate was able to decrease the solubility of U (by 96%), Ni (by 83%), Al, Ba, Co, Mn and Zn. As and Se solubilities increased, suggesting that phytate increased competition for sorption sites, releasing sorbed oxyanion contaminants. Dodeca sodium-phytate actually increased solubility of many metals at high concentrations, showing that adequate concentrations need to be investigated for application of this chemical *(158)*.

A modeling study of the Anacostia River by Roberts *(159)* investigated the ability of apatite, sand, Aquablok™ and coke breeze to minimize the release of PAH contaminants from sediments to the water column . It showed that an apatite cap layer of 15 cm has little efficiency to retard PAH migration from sediments to the water column. Whenever a site is contaminated with both heavy metal and organic contaminants, apatite may not be the best option. The author observed that Aquablok™ (15 cm) and coke breeze (15 cm) were the most effective caps between the studied cap materials. Time for phenanthrene breakthrough for the apatite and sand cap layers was around 60 d. In another study testing three different kinds of apatite, time for phenanthrene and benzo[a]pyrene to break through a 2.5 cm apatite cap varied from 6 to 47 yrs and 574 to 5800 yrs, respectively, considering only diffusion *(50)*.

2.17. Organoclay for Metal Contaminated Sediment Remediation

OC has been used to minimize non-polar contaminant transport, such as oil, chlorinated hydrocarbons and PAHs *(160-161)*. For example, Knox et al. *(50)* simulated the time required for some PAHs to breakthrough a 2.5 cm layer of a variety of active capping materials and they found that two types of OC were the most sorptive materials for the PAHs tested. Time for phenanthrene, pyrene and benzo[a]pyrene breakthrough a 2.5 cm OC was higher than 600 yr for those two OC tested for diffusion only. However, the type of organoclay selected is very

important as they also observed a time as low as 5 yr for phenanthrene breakthrough for a different tested organoclay. One other study suggested that long-chain OCs are probably superior to short-chain ones for sorption of highly hydrophobic compounds, while short-chain OCs may be better sorbents for slightly hydrophobic non-ionic organic materials *(162)*. Particle diameter and thus surface area and hydraulic conductivity are important parameters when evaluating OC efficiency *(15, 163)*. The degree of clay modification (affecting its cation exchange capacity - CEC) and organic carbon content of the OC strongly affect its adsorption capacity *(163-164)*.

Several studies provide clear data demonstrating the ability of OC to minimize metal contaminant transport *(15, 50)*, as clay can be modified to increase its efficiency to remove metal contaminants. A key parameter indicating the ability of clay to remove contaminants through ion exchange is the CEC. Ions, such as Na and Ca, can be exchanged for cations like Pb, Hg and Cd *(85)*. Clay is made up of layered silicates of very fine particle size. The clay structure allows isomorphous substitution in the lattice by smaller and/or lower valent ions. For example, sites normally occupied by Al^{3+} can be substituted by Cr^{3+}. Therefore, ion exchange may result in immobilizing the metal. Depending on the clay layer structure, the clay may be more prone to swell and thus the interlayer cation can undergo exchange with cations from external solutions. The smectite group is a particularly promising group to use in metal and organic sequestration. Clay minerals that have properties mainly governed by smectites are known as bentonites, where the montmorillonite smectite sub-group is the major constituent. This kind of clay usually presents the highest CEC. Additionally, this kind of clay facilitates insertion of large cationic species into the lattice (e.g. quaternary ammonium cations), which act as pillars, propping apart the clay layers and creating a micropore system increasing its surface area *(165)*. Adsorption also contributes to immobilization of the metal. Adsorption usually results in rapid removal of the

adsorbate followed by a much slower uptake until the equilibrium is reached *(166)*. The modification of this clay group is very often applied envisioning to improve adsorption.

Care should be taken with clay modification. When clay is modified to increase its capacity to adsorb a certain group of contaminants, undesired environmental impact may occur, including changes in pH and potential leaching of organo-modifiers to the water. For example, an OC with high efficiency to adsorb metals when left in contact for one week with a metal solution prepared with de-ionized water increased the solution pH from 3 to 12 (samples were prepared with 200 mg of sorbent and 15 ml of metal solution) . However, this behavior is likely not representative of the behavior of this OC in the field. For example, when the same experiment was repeated with a metal solution prepared with salt water, the pH only changed from 7.2 to 7.6 *(50)*. Further, the liquid to solid ratio was not representative of the ratio found in a thin-layer amendment. Finally, the deionized water used in the study is clearly not representative of in situ porewater, which would present greater buffering capacity than the tested de-ionized water solution. Despite these concerns, it is important to perform experiments with amendments to check if they would not cause substantial changes in pH, which could affect metal speciation and other un-desirable effects.

Kaufhold et al. *(167)* tested 38 bentonite suspensions with respect to the pH of 2% w/w suspensions with de-ionized water and they observed changes in pH from 6 to a maximum of 10 depending on the sample. The authors mentioned this behavior was only observed if excess salts were removed from the system. They concluded that the pH of the samples was influenced by calcite dissolution, with calcite providing substantial alkalinity, and by Na^+, with pH increase caused by increasing exchangeable Na^+. Hydrolysis of montmorillonite (Na^+ exchanged for H^+

of water) helps to explain the results. Ca^{2+}- and Na^{+}-bentonites behaved differently, with Ca^{2+}-bentonites showing less increase in pH.

Gupta and Bhattacharyya *(168)* obtained the CEC for kaolinite and montmorillonite as 13 and 153 meq/100g, respectively. The authors observed that montmorillonite adsorbs much more Cd(II), Pb(II) and Ni(II) than kaolinite. Another important conclusion was the increase in adsorption for those metals with pH increase (until the metal ions precipitated out as metal hydroxides). The authors explained this finding mainly as a result of competition between the metal ions and H_3O^{+} ions for adsorption on clay surface. At lower pH, there is much more H_3O^{+} ions than metal ions and the clay surface is mostly covered with H_3O^{+} ions. They also observed a decrease in amount of metal ion adsorbed per unit mass of clay with high clay loading, which is probably due to particle aggregation, decreasing the total surface area, and due to reduction of adsorption sites per unit mass of adsorbent. At high metal ion loading, the increase of metal ions adsorbed per unit mass of clay increased in the experiment with the increase of metal ion concentration in the adsorbate solution limited by adsorption sites and competition for them *(168)*. OCs also perform very well for non-aqueous phase liquids (NAPLs); low permeability may be one of the factors that enhances its performance *(169)*.

Knox et al. *(50)* observed that one of the OC they tested or a mixture of the same OC mixed with one of the rock phosphates they tested (among three types of OCs, two types of rock phosphates, biological apatite, calcium phytate, two types of zeolite and a biopolymer) would be the most suitable treatment for a wide range of metal contaminants. Quantifying how strongly these metals may bind to active materials is also very important to guarantee they will not be remobilized and released back to the water. In the same study, they observed Cr, Cu, Pb and Zn were highly retained to all the amendments tested, with one of the tested OC, the biopolymer and

the mixture of OC and rock phosphate presenting the best performances. Arsenic was retained by more than 50% for only one of the OCs tested. Clearly there are substantial differences in performance between OCs. For example, K_d values varied from 1 to 33,864 for As and from 440 to 207,270 mL g^{-1} depending on the OC type used in the experiment. The authors did not find such wide variation for different types of apatite, with the highest variation for Cr (172 - 19,278 ml g^{-1}) and the lowest for Zn (1,784 - 2,157 ml g^{-1}).

2.18. Activated Carbon (AC) for Metal Contaminated Sediment Remediation

AC may be found in a wide range of particle sizes (from <325 mesh (45 μm) to 4x6 mesh (4.75-3.35 mm), pore size distribution and internal micro-porosity structure. The American Society for Testing and Materials (ASTM D5158) classifies powdered activated carbon as AC in particle sizes predominantly smaller than an 80 mesh sieve (0.177 mm) *(170)* while GAC is defined as a minimum of 90 % of the sample weight being retained on a 80 mesh sieve *(171)*. Activation modifies the pore structure, forming mesopores and micropores yielding surface areas ranging from 500 to 2000 m^2 g^{-1} *(172-174)*.

AC can be produced from a variety of raw materials. Norit Americas, Atlanta, GA, produces a GAC by steam activation of lignite coal and washes it with acid. They also produce a GAC by a phosphoric acid process of coal. Wilson et al. *(174)* used peanut shells to produce activated carbon. They milled peanut shells to a 10x20 mesh (2.0-0.85mm) US sieve particle size, mixed it with molasses and placed the mixture under 5,000 psi for 30 min. The resultant block was placed in a furnace at 800° C for 2 hr with N_2 flowing into the sealed retort. Water was also pumped into the gas flow line. After the block was cooled overnight under N_2, it was crushed and placed back into the furnace (300° C for 4hr under compressed air). Once cooled again, the crushed material was washed with HCl to remove surface ash and then washed with distilled water and

dried at 110° C overnight. The authors indicated that changing the steam activation time makes possible to increase adsorption capacity. AC thus can be produced by crushing a high-carbon material, such as coal, wood and coconut shells, and then roasting it to make charcoal. When a second roasting is performed in the presence of steam, a highly porous material is produced, providing AC high surface area. In general, larger surface area results in more sites available for contaminant sorption *(175)*. The sorption mechanism that usually occurs for hydrophobic organic contaminants is sorption into the inner surface of pores. However, the mechanism for metals is more complex as ionic charges affect removal of the metal from solution *(172)*.

AC can be modified to better remove different kinds of contaminants with presence of different surface functional groups *(176)*. For example, Ahn et al. *(177)* modified an AC with anionic surfactants to increase its capacity to adsorb cations. The researchers observed AC can remove metal contaminants predominantly due to surface complex formation between the species and the surface functional groups by electrostatic attraction of metal ions to mainly surface oxygen-containing functional groups such as carbonyl groups. This functional group seems to be the main responsible for metal adsorption as alkaline-earth metal cations can be integrated with these groups to form complexes. In general modification by acidic treatment enhances chelation with metals while basic treatment enhances uptake of organics *(172, 176)*. Additionally, pretreatment of carbon with Cu(II), for example, has been proven to enhance As removal by formation of insoluble metal arsenates with the Cu impregnated in the carbon and also by As adsorbed into carbon independently *(178)*.

Several studies have shown that GAC, coke and/or OCs can sequester hydrophobic organic compounds (HOC), retarding transport through the cap layer and potentially decreasing HOC bioavailability *(14, 164, 179-180)*. According to McDonough et al. *(181)*, AC has a high PCB

adsorption capacity. The authors also emphasized the AC properties are an important factor affecting its performance and further research should be done to enhance PCB adsorption. Murphy et al. *(14)* reported that a thin layer of GAC can provide 1000 yr of isolation time for 2,4,5-polychlorinated biphenyl, even under moderate porewater seepage, while coke provides a few decades. According to the authors, the groundwater seepage substantially affects cap performance and thus site specific characteristics are very important to correctly predict cap performance. Coke has a poor performance as a sorbent when compared to other sorbents, which may be due to low specific surface area and slow kinetics of contaminants into the coke particles *(182-183)*. Experiments have shown that its sorptive capacity is similar to moderate organic carbon sediments *(14, 139)*. Zimmerman et al. *(182)* observed 77% and 83% reduction of PCB and PAH uptake by semi-permeable membrane devices for sediment treated with 3.4 % wt AC. Millward et al. *(183)* observed that after one month of sediment contact with AC, PCB bioaccumulation in a polychaete (class of annelid worms) was reduced by 82% (and by 87% after 6 months of contact).

Even though GAC is known for its efficiency as sorbent for organic contaminants, there are relatively few studies analyzing its efficiency for remediation of metal contaminated sediments. This is important because typically organic contaminated sediments are also co-contaminated with metals, and the efficacy of GAC for metals should be investigated. There are some studies applying AC for metal contaminant removal from water and wastewater. Researchers tested AC (particle size 250 – 500 μm) prepared from coirpith (an agricultural solid waste, which constitutes as much as 70% of the coconut husk) for Cd(II) and Hg(II) adsorption. The adsorption capacity was 93.4 mg Cd(II) g^{-1} and 154 mg Hg(II) g^{-1} at pH 5. The tested AC had a Cd(II) removal of 98 and 85% for Cd(II) concentrations of 20 and 40 mg L^{-1} at pH 4. They

observed that efficiency of Cd(II) removal decreased with Cd(II) concentration increase due to adsorption involving first higher energy sites. Once those become saturated adsorption occurs on lower energy sites *(184-185)*. AC from coconut and palm shells was modified and considered efficient to remove Cd and Pb from a solution containing 20 mg L^{-1} of each metal. Efficiency of removal was above 99.5% *(186)* Aggarwal et al. *(187)* modified AC with nitric acid, ammonium persulfate, hydrogen peroxide and oxygen gas. They observed that the presence of acidic carbon-oxygen surface groups enhanced the adsorption of Cr(III) cations and decreased Cr(VI) adsorption. Elimination of these groups resulted in the opposite behavior. Studies showing AC efficiency for metal removal from sediments are needed, but clearly the kind of AC applied is key to enhance metal contaminant removal.

It is also important to consider that very fine particle materials, such as powdered activated carbon (PAC), with a typical diameter of 75-300 μm, should be applied in core mats due to the PAC low bulk density and ease of re-suspension and transport. These kind of materials can become an environmental concern as they could be transported long distances carrying with them a high amount of contaminants that will be sorbed on them *(188)*. Sorbent-filled geotextiles can be used to place these sorbents as sediment caps *(141)*.

2.19. Hydraulic Barriers for Metal Contaminated Sediment Remediation

Low hydraulic conductivity seems to considerably contribute to active capping material performance due to minimization of contaminant mobility for sites with advection *(15)*. In the absence of advection (i.e. sites with diffusion only), these types of barriers have no additional benefit. Clays usually present high binding capacity to organic contaminants, however their high degree of cohesiveness and low aqueous permeability are characteristics that contribute to their capacity to immobilize a variety of contaminants under advection, and minimize bioturbation and erosion impact in the material as well.

AquaBlok™ is an example of hydraulic barrier that has been applied in active capping *(10)*. It is formed of bentonite clay with polymer additives covering a small aggregate core. The polymer is used to promote adhesion between the clay and the aggregate core. It can be modified with reagents to enhance its contaminant sequestration capacity or it can incorporate plant seeds to promote vegetation habitat establishment *(142)*. The hydrated material has a very low hydraulic conductivity (on the order of 10^{-9} cm s^{-1}), and thus upon swelling it forms a continuous hydraulic barrier, reducing contaminant breakthrough to the water column.

A potential major drawback in using cap materials with very low hydraulic conductivity may be the accumulation of gas beneath the cap, resulting in cap failure with release of gas bubbles and contaminant transport to the water column due to gas ebullition. This effect should be considered in the cap design *(10)* and its importance has been demonstrated in the field. For example, inclinometers placed on the top of the ~10 cm (11.25±5.0 cm) Aquablok™ layer installed in the Anacostia River active capping project, Washington, D.C., indicated cap vertical uplift with time with rapid deflection from time to time. The outboard end of the inclinometer was also subjected to uplift and rapid deflection. The researchers involved in the project attributed this behavior to rapid releases of gases that accumulated under the cap *(10)*.

2.20. Sand for Metal Contaminated Sediment Remediation

Passive capping consists of covering the contaminated sediment with a clean inert material, such as clean sand or sediment layer. Sand caps are efficient to minimize the release of many contaminants to the water column when contaminants are strongly sorbed to the sediment solid phase and/or diffusion is the main mechanism of transport. However, under advective transport, passive caps are usually not efficient *(10, 15, 159)*. As passive capping contributes mostly as a physical barrier than as a chemical one, very thick caps are usually needed to minimize contaminant transport. Caps varying from 30 cm up to 1.5 m cm have been applied in the field

(11, 144, 148, 189). Additionally, gas bubbles produced in sediments with a high content of OM may easily open preferential paths in sand caps, frequently releasing contaminants to the water column. NAPL may migrate due to disturbance during capping placement and/or gas ebullition *(169)*.

In a study by Zimmerman et al. *(182)* performed for five months, sand was efficient to reduce PCB flux only by 23% compared to untreated sediment. The experiment was performed in 250 ml beakers filled with 20 g of wet sediment, 2g of sand or untreated sediment placed on top of the sediment and the beakers were filled to 200 ml with 17 ppt seawater with 1 g L^{-1} sodium azide. Sand also would not be efficient to remove metal contaminants under advection conditions, as sorption of metals on sand is near zero *(50)*.

2.21. Other Potential Active Capping Materials for Metal Remediation

In addition to coke and phytate that were previously discussed in this chapter, other potential materials that have been tested or proposed for active capping are zeolite and biopolymers. Natural zeolites are crystalline hydrated alumino-silicates of alkali and alkaline earth metals. They are able to sorb cationic contaminants due to their high CEC as well as demobilize non-polar organic pollutants and anionic contaminants by surface modification with cationic surfactants. This treatment modifies only the external surface, which becomes neutral or even positively charged, while the internal cage and tunnel structure remains an active cation exchanger *(190)*. A study from Knox et al. *(50)* showed that zeolites can effectively remove Cd, Cr, Co, Cu, Pb and Zn in freshwater; however its efficiency in salt water was smaller maybe due to sorption of Na^+ occupying partially its internal pores. In addition, anionic metals, like Cr(VI) as $Cr_2O_7^{2-}$ or as CrO_4^{2-} or As as AsO_3^{3-} or as AsO_4^{3-}, would largely be unaffected by the use of zeolites.

Biopolymers are also materials that could be used in active capping as they may contain multiple reactive sites with potential for chemical interaction with other compounds. They can effectively sequester Cd, Co, Cu, Ni, Pb and Zn in fresh and salt water, although they are not effective for As and Se *(50)*. Other study also pointed the capacity of naturally occurring polymers from seafood processing waste (such as chitin and chitosan) to bind with Cu, Cr, Cd and Pb *(191)*. Chitin is the second most prevalent biopolymer on earth after cellulose and it has been used as an amendment for groundwater remediation as an electron donor to drive reductive dechlorination. Wang et al. *(192)* chemically modified biopolymers (lignin, chitin and cellulose) to increase their organic sorption capacity. Mixture of biopolymers with other cap materials could enhance the cap ability to remove a wide range of contaminants.

Srivastava *(193)* tested hollow fiber polymeric membranes for remediation of PAH contaminated sediment. The membranes supplied the necessary electron acceptors controlling the redox potential and enhancing biodegradation and chemical binding of PAH to OM. Diffusion governed the transport of electron acceptors in the membrane assembly inside a geotextile fiber to the sediment transporting electron acceptors from the water column to the sediment.

2.22. Transport of Contaminants through Cap Materials

Physical and chemical isolation should be considered in the cap design. Transport of contaminants may occur through diffusion, advection and gas ebullition. Sediment composition and cap parameters need to be considered when estimating the contaminant flux to the water column by these processes. Sediment consolidation during initial placement may also account for contaminant transport to the water column. If substantial gas ebullition occurs at the site, it is necessary to adopt a system to capture and properly release the gas to the atmosphere,

guarantying cap integrity and minimizing ebullition-facilitated contaminant transport to the water column.

Physical isolation thickness should account for bioturbation, for cap erosion and for cap construction technique, which affects cap consolidation and stability. An armor layer is usually applied on the top of a cap to protect it against erosion due to hydraulic and environmental forces. Additionally, if cap material is placed in bulk instead of in reactive mats, operational technique will affect cap thickness and this should be considered.

Site characterization and implementation of source control prior to cap installation are fundamental to design the cap and to avoid cap contamination from the top to the bottom. Post-capping monitoring should verify if erosion has been a problem in the site, if there is contaminant flux into the cap material and into the water surface and if re-colonization is occurring as specified in the design *(127)*.

These processes involved in the chemical and physical isolation of contaminated sediments are described in more detail below.

2.22.1. Pre and Post-Capping Monitoring

Pre and post-capping monitoring is very important to assess cap efficiency. Pre-capping monitoring is necessary to correctly design the cap, to assess cap viability and to help evaluate capping efficiency after the cap is placed. It is necessary to know which contaminants are present and their concentration to correctly choose the cap material and its thickness. OM content and gas ebullition rates help to decide if a gas control system should be adopted and to evaluate how impermeable the cap material can be. Site characterization is also necessary to evaluate the best cap placement method as hydrodynamic stability is important when placing a cap. Evaluation if there is advective flux is necessary to correctly design the cap and armoring against river flow,

wave action, propeller wash forces and ice scour may be necessary. Control of contaminant sources should be implemented as contaminated sediment deposition may lead to cap contamination from the top to the bottom. A guidance for in-situ capping has been elaborated by the USEPA *(189)*.

Post-capping monitoring should verify if erosion has been a problem in the site, if there is contaminant flux into the cap material and into the water surface, and if re-colonization is occurring as specified in the design *(127)*. If levels of contaminants above-cap increase, care should be taken to evaluate if this was due to new contaminated sediment deposited on the top of the cap. However, continuous deposition of clean sediment above the cap is a good finding as it contributes to natural recovery and to contaminant isolation from the water column. Cap maintenance should be performed to guarantee long-term integrity of the cap.

In the Anacostia River project, the cap was placed by conventional clamshell controlled from the crane barge through the Offshore Positioning Software (WinOPS) system that tracked each bucket placed. Monitoring after cap placement through more than 50 cores allowed calculation of average and standard deviation of actual cap thickness implemented in the field (Table 2.13).

Table 2.13. Target and observed cap thickness[a]

Cap	Target thickness (cm)	Observed thickness ± σ (cm)
Sand	30	(22.3±8.0)
Aquablok™ / sand	10 / 15	(11.3±5.0) / (13.3±4.5)
Apatite / sand	15 / 15	(12.3±3.0) / (11.3±3.0)
Coke / sand	2.5 / 15	2.5 (mat) / -

[a] Source: *(10)*

Long-term active capping monitoring data is not available yet as this is a relatively recent developed technology. However, modeling studies have been performed demonstrating long-

term active capping efficacy to minimize the release of a wide range of contaminants to the water column *(14-15, 159)*.

2.22.2. Molecular Diffusion

Diffusion occurs due to differences in concentration of a compound in space through the cap material to the water column. The diffusive transport rate may increase or decrease depending on the molecular weight and structure of the compound. In general, the smaller the molecular weight and more compact its molecular dimensions, the faster its rate of diffusion. Diffusion happens through random motions of dissolved molecules, ions, or suspended particles of the containing phase and through thermal kinetic energy of the solute in response to concentration gradients as most successfully described in a mechanistic theory by Fick *(47)*. Fick's first law relates the diffusion mass flux J_{diff} to the concentration gradient. In one spatial dimension x:

$$J_{diff} = -D\frac{\partial C}{\partial x} \tag{2.17}$$

Where D is the diffusion coefficient [L^2T^{-1}].

Fick's second law is the mass conservation equation for a fluid phase and states how diffusion causes the concentration C to change with time t. In one spatial dimension x:

$$\frac{\partial C}{\partial t} = D\frac{\partial^2 C}{\partial x^2} \tag{2.18}$$

Eq. 2.18 can be solved considering a system where mass is introduced in a uniform vertical sediment column maintaining a constant concentration at x=0 and diffusion occurring with time t into the domain x>0 under initial and boundary conditions given by c(x,0)=c(∞,t)=0, c(0,t)=C_0 *(194)*:

$$\frac{C}{C_0} = erfc\left(\frac{x}{\sqrt{4D_{obs}t}}\right) \tag{2.19}$$

Where D_{obs} is the observed diffusion coefficient. D_{obs} is calculated considering the effective diffusion coefficient D_{eff} and the contaminant retardation factor (R), which represents how much slower the chemical species migrates in comparison to water. Most chemicals move slower than water because of sorption mechanisms on the soil/sediment matrix:

$$D_{obs} = \frac{D_{eff}}{R} \tag{2.20}$$

The effective diffusion coefficient D_{eff} is smaller than the molecular diffusion coefficient D_{mol} because the chemical species moves along a tortuous path through the pore space. Thus, D_{mol} should be corrected for tortuosity τ, which is related to the effective porosity φ_e (unitless). While porosity is the total volume of voids per bulk volume, the φ_e is calculated by the relation of the total volume of voids that can become filled with water (or other fluids) able to migrate under an induced hydraulic gradient per bulk volume. Hence, the φ_e considers only the water in interconnected pore space that is able to migrate at an appreciable rate because some of the water might be isolated, adsorbed or held in "dead-end" pores *(194)*.

$$D_{eff} = D_{mol} * \ \tau, where\ \tau = \varphi_e{}^{4/3} \tag{2.21}$$

The factor R is related to the contaminant partitioning coefficient K_d [L^3 M^{-1}], dry bulk density ρ [M L^{-3}] and φ_e by the following relation (eq. 2.18) *(194)*:

$$R = 1 + K_d \frac{\rho}{\varphi_e} \tag{2.22}$$

Substituting equations 2.20, 2.21 and 2.22 in equation 2.19, we obtain:

$$\frac{C}{C_o} = erfc\left(\frac{x}{2\sqrt{D_{mol}\varphi_e^{7/3}}}\frac{\sqrt{\varphi_e + \rho K_d}}{\sqrt{t}}\right) \quad (2.23)$$

2.22.3. Advection and Groundwater Flow

Advection occurs through bulk water phase mass transport in response to a gradient in total head with the chemical being carried along with the bulk fluid movement *(47)*. For one spatial dimension flow, the general formulation below can be used: *(194)*

$$\frac{\partial C}{\partial t} + v\frac{\partial C}{\partial x} = D\frac{\partial^2 C}{\partial x^2} \quad (2.24)$$

Where: v is the porewater chemical velocity and D is the combined mechanical dispersion and diffusion coefficient. Site characteristics, such as hydraulic gradient d_h/d_x [L L^{-1}] and hydraulic conductivity k_h [L T^{-1}], are important parameters affecting the porewater chemical velocity v, which is corrected to R (eq 2.22).

$$v = \frac{K_h\frac{d_h}{d_x}}{R\varphi_e} \quad (2.25)$$

Considering a system where mass is introduced in a uniform vertical sediment column with inlet boundary condition c(0,t)=C_0 *(194)*:

$$\frac{c}{c_o} = \frac{1}{2}\left(erfc\left(\frac{x-\upsilon t}{\sqrt{4D_{obs}t}}\right) + \exp\left(\frac{x\upsilon}{D_{obs}}\right)erfc\left(\frac{x+\upsilon t}{\sqrt{4D_{obs}t}}\right)\right) \quad (2.26)$$

Substituting equations 2.20, 2.21 and 2.22 in equation 2.26, we obtain:

$$\frac{C}{C_o} = \frac{1}{2}\left(erfc\left(\frac{x\sqrt{(\varphi_e + \rho K_d)}}{2\sqrt{D_{mol}\varphi_e^{7/3}}\sqrt{t}} - \frac{k_h}{\sqrt{(\varphi_e + \rho K_d)}} \frac{d_h/d_x}{2\sqrt{D_{mol}\varphi_e^{7/3}}}\sqrt{t} \right) + \ldots \right. \quad (2.27)$$

$$\left. \exp\left(\frac{x k_h (d_h/d_x)}{D_{mol}\varphi_e^{7/3}} \right) erfc\left(\frac{x\sqrt{(\varphi_e + \rho K_d)}}{2\sqrt{D_{mol}\varphi_e^{7/3}}\sqrt{t}} + \frac{k_h}{\sqrt{(\varphi_e + \rho K_d)}} \frac{d_h/d_x}{2\sqrt{D_{mol}\varphi_e^{7/3}}}\sqrt{t} \right) \right)$$

2.22.4. Gas Ebullition

Gas ebullition due to methanogenic and, potentially, denitrifying activity in sediments is one of the critical processes in sediments because bubbles are hydrophobic and tend to accumulate hydrophobic contaminants and colloids on their surface. This may possibly result in larger contaminant fluxes to the overlying water column than would occur due to even high porewater velocity advective flow. Gas bubble migration may not only release contaminants to the water column and atmosphere *(195)*, but may also cause cap damage and even rupture the cap, particularly in unconsolidated surface layers *(196)*, providing additional pathways for contaminant release.

Methane and carbon dioxide are end products of the degradation of OM under methanogenic conditions. In the complex process of OM degradation, fermenters degrade the more complex OM producing monosaccharides, fatty acids/alcohols and hydrogen. Syntrophic bacteria consume those fatty acids and alcohols producing acetate, carbon dioxide and hydrogen that may be consumed by homoacetogens to produce acetate, and also by hydrogenotrophic methanogens to produce methane. Homoacetogens degrade monosaccharides producing acetate, which can then be converted to methane and carbon dioxide by acetoclastic methanogens (Figure 2.7) *(197)*.

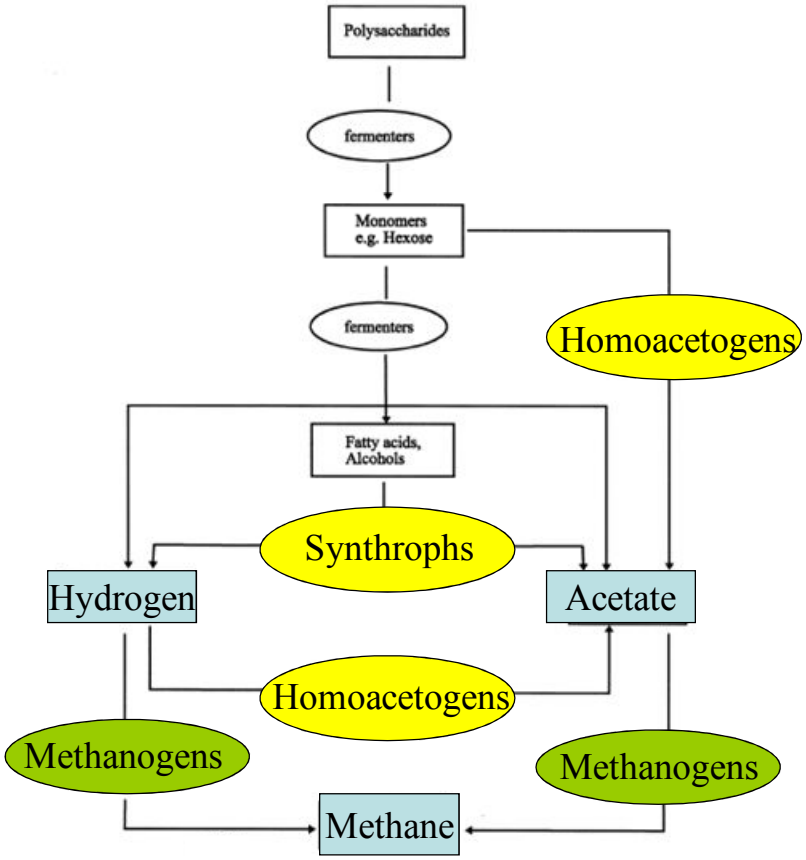

Figure 2.7. Organic matter degradation under methanogenic conditions.

The microbial community structure (and thus the volume and type of gas produced) is strongly affected by temperature changes. Hydrogenotrophic methanogens are stimulated by increased temperature to a greater extent than are acetoclastic methanogens *(198)*. Hydrogenotrophs produce only methane, consuming carbon dioxide and hydrogen, while acetoclasts produce methane and carbon dioxide as shown in equations 2.28 and 2.29.

Hydrogenotrophic methanogenesis

$$CO_2 + 4H_2 \rightarrow CH_4 + 2H_2O \qquad \Delta G_0 = \text{-131 kJ/mol} \tag{2.28}$$

Acetoclastic methanogenesis

$$CH_3COO^- + H^+ \rightarrow CH_4 + CO_2 \qquad \Delta G_0 = \text{-76 kJ/mol} \tag{2.29}$$

Widely varying gas production fluxes have been reported in the field. Tanner et al.*(199)* observed methane fluxes varying from 0.07 to 0.67 L m^{-2} d^{-1} for a wetlands used to treat wastewater. Sovik et al.*(200)* measured gas production in ten constructed wetlands with fluxes of methane and carbon dioxide up to 53 and 47 L m^{-2} d^{-1}, respectively. Ostrovski et al.*(201)* reported a flux of 0.23 L m^{-2} d^{-1} from hypolimnetic sediments,*(201)* and Hughes et al.*(202)* observed gas production fluxes of 2.7 L m^{-2} d^{-1} on a laboratory study with sediment from the Anacostia River, Washington, DC.

Knowing the composition of gas produced is also important as three of the most important greenhouse gases worldwide may be produced through methanogenic and denitrification activity. Carbon dioxide and methane are the common products of methanogenic degradation, but N_2O can also be produced as an intermediate of the denitrification process. Stadmark and Leonardson *(203)* have shown that seasonal variation in the emission of greenhouse gases occur due to changing temperature and to varying composition and bioavailability of organic bacterial substrates in aquatic sediments. Huttunen et al. *(204)* observed bubble gas content of CH_4 and CO_2 equal to 48-67% and 0.01-1.1%, respectively, while Casper et al. *(205)* observed mean gas content of CH_4, CO_2 and N_2 equal to 66, 3 and 36%, respectively. Both studies were performed *in situ* with lake sediment.

Gas ebullition-facilitated transport of contaminants in caps has yet to be fully investigated. It is known that methanogenic OM degradation facilitates contaminant transport through caps and

gas accumulation may cause cap damage *(195)*, but studies quantifying ebullition-facilitated transport of contaminants to the water column and research on methods to properly collect gas in the field to protect cap are scarce.

Yuan et al. *(3)* found that significant amounts of both solid particulate matter and contaminant can be transported from the sediment to the water column by gas movement. The authors observed that the amount of contaminant and solid particulate transported is related to the volume of gas released. Hulls and Costello *(206)* observed in their bench tests with sediment from Stryker Bay, Duluth Minnesota, that PAH are transported to the water column due to groundwater advection and gas ebullition. The authors concluded that a sand cap can be effective to minimize contaminant release and to prevent gas from forming due to sediment insulation. Fendinger et al. *(20)* noted that sediment contaminant transport may be a function of gas ebullition rates, Henry's law constant and porewater contaminant concentration. According to the researchers, organic contaminant partitioning occurs mainly between sediment gas and porewater, which is determined by gas/water partition coefficients of each compound in the sediment porewater. The process of organic contaminant partition between sediment solid material and gas bubbles is probably negligible due to the high liquid water content of many sediments.

2.22.5. Bioturbation

Bioturbation is related to the disturbance and mixing of sediment particles or porewater due to processes associated with benthic animals. Movement of contaminants due to benthic animals occurs by ingestion of contaminants at depth and defecation at the surface, by irrigation of burrows, by increasing the surface area of sediments exposed to the water, etc. *(207)*

Active sediment and cap mixing by benthic organisms due to biological activity usually occurs in the top 5 – 10 cm layer, but can occur at depths reaching 1 m by benthic animals such as ghost shrimp *(123)*. Thus a key design parameter is the cap thickness necessary for preventing bioturbation effects as benthic organisms may redistribute pollutants by bringing sediment contaminants from beneath the cap to the surface *(7, 208)*.

The mix of the top contaminant layer by benthic organisms, such as tube-dwelling amphipods and polychaetes, results in higher contaminant release than diffusion through the porewater *(209)* as it may cause sediment particle re-suspension and change metal speciation through actively irrigating the sediments with oxygen-rich overlying water. Over long re-suspension periods, AVS decreases mostly due to oxidation of iron monosulfides and a significant fraction of metal sulfides may become bioavailable *(210)*.

Reible and others have developed a model of contaminant migration by bioturbation *(211)*. Bioturbation-facilitated contaminant transport from sediment is rapid due to bioturbation of particle-bound contaminants through the upper 10 cm of the sediment bed to the interface and rapid chemical desorption at the sediment-water interface followed by contaminant transport through the benthic boundary to the water column *(212)*. Thus, the chemical migration rate within the bioturbation zone is usually much faster.

Factors affecting depth of bioturbation (L_{bio}, cm) are capping material, cap compaction, and type, size and density of organisms populating the cap. Due to difficulties to correctly estimate these factors, a conservative depth equal to the deepest penetrating organism present in the site is chosen. L_{bio} affects the bioturbation mass transfer coefficient K_{bio} (cm d^{-1}) by the following relation:

$$K_{bio} = \frac{dD_{bio}R}{L_{bio}} \quad (2.30)$$

Where d is the desorption efficiency of contaminant from sediment particles (unitless); D_{bio} is the biodiffusion coefficient ($cm^2\ d^{-1}$) and R is the retardation factor. Biodiffusion is related to the diffusion of materials through the sediment column due to biological activity According to Reible *(213)*, general values for L_{bio} can be set as 10 cm and D_{bio} as 10 $cm^2\ yr^{-1}$. However, Palermo and others *(207)* suggested that 30 cm should be adopted as L_{bio} due to different stages of cap colonization: early colonizers are represented mainly by small-bodied polychaetes and mollusks, mixing mostly surficial sediments, while later colonizers (after several months or 1-2 years) are represented by deeper penetrating organisms, reaching depths around 30 cm. D_{bio} values varying from 23 to 50 $cm^2\ d^{-1}$ were suggested by Wheatcroft and Martin *(214)* in the upper 10 cm of Palos Verdes Shelf sediment, with exponentially decreasing D_{bio} values below 10 cm.

K_{bio} should be accounted for when estimating the overall mass transfer coefficient and thus to estimate the overall cap thickness. However, for simplification purposes, a cap thickness is usually added to the chemical isolation thickness to account for the depth of bioturbation and thus this thickness is assumed to pose no resistance to mass transfer between the sediment layer and the water phase. In this case, K_{bio} would be considered negligible *(213)* when calculating the cap thickness to account for contaminant flux to the overlying water. Table 2.14 shows a summary of recommended cap thickness to account for the cap bioturbation component.

Table 2.14. Recommended cap thickness for the bioturbation component of cap thickness[a]

Environment	Cap material	L_{bio} for surficial zone of sediment mixing (cm)	L_{bio} for mid-depth zone of mixing (cm)	Total bioturbation thickness (cm)
Coastal/marine	sand	10	10 - 35	20 - 45
	silt/clay	10 – 15	10 - 45	20 - 60
Freshwater	sand	10	10 - 20	20 - 30
	silt/clay	10	10 - 30	20 - 40

[a] Source: *(215)*

2.22.6. Cap and Sediment Consolidation

The cap weight generates an initial excess pore pressure in the sediments, which produces a transient advective flux of contaminant that substantially impacts the overall flux *(216)*. Alshwabkeh et al. *(216)* developed a model that accounts for the effect of consolidation and excess pore pressure dissipation on transient nonlinear advective transport through sediment and the cap. There is also a module called Primary Consolidation, Secondary Compression and Desiccation of Dredged Fill (PSDDF) of the Automated Dredging and Disposal Alternatives Modeling System (ADDAMS) *(217-218)* that can be used to predict consolidation of the sediment underlying a cap, even though it was proposed for consolidation in thick deposits of fine-grained material.

Soil mechanics properties will dictate the excess pore pressure dissipation and consolidation process. Prior to cap placement, the total compression of native in-place sediments under a specific load should be estimated to compute the compression caused by the volume decrease caused by squeezing of porewater from the sediments *(6)*. The Terzaghi's consolidation theory *(219)* can be used to estimate the average consolidation/settlement of the particular sediment. Standard methods for consolidation properties are available from ASTM *(220)*.

Sediment consolidation is an important parameter of contaminant flux from sediments in the first weeks after capping as contaminant transport is enhanced by porewater expelled from the

sediments. Contaminant breakthrough the cap may be accelerated up to 150 times compared to diffusion-only breakthrough *(216)*. Thus, it is pertinent to state that even a site usually only subjected to diffusive conditions will be subjected to advection due to sediment consolidation during and sometime after cap placement. Moo-Young and others *(218)* performed experiments (centrifuge tests) with a fluorescent dye tracer (Rhodamine WT) to simulate the effects of consolidation in capped sediments and they observed that consolidation-induced advective transport of contaminants is an important factor affecting contaminant transport through a cap and they suggested contaminant flux due to sediment consolidation should be considered on cap design.

Cap thickness should also account for cap consolidation. According to Horne Engineering Services *(221)*, a consolidation compensation thickness of up to 4 cm should be considered to account for consolidation of a 20 - 30 cm cap. This value will vary according to the cap material, cap thickness and cap construction method. According to the technique chosen to place the cap material, the resulting density and rate of application of capping material should be specified and some thickness should be added to account for cap consolidation.

Another relevant point is that after sediment/cap consolidation, cap and sediment will have a reduced porosity and permeability, which results in reduction in chemical migration rates by diffusion and advection *(213)*.

2.22.7. Armor layer

An armor layer is usually applied on the top of a cap to protect the cap against erosion due to hydraulic and environmental forces. Scouring of the cap may occur due to high flow velocities in the overlying water column during discharge events, for example. Mohan et al. *(6)* described the necessity to armor against river flow, wave action, propeller wash forces and ice scour. In cold

areas, frazil and anchor ice may contribute to sediment cap scouring *(222)*. The EPA Assessment and Remediation of Contaminated Sediments (ARCS) program developed a manual for design of capping armor layers *(189)*.

Palermo et al. *(207)* suggested that significant erosion occurs in a sand cap in water depths shallower than 40 m and that caps composed of silt and clay materials are more subjected to erosion.

A simple initial analysis through maximum and mean depth of scour (D_s) calculation could be performed to estimate scouring potential of a sand cap as a function of cap particle size using the following equations *(223)*:

$$D_{s,\max} = 6.5 D_{50}^{-0.115} \tag{2.31}$$

$$D_{s,mean} = 1.42 D_{50}^{-0.115} \tag{2.32}$$

Where D_{50} refers to the median diameter of the sand cap material. A water flow velocity varying from 1.2 to 2.3 m s^{-1} in 21 channels was used to obtain equations 2.31 and 2.32.

The critical velocity for initiation of particle suspension can be calculated from Van Rijn *(224)* (Figure 2.8). This graph allows estimation of the approximate critical vertically average velocity value for the initiation of sediment movement (u_{cr}) for a fixed D_{50} and water depth h. At these values, the particles will start to roll or move across the bottom in fairly regular jumps. The critical velocity for initiation of suspension ($u_{cr,s}$), where particles will leave the turbulent bottom boundary layer and be brought into suspension, is also defined. If the velocities are frequently above u_{cr}, then there is a potential for site erosion. There is a strong likelihood for severe erosion if the velocities frequently exceed $u_{cr,s}$. Bottom velocities above 0.3 m s^{-1} are often able to initiate erosion and the erosion rate is very sensitive to large currents, where the bed load transport increases as the 4^{th} power of the water velocity *(6, 225)*.

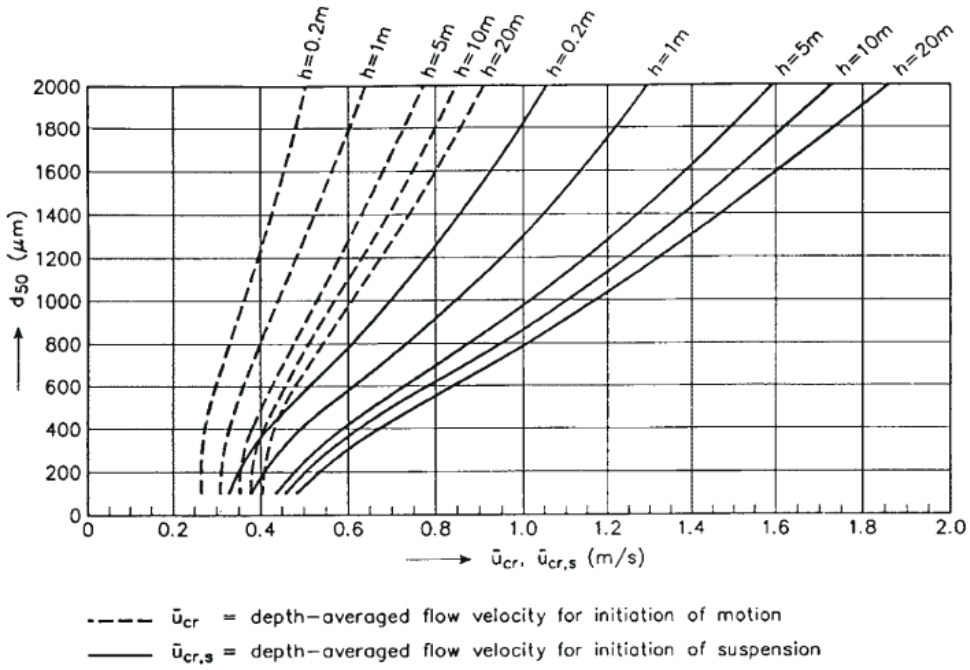

Figure 2.8. Critical vertically averaged velocities for a plane bed *(224)*.

2.23. Modeling Theory

For the purposes of my proposed research, I have decided to use a simplified model that accounts only for diffusion and advection because, although these are the most understood processes affecting contaminant fate in sediments, they have not been adequately investigated in capping systems. Thus my focus is not to evaluate bioturbation, cap consolidation and/or decay of contaminants; which should be focused on at a later time once sufficient understanding of the former is achieved. I have focused on comparing a broad range of cap materials and contaminants to indicate which cap works better under unified conditions for each contaminant. Models considering bioturbation, decay, volatilization and other processes can be found elsewhere *(226-227)*, and they usually require more parameters. Even though they are probably more precise, they require more site specific data, requiring a narrower focus. As example of other models, Dueri et al. *(226)* developed a model (TRANSCAP-ID) to simulate migration of

dissolved contaminants through a sediment cap. It includes diffusion, advection, dissolution of the chemical species and bio-irrigation. Another model, called RECOVERY and developed by USACE, considers dissolved and particulate flux through a deep sediment layer, followed by a mixed active sediment layer (which could be a cap as well), followed by the well mixed vertically water column. However, it is limited to organic contaminants. The processes considered in the model are sorption, decay, volatilization, burial, resuspension, settling, bioturbation, and porewater diffusion *(227)*.

The variability in model parameters obtained from the literature may require the use of a Monte Carlo method to evaluate how sensitive model results are to uncertainty in model parameters. The simulation result gives the full range of possible outcomes and the likelihood, or probability, of each outcome to be above or below a certain value. It is obtained by repeated calculations (such as 50,000 times) using randomly selected parameter values for each calculation *(228)*.

Monte Carlo methods rely on computational algorithms for sampling random draws of variables that share the same underlying probability distribution. Monte Carlo schemes have a broad range of applications. They are often used when simulating physical and mathematical systems, generating random numbers, numerical integration, searching for solutions for complex optimizations and specially for generating the distributions of random variables whose closed form solution seems to be mathematically intractable. Because of Monte Carlo reliance on repeated computation and random or pseudo-random numbers, Monte Carlo methods have become more popular as the speed of processing increases.

Each of the model parameters should follow a probability distribution function (PDF), which should reflect the range of value variation for the parameter and uncertainties related to specific

conditions at the site. Variability is related to heterogeneity of a well-characterized parameter. For example, OC may be found in different particle size ranges, which greatly affects its hydraulic conductivity values. Uncertainty is related with the lack of knowledge about factor and processes for that parameter. For example, metal K_d values are difficult to predict as site conditions are highly variable with time and affect metal solubility, which affects K_d.

In the next step, random values from the PDF for each input parameter (except the derivated and constant parameters) are generated, resulting in a set of values varying within some defined range for each input variable. These values are used to derive the final density function of the variable of interest.

Monte Carlo is especially useful for avoiding the daunting task of finding the analytical density function of final random variables constructed upon original input variables. Monte Carlo methods were used in chapter 3 to perform an analysis of previous research to specify the probability distribution of parameters such as hydraulic conductivity, porosity, density and distribution coefficient, which in turn were used to derive the final density of the ratio of C/C_o (which is defined by the breakthrough porewater concentration C of contaminant at the top of the cap at time t by the initial concentration of contaminant in the sediment porewater C_o). In summary, I used hydraulic conductivity, porosity, density and distribution coefficients based on the best available information on the distribution of such parameters. I then computed C/C_o for each previously simulated sample based on a known relationship of those parameters and C/C_o. The collection of final numerical values of C/C_o represents the estimation of the final distribution of C/C_o.

For a clarification of the general setup of our method, let *Y* be some variable of interest. Variable *Y* is associated with other variables $\{X_i\}_{i=1}^{I}$ by a known relation described by the function f , that is:

$$Y = f(X_1, \dots, X_I, \psi) \tag{2.33}$$

Where ψ are known fixed parameters. Previous works found in the literature provided a range of distribution functions for variables $\{X_i\}_{i=1}^{I}$, say (f_{Xi} : i = 1,…,I). Thus the numerical computation of the distribution of variable *Y* relies on the sampling of all variables $\{X_i\}_{i=1}^{I}$ according to the density functions (f_{Xi} : i = 1,…,I) and application of the formula 2.33. The resultant histogram of computed values of Y mimics the exact density function of variable *Y* based on the distribution of its former variables *X*. This process avoids the calculation of the analytical solution of the distribution of *Y*, which could, in principle, be obtained by the Jacobian method of change of variables. It is worth noting that by increasing the number of draws, the distribution of *Y* can be obtained as precisely as wanted.

CHAPTER III. MODELING ACTIVE CAPPING EFFICACY FOR METAL AND ORGANOMETAL CONTAMINATED SEDIMENT REMEDIATION

The following is a first-authored manuscript published in the *Environmental Science and Technology* Journal in 2008 *(15)*. I worked on this project with the fellow student Ke Yin from the Environmental Engineering Laboratory of Professor Rockne at the University of Illinois at Chicago. The research included modeling Cd, Cr, Pb, Ag, As, Ba, Hg, CH_3Hg and CN transport through sand, GAC, organoclay, shredded tires and apatite caps by deterministic and Monte Carlo methods. The University of Illinois graduate college guidelines allow the inclusion of first-authored publications in the body of the PhD dissertation.

3.1. Abstract

Cd, Cr, Pb, Ag, As, Ba, Hg, CH_3Hg and CN transport through sand, granular activated carbon (GAC), organoclay, shredded tires and apatite caps was modeled by deterministic and Monte Carlo methods. Time to 10% breakthrough, 30 and 100 yr cumulative release were metrics of effectiveness. Effective caps prevented above-cap concentrations from exceeding USEPA acute criteria at 100 yr assuming below-cap concentrations at solubility. Sand caps performed best under diffusion due to the greater diffusive path length. Apatite had the best advective performance for Cd, Cr and Pb. Organoclay performed best for Ag, As, Ba, CH_3Hg and CN. Organoclay and apatite were equally effective for Hg. Monte Carlo analysis was used to determine output sensitivity. Sand was effective under diffusion for Cr within the 50%

confidence interval (CI), for Cd and Pb (75% CI) and for As, Hg and CH_3Hg (95% CI). Under diffusion and advection, apatite was effective for Cd, Pb and Hg (75% CI) and organoclay for Hg and CH_3Hg (50% CI). GAC and shredded tires performed relatively poorly. Although no single cap is a panacea, apatite and organoclay have the broadest range of effectiveness. Cap performance is most sensitive to the partitioning coefficient and hydraulic conductivity, indicating the importance of accurate site-specific measurement for these parameters.

3.2. Introduction

The two most commonly used technologies to reduce exposure to sediment contaminants are capping and dredging with subsequent disposal *(5-7)*. Dredging can lead to re-suspension and re-mobilization of contaminants. In addition, the large amount of entrained water during dredging necessitates extensive dewatering periods, which may lead to release of volatile contaminants *(124)*. Conventional capping works as a physical barrier to isolate the contaminated sediments from the overlying water and minimize flux. Although caps are frequently cited as being more effective from a short term risk standpoint, they do not result in contaminant removal and they are limited to sites where water depth limitations are not an issue. Capped sediment can also represent a future risk if the confinement structure is compromised due to gas ebullition or cap scouring; or by excessive contaminant breakthrough due to diffusion or advection.

A relatively new alternative termed “active capping” replaces the thick cap with a thin layer modified to promote contaminant sequestration, enhanced retardation and/or chemical or biological degradation processes to increase efficacy. We classify here modifications as bioaugmentation (addition of benthic animals or microorganisms), biostimulation (addition of nutrients, electron acceptors or donors, or other agents to stimulate benthic organisms), contaminant sequestration (addition of granular activated carbon (GAC), apatite or other agents

to bind pollutants) and hydraulic sequestration (addition of water-expanding clay or other agents to decrease hydraulic conductivity) *(10, 14, 128-129)*.

Several studies have shown that GAC, coke and/or organoclays can sequester hydrophobic organic compounds (HOC), retarding transport through the cap layer and potentially decreasing HOC bioavailability *(14, 164, 179)*. Murphy et al. *(14)* reported that a thin layer of GAC can provide 1000 yr of isolation time for 2,4,5-polychlorinated biphenyl, even under moderate porewater seepage, while coke provides only a few decades.

Apatite is gaining favor as a counterpart to GAC for metals. Apatite has two modes of action: it binds certain metals into insoluble phases that are extremely stable by replacing Ca^{+2}, PO_4^{-3} and OH^- ions by metal ions *(139)* and it can act as geosorbent for other metals with binding strength affected by solution pH *(125, 140)*. Crannell et al. *(138)* showed that apatite reduced Pb diffusivity by 67%, Zn by 50%, but Cu diffusivity remained unchanged. Bostick et al. *(150)* concluded that biogenic apatite has the potential to successfully retard migration of U, Pb, Cd, Cu and Hg, but was less effective for As, Se, Ba and Cr.

Several initiatives have been taken by the US Environmental Protection Agency (USEPA) and the US Army Corps of Engineers to explore capping effectiveness, and a major field study with apatite, coke, aquablok™ and sand has been undertaken in the Anacostia river; however no studies have yet been published comparing the effectiveness of both a wide variety of cap materials and contaminants. Because many contaminated sediment sites have a mixture of both metal and organic contaminants, active media may be required to sequester both metals and organics. Thus, the first objective of this paper was to compile model parameter data for a range of cap materials and for a range of contaminants from the literature. We then model the transport of Cd, Cr, Pb, Ag, As, Ba, Hg, CH_3Hg and CN (although not technically a metal, CN is a

common co-contaminant with metals) through five different cap configurations. Finally, we use a Monte Carlo method to evaluate how sensitive model results are to uncertainty in model parameters.

3.3. Materials and Methods

Five capping materials and ten common metal contaminants were considered under diffusion only (diffusion) or with porewater advection flow. Contaminated near-shore areas (commonly selected as capping sites) are frequently subjected to submarine groundwater discharge *(229)*. The hydraulic gradient (d_h/d_x) across the cap in the simulations was given a fixed value of 0.005 and 0.05 $m \cdot m^{-1}$ for advection flow conditions, which comprises the typical hydraulic gradient range of near shore areas in North America. The cap thicknesses were chosen based on configurations used in laboratory and field studies reported in the literature *(10, 14)*. GAC, apatite and organoclay were 2 cm, shredded tires were 10 cm and sand was 25 cm. In applications, GAC, organoclay, and apatite would likely be employed in a geotextile "sandwich" to facilitate field application. In practice, the low density of GAC necessitates addition of sand to weigh the mat down. We assume that the geotextile, added sand, and the presence of mixed contaminants do not affect the transport of the contaminants in these simulations *(230)*. It is assumed that the contaminant source is infinite below the cap and desorption is rapid relative to porewater transport and thus the porewater concentration is at equilibrium with the solid phase.

We treat the system as a uniform vertical sediment column with an active cap at the top and porewater flux by diffusion and advection under two fixed gradients (0.005 and 0.05 $m \cdot m^{-1}$) across the active cap itself. Additional sand and/or armoring layers above the cap are not included in the analysis to provide a uniform comparison across different cap types. Under these conditions, the transport of contaminants is only affected by the properties of the contaminant

and the capping materials: porosity, bulk density, cap thickness, hydraulic conductivity, tortuosity, partitioning coefficient and molecular diffusivity. All parameters are either assumed in the test conditions (hydraulic gradient and cap thickness) or derived from an analysis of literature values (described in detail below). Transport thus follows equations 3.1 and 3.2 (more detailed description of the equations below can be found in chapter 2) *(194)*:

I) Diffusion

$$\frac{C}{C_o} = erfc\left(\frac{x}{2\sqrt{D_{mol}\varphi_e^{7/3}}}\frac{\sqrt{\varphi_e + \rho K_d}}{\sqrt{t}}\right) \tag{3.1}$$

II) Advection

$$\frac{C}{C_o} = \frac{1}{2}\left(erfc\left(\frac{x\sqrt{(\varphi_e + \rho K_d)}}{2\sqrt{D_{mol}\varphi_e^{7/3}}\sqrt{t}} - \frac{k_h}{\sqrt{(\varphi_e + \rho K_d)}}\frac{d_h/d_x}{2\sqrt{D_{mol}\varphi_e^{7/3}}}\sqrt{t}\right) + \ldots\right. \tag{3.2}$$

$$\left.\exp\left(\frac{xk_h(d_h/d_x)}{D_{mol}\varphi_e^{7/3}}\right)erfc\left(\frac{x\sqrt{(\varphi_e + \rho K_d)}}{2\sqrt{D_{mol}\varphi_e^{7/3}}\sqrt{t}} + \frac{k_h}{\sqrt{(\varphi_e + \rho K_d)}}\frac{d_h/d_x}{2\sqrt{D_{mol}\varphi_e^{7/3}}}\sqrt{t}\right)\right)$$

Where $C(x,t)$ is the breakthrough porewater concentration ($mg \cdot L^{-1}$) of contaminant at the top of the cap of thickness x at time t (yr); C_o is the initial concentration of contaminant in the sediment porewater ($mg \cdot L^{-1}$); φ_e is the effective cap porosity (unitless); ρ is bulk density ($kg \cdot L^{-1}$); k_h is the hydraulic conductivity of the cap ($m \cdot yr^{-1}$); d_h/d_x is the hydraulic gradient across the cap ($m \cdot m^{-1}$); D_{mol} is the molecular diffusivity ($m^2 \cdot yr^{-1}$) and K_d is the cap-porewater partitioning coefficient ($L \cdot kg^{-1}$).

Mass breakthrough per unit cross-sectional area A ($mg \cdot m^{-2}$) over time was calculated from the porewater Darcy velocity using a finite difference form of equation 3.3:

$$M_t = \varphi_e A \left(\frac{d_h}{d_x} \frac{k_h}{\varphi_e \left\{ 1 + \frac{K_d \rho}{\varphi_e} \right\}} \right) \int_0^t C_t dt \qquad (3.3)$$

Where C_t is the ratio C/C_o determined by equations 1 or 2 at time t, multiplied by the underlying sediment concentration C_o.

The values for metal solubility from the literature used in the cumulative mass breakthrough analyses are shown in Table 3.1: it should be noted that these are broad estimates because metal speciation and porewater chemistry greatly affect these values. Data were log-normally distributed so geometric mean (P50) values were considered as the solubility concentration C_s. We chose a 100 yr C/C_o target value to classify a cap as effective based on the USEPA criterion maximum concentration (CMC) for metals in freshwater *(29)*. This criterion defines the "highest concentration of a material in surface water to which an aquatic community can be exposed briefly without resulting in an unacceptable effect". We also show in Table 3.1 the criterion for continuous concentration (CCC), which is an estimate of the "highest concentration of a material in surface water to which an aquatic community can be exposed indefinitely without resulting in an unacceptable effect" *(29)*. For our simulations, C_o was set conservatively as the literature-derived solubility value (C_s, Table 3.1) and C as the USEPA CMC for freshwater (Table 3.1). The geometric mean was applied to establish the CMC and CCC for Cr due to wide differences in reported values for Cr (III) and (VI).

Table 3.1. Metal solubility values from the literature, USEPA CMC and *CMC/C_s* target values[a]

Compound	P10 ($mg \cdot L^{-1}$)	P50 (=C_s) ($mg \cdot L^{-1}$)	P90 ($mg \cdot L^{-1}$)	Geom std dev	CMC ($mg \cdot L^{-1}$)	*CMC/C_s* target	CCC ($mg \cdot L^{-1}$)	*CMC/C_s* target
Cd, pH 7	0.008	3	1240	110	2.0E-03	6.6E-04	2.5E-04	8.3E-05
Cr, pH 7	0.021	20	20500	220	1.0E-01	4.8E-03	2.9E-02	1.4E-03
Pb, pH 7	0.26	4	60	8	6.5E-02	1.7E-02	2.5E-03	6.4E-04
Ag	0.17	8	390	20	3.2E-03	3.9E-04		
As	0.018	5	1470	80	3.4E-01	6.5E-02	1.5E-01	2.9E-02
Ba	0.67	60	5970	40	n.a.		n.a.	
Hg	0.002	15	101000	1000	1.4E-03	9.5E-05	7.7E-04	5.2E-05
CH_3Hg		100			1.4E-03	1.4E-05	7.7E-04	7.7E-06
CN	0.35	280	232000	190	2.2E-02	7.7E-05	5.2E-03	1.8E-05

[a] P10, P50, P90 = percentiles; sources: *(29, 70, 231)*; n.a.=there is no EPA CCC criteria for the compound

Variability in model parameters obtained from the literature necessitated an uncertainty analysis for model output. We used a Monte Carlo method to obtain the distribution of model output based on the range of parameter values. Analyses were performed for 5000 draws of the random variables K_d, φ_e, ρ and k_h to obtain the distribution of C/C_o over time within the 95% confidence interval (CI). As there is no simple way to know *a priori* the metal speciation in the field (which accounts for the high variability of reported K_d values) and that speciation may be affected by changing environmental conditions over time, the Monte Carlo simulations allowed us to incorporate these uncertainties into model output to account for the possible forms of metal speciation with a statistically significant result. An extensive review of literature values was used to establish probability distribution functions for the variables (Tables 3.2 and 3.3). The data showed that K_d values followed a log-normal distribution (truncated at zero) and normal distributions (truncated at zero) best fit the φ_e, ρ and k_h data (except k_h values for organoclay, shredded tires and GAC, which were log-normally distributed, see below). Matlab (v. 7, MathWorks, Inc.) was used as the Monte Carlo platform.

Table 3.2. Model compounds used in the active cap transport simulations[a]

Compound	Relevant environ. state	D_{mol} (m^2 yr^{-1})	log K_d (L kg^{-1})	Std dev log K_d	f_i
Cd, pH 4	**Cd^{2+}**	2.27E-02	1.3		2.9
Cd, pH 7	"	2.27E-02	2.6	1.4	1.9
Cd, pH 9	"	2.27E-02	3.5		1.7
Cr, pH 4	**Cr^{3+}, Cr^{6+}**	1.86E-02	2.7		1.5
Cr, pH 7	"	1.86E-02	2.1	1.7	1.7
Cr, pH 9	"	1.86E-02	0.88		2.6
Pb, pH 4	**Pb^{2+}**, Pb^{4+}	3.00E-02	2.6		1.8
Pb, pH 7	"	3.00E-02	3.4	1.4	1.6
Pb, pH 9	"	3.00E-02	3.8		1.5
Ag	**Ag^{+}**	5.23E-02	3.6	1.1	1.0
As	**As^{+3}**, As^{+5}	3.82E-02	2.4	0.70	1.0
Ba	**Ba^{2+}**	2.68E-02	2.5	0.80	1.0
Hg	Hg^{0}, Hg^{+}, **Hg^{2+}**	5.68E-02	4.9	0.60	1.0
CH_3Hg	**CH_3Hg^{+}**	1.92E-02	3.9	0.50	1.0
CN	**HCN**	7.03E-02	1.6	1.7	1.0

[a] bold represents main species used in simulations; log K_d for apatite=log K_d*f_i, f_i=immobilizing factor; sources: *(49, 51, 138, 232-233)*

Table 3.3. Parameter values considered in the Monte Carlo simulations[a]

Cap material	x (m)	φ_e		ρ (kg·L^{-1})		k_h (m·yr^{-1})[b]	
		μ	σ	μ	σ	μ (or μ_g)	σ (or σ_g)
sand	0.25	0.31	0.03	2.0	0.30	21,000	27,000
organoclay	0.02	0.36	0.07	1.8	0.35	10	207
shredded tires	0.10	0.48	0.20	0.7	0.05	280,000	10
apatite	0.02	0.44	0.02	1.7	0.10	22	25
GAC	0.02	0.45	0.11	0.6	0.12	60	26

[a] sources: *(14, 47, 138, 159, 164, 232, 234-253)*; [b]organoclay, shredded tires and GAC k_h values are reported as geometric mean (μ_g) and geometric standard deviation (σ_g)

Organoclay k_h values vary greatly depending upon the product. Some commercially available organoclays have very high conductivity (3,000 m·yr^{-1}) *(252)*, whereas other studies report much lower k_h values for organo-modified clays (5 m·yr^{-1}) *(239)*. Further, at least one commercially-available organoclay has very low permeability (0.1 m·yr^{-1}) *(253)*. Together, these organoclay k_h data were better fit with a log-normal distribution. Shredded tire k_h values reported

in the literature present high variability due to bed compressibility and variable particle size *(241, 244, 249)* and thus a log-normal distribution better fit the data. Much of the literature-reported k_h values for GAC are relevant to in-line processes with large particle sizes (where very high k_h values are desirable). We assume in the field much lower values would be preferable for sediment applications and thus we have chosen lower k_h values that would be similar to those for very small GAC (or large powder activated carbon). Data on k_h for activated carbon in this size range are sparse, so we supplemented commercially-available values (300 $m \cdot yr^{-1}$) *(252)* with those derived from equations to estimate k_h from particle size *(47)*, as well as those from our own column experiment measurements *(16)*. Similar to the case with organoclay and shredded tires, the range of GAC k_h data were best fit with a log-normal distribution.

3.4. Results and Discussion

The literature best estimate D_{mol} values used in the simulations varied from 0.019 (Cr) to 0.070 $m^2 \cdot yr^{-1}$ (CN), and log K_d varied widely from 0.88 (Cr at pH 9) to 4.9 $L \cdot kg^{-1}$ (Hg) (Table 3.2). Porosity varied from 0.30 (sand) to 0.50 (GAC), ρ from 0.66 (GAC) to 1.86 $kg \cdot L^{-1}$ (sand) and k_h from 10 (organoclay) to 4,000 $m \cdot yr^{-1}$ (sand) (Table 3.4). I present here results for each capping material for metals with literature-reported pH dependent K_d values (Cd, Cr, Pb), followed by metals with no reported pH-dependency for K_d (Ag, As, Ba) and then Hg, CH_3Hg and CN. Although Ba is not considered a priority pollutant by the USEPA CMC and CCC criteria, I also modeled Ba behavior as it is included in the RCRA 8 metals. Even though pH is likely to affect sorption behavior for all metals analyzed (as well as some of the cap materials), a detailed analysis of these effects is beyond the scope of this part of the study. A primary source

for the K_d values used in this study is a recent comprehensive literature compilation of metal K_d values reported by USEPA *(49, 51)*.

Table 3.4. Literature best estimate values used in the simulations[a]

Cap material	x (m)	φ_e	ρ (kg L^{-1})	k_h (m yr^{-1})
sand	0.25	0.30	1.86	4,000
organoclay	0.02	0.36	1.80	10
shredded tires	0.10	0.40	0.73	100,000
apatite	0.02	0.45	1.60	30
GAC	0.02	0.50	0.66	60

[a] sources: *(14, 47, 232, 234-244, 252-253)*

Under diffusion conditions, sand efficiently hinders Cd release (Figure 3.1 a–c). Diffusive path length greatly affects breakthrough time, thus leading to the relatively effective performance of the thicker sand cap. Cd breakthrough is predicted in the sand cap (d_h/d_x=0.05 $m \cdot m^{-1}$) in less than 50 d, one yr and 80 yr at pH 4, 7 and 9, respectively (Figure 3.1 d-f). Sand is predicted to effectively minimize the release of Cr (except at pH 9) and Pb under diffusion (Figures 3.2 and 3.3 a-c). Sand performed best under diffusion for Ag, As and Ba. Ag and As release is less than their USEPA CMC after 5000 and 1500 yr, respectively (Figure 3.4 a, b). Under advection, the sand cap does not perform well for all contaminants except Hg. Sand will likely minimize Hg release under both diffusion and advection (Figure 3.5 a, d), keeping Hg release below the CMC (1.4 10^{-3} $mg \cdot l^{-1}$) for 175 yr, even under advection. CH_3Hg releases are predicted to reach the CMC after 5000 and 18 yr for diffusion and advection, respectively (Figure 3.5 b, e). CN releases are predicted to reach the CMC in 35 yr and <1 yr for diffusion and advection, respectively (Figure 3.5 c, f).

Shredded tire caps efficiently hinder Cd release (Figure 3.1 a–c) under diffusion conditions. Similar to the sand cap, the shredded tire cap is thicker than the other cap materials, thus leading

to the more effective performance of the thicker shredded tire cap. The shredded tire cap is predicted to perform satisfactorily for Cr only at pH 4 (Figure 3.2 a–c) and for Pb (at all pH) under diffusion. Ag, As and Hg releases are lower than their USEPA CMC after 180, 65 and 2800 yr, respectively, under diffusion. However, under advection, the shredded tire cap does not perform well for any contaminant. Cd, As and CN breakthrough, for example, is predicted in <1 yr. Hg breakthrough occurs in <2 yr.

Organoclay performed well for Cd at pH 9 (Figure 3.1 c, f), but it is not predicted to prevent Cd release to the water column at 100 yr at lower pH, even under diffusion-only conditions. Organoclay is predicted to prevent Cr releases from exceeding the USEPA CMC for 15, 3.5, and 0.2 yr at pH 4, 7 and 9, respectively, under advective conditions (d_h/d_x=0.05). Organoclay is effective at minimizing Pb release under diffusion, except at pH 4. However, under advection it is effective only at pH 9 (Figure 3.3 a-f). Organoclay performed best among the caps for Ag, As and Ba under advection; followed by apatite, GAC, sand and shredded tires (figure 3.4 d-f). The very low hydraulic conductivity of organoclay is responsible primarily for its better performance. Organoclay Ag and As releases are predicted to reach the CMC after 20 yr and 5 yr, respectively (d_h/d_x=0.05). A thicker layer of both organoclay and apatite would likely be necessary to successfully minimize the release of these contaminants to the water column. Hg is predicted to reach the CMC after >300 yr under both diffusion and advection (Figure 3.5 a, d). Organoclay CH_3Hg releases are predicted to reach the CMC after 90 and 70 yr for diffusion and advection, respectively (Figure 3.5 b, e). Organoclay CN releases are predicted to reach the CMC in <1 yr for both diffusion and advection (Figure 3.5 c, f).

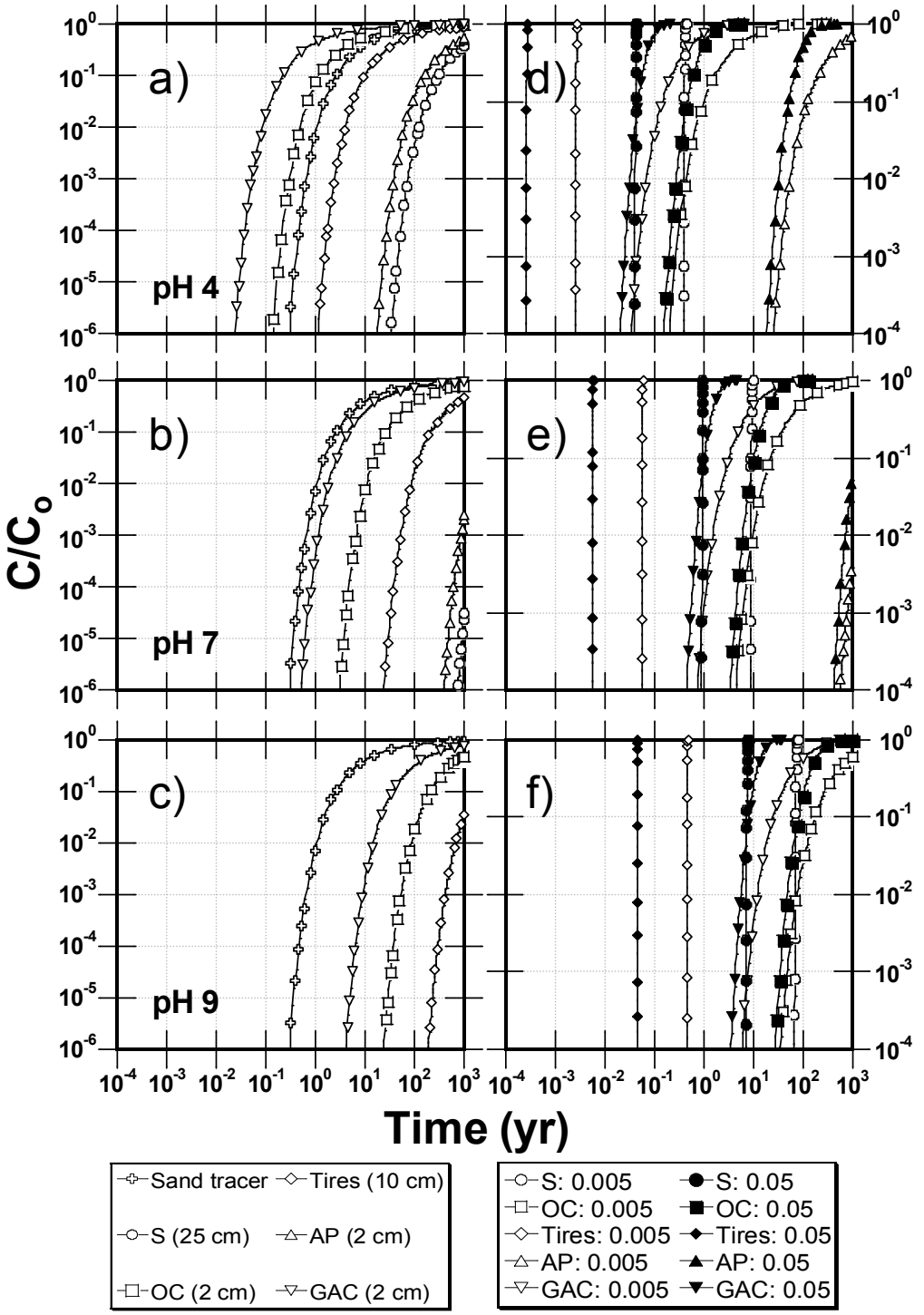

Figure 3.1. Simulated breakthrough concentration curves of Cd in different caps under diffusion (a, b, c) and advection under two gradients (d, e, f) as a function of pH. Shown are pH 4 (a, d), pH 7 (b, e) and pH 9 (c, f) in sand, shredded tires, organoclay, GAC and apatite caps. Also shown is a conservative tracer in the sand cap under diffusion for comparison.

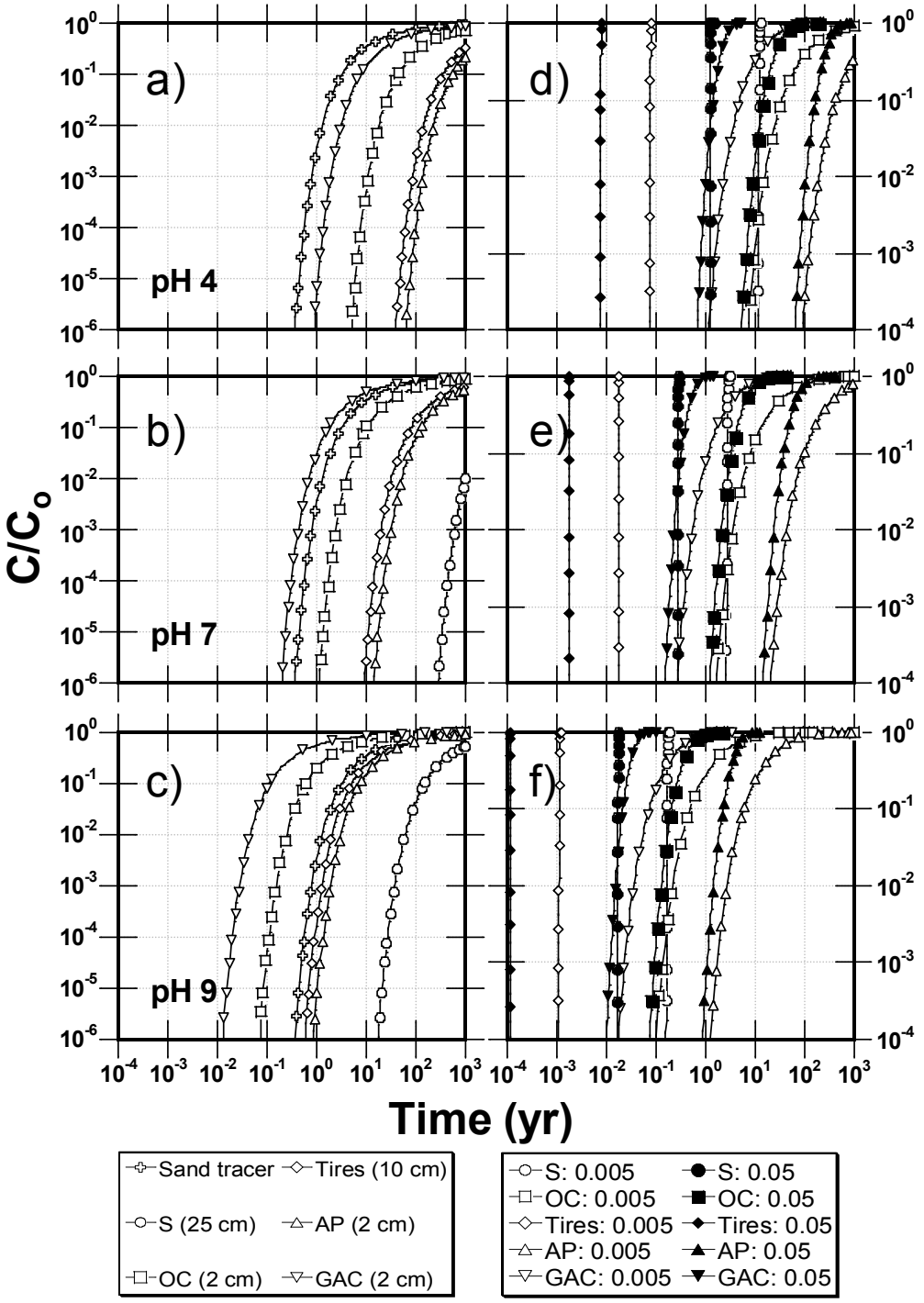

Figure 3.2. Simulated breakthrough concentration of Cr in different caps under diffusion (a, b, c) and advection under two gradients (d, e, f) as a function of pH. Shown are pH 4 (a, d), pH 7 (b, e) and pH 9 (c, f) in sand, shredded tires, organoclay, GAC and apatite caps. Also shown is a conservative tracer in the sand cap under diffusion for comparison.

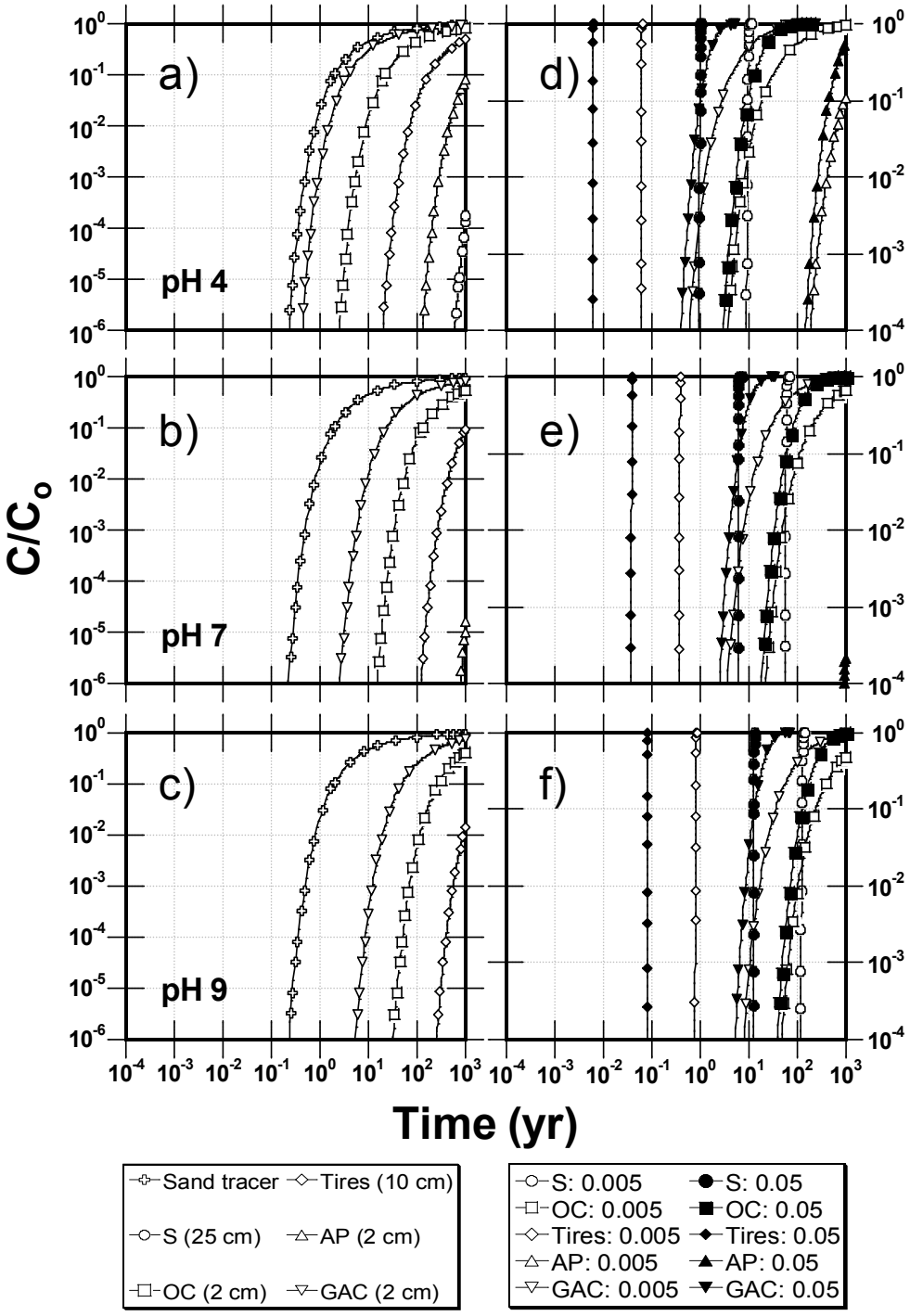

Figure 3.3. Simulated breakthrough concentration of Pb in different caps under diffusion (a, b, c) and advection under two gradients (d, e, f) conditions as a function of pH. Shown are pH 4 (a, d), pH 7 (b, e) and pH 9 (c, f) in sand, shredded tires, organoclay, GAC and apatite caps. Also shown is a conservative tracer in the sand cap under diffusion for comparison.

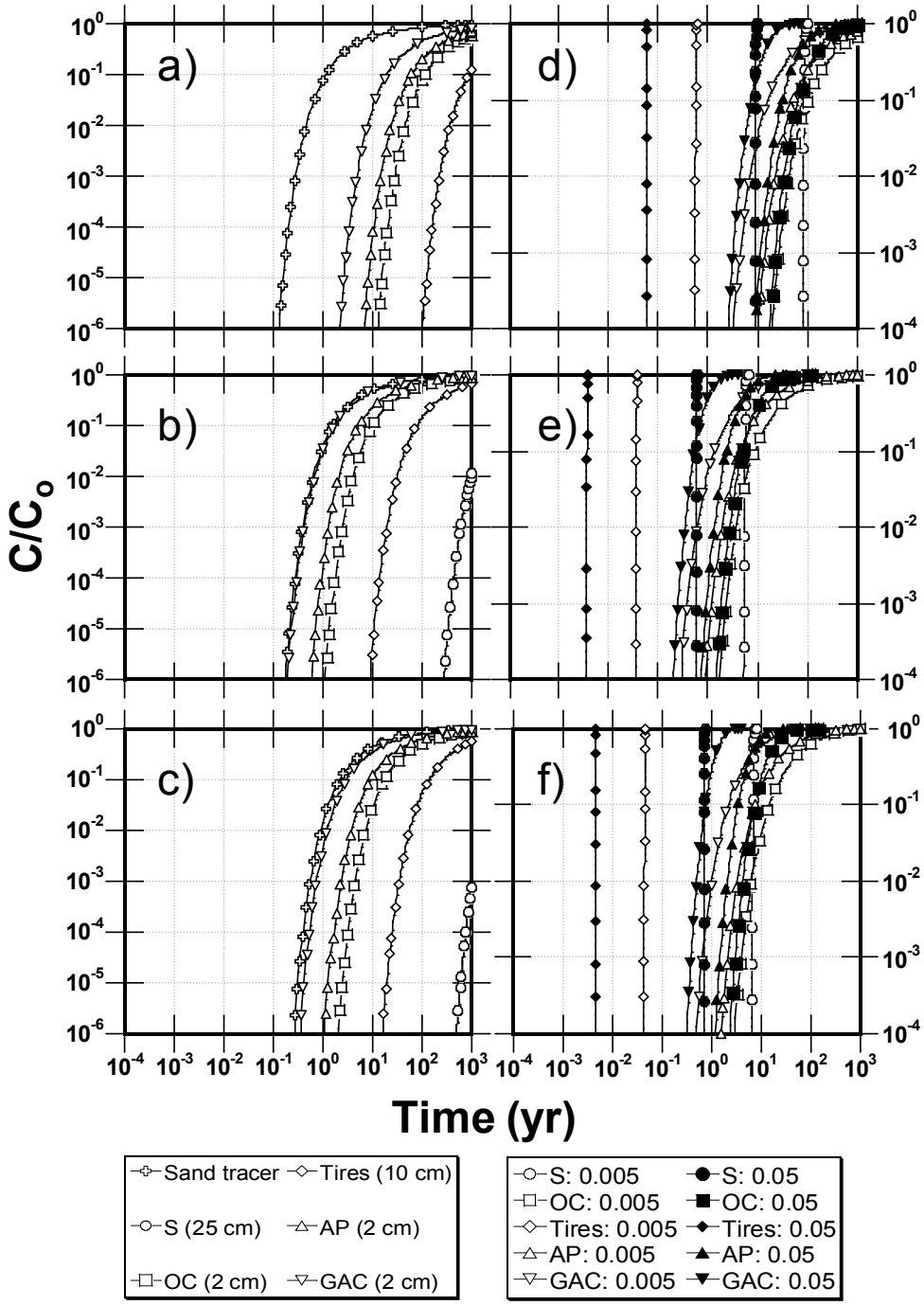

Figure 3.4. Simulated breakthrough concentration of putatively non-pH sensitive partitioning metals in different caps under diffusion (a, b, c) and advection under two gradients (d, e, f). Shown are Ag (a, d), As (b, e) and Ba (c, f) in sand, shredded tires, organoclay, GAC and apatite caps. Also shown is a conservative tracer in the sand cap under diffusion for comparison.

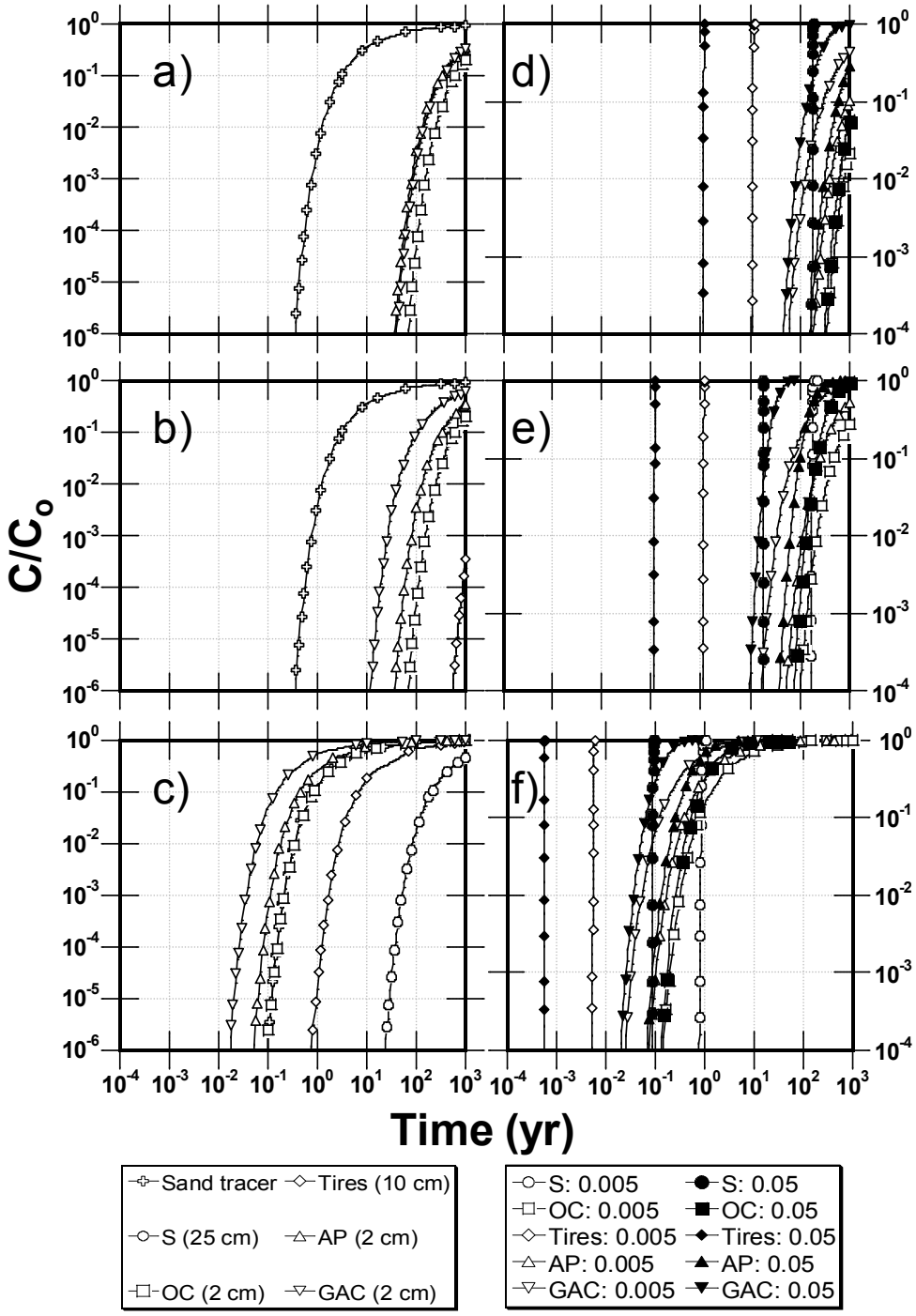

Figure 3.5. Simulated breakthrough concentration of mercury and organo-metals in different caps under diffusion (a, b, c) and advection under two gradients (d, e, f). Shown are Hg (a, d), CH_3Hg (b, e), CN (c, f) in sand, shredded tires, organoclay, GAC and apatite caps. Also shown is a conservative tracer in the sand cap under diffusion for comparison.

Apatite had the best performance for Cd at all pH; and releases under advection were less than the USEPA CMC ($2.0\ 10^{-3}$ mg·l^{-1}) after 23, 500, and 4000 yr at pH 4, 7 and 9, respectively (Figure 3.1 d-f). Apatite is predicted to have the best performance for Cr under advection at d_h/d_x=0.05 (Figure 3.2 d-f), with releases less than the CMC value after 100, 23, and 1.5 yr at pH 4, 7 and 9, respectively. A thicker apatite layer may be necessary to minimize the release of Cr at pH 7 or 9 under a similar gradient. Under advection, apatite had the best performance for Pb at all pH, with predicted Pb release less than the CMC after 300, 2000, and 4000 yr at pH 4, 7 and 9, respectively (Figure 3.3 d-f). Apatite Ag and As releases are predicted to reach the CMC at 13 and four years, respectively, for diffusion (Figure 3.4 a, b) and at 11 yr and two yr, respectively (figure 3.4 d, e) under advection. Hg is predicted to reach the CMC after >160 yr under both diffusion and advection (Figure 3.5 a, d), whereas CH_3Hg releases are predicted to reach the CMC after >35 yr for both diffusion and advection (Figure 3.5 b, e). Apatite CN releases are predicted to reach the CMC in <1 yr for both diffusion and advection (Figure 3.5 c, f).

GAC does not prevent Cd (Figure 3.1 a-c), Cr (Figure 3.2 a-c), Pb (Figure 3.3 a-c), Ag and As (Figure 3.4 a, b) breakthrough, even under diffusion only conditions. All five contaminants reach their USEPA CMC under diffusion in <25 yr. Under advection, GAC allows Cd, Cr, Pb, Ag and As release to the water column to reach their EPA CMC after <4 yr. GAC performs relatively better for Hg and CH_3Hg. Above-cap concentrations were not predicted to exceed the CMC until after >50 yr and >9 yr for Hg and CH_3Hg, respectively (Figure 3.5 a, b, d, e). As with the other caps, CN release from a GAC cap is predicted to exceed the CMC in <1 yr for both diffusion and advection (Figure 3.5 c, f).

In all cases, Cd and Pb breakthrough times were predicted to increase as the pH increased (Figures 3.1 and 3.3 a-f), while Cr breakthrough time decreased for all caps as the pH increased (Figure 3.2 a-f) due to the strong influence pH has on the partitioning coefficient or these metals.

All test compounds had 10% breakthrough times in excess of 100 yr in the sand cap under diffusion. Similarly long breakthrough times are predicted for the shredded tire cap at neutral pH (with the exception of CN). For several metals, apatite is predicted to perform effectively under diffusion with 10% breakthrough times of 7000, 3000 and 1000 yr for Pb, Cd and Hg, respectively. Other contaminants were not as effectively retarded by apatite; 100 – 300 yr for Cr and CH_3Hg, 60 yr for Ag and less than 10 yr for As, Ba and CN. GAC had 10% breakthrough times of 350 and 100 yr for Hg and CH_3Hg, respectively; and less than 25 yr for the other metals (Figure 3.6 a).

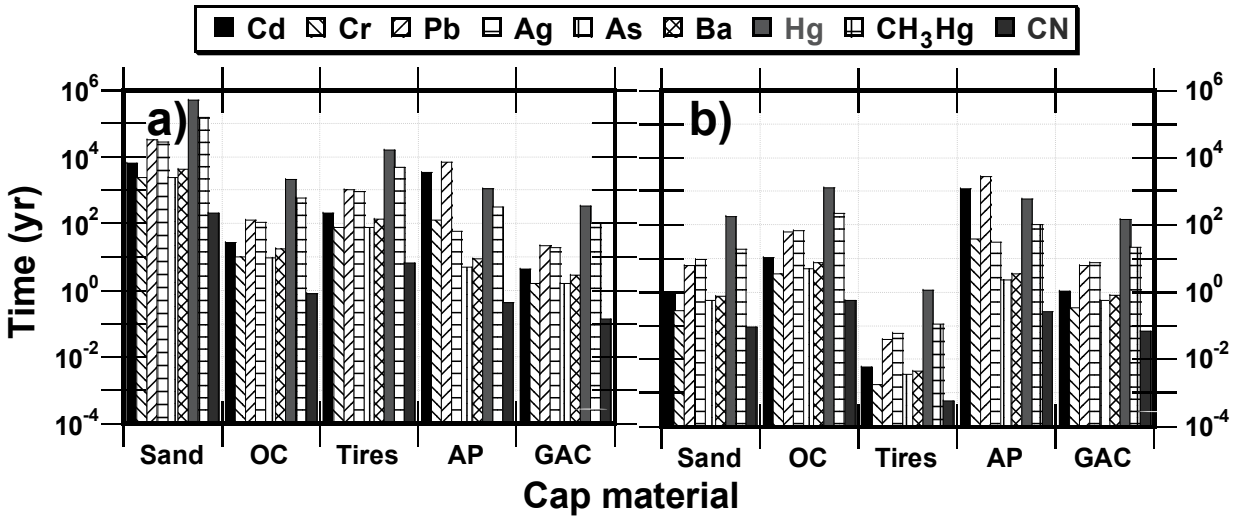

Figure 3.6. Comparison of time required for 10% contaminant simulated breakthrough in five cap materials under diffusion (a) and advection (b) flow conditions (d_h/d_x=0.05).

The relative performance of the caps (by 10% breakthrough time) was predicted to be much different under advective flow conditions (Figure 3.6 b). Cap materials with either higher metal

sequestration capability (apatite) or lower permeability (organoclay) minimized contaminant breakthrough under advection relative to sand or shredded tires, which both had predicted times to 10% breakthrough frequently <1 yr. Such short breakthrough times are not likely to be considered acceptable performance for any conceivable capping scenario. Cd, Pb, Hg and CH_3Hg are predicted to have 10% breakthrough times in excess of 100 yr under advection for apatite, whereas only Hg and CH_3Hg had similarly long 10% breakthrough times in the organoclay cap. However, both apatite and organoclay were less effective for Cr, As, Ba and CN; and may require thicker layers of cap material to perform efficiently.

Although porewater concentration is the most useful metric to quantify exposure risk, I include cumulative mass breakthrough as an additional performance metric because it takes into account the actual volumetric porewater flowrate and provides a better measure of impacts to the overlying water body (Figure 3.7). Apatite is predicted to perform effectively for Cd, Pb and Hg, while organoclay is predicted to perform effectively for Hg and CH_3Hg. Although not meeting the 100 yr effectiveness criterion, apatite is predicted to perform better than all other caps for Cr, while organoclay would be better than the other caps for Ag, As, Ba and CN. Even though apatite prevents release of Cr better than organoclay (time to reach CMC is 30 and 1.5 yr for apatite and organoclay, respectively), I predict a 6 cm apatite cap layer would be necessary to prevent Cr release from reaching the CMC for 100 yr. Due to poor sequestration of CN, the cap size and resultant cost to prevent its release from reaching CMC likely would be prohibitive (if the underlying porewater is at C_s).

Advective areal mass release from the sand cap varied greatly by contaminant. After 100 yr, Pb, As and Hg mass release is predicted to be 4300 $mg \cdot m^{-2}$, 64,000 $mg \cdot m^{-2}$ and < 10^{-6} $mg \cdot m^{-2}$, respectively. The 100 yr mass release is smaller for the apatite cap, with values < 10^{-6} $mg \cdot m^{-2}$ for

Cd, Pb and Hg and < 700 mg·m^{-2} for all other metals except CN (Figure 3.7). Organoclay also performed well, with predicted 100 yr release all <2 mg·m^{-2} for Pb, Ag, Hg and CH_3Hg.

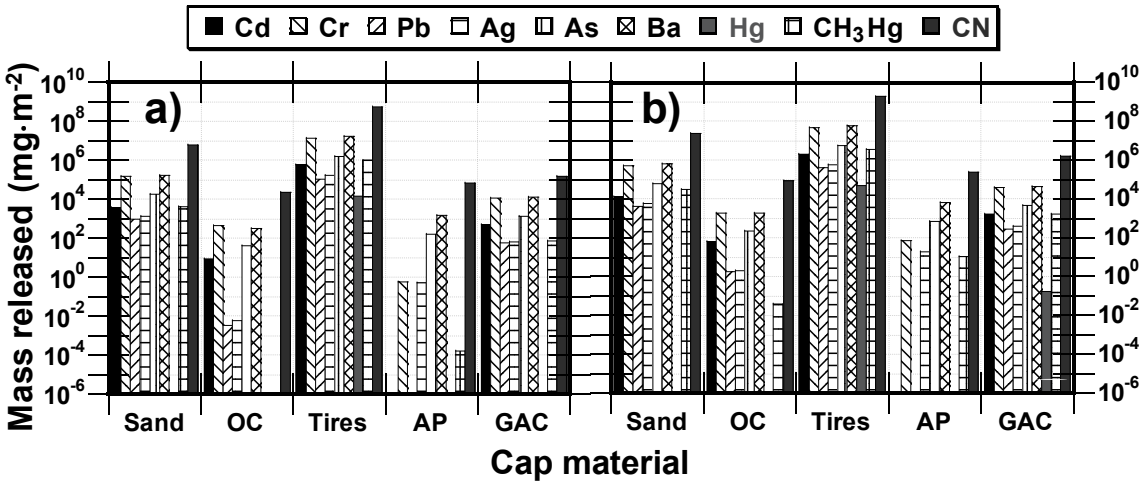

Figure 3.7. Simulated cumulative contaminant mass breakthrough (mg m^{-2}) in five cap materials after 30 yr (a) and 100 yr (b) under advection flow conditions (d_h/d_x=0.05).

Combined cumulative 30 and 100 yr areal mass release shows that organoclay is predicted to have the best overall performance (Figure 3.8 a). Surprisingly, GAC is predicted to have a reasonable performance when compared to apatite from a mass release standpoint. Although apatite works very well for Cd, Pb and Cr (where GAC is relatively ineffective), GAC differs by less than an order of magnitude for Ag, As, Ba and CN.

The 30 and 100 yr concentration data were normalized to the CMC to better compare the relative performance (Figure 3.8 b). Organoclay risk is driven by CN, Cd and Ag, while apatite risk is driven by CN, CH_3Hg and Ag. GAC risk is driven by CN, CH_3Hg and Cd, whereas both sand and shredded tire risk is driven primarily by CH_3Hg. By this metric, apatite performed best for Pb, Cd and Cr, and organoclay performed best for Ag, As, and CH_3Hg. Both apatite and organoclay were equally effective towards Hg and equally ineffective towards CN.

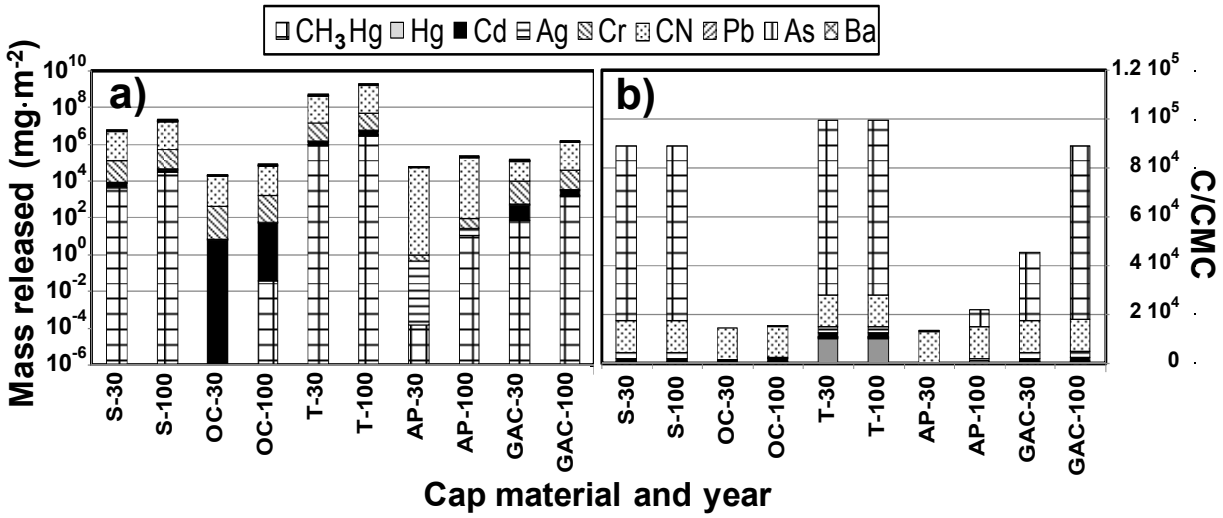

Figure 3.8. Simulated total mass and toxicity-normalized concentration measures of contaminant release through five cap materials after 30 and 100 years under advection flow conditions (d_h/d_x=0.05). Shown are cumulative areal mass release (a) and the 30 and 100 yr contaminant concentration at the cap surface (b) normalized to the toxicity criteria for maximum concentration (CMC).

The variability in reported parameter values used in these simulations indicates the need to perform a sensitivity analysis. Because multiple parameters are used in the model, I chose a Monte Carlo method to investigate sensitivity to multi-parameter variability. The complex metal partitioning process is affected by speciation, redox state and pH, which in turn greatly affects K_d values and thus results in the large variability in reported values, e.g. CN (1.6±1.7 l·kg^{-1}) and Cd at pH 7 (2.6±1.4 l·kg^{-1}). Porosity (φ_e) varied from 0.31±0.03 (sand) to 0.48±0.20 (shredded tires), ρ from 0.60±0.12 kg·l^{-1} (GAC) to 2.0±0.30 kg·l^{-1} (sand), and k_h varied from 10±207 m·yr^{-1} (organoclay μ_g) to (2.8 10^{+5})±(10) m·yr^{-1} (shredded tires μ_g) (Table 3.3). I report the distribution of C/C_o over time within various confidence intervals (Figure 3.9 – 3.13). The area between the boundary lines represents all breakthrough results under all possible values for K_d, φ_e, ρ and k_h within the CI. A summary of all results is presented in Table 3.5.

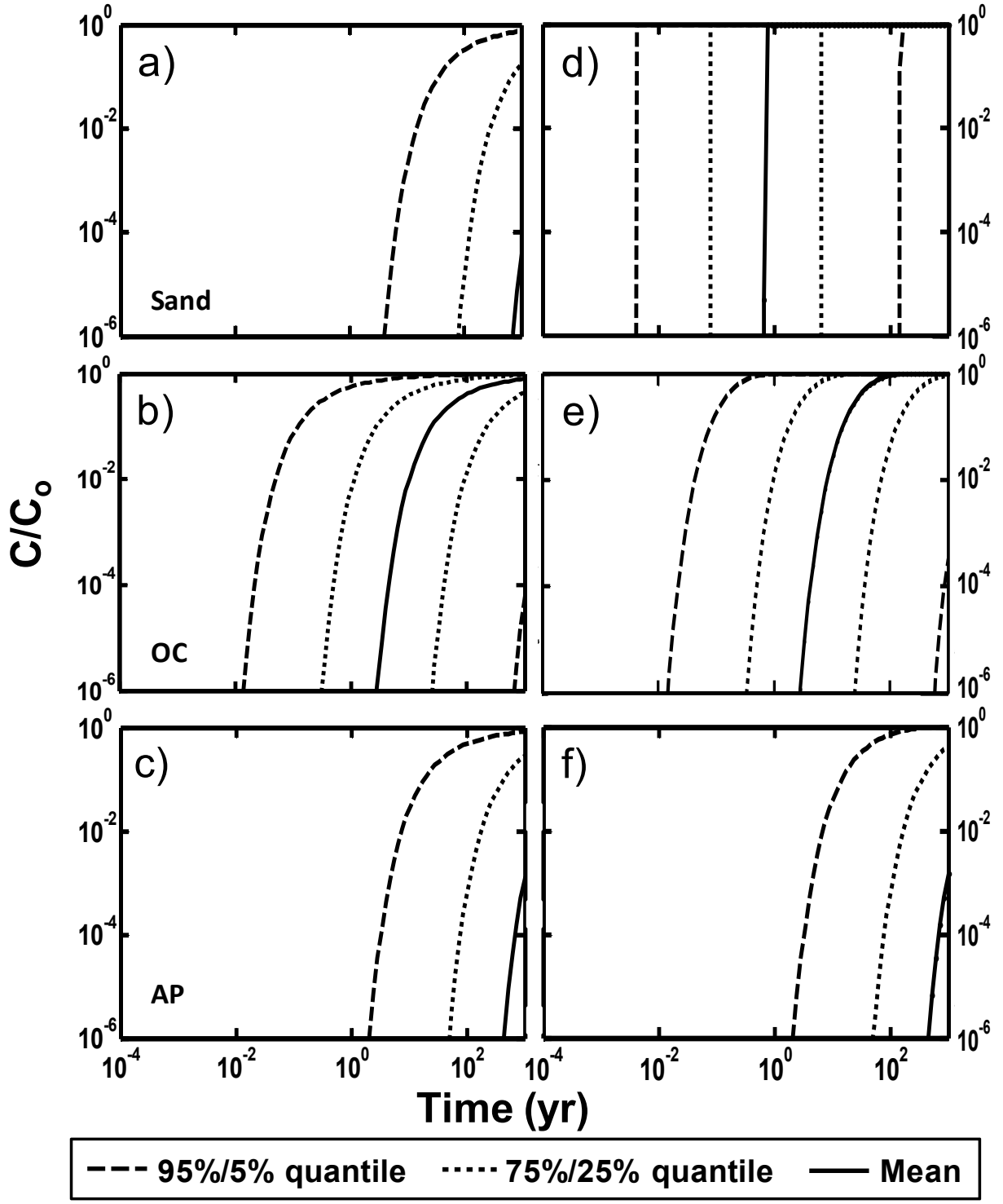

Figure 3.9. Representative Monte Carlo simulation curves of breakthrough concentration for Cd at pH7. Shown are simulations under diffusion (a, b, c) and advective (d, e, f) conditions in sand (a, d), organoclay (b, e) and apatite (c, f).

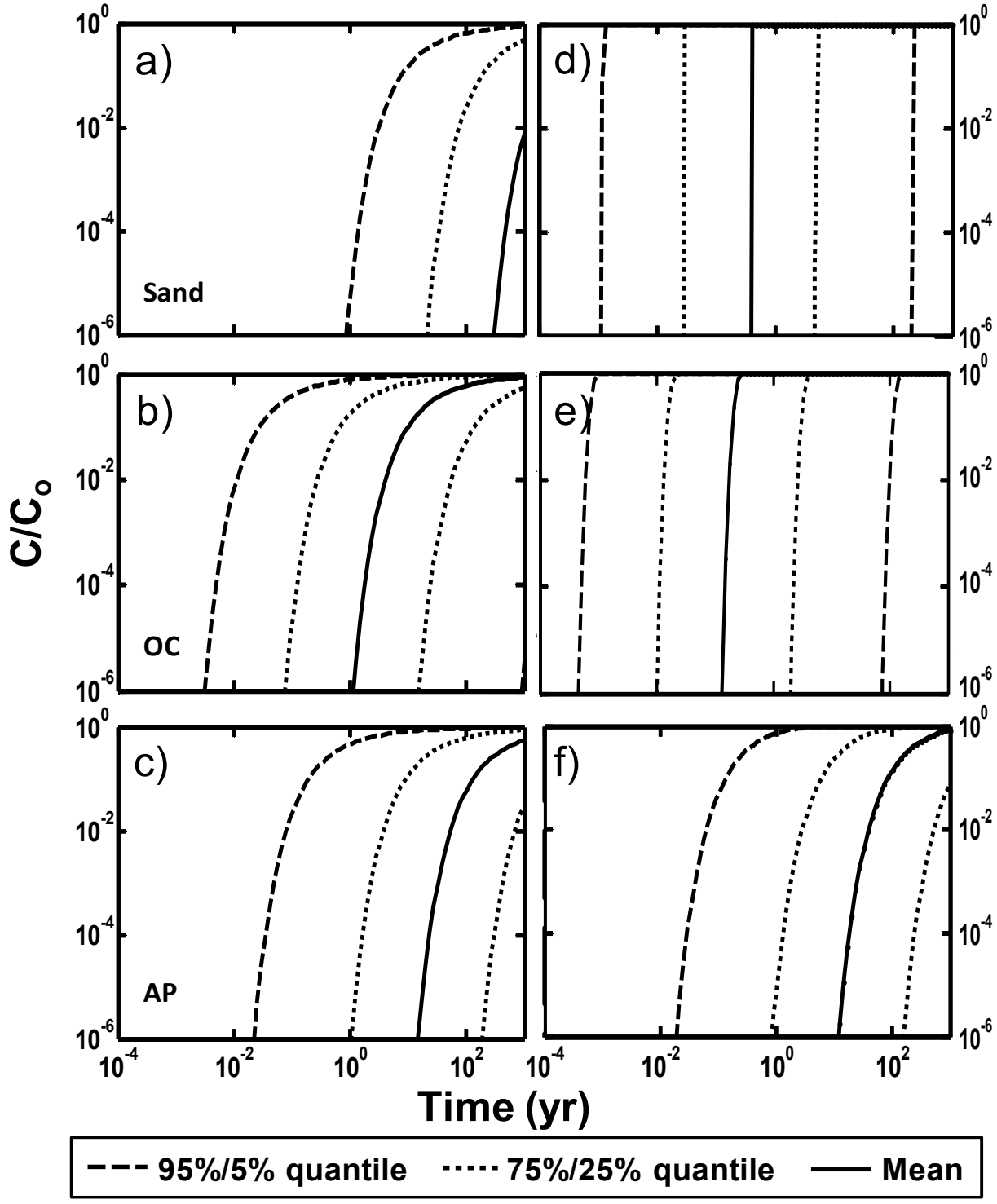

Figure 3.10. Monte Carlo simulation of breakthrough concentration for Cr at pH7. Shown are simulations under diffusion (a, b, c) and advective (d, e, f) conditions in sand (a, d), organoclay (b, e) and apatite (c, f).

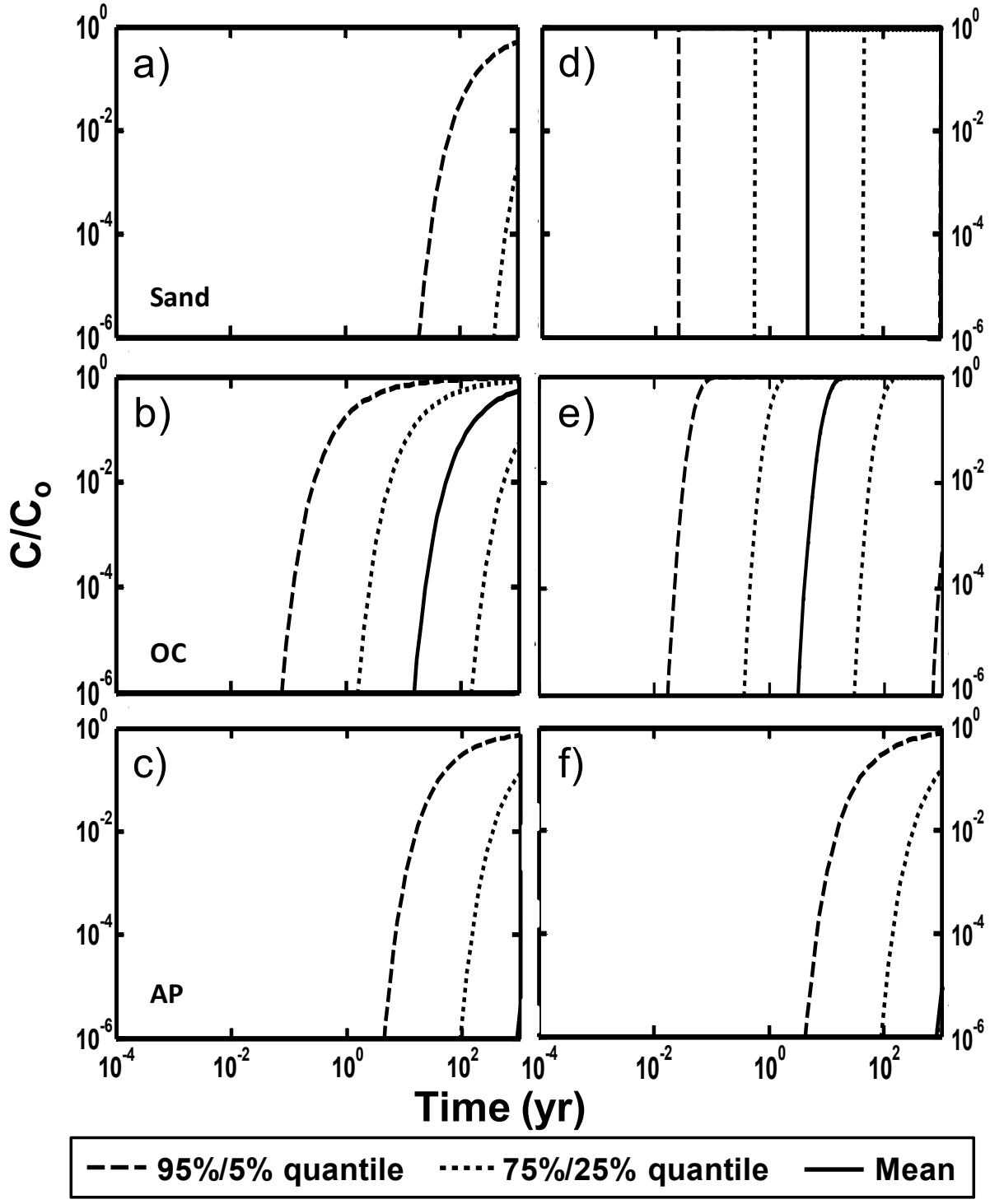

Figure 3.11. Monte Carlo simulation of breakthrough concentration for Pb at pH7. Shown are simulations under diffusion (a, b, c) and advective (d, e, f) conditions in sand (a, d), organoclay (b, e) and apatite (c, f).

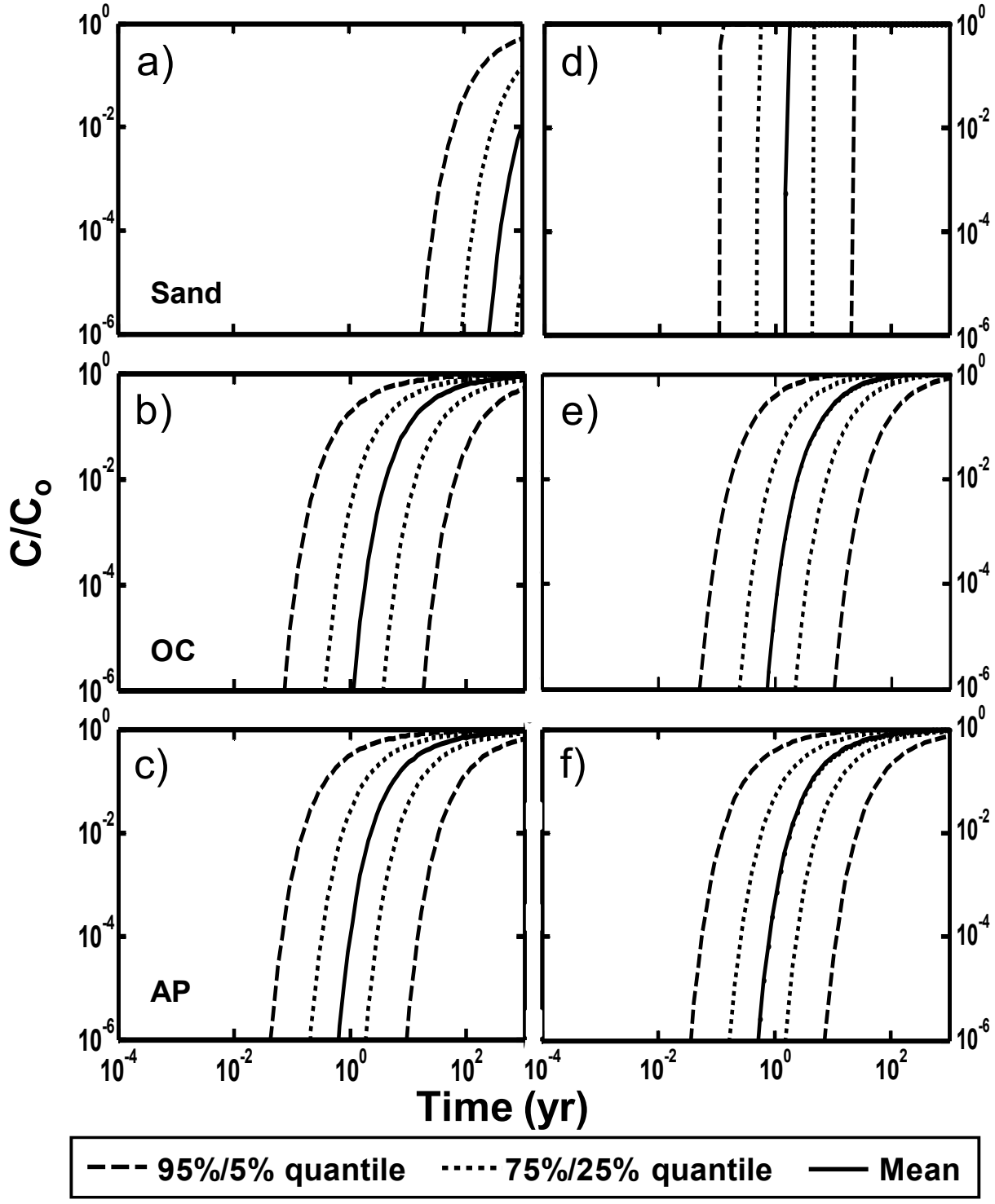

Figure 3.12. Monte Carlo simulation of breakthrough concentration for As. Shown are simulations under diffusion (a, b, c) and advective (d, e, f) conditions in sand (a, d), organoclay (b, e) and apatite (c, f).

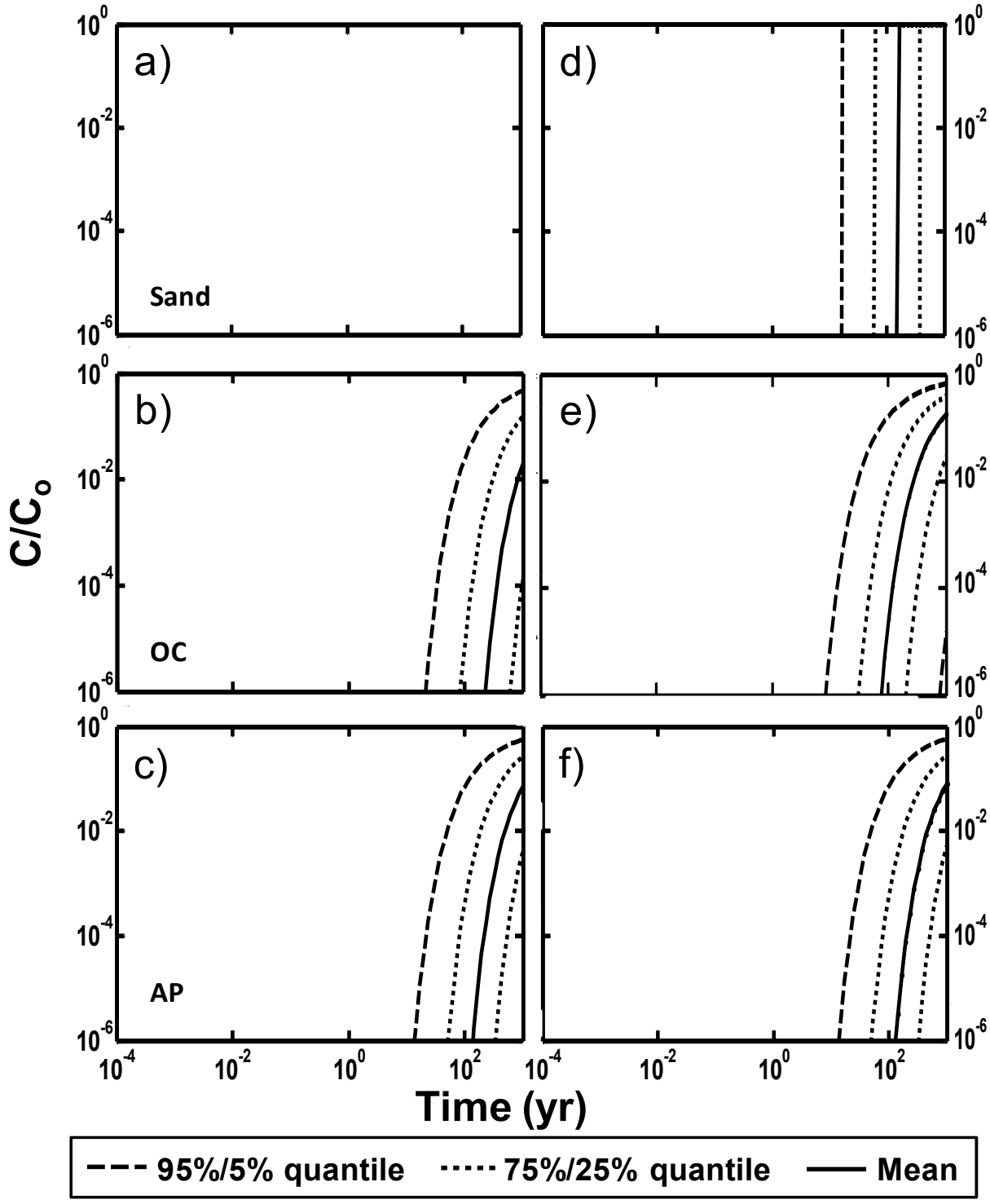

Figure 3.13. Monte Carlo simulation of breakthrough concentration for Hg. Shown are simulations under diffusion (a, b, c) and advective (d, e, f) conditions in sand (a, d), organoclay (b, e) and apatite (c, f).

Table 3.5. Summary of the Monte Carlo simulation results[a]

Compound	Cap material									
	Sand		OC		Tires		AP		GAC	
	CMC	CCC	CMC	CCC	CMC	CCC	CMC	CCC	CMC	CCC
Cd, pH 7	++/-	++/-	-/-	-/-	-/-	-/-	++/++	++/++	-/-	-/-
Cr, pH 7	+/-	+/-	-/-	-/-	-/-	-/-	-/-	-/-	-/-	-/-
Pb, pH 7	+++/-	++/-	+/-	-/-	+/-	+/-	++/++	++/++	-/-	-/-
Ag	+++/-	n.a.	-/-	n.a.	+/-	n.a.	-/-	n.a.	-/-	n.a.
As	+++/-	+++/-	-/-	-/-	-/-	-/-	-/-	-/-	-/-	-/-
Hg	+++/++	+++/+	++/+	++/+	+++/-	++/-	++/++	+/+	+/+	-/-
CH_3Hg	+++/-	+++/-	++/+	+/-	++/-	++/-	-/-	-/-	-/-	-/-
CN	-/-	-/-	-/-	-/-	-/-	-/-	-/-	-/-	-/-	-/-

[a] - means cap complies with the USEPA CMC or CCC after 100 yr within <50% CI; +, ++ and +++ means cap complies with the CMC or CCC within mean, 75% and 95% CI, respectively. First symbol means result for diffusion, second symbol means result for advection (d_h/d_x=0.05). n.a.=there is no EPA CCC criteria for the compound

Sand achieved USEPA CMC under diffusion for Cd within the 75% CI (Figure 3.9 a) and for Pb (Figure 3.11 a), Ag, As (Figure 3.12 a), Hg (Figure 3.13 a) and CH_3Hg (95% CI). Sand does not perform satisfactorily for Cr and CN, even under diffusion only. With the exception of Hg, all other compounds would rapidly breakthrough the sand layer under advection and therefore it does not appear likely that sand alone would perform acceptably.

Shredded tires were only effective for Hg (95% CI) and for CH_3Hg (75% CI) under diffusion. All compounds would rapidly breakthrough the shredded tire layer under advection.

Organoclay was effective for Hg and CH_3Hg under diffusion (75% CI), and within the 50% CI under advection. Organoclay did not perform satisfactorily for the other compounds. Although organoclay performed better than apatite in the sensitivity analysis for Ag, As and CH_3Hg, it was not effective (75% CI) for these metals under advection and a thicker layer, >15 cm, may be needed to remediate sites with these contaminants.

Apatite achieved the CMC after 100 yr under diffusion and advection (d_h/d_x=0.05) for Cd, Pb and Hg (75% CI). The performance of apatite was not as satisfactory for other metals analyzed.

GAC performed poorly for all metals under the 100 yr CMC criterion.

3.5. Conclusions and Implications

Cap thickness is clearly the most important factor under diffusion; sand caps performed best under diffusion and shredded tires also performed well. However, an inadequately armored sand cap layer alone may not work satisfactorily, even in sites that are only under diffusive transport conditions due to erosive losses of cap material over time. Under advection, decreased hydraulic conductivity may be as or more important than increased K_d; apatite had the best performance for Cd, Cr and Pb and low hydraulic conductivity organoclay performed best for Ag, As, Ba, CH_3Hg and CN. My results are comparable to those obtained by Bostick et al. *(150)*, who observed that apatite successfully retards migration of Pb, Cd and Hg, but is less effective for As, Ba and Cr. In some cases, organoclay behaved similarly under diffusion and advection because this cap material is both a sorbent and a hydraulic barrier, while the thick sand cap effectiveness was completely different under advection because it is not a sorbent and is highly permeable.

Overall, no cap is predicted to be effective for Cr and CN. Although sand would reduce Cr flux to the water column for 80 yr under diffusion (75% CI), no cap reduced Cr release at a high CI under advection (Figure 3.10). Thicker caps could thus be applied to ensure effective performance, although this would result in increased cost. Sand and apatite are the most effective caps for Hg, but organoclay may be effective as well. Sand, organoclay and tires are predicted to be effective for CH_3Hg under diffusion only, but a thicker cap of organoclay would probably be more effective under advection. Sand is predicted to be effective for Ag and As under diffusion,

but a thicker cap of organoclay would likely be the best alternative for these metals under advection. Sand and apatite are predicted to be effective for Cd and Pb at neutral pH, but only apatite is predicted to be effective under advection.

Cap combinations (e.g. apatite or organoclay followed by sand) may be the most economically efficient capping formulation. The apatite or organoclay mat providing effective advective sequestration and the sand layer contributing for both stability and as a thick diffusive pathway.

My results demonstrate the need for uncertainty analysis, which is driven primarily by sediment chemistry that greatly affects K_d and the variety of cap materials with different permeabilities. More K_d data under realistic field conditions are needed to reduce uncertainty to a level more acceptable in managing risk. Knowing site specific conditions would also contribute to decrease uncertainty in my simulations for a specific site, but the utility of a broader comparison is the ability to focus data-gathering efforts on the caps that are likely to be more effective and the contaminants that are driving risk. Further, the importance of k_h is clearly demonstrated by my simulations. These results may lead to modified cap formulations to decrease permeability and thus improve performance.

There are currently >100 contaminated sediment projects were capping is planned or has been implemented *(254)*. However, capping tends to be "harder sell" for regulatory agencies and the public *(255)*. I hope the experimental and modeling results from cap efficiency for different metal contaminants under a variety of environmental conditions and cap characteristics contribute to a better understanding of the effectiveness of capping and to focus efforts on future studies.

CHAPTER IV. METAL ADSORPTION ISOTHERM AND COLUMN TRANSPORT STUDIES WITH ACTIVE CAPPING AMENDMENTS

Equilibrium adsorption studies were conducted with the cationic metal Cd and the anionic metal As, and the cap materials sand, organoclay (OC), apatite and granular activated carbon (GAC) to provide more confident model predictions based upon measurement of the most sensitive parameter identified in the Monte Carlo analyses shown in chapter 3, the partitioning coefficient K_d. Laboratory-scale column studies were also performed to validate the model simulations.

4.1. Abstract

The partitioning coefficient K_d was measured by adsorption isotherm experiments for Cd, a cationic metal, and As, an anionic metal, and four cap materials (sand, organoclay OC, apatite and granular activated carbon GAC). Results indicate that Cd adsorption isotherms are likely nonlinear for all cap materials, and As isotherm is nonlinear at least for organoclay. Although none of the caps exhibited a high sorption capacity for As, OC and apatite performed clearly better than sand and GAC. Surprisingly, OC exhibited a significantly higher sorption capacity than apatite for Cd. The K_d results indicate close agreement between the experimental and literature K_d values with the exception of As and Cd with apatite. Apatite performed well for Cd in the column study with full breakthrough after 12000 pore volumes. Sand did not exhibit such a poor sorption capacity as expected for Cd with full breakthrough after 4000 pore volumes. Based on the column experiment results, GAC performed poorly both for As and Cd. The results from simulations performed with measured K_d and cap parameters compared to literature-derived model simulations demonstrate the need for uncertainty analysis. The measured K_d values under

realistic field conditions (circumneutral pH and close to anaerobic conditions) contribute to reduce uncertainties in parameters used for project design to a level more acceptable in managing risk.

4.2. Introduction

There are relatively few field capping projects that have been implemented *(10-13)*. Thus, guidance for project design from theoretical and practical aspects is not well established. Our literature-derived model simulations *(15)* shown in chapter 3 demonstrated the substantial uncertainties in parameters used for project design. Thus, experiments were conducted to provide more bounded values for model predictions of field performance based upon the parameters identified as most sensitive to model output in the Monte Carlo analyses. The partitioning of contaminants between the cap material solid phase and the aqueous porewater phase was investigated in this study to decrease the uncertainty in this parameter. Column experiments were performed to evaluate cap performance to minimize the release of contaminants. Simulations using the models described in chapter 3 were performed with measured K_d and cap parameters (porosity, density and hydraulic conductivity) values, and results compared to the literature-derived model simulations shown in chapter 3.

Sorption describes the attachment and release of compounds between the aqueous and particulate phases. There are a multitude of mechanistic and empirical models to describe the solid-liquid sorption process. At equilibrium, these are frequently referred to as isotherms as their measurements are performed at constant temperature. Mechanistic models include the Langmuir and Brunaur, Emmett, Teller (BET) isotherms, and empirical or semi-mechanistic models include the Freundlich and linear equilibrium partitioning isotherms. The latter is the simplest model as the partitioning is a direct linear function of concentration (i.e. the partitioning

parameter does not change as a function of concentration). The partitioning coefficient (K_d) is the ratio of concentrations of a compound in the two phases of a mixture of two immiscible phases at equilibrium. More specifically in our case it is the ratio of sorbed metal concentration on the solid matrix (mg kg^{-1} of sorbing material) to dissolved metal concentration in the aqueous phase (mg L^{-1} of solution) at equilibrium.

Limitations of assuming a linear mathematical model consist in not imposing a limit to the amount of pollutant that can be sorbed on the solid matrix, and a limited dataset may lead to the conclusion that the relation is linear when it is actually not. For non-linear sorption, partitioning is a function of concentration. Freundlich and Langmuir models are most frequently used to represent such adsorption isotherms:

Freundlich: $$C_{sorb} = K_d C_w^f \text{ or } logC_{sorb} = logK_d + flogC_w \quad (4.1)$$

Langmuir: $$C_{sorb} = \frac{M_s K_d C_w}{1+K_d C_w} \quad (4.2)$$

Where C_{sorb} (mg kg of $sorbent^{-1}$) is the contaminant equilibrium concentration on the sorbent phase; C_w (mg L^{-1}) is the contaminant equilibrium concentration in the aqueous phase; K_d is the solid-aqueous partitioning coefficient (L kg^{-1}) and M_s is the maximum mass of contaminant that the adsorptive material can hold (mg kg of $sorbent^{-1}$). For the Freundlich model, when $f = 1/n = 1$, the relationship is linear; when $0<f<1$ (or $n>1$) there is a higher affinity of the contaminant for the sorbent; when $f>1$ (or $0<n<1$), there is a lower affinity of the contaminant for the sorbent relative to the affinity of the contaminant for the solution (Figure 4.1). The Langmuir model describes the high affinity of the contaminant for the sorbent at low aqueous concentration with lower or invariant affinity at higher contaminant aqueous concentrations *(47)*.

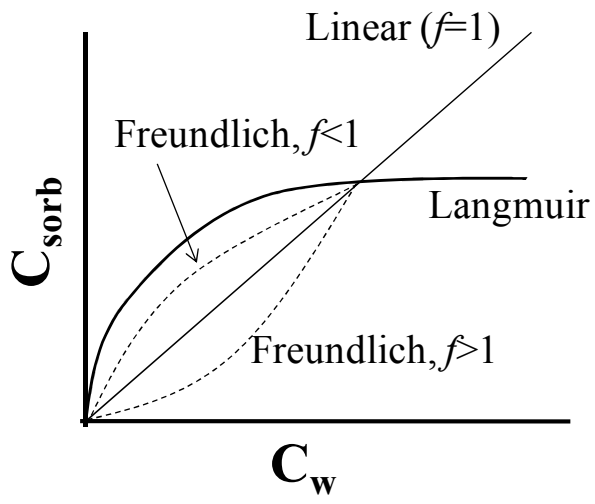

Figure 4.1. Isotherm models (adapted from Alvarez and Illman *(47)*).

In the case of organic compounds, the partition coefficient is a measure of the degree of the hydrophobicity of the sorbate. Hydrophobic compounds (high partition coefficients) partition preferentially to hydrophobic materials, while hydrophilic compounds partition preferentially to the water phase. Compilations of K_d values for many organic contaminants of concern have been performed, and there are numerous reports in the literature of free energy relationships used to predict unknown K_d for compounds and sorbents (e.g. the well known Karickhoff equation *(48)*).

Solid-aqueous phase partitioning is not as simple for heavy metal contaminants, as K_d values are also a function of geochemical characteristics of the solid matrix and the porewater composition, pH and nature and concentration of sorbents *(49)*. Despite these difficulties, attempts have been made to compile K_d data for some metals (Table 4.1) *(49-51)*. More research is needed, however, to decrease the uncertainty in this parameter as demonstrated by our previously reported modeling results *(15)*. For example, uncertainties in K_d value for Cr affect Cr predicted reference breakthrough times by as long as several hundred years *(15)*. Such uncertainties dramatically impact risk-based cap design.

Table 4.1. Summary of solid-aqueous partitioning coefficients for selected metals in the cap media[a]

Cap material	log K_d (L kg^{-1})									
	Cd		Pb		Cr		As		Ag	
	μ	σ	μ	σ	μ	σ	μ	σ	μ	σ
Sand	2.6	1.4	3.4	1.4	2.1	1.7	2.4	0.7	3.6	1.1
Apatite	3.5	0.4	3.9	0.6	3.4	1.0	1.4	0.4	3.6	1.1
GAC	2.6	1.4	2.8	0.	1.0	1.7	1.4	0.4	3.6	1.1
Organoclay	3.6	1.5	2.8	0.4	3.1	0.8	1.7	2.4	3.6	1.1

[a] Sources: *(49-51)*. When K_d literature data was not available, K_d is shown for sediment as the solid phase (instead of the specific cap material).

Thus, the first objective of this study was to measure K_d values for adsorption of Cd and As on the four cap materials: sand, organoclay (OC), apatite (AP), and granular active carbon (GAC), and compare the measured K_d values to literature values (Table 4.1). A second objective was to characterize cap material properties (surface area, porosity, density and hydraulic conductivity) to decrease uncertainties and re-perform simulations using the model described in chapter 3. As experimental validation is a much larger undertaking than model simulation, I limited the number of test compounds and active cap materials. Adsorption isotherm and column experiments were performed for Cd, a cationic metal at circumneutral pH, and As, an anionic metal at circumneutral pH, with only four of the five cap materials in the modeling study. The metals Cd and As were chosen because Cd is classified as a class B1 carcinogen (i.e., probably human carcinogen) and inorganic As is classified as a Class A carcinogen (i.e., known human carcinogen) by the U.S. Environmental Protection Agency (USEPA).

4.3. Materials and Methods

Organoclay (PT-1E powdered organoclay), apatite (EC-MB hydroxyl-apatite, bone char) (both from Biomin Inc., Ferndale, MI), sand, and granular activated carbon (GAC, 8325 from Buy.Activated.Charcoal.com, Crawford, NE, USA) were used in the experiments. Apatite was size reduced down to <0.3 mm by mortar and pestle and sieved with 0.3 mm standard sieve. Sand collected from the 12th street beach on Lake Michigan (Chicago, IL) was sieved in 0.3 – 0.5 mm standard sieves.

Isotherm study. Adsorption isotherm experiments of Cd, a cationic metal at circumneutral pH, and As, an anionic metal at circumneutral pH, were performed with four cap materials (sand, OC, AP and GAC). Shredded tires were not tested as the results from the simulations demonstrated its relatively poor performance in minimizing metal release to the water column (see chapter 3, also Viana et al. *(15)*). Adsorption isotherms were performed in serum bottles filled with 100mL of aqueous metal solution. Different masses of sorbent were added based upon their predicted sorption capacity: 2 g of sand, 0.5 g of AP, 2 g of GAC and 0.5 g of OC were added to each bottle to ensure a range of C_w values that could be measured. The concentrated metal solution was composed of $CdCl_2$ (0.85 mM) and $NaAsO_2$ (0.20mM) in a synthetic freshwater sediment porewater. Synthetic fresh porewater solution was based upon De Schamphelaere et al. *(256)*, Heijerick et al. *(57)* and Taillefert et al. *(257)* and composed of $NaHCO_3$ (1 mM), $CaCl_2.2H_2O$ (0.25 mM), $MgSO_4.7H_2O$ (0.1 mM) and $Fe(NH_4)_2(SO_4)_2.6H_2O$ (0.2 mM) (Fisher Scientific, Pittsburgh, PA) added to de-ionized water. Different volumes of the concentrated metal solution were added to each serum bottle with a total of 20 bottles (five ranges of concentrations and four cap materials, Table 4.2). The pH was adjusted to 6.8 by

adding 1N NaOH or 1N HCl. MOPS-buffer (3-[N-morpholino] propane sulfonic acid, sodium salt from Sigma-Aldrich, M-9381) was added to maintain a constant pH during the experiment. This synthetic buffer is designed to be non-reactive with metals *(54, 57)* to replace the more typically used phosphate, carbonate, or organic buffers that would affect metal speciation and thus solubility. With the exception of OC incubations, the maximal pH change after five weeks was 0.2 pH units. OC had an increase of 0.2-0.59 pH units after five weeks incubation. Sodium azide (1 mL of a 0.1 M solution) was added to prevent microbial growth. The serum bottles were heated and sparged with N_2, sealed, and incubated in a dark rotating tumbler for five weeks at 20 °C.

Table 4.2. Input mass and pH change in test system consisting of water and sand, GAC, OC and AP capping material slurry.

	Sand					GAC				
	B1	B2	B3	B4	B5	B6	B7	B8	B9	B10
C_{As} (mg L^{-1})	0.15	0.60	1.2	7.5	15	0.15	0.60	1.2	7.5	15
C_{Cd} (mg L^{-1})	1.0	3.8	7.7	48	96	1.0	3.8	7.7	48	96
pH at t=0	6.8	6.8	6.8	6.8	6.8	6.8	6.8	6.8	6.8	6.8
pH after 5 weeks	6.9	6.64	6.58	6.44	6.38	7.24	7.14	7.03	6.84	6.54
	OC					**AP**				
	B11	B12	B13	B14	B15	B16	B17	B18	B19	B20
C_{As} (mg L^{-1})	0.15	0.60	1.2	7.5	15	0.15	0.60	1.2	7.5	15
C_{Cd} (mg L^{-1})	1.0	3.8	7.7	48	96	1.0	3.8	7.7	48	96
pH at t=0	6.8	6.8	6.8	6.8	6.8	6.8	6.8	6.8	6.8	6.8
pH after 5 weeks	7.4	7.39	7.24	6.97	7.24	6.9	6.76	6.7	6.55	6.5

After aging, a supernatant sample (20 mL) from each of the 20 bottles was collected in falcon tubes (Fisher Scientific, Pittsburgh, PA), preserved using nitric acid, sealed and refrigerated at 4° C for transfer to a National Environmental Laboratory Accreditation Program (NELAP)-certified laboratory for analysis of Cd and As. The metals Cd and As were analyzed according to USEPA SW-846 method 6020 *(258)* by Inductively Coupled Plasma Mass

Spectrometry (ICP-MS). Sorbent samples were also analyzed for Cd and As C_{sorb} according to USEPA SW-846 method 6020 *(258)*.These data were used to determine the adsorption isotherm behavior of each metal by comparing C_{sorb} to C_w (eq. 4.3 and 4.4) and the mass balance on sorbate:

$$V_w C_w + M_{sorb} K_d C_w = M_{total} \tag{4.3}$$

Where V_w is the solution volume (L); C_w (mg L^{-1}) is the metal equilibrium concentration in the liquid phase; M_{sorb} is the mass of sorbent added to the bottle (kg); and M_{total} is the total mass of metal. C_{sorb} can then be obtained from equation 4.3:

$$C_{sorb} = \frac{M_{total} - C_w V_w}{M_{sorb}} \tag{4.4}$$

The cap material porosity (φ_e), bulk density (ρ) and hydraulic conductivity (k_h) were measured in the laboratory as described elsewhere *(16, 259)* and values are shown in Table 4.3. Nitrogen adsorption and desorption isotherms, surface area and pore volumes of the tested cap materials were determined by Micrometrics Analytical Services (Norcross, GA). Nitrogen adsorption was performed at 77 K with 10 s equilibration intervals. Data were collected from a relative pressure (p/p_0) of 0.01 to 0.99. Total surface area was calculated using the Brunauer Emmett Teller (BET) adsorption isotherm model *(260-261)* for the nitrogen isotherm data.

Table 4.3. Measured transport parameters for cap material used in this study[a]

Cap material	φ_e		ρ (kg·L^{-1})		k_h (m·yr^{-1})	
	μ	**σ**	**μ**	**σ**	**μ**	**σ**
Sand	0.35	0.008	1.63	0.003	4,300	2,000
Apatite	0.43	0.04	1.33	0.05	27	7
GAC	0.70	0.02	0.57	0.005	76	20
Organoclay	0.45	0.07	0.80	0.04	21	7

[a] Source: *(16)*

Column study. The column experiments were performed using Omnifit adjustable columns with L×I.D. 100×10 mm from Fisher Scientific (Pittsburgh, PA). A low-pressure diaphragm gauge (1.6% Accuracy, 1/4" NPT bottom with 0 - 5 psi range) and a brass-case dual-scale gauge (2% Accuracy 3-1/2" Dial, 1/4" NPT Male Bottom, 0-15 psi, both from McMaster-Carr Co. (Robbinsville, NJ), were used to provide uniform hydraulic gradients across the column. Cap thickness and flowrate were varied based on predicted behavior of each cap material (e.g. metal breakthrough in a sand column is expected to be much faster than through OC or apatite). Filters were used at the end of each column to prevent sorbent material from exiting the column. A peristaltic pump Masterflex® console driver with a L/S® Easy-Load® II pump head (flow rates of 0.06 to 2300 mL min^{-1}) from Cole-Parmer (Vernon Hills, IL) was used to pump the metal solution through the column (Figure 4.2).

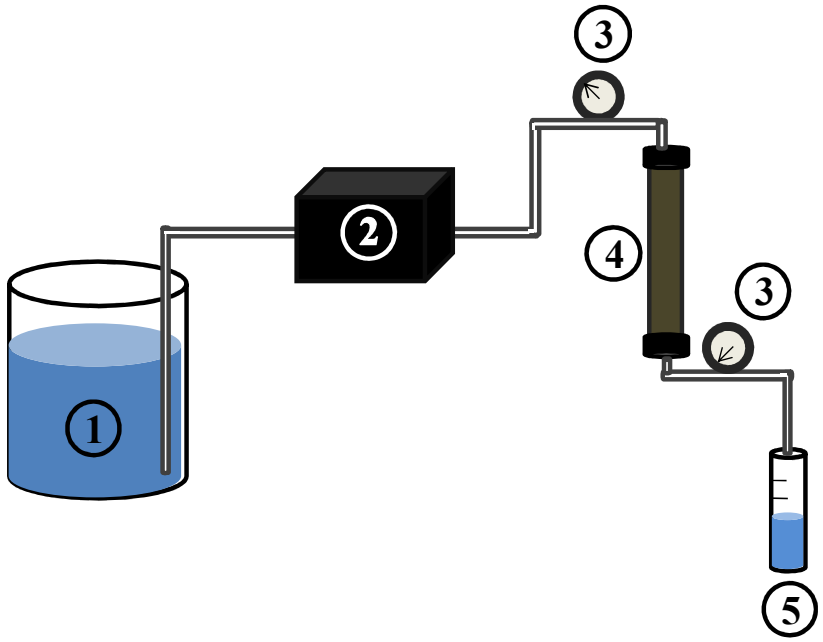

Figure 4.2. Schematic of the column test system. Shown are (1) feed vessel containing metal influent solution, (2) peristaltic feed pump, (3) upstream and downstream pressure gauges, (4) test column and (5) effluent graduated cylinder to measure volume of sample.

The experiments were performed for the cationic metal Cd and the anionic metal As. The metal solution was prepared as described in the adsorption isotherm experiment. A mass of 0.7, 0.7, 0.7 and 0.27 g of sand, AP, GAC and OC were packed in the column with a correspondent cap thickness of 0.4, 0.6, 1.8 and 0.4 cm, respectively. The cap thickness was varied to achieve full contaminant breakthrough in each cap material in a reasonable time-frame. However, different cap thicknesses made comparisons of breakthrough curves between columns based on the time scale more difficult, and thus number of pore volumes (PV) of the solution passed through the cap material with thickness *x* (cm) in time *t* (min) was used instead *(262)*:

$$PV = \frac{Qt}{Ax\varphi} \qquad \text{(eq. 4.5)}$$

Where: Q is the flow through the cap material (mL min^{-1}); A is the cross-sectional area (cm^2); and φ is the porosity. Therefore, flow was monitored during the experiments to calculate PV. Before running the metal solution through the system, de-ionized water was run through the column until negligible conductivity was detected from the effluent. Effluent samples were collected in intervals chosen according to the time expected for metal breakthrough in each of the cap materials. Flow rates were adjusted using a peristaltic pump by increasing water flow through the column (and thus hydraulic gradient). The system is designed to have the flexibility to increase or decrease flow by orders of magnitude and cap thickness up to 10 cm to properly run the experiments in a reasonable time frame.

Comparison of laboratory data for the transport through the column was performed in dimensionless form by calculating the Peclet number, which is a measure of the relative importance of advection to dispersion (mixing) (eq. 4.6) *(194)*. By using this measure, the column experiments with each capping material may be compared. Experimental parameters

were selected to achieve a Peclet number P_L similar for a given metal and all cap materials. Table 4.4 shows P_L values based on a range of possible hydraulic gradients d_h/d_x.

$$P_L = \frac{xv}{D_{obs}}, \quad \text{where} \quad v = \frac{K_h \frac{d_h}{d_x}}{R\varphi_e} \;, \quad R = 1 + K_d \frac{\rho}{\varphi_e} \quad \text{and} \quad D_{obs} = \frac{D_{mol}\varphi_e{}^{4/3}}{R} \qquad \text{(eq. 4.6)}$$

Where: v is the chemical velocity in the porewater (m yr^{-1}) corrected by the retardation factor R; D_{obs} is the observed diffusivity of each contaminant in each cap (m^2 yr^{-1}); and D_{mol} is the contaminant molecular diffusivity ($m^2 \cdot yr^{-1}$).

Substituting v and D_{obs} equations in the P_L equation, we obtain:

$$P_L = \frac{xk_h\left(d_h/d_x\right)}{D_{mol}\varphi_e{}^{7/3}} \qquad \text{(eq. 4.7)}$$

Table 4.4. Peclet number for As and Cd and the tested cap materials based on different hydraulic gradients.

	Sand (0.4 cm)		Apatite (0.6 cm)		GAC (1.8 cm)		OC (0.4 cm)	
Compound	***dh/dx***	***P_L***	***dh/dx***	***P_L***	***dh/dx***	***P_L***	***dh/dx***	***P_L***
As	10	52,156	10	304	10	823	10	142
	100	521,562	100	3,039	100	8,231	100	1,417
	1,000	5,215,624	1,000	30,387	1,000	82,312	1,000	14,171
	10,000	52,156,245	10,000	303,873	10,000	823,115	10,000	141,706
	100,000	521,562,447	100,000	3,038,729	100,000	8,231,152	100,000	1,417,055
Cd	10	87,770	10	511	10	1,385	10	238
	100	877,695	100	5,114	100	13,852	100	2,385
	1,000	8,776,954	1,000	51,136	1,000	138,515	1,000	23,846
	10,000	87,769,539	10,000	511,363	10,000	1,385,154	10,000	238,465
	100,000	877,695,395	100,000	5,113,631	100,000	13,851,543	100,000	2,384,648

The experiments were planned based on simulation results (Table 4.5) performed to predict the time for breakthrough of As and Cd in each cap material using the model described on chapter 3 (see also Viana et al. *(15)*) and parameter values shown in tables 4.1 and 4.3. Hydraulic gradient value were selected to result on a Peclet number P_L similar for a given metal and all cap materials.

Table 4.5. Time for complete breakthrough (C/C_0=1) and Peclet number (P_L) considering a 0.4, 0.6, 1.8 and 0.4 cm cap thickness for sand, apatite, GAC and OC. A hydraulic gradient of 2, 300, 150 and 800 m m^{-1} was considered for sand, apatite, GAC and OC simulations, respectively.

Compound	Time for complete breakthrough the capping material (min) and P_L							
	Sand		Apatite		GAC		OC	
	t (min)	P_L	t (min)	P_L	t (min)	P_L	t (min)	P_L
As	110	10,500	16	9,000	14	12,000	10	11,500
Cd	170	17,500	1800	15,500	200	20,500	800	19,000

Effluent samples for each column experiment were collected in falcon tubes (Fisher Scientific, Pittsburgh, PA), preserved using nitric acid, sealed and refrigerated at 4° C for transfer to a NELAP-certified laboratory for analysis of Cd and As. The metals Cd and As were analyzed according to USEPA SW-846 method 6020 *(258)* by ICP-MS.

The methodology proposed by Buergisser et al. *(52)* was used to confirm the isotherm behavior. The isotherm is linear if the adsorption and desorption front have exactly the same shape, convex (i.e. Freundlich $0<f<1$ or $n>1$) if there is a substantial tailing in the desorption front or concave (i.e. Freundlich $f>1$ or $0<n<1$) if the adsorption front is diffuse while the desorption front is sharp (Figure 4.3).

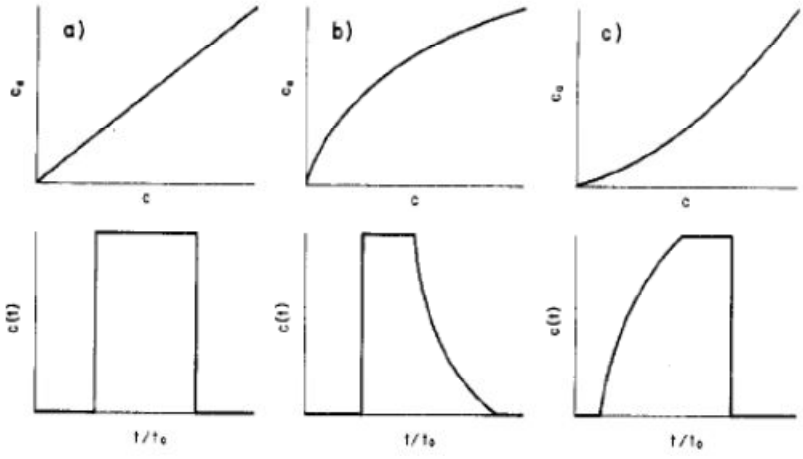

Figure 4.3. Column experiment breakthrough curve of a step concentration change without dispersion effects for (a) linear, (b) convex and (c) concave isotherms *(52)*.

4.4. Results and Discussion

Adsorption Isotherm Results. As and Cd were selected for the isotherm study representing an anionic and a cationic metal. Compound aqueous phase concentrations were measured and plotted as a function of calculated solid phase concentration (Figure 4.4). Also shown are linear regression fits to yield the K_d as the slope of the trendline (Table 4.6). The relatively low coefficient of determination (R^2) values demonstrate that the metals As and Cd may have non-linear adsorption isotherms (Figure 4.4). The results demonstrate that sand and GAC have similar sorption capacity for As, while GAC performs significantly better than sand for Cd. Apatite and OC exhibited more sorption capacity than sand and GAC with OC exhibiting slightly higher sorption capacity for As.

Table 4.6. Linear K_d and R^2 for contaminant-cap equilibrium isotherms.

	As		Cd	
Cap material	K_d	R^2	K_d	R^2
Sand	80.8	0.76	417	0.85
Apatite	354	0.83	1787	0.86
GAC	90.1	0.73	880	0.86
OC	436	0.79	1819	0.78

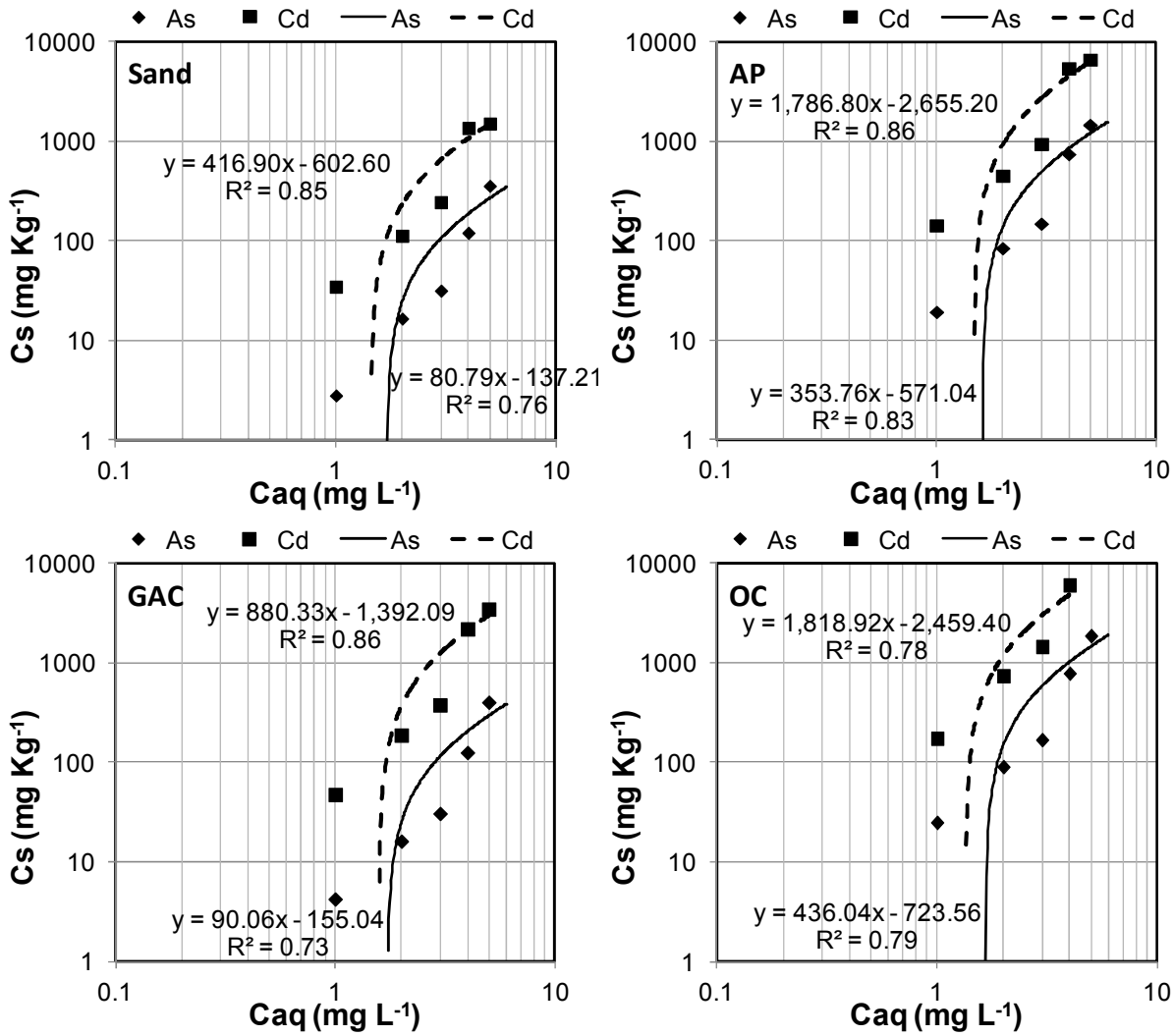

Figure 4.4. Isotherm testing of aqueous concentration versus solid phase concentration with a linear fit of As and Cd in cap materials sand (upper left), apatite (upper right), GAC (lower left), and organoclay (lower right).

As the linear isotherm model does not describe well the data, the Freundlich model was used (Figure 4.5 and Table 4.7).

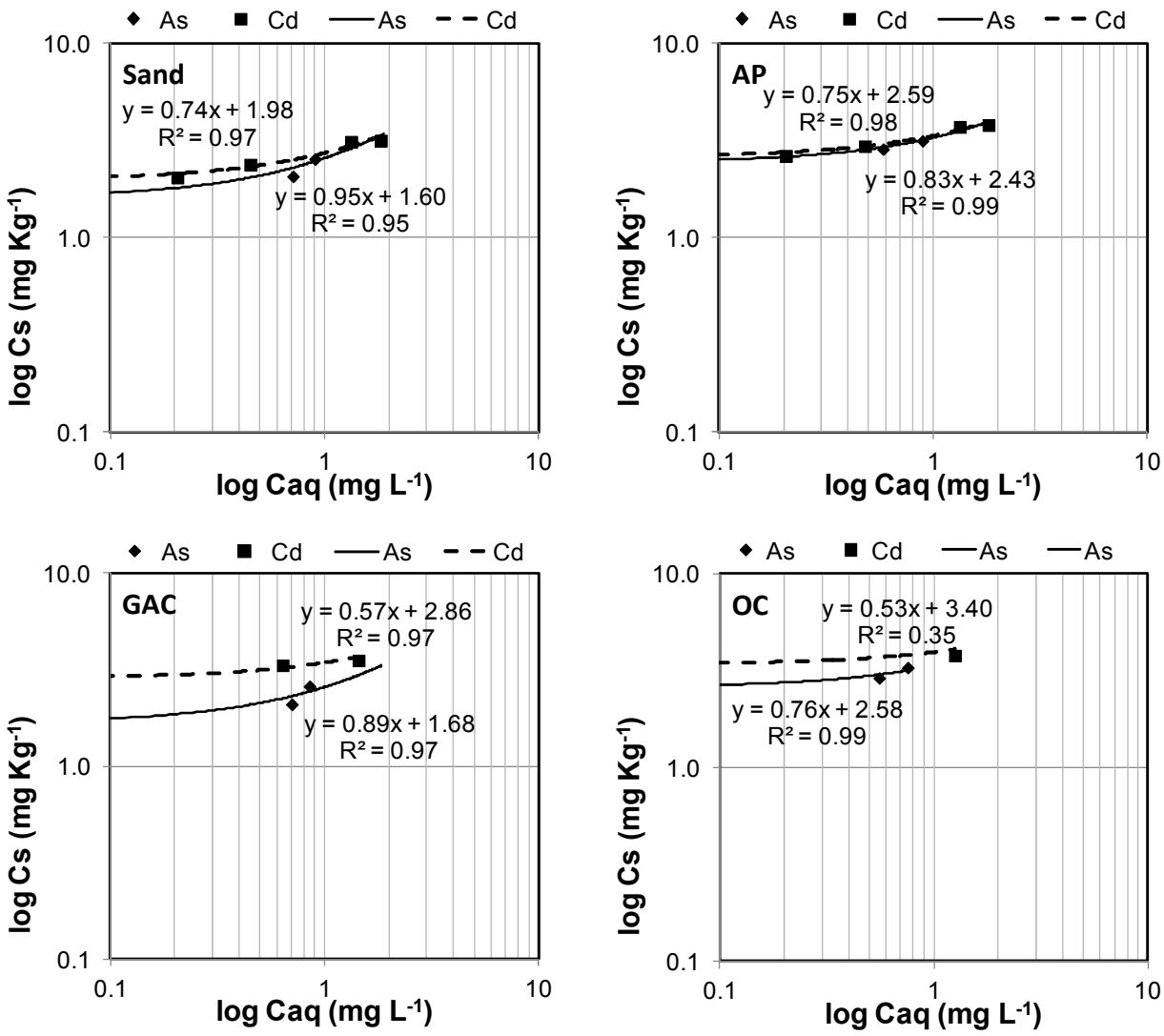

Figure 4.5. Freundlich isotherm plots for adsorption of As and Cd in cap materials sand (upper left), apatite (upper right), GAC (lower left), and organoclay (lower right).

Although none of the caps exhibited a high sorption capacity for As, OC and apatite performed clearly better than sand and GAC (Table 4.7). Surprisingly, apatite exhibited a relatively low sorption capacity compared to OC for Cd, which differs from the literature values were a sound performance was observed for both apatite and OC (table 4.1). Note, however, the low R^2 for K_d of Cd in OC. With the exception of the latter, the Freundlich isotherm model fits

the data with $R^2 \geq 0.95$. The *n* values were higher for Cd, which demonstrates its higher affinity for the cap materials at lower concentrations and non-linear isotherm behavior.

Table 4.7. Freundlich isotherm model parameters for adsorption of As and Cd in cap materials sand, apatite, GAC and OC.

Cap material	As					Cd				
	Log K_d		*n*		R^2	*Log* K_d		*n*		R^2
	μ	σ	μ	σ		μ	σ	μ	σ	
Sand	1.60	0.09	1.05	0.13	0.95	1.98	0.08	1.36	0.14	0.97
Apatite	2.43	0.04	1.20	0.07	0.99	2.59	0.07	1.34	0.12	0.98
GAC	1.68	0.07	1.13	0.11	0.97	2.86	0.07	1.75	0.17	0.97
OC	2.58	0.04	1.31	0.08	0.99	3.40	0.35	1.89	1.48	0.35

Measured values were compared to the literature values shown in table 4.1. The K_d results indicate close agreement between the experimental and literature K_d values with the exception of As and Cd with apatite (Figure 4.6). Apatite was expected to exhibit a higher sorption capacity for Cd because in the apatite chemical formula ($Ca_5(PO_4)_3(OH, F, Cl)$) Ca can be easily replaced by Cd *(125, 138)*. Isomorphous substitution and diffusion are more likely to occur for cations with ionic radii close to that of Ca^{2+}. Ca can be substituted with ionic radii between 0.80 and 1.35 Å, which includes Cd (0.97 Å) *(138)*. However, this was not verified in these experiments given the low measured K_d value for Cd with apatite compared to the literature value. On the other hand, the literature may be underestimating the apatite capacity to sorb As because PO_4 can be substituted with oxyanion-forming elements with ionic radii between 0.29 and 0.60 Å, which includes As (0.46 Å) *(138)*.

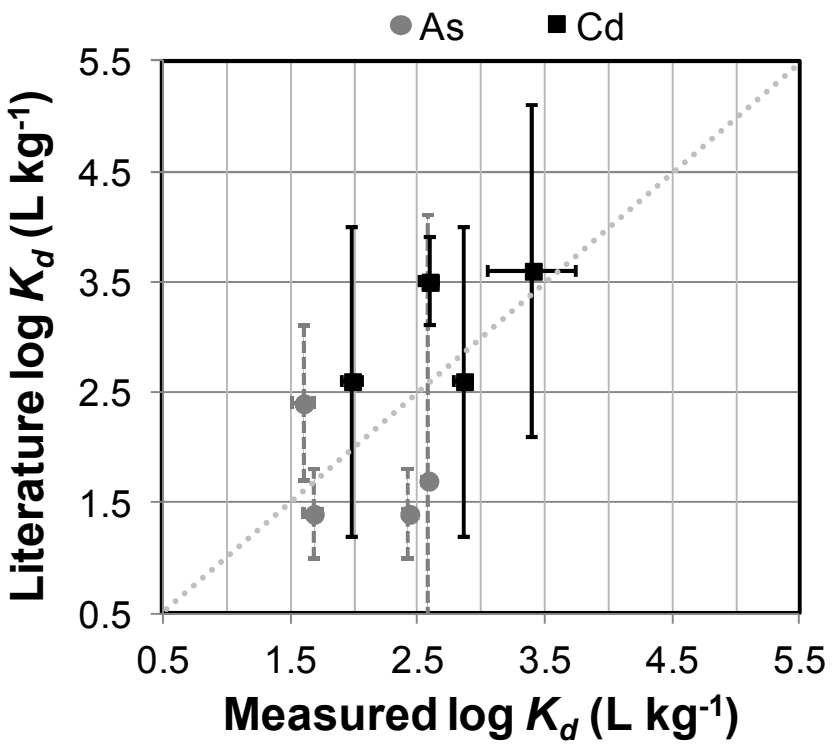

Figure 4.6. Comparison of K_d between measured and literature values.

The nitrogen adsorption and desorption isotherms, porosimetry surface area and pore volumes for the tested cap materials are shown in figures 4.7-4.9 and table 4.8. Sand and OC have low surface areas of 0.41 and 1.0 m^2 g^{-1}, respectively, by BET analysis. On the other hand, GAC has a surface area of 1200 m^2 g^{-1}. The average pore diameter was determined to vary between 27 (for GAC) and 254 Å (for OC). Clearly GAC is nanoporous with a strong sorption capacity even in the low pressure region. A sharp adsorption occurs when the pressure is higher than 0.9 P/P_0 for apatite and OC. The total volume of nitrogen adsorbed varied from 1.1 to 350 cm^3 g^{-1} STP for sand and GAC, respectively. The high surface area of GAC may have contributed to its higher K_d values compared to sand. However, GAC K_d values for As and Cd are still lower than the OC ones (Table 4.7). This is likely due to the modification of clay to increase its ion exchange capacity, which increases its efficiency to sorb metal contaminants.

The smectite group is a particularly promising clay group to use in metal sequestration. Clay minerals that have properties mainly governed by smectites are known as bentonites, where the montmorillonite smectite sub-group is the major constituent. This kind of clay usually presents the highest cation exchange capacity. Additionally, this kind of clay facilitates insertion of large ion species into the lattice, which act as pillars, propping apart the clay layers and creating a micropore system increasing its surface area *(165)*. Ions, such as Na and Ca, can be exchanged for cations like Cd *(85)*. This would help to explain the high K_d for Cd in OC.

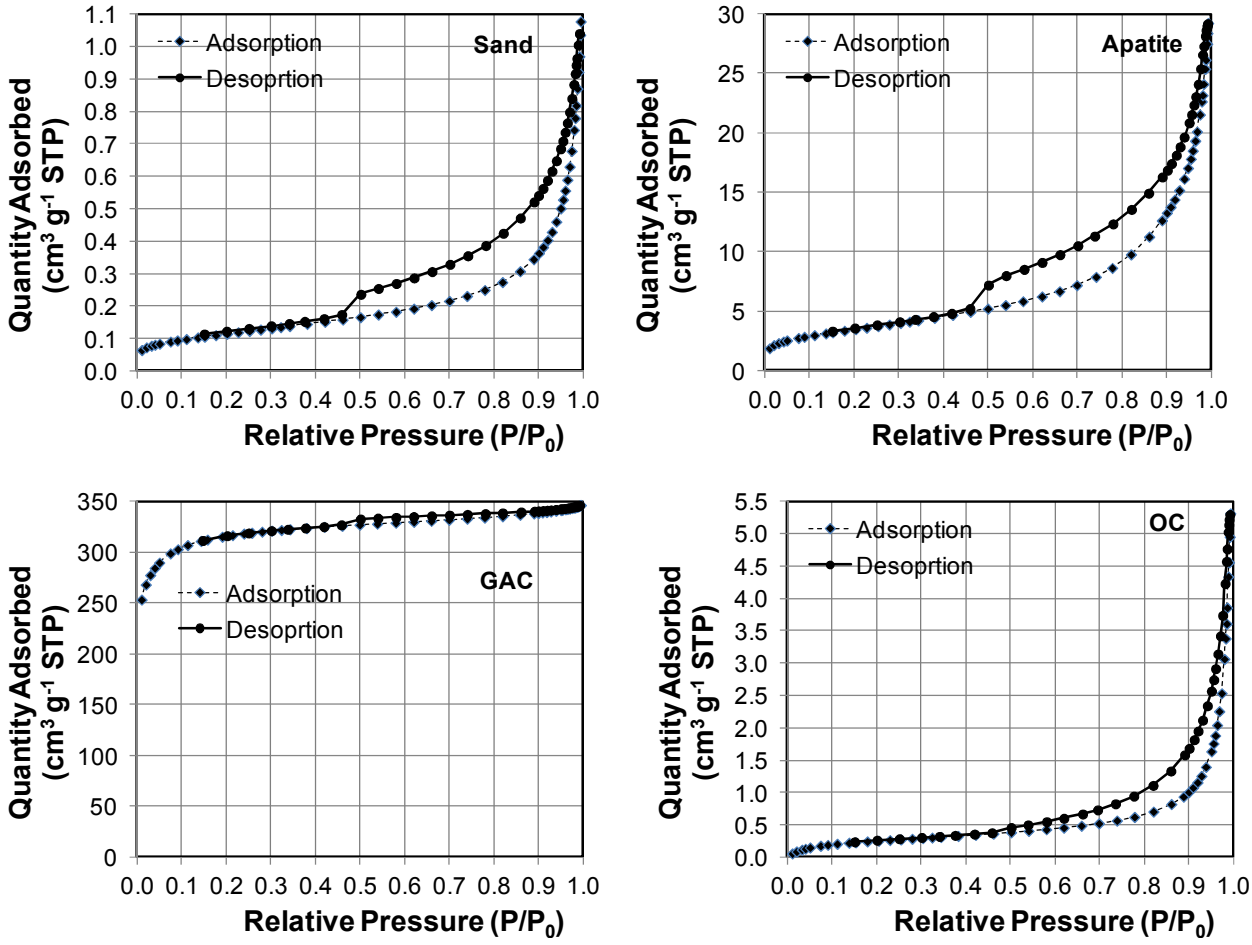

Figure 4.7. N_2 adsorption and desorption isotherms for active capping amendments sand (upper left), apatite (upper right), GAC (lower left), and organoclay (lower right). Y axes have different scales. Note hysteresis in the desorption isotherms.

Table 4.8. Porosimetry surface area and pore volumes for active capping amendments.

	Sand	Apatite	GAC	Organoclay
BET SA ($m^2 g^{-1}$)	0.412	12.5	1200	1.00
17-3000 Å SA[1] ($m^2 g^{-1}$)	0.465	15.1	207	1.34
External SA[2] ($m^2 g^{-1}$)	0.355	13.6	40.4	0.98
Micropore SA[2] ($m^2 g^{-1}$)	0.057	0	1170	0.022
Micropore PV[2] ($cm^3 g^{-1}$)	$2.7x10^{-5}$	0	0.48	0
17-3000 Å PV[1] ($cm^3 g^{-1}$)	$1.7x10^{-3}$	0.047	0.14	0.0085
Avg. Pore Diameter[1] (Å)	142	125	27	254

[1]-BJH method using standard Halsey equation
[2]-t Plot method using Harkins and Jura equation

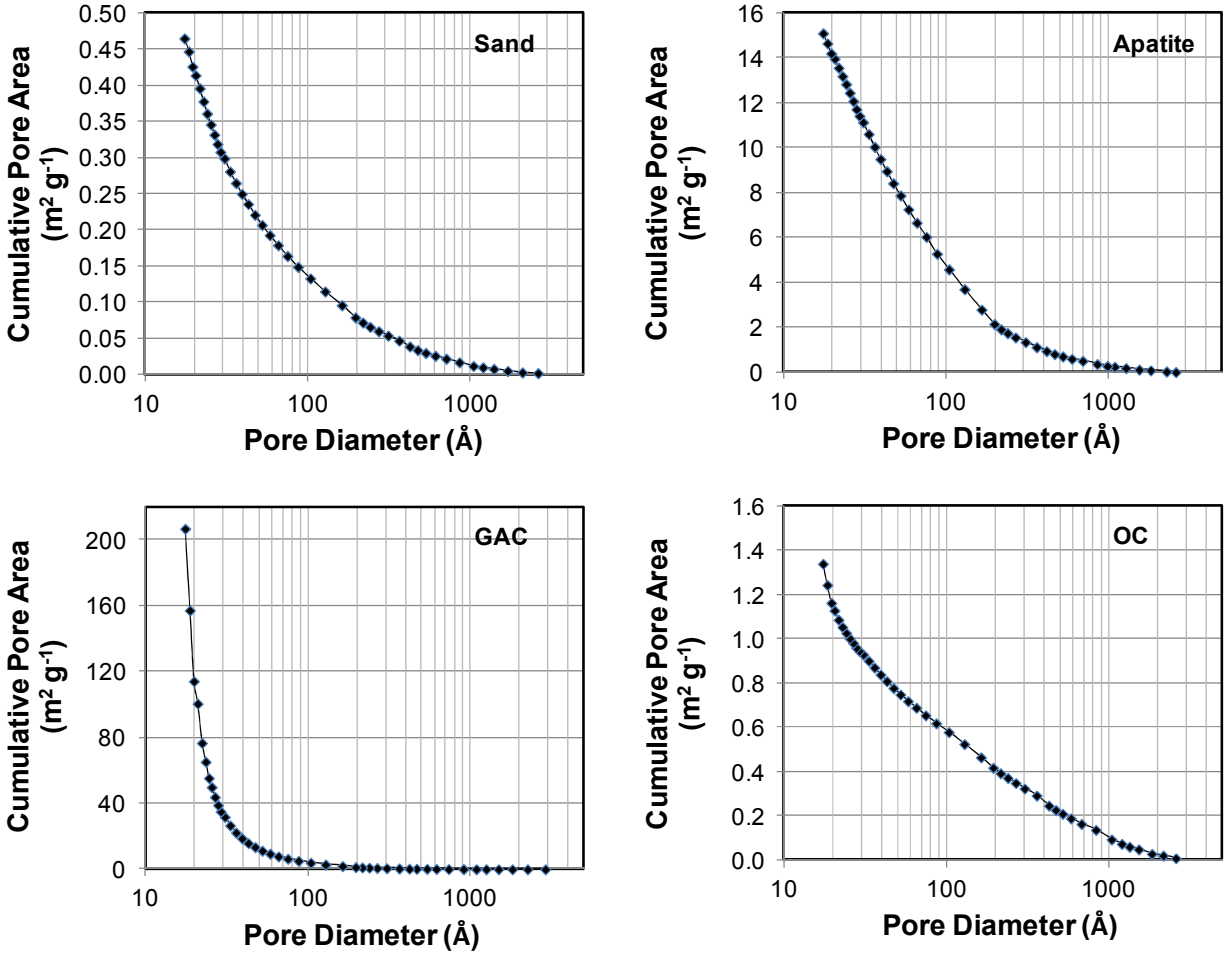

Figure 4.8. Cumulative pore area versus pore diameter from N_2 adsorption isotherms for active capping amendments sand (upper left), apatite (upper right), GAC (lower left), and organoclay (lower right). Y axes have different scales. Pore surface areas calculated from BJH standard Halsey equation.

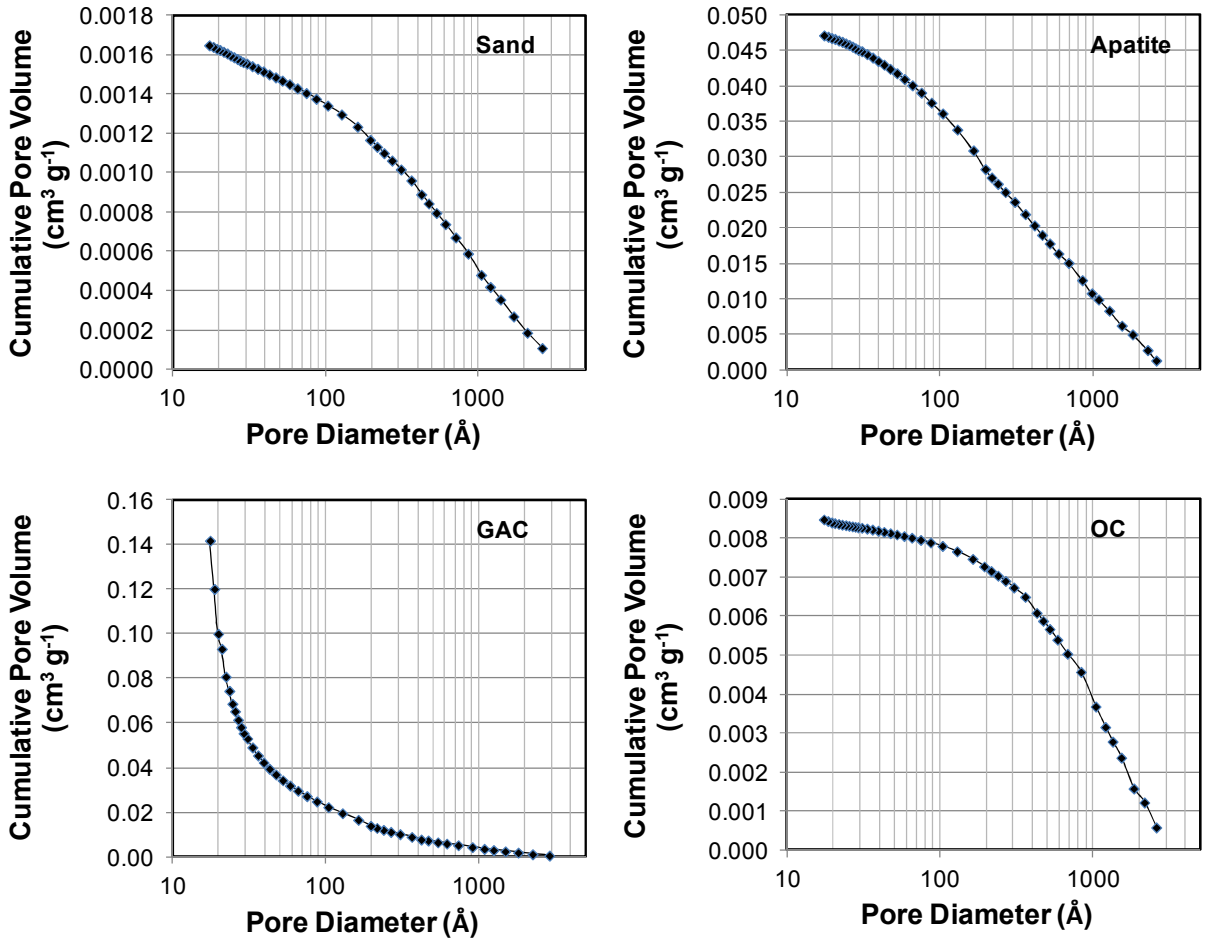

Figure 4.9. Cumulative pore volume versus pore diameter from N_2 adsorption isotherms for active capping amendments sand (upper left), apatite (upper right), GAC (lower left), and organoclay (lower right). Y axes have different scales. Pore volumes calculated from BJH standard Halsey equation.

Colum Study Results. Not unexpectedly, apatite performed very well for Cd (Figure 4.11) with full breakthrough after 12000 pore volumes likely due to the Cd capacity to replace Ca in the apatite chemical formula ($Ca_5(PO_4)_3(OH, F, Cl)$) *(125, 138)*. Surprisingly, sand did not exhibit such a poor sorption capacity for Cd with full breakthrough after 4000 pore volumes. Based on the column experiment results, GAC performed poorly for both metals. There is a substantial tailing in the desorption front for the Cd breakthrough curve in the column with GAC

and for the As breakthrough curve in the column with apatite (Figures 4.10 and 4.11). This suggests a convex isotherm with $n>1$ *(52)*, which is in agreement with the obtained log K_d values using the Freundlich model. The As breakthrough curve for the column with sand exhibited the same shape for the adsorption and desorption front, indicating the isotherm is linear. Indeed, The Freundlich n is very close to 1.0 (1.05±0.13) confirming the isotherm linearity.

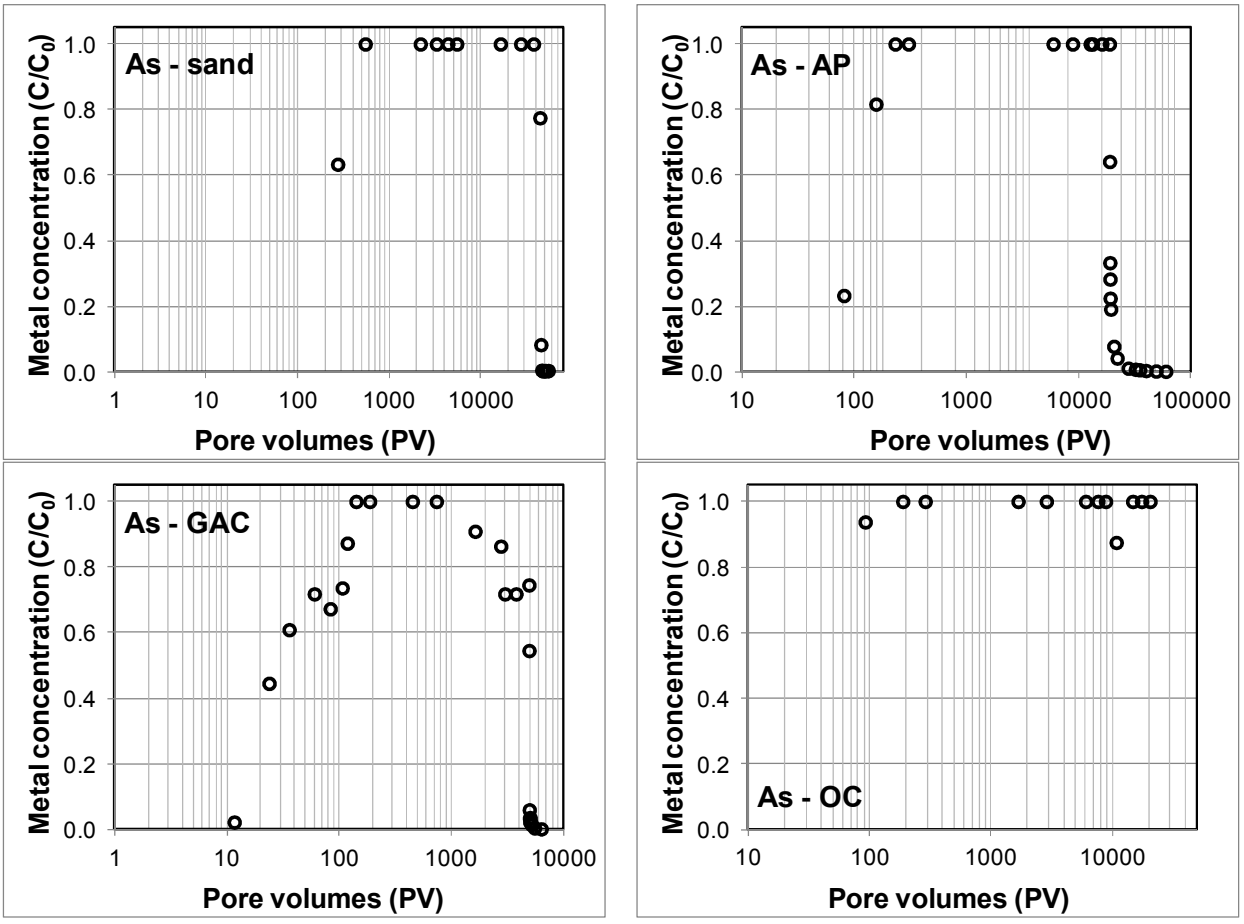

Figure 4.10. Arsenic breakthrough curve (C/C_o) with pulse input in active capping column of sand (upper left), apatite (upper right), GAC (lower left), and organoclay (lower right). Note different X axes scales.

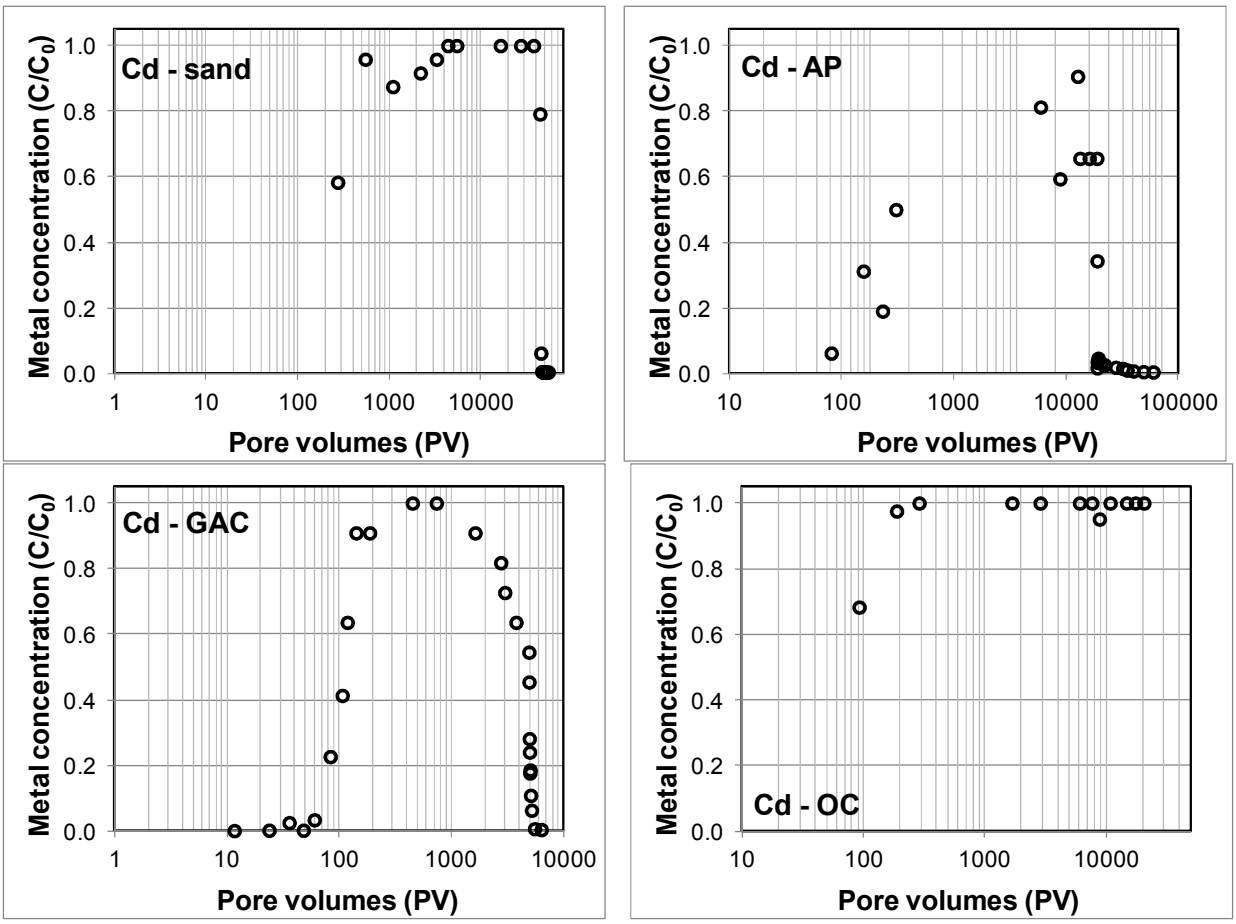

Figure 4.11. Cadmium breakthrough curve (C/C_o) with pulse input in active capping column of sand (upper left), apatite (upper right), GAC (lower left), and organoclay (lower right). Note different X axes scales.

Comparison between model simulations with measured and literature values. The literature-derived model simulations shown in chapter 3 (see also Viana et al. *(15)*) were compared to simulations performed with measured K_d and cap parameters (porosity, density and hydraulic conductivity). The Monte Carlo method described in chapter 3 was used to obtain the distribution of model output based on the range of parameter values. Matlab (v. 7.12, MathWorks, Inc.) was used as the Monte Carlo platform. Analyses were performed for 50000 draws of the random variables K_d, φ_e, ρ and k_h to obtain the distribution of C/C_o over time within the 95% confidence interval (CI).

Overall agreement between the literature-derived model simulations and the simulations performed with measured parameters was achieved for most metals and cap material combinations, although the literature-derived model simulation graphs exhibit higher uncertainties likely due to the higher standard deviations for the literature K_d values and some of the cap parameters (Figure 4.12 to 4.15). Overall, the sand cap performed best under diffusion due to the greater diffusive path length. Apatite and sand performed relatively poorly for Cd in the model simulations performed with measured parameters in comparison to the literature-derived simulations. This can likely be explained by lower measured log K_d values (2.6 and 2.0 for apatite and sand) in comparison to literature values (3.5 and 2.6 for apatite and sand).

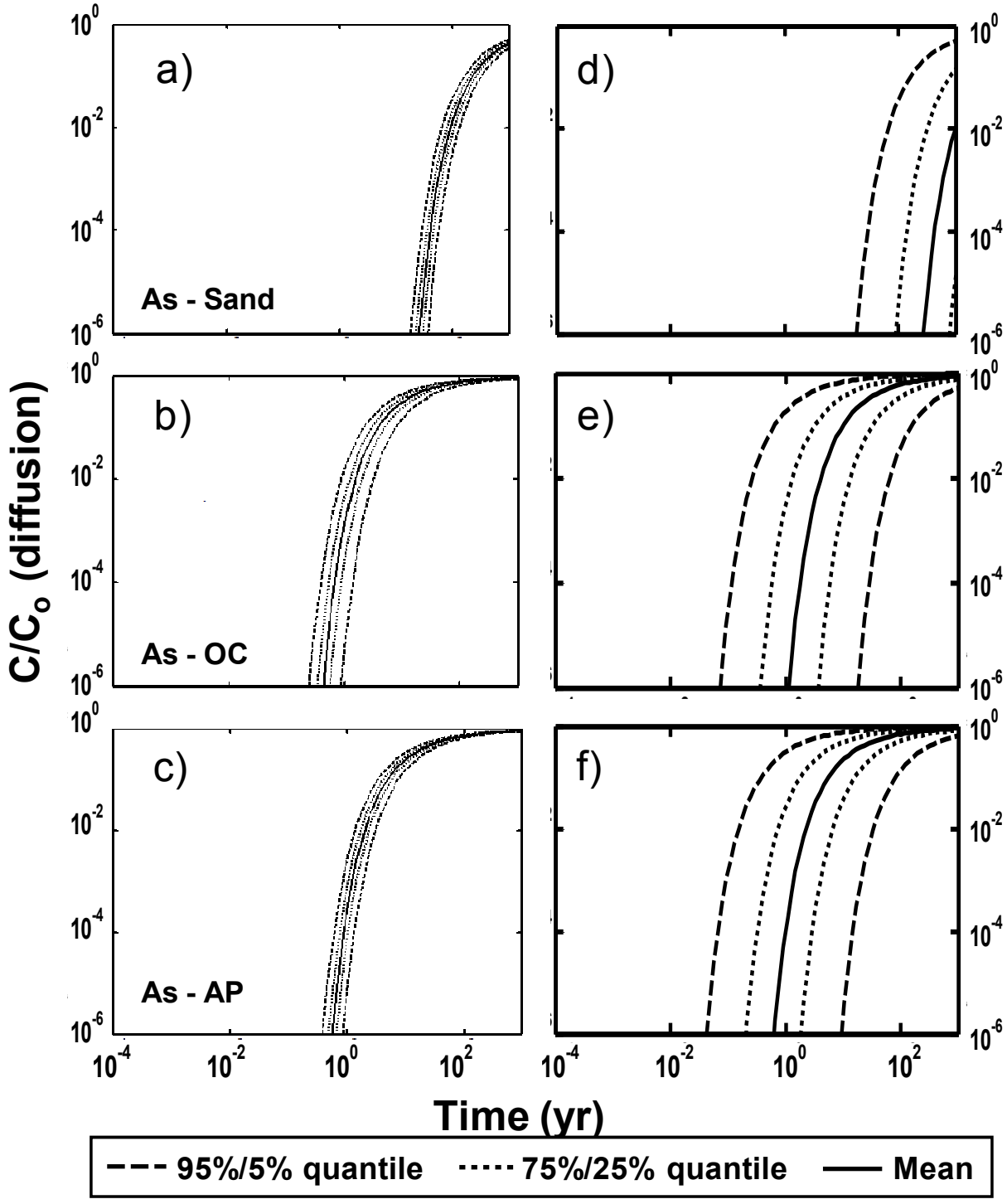

Figure 4.12. Comparison between simulations performed with measured parameters (a, b, c) and literature-derived model simulations (d, e, f) for As under diffusion conditions.

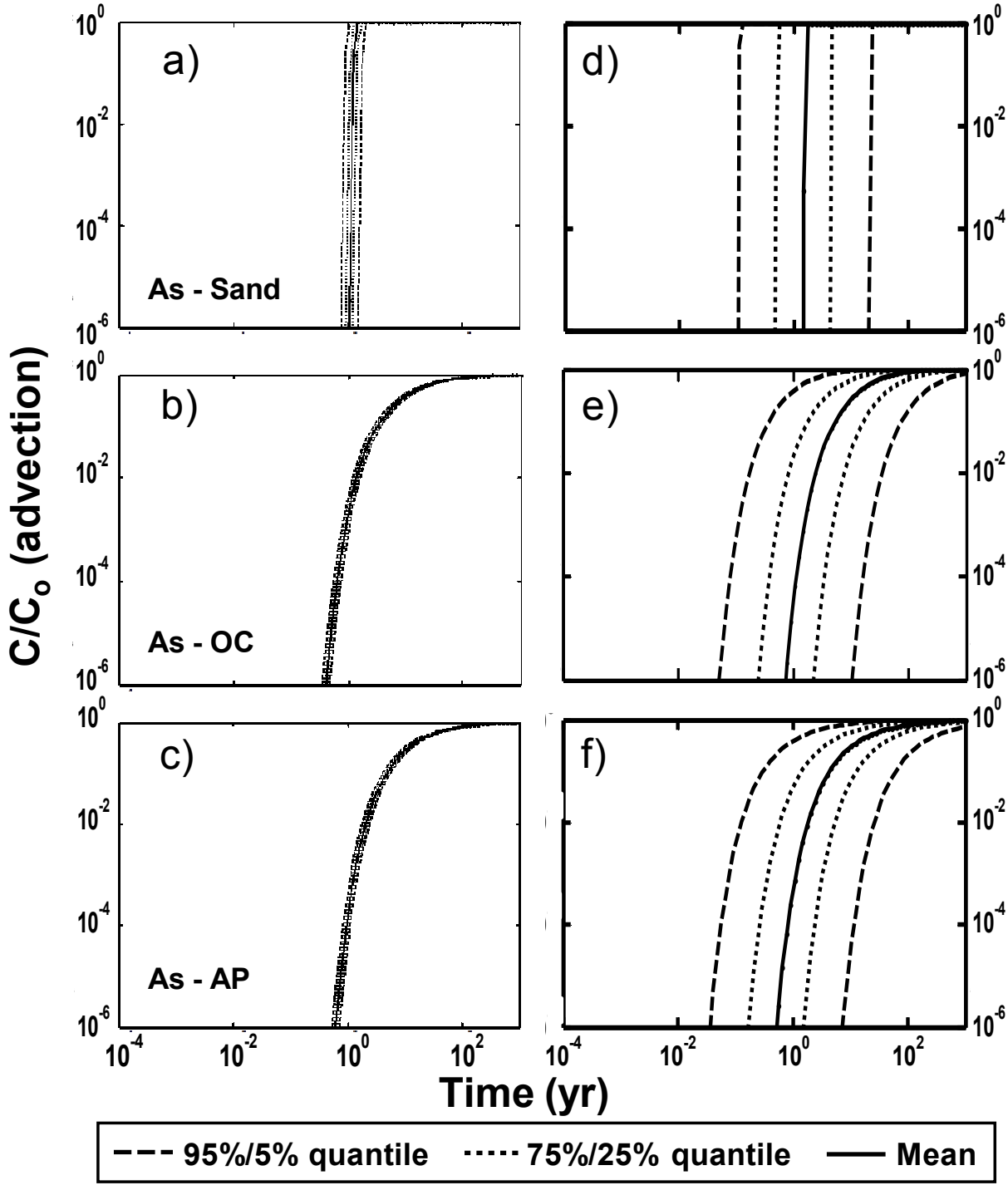

Figure 4.13. Comparison between simulations performed with measured parameters (a, b, c) and literature-derived model simulations (d, e, f) for As under advection conditions (d_h/d_x=0.005).

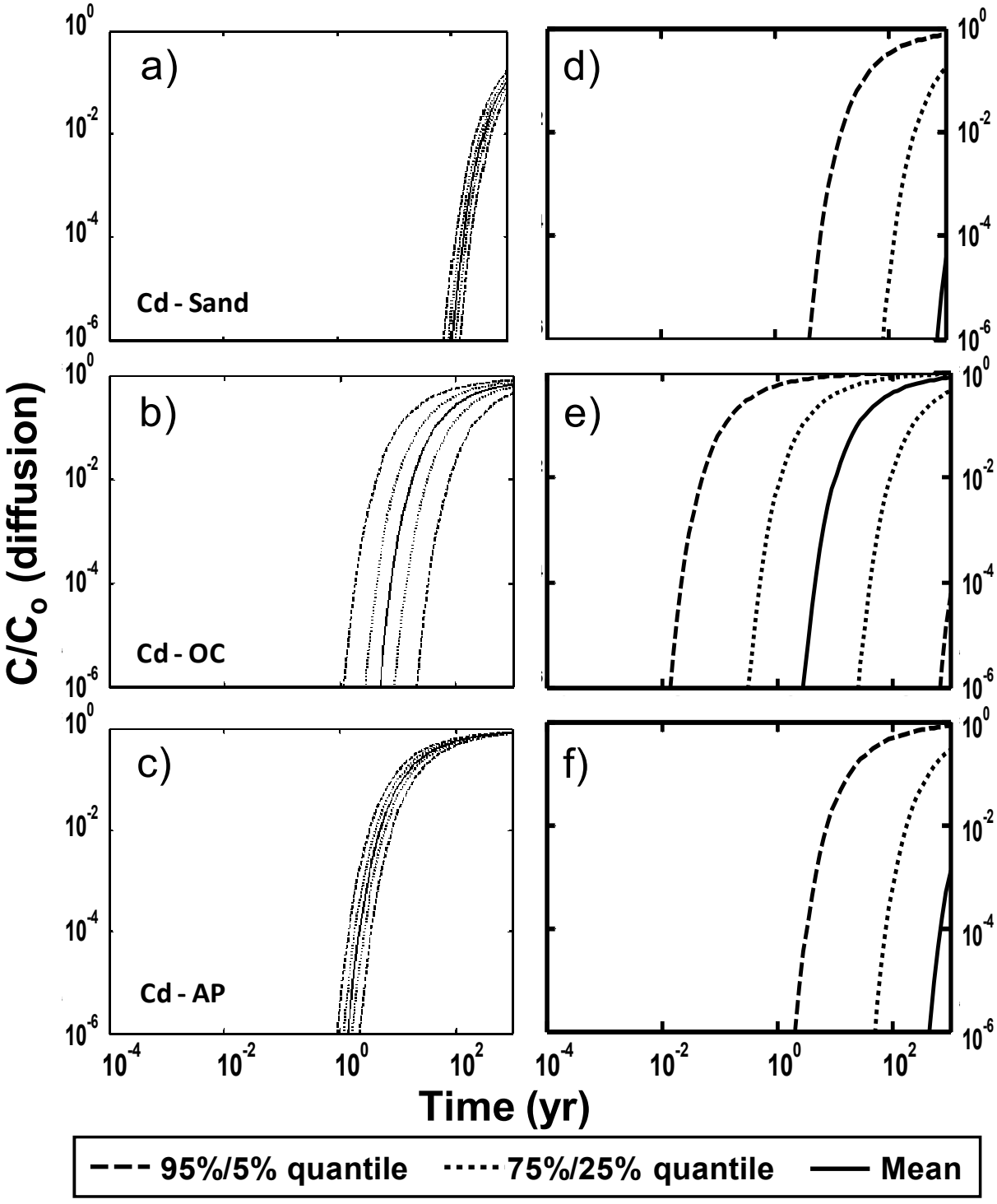

Figure 4.14. Comparison between simulations performed with measured parameters (a, b, c) and literature-derived model simulations (d, e, f) for Cd under diffusion conditions.

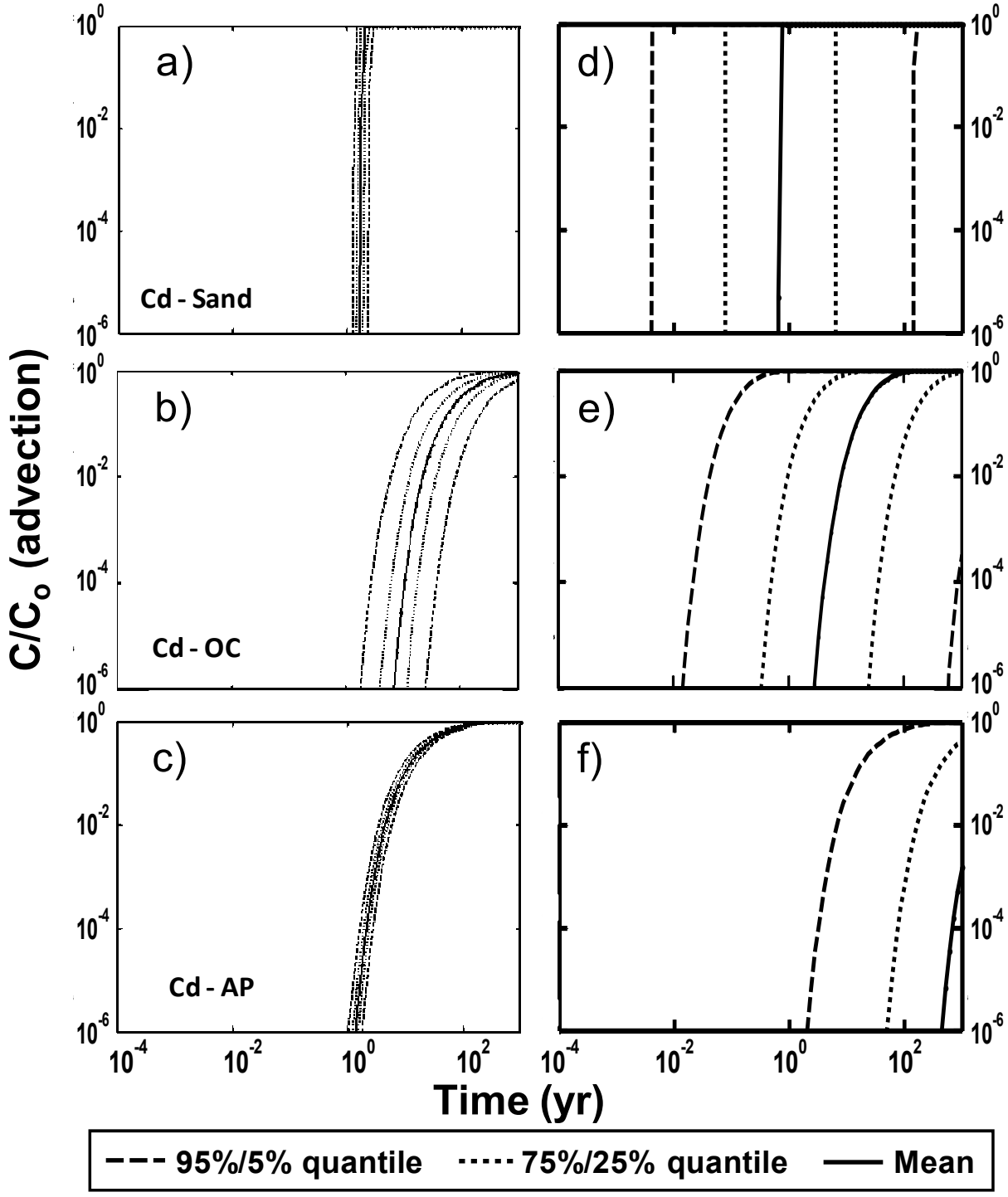

Figure 4.15. Comparison between simulations performed with measured parameters (a, b, c) and literature-derived model simulations (d, e, f) for Cd under advection conditions (d_t/d_x=0.005).

4.5. Conclusions and Implications

The metal Cd likely has non-linear adsorption isotherm behavior with all cap materials. This is demonstrated by the relatively low R^2 values for the linear equilibrium partitioning isotherm model and the statistically significant different from one Freundlich n values. Additionally, the substantial tailing in the desorption front for the Cd breakthrough curve in the column with GAC and for the As breakthrough curve in the column with apatite suggests a convex isotherm with $n>1$. The K_d values increase for As in the following order for the tested cap materials: sand≅GAC<AP≅OC. Although none of the caps exhibited a high sorption capacity for As, OC and apatite performed clearly better than sand and GAC. The K_d results indicate close agreement between the experimental and literature K_d values with the exception of As and Cd with apatite. Surprisingly, apatite exhibited a relatively low sorption capacity compared to OC for Cd. Apatite was expected to exhibit a higher sorption capacity for Cd because Ca can be easily replaced by Cd in the apatite chemical formula *(125, 138)*.

Not unexpectedly, apatite performed very well for Cd in the column study with full breakthrough after 12000 pore volumes. Sand did not exhibit such a poor sorption capacity as expected for Cd with full breakthrough after 4000 pore volumes. Based on the column experiment results, GAC performed poorly for both As and Cd.

The results from simulations performed with measured K_d and cap parameters compared to literature-derived model simulations demonstrate the need for uncertainty analysis, which is driven primarily by sediment chemistry that greatly affects K_d and the variety of cap materials with different permeabilities. The measured K_d values under realistic field conditions (circumneutral pH and close to anaerobic conditions) contribute to reduce uncertainties in parameters used for project design to a level more acceptable in managing risk.

CHAPTER V. PRE-CAPPING CHARACTERIZATION

I worked on this project with the students Ke Yin and Xiuhong Zhao from the Environmental Engineering Laboratory of Professor Rockne at the University of Illinois at Chicago. The research included sample collection in the field and laboratory sediment characterization envisioning the installation of a demonstrative active capping project in the turning basin of Bubbly Creek, Chicago, IL. The University of Illinois graduate college guidelines allow the inclusion of first-authored publications in the body of the PhD dissertation.

5.1. Abstract

Sediments in “Bubbly Creek” located in the South Fork of the South Branch of the Chicago River (Illinois, USA) were characterized for selection of amendments for an active capping demonstration project. Bubbly Creek is a 2000 m creek that starts at the Racine Avenue pumping station (RAPS), the largest sewage pumping station in the world at the time it was built. During large storm events, the RAPS can discharge up to 175 $m^3 s^{-1}$ of combined storm and wastewater into the creek. These high flow rates result in large shear flows on the sediment. Both heavy

metal levels (up to 900, 2900 and 6200 mg kg^{-1} of Pb, Cr and Zn, respectively) and polycyclic aromatic hydrocarbons (up to 3300 mg kg^{-1}) were identified as contaminants of concern in the creek sediments. A complicating issue in the creek is the copious gas ebullition from organic matter biodegradation in sediments. These gases can open advective channels that may result in substantial pollution release and compromise cap effectiveness. The capping project is proposed to be carried out in conjunction with overlaying wetlands in the shallow regions of the creek to remove nutrients from the river and pollutants discharged from combined sewer outflows. Metal and organic contaminant sequestration and oxidizing agents coupled with a gas collection system will be evaluated and compared to a sand reference cap.

5.2. Introduction

Prior to the enactment of the Resource Conservation and Recovery Act in 1976 and the Comprehensive Environmental Response, Compensation and Liability Act in 1980, indiscriminant releases of contaminants to the air, water and soil were largely unregulated and led to substantial pollution of the environment. Contaminants like polycyclic aromatic hydrocarbons (PAHs) and polychlorinated biphenyls (PCBs) accumulated on the bottom of rivers and lakes due to their hydrophobicity and relatively long environmental persistence. Contaminated sediment remedial alternatives include dredging, *in situ* capping with sand or clean sediment and active capping *(5-7)*. Like normal capping, active capping is also subject to contaminant migration through the cap. However, the selection of appropriate active materials and cap thicknesses can minimize contaminant flux to the water column to levels that are not significant from a risk standpoint; even with significant advective sediment-to-water-column porewater fluxes. A detailed evaluation of *in situ* conditions is vital to guarantee cap effectiveness. Before choosing the active capping material, site characterization including

sediment depth, organic matter and organic carbon content, contaminant concentration, presence of outfalls and other hydraulic structures, is necessary for cap design. Relevant geotechnical properties such as shear strength, compressibility, unit weight and water content should be taken into account. Further, scouring of the cap may occur due to high flow velocities in the overlying water column during discharge events.

The site of the present study is known as "Bubbly Creek." Bubbly Creek is the South Fork of the South Branch of the Chicago River, connecting with the main south branch of the Chicago River at the turning basin. In the early-1900's, Bubbly Creek became a notorious open sewer as industrial effluents went directly into the stream, as well as wastes from the adjacent stock yards *(263)*. Although direct wastewater discharge is prohibited now, the creek still is impacted by combined sewer outflow (CSO) effluent on an approximately monthly basis from the Racine Avenue pumping station (RAPS). Although these flows can be quite large, up to 175 $m^3 s^{-1}$ in the 46 m wide creek, the water in Bubbly Creek is normally stagnant and susceptible to gas ebullition events. The City of Chicago is interested in remediating this historical waterway to provide additional green space to the Canal Origins Park and newly developed residential housing in the area as it transitions from industrial to mixed-residential. Towards this goal, a field scale active capping demonstration project is being implemented for the turning basin by our research group in collaboration with the Metropolitan Water Reclamation District of Greater Chicago (MWRD), the Wetlands Initiative (TWI), the US Army Corps of Engineers (USACE) and the City of Chicago Department of the Environment (DOE).

5.3. Materials and Methods

Sampling of Bubbly Creek was performed onboard the MWRD RV *PC1* in October and November 2005. A total of 15 sediment cores and 13 surface grabs were collected (Figure 5.1). Four of the cores were full depth to the clay/hardpan layer at a mean depth of 8 m below water surface and the remainder were partial cores to a depth of 2 m below the sediment-water interface. A field technician pushed a 2 m x 5 cm diameter plastic core tube into the sediment *in situ* to retrieve intact cores. The cores were sectioned in the field into 20 cm intervals and placed in clean 250 mL glass sample jars with Teflon® caps (Fisher Scientific, Pittsburgh, PA). The grab samples were obtained using a nine inch (23 cm) stainless steel dredge and placed in gasketed plastic buckets (5 L, Fisher Scientific, Pittsburgh, PA) and stored in the refrigerator (4° C) until analysis.

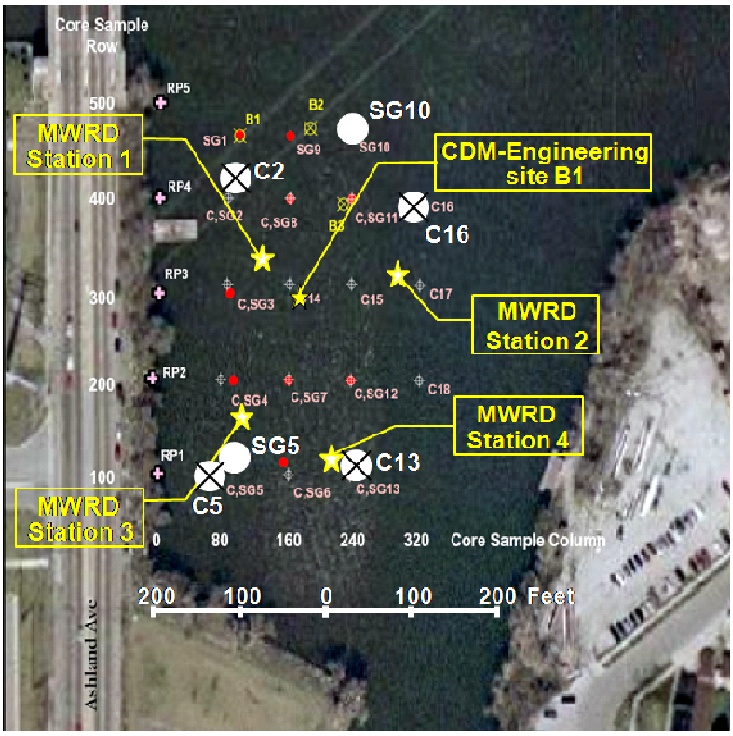

Figure 5.1. Aerial view at the Bubbly Creek turning basin. Highlighted are selected core (C) and surface grab (SG) locations from the current study. Also shown are MWRD sampling stations and the site of a core sample taken by the USACE *(264)*. Base sample location map courtesy of Wetlands Initiative.

Sediment samples were volumetrically sampled from thoroughly homogenized interval segments using a 3 cm^3 syringe as described by Buckley et al. *(265)*. Sediment samples were weighed on a tared, clean disposable aluminum tray and dried (105 °C, 48 hr). Wet bulk density, percent moisture, dry bulk density, percent solids, organic carbon (OC) and organic matter (OM) were analyzed *(265)*. Anion concentrations in filtered (0.45 μm) pore water were measured by ion chromatography (Dionex IC25, Sunnyvale, CA) as described previously by Rockne and Brezonik *(266)*.

The 16 EPA priority-pollutant PAHs were extracted from the sediments using a modified Soxhlet extraction method. Wet sediment was ground with anhydrous Na_2SO_4 to complete dryness. The dehydrated sample was transferred to a Whatman cellulose thimble (33 mm x 94 mm, Fisher Scientific, Pittsburgh, PA) and spiked with known amounts of PAH surrogate phenanthrene-D10 (Supelco, Bellefonte, PA). The sediment was then extracted as described in Song et al. *(267)* in a Soxhlet extractor (Fisher Scientific, Pittsburgh, PA) for 24 hr in 150 mL 1:1 (v/v) hexane:acetone mixture. The extract was then cleaned-up by elution through a glass column (30 cm, 1.9 cm i.d. with 250 mL reservoir, Fisher Scientific, Pittsburgh, PA) filled with 20 g of fully activated silica gel (100-200 mesh, Fisher Scientific, Pittsburgh, PA) and dichloromethane to obtain a 1:1 (v/v) hexane:dichloromethane mixture in the column. Extracts were concentrated on a Kuderna-Danish (K-D) concentrator (Fisher Scientific, Pittsburgh, PA) to approximately 5 mL. The volume of sample was then brought up to 10 mL by adding clean solvent. PAH internal standards anthracene-D10, triphenylmethane, benz(a)anthracene-D12 and perylene-D12 (Supelco, Bellefonte, PA) were added to the sample before analysis by gas chromatography mass spectrometry (GC/MS) in EI mode on an Agilent 6890 GC coupled to an Agilent 5973 mass selective detector. Separation was achieved using an HP-5 MS fused silica

capillary column (30 m x 0.25 mm i.d.; 0.25 μm film thickness) and a 5 μL injection volume. The injector temperature was 250° C. The initial column temperature was 50° C, followed by a temperature increase of 10° C min^{-1} to a temperature of 180° C, a temperature increase of 6° C min^{-1} to a temperature of 250° C and a temperature increase of 3° C min^{-1} to a temperature of 300° C and kept for 5 min. Helium was used as the carrier gas.

Polychlorinated biphenyls (PCBs) data were obtained from a complete composited sediment core taken in the center of the turning basin by the USACE *(264)*. PCBs were analyzed for total and specific aroclors using USEPA SW-846 method 8082. Heavy metal levels were performed by a contract laboratory for the MWRD according to USEPA SW-846 method 6010B *(268)*.

Gas production assays were performed with surface sediment grab samples homogenized (100 ml) and placed into stoppered serum bottles (125 mL, Fisher Scientific, Pittsburgh, PA). The bottles were sparged with N_2 gas and sealed for quiescent incubation at 5°, 20°, 25° or 35° C upside-down to prevent gas release. Gas production was measured at time points by volume displacement using a 10 cm^3 syringe and the gas phase composition was determined by isothermal gas chromatography with thermal conductivity detection (SRI instruments 9300B, Torrance, CA). The column temperature was maintained at 80°C for five minutes with Helium carrier gas.

To better understand the relative efficacy of selected cap materials for containing and/or degrading organic and metal pollutant mixture, simulations were performed as described in Yin et al.*(129)*. Five capping materials and 22 contaminants were used in the simulations. Performance (as defined by breakthrough curves) was assayed under diffusion only as follows *(194)*:

$$c(x,t) = c_o erfc\left(\frac{x}{\sqrt{4D_{obs}t}}\right) \quad (5.1)$$

$$D_{obs} = \frac{D_{mol}\tau}{R} \quad (5.2)$$

Where *c(x,t)* is the breakthrough porewater concentration of contaminant (mg L^{-1}) at the top of the cap of thickness *x* at time *t (yr)*; c_o is the initial concentration of contaminant in the sediment porewater (mg L^{-1}); *R* is the retardation factor (unitless); D_{obs} is observed diffusivity (m^2 yr^{-1}); D_{mol} is the molecular diffusivity (m^2 yr^{-1}) and τ is the tortuosity of the cap media (unitless). All parameters were assumed according to Yin et al. *(129)*.

The mean and maximum depth of scour was calculated to estimate scouring potential of a sand cap in the creek. The equations for maximum and mean scour depth as a function of cap particle size are as follows *(223)*:

$$D_{s,\max} = 6.5D_{50}^{-0.115} \quad (5.3)$$

$$D_{s,mean} = 1.42D_{50}^{-0.115} \quad (5.4)$$

Where D_{50} refers to the median diameter of the sand cap material, estimated to be 0.6 mm for a sand cap.

Although these equations were developed primarily for non-cohesive (*i.e.* sand and gravel) soils and the sediments in Bubbly creek are dominated by cohesive silts and clays (>60%), these results can help us understand the possibility of cap scouring at the creek. The water flow velocity in the 21 channels used to obtain equations 3 and 4 varied from 1.2 to 2.3 m s^{-1} *(223)* and turning basin velocities during peak discharge are within this range.

The critical velocity for initiation of particle suspension in the turning basin was obtained from the data in van Rijin *(224)*. The mean water depth in Bubbly Creek was used for calculation

of the critical velocity with a D_{50} of 6 mm as before. There is a strong likelihood for severe erosion if water column velocities frequently exceed the critical velocity for initiation of suspension.

5.4. Results and Discussion

The water depth in the Bubbly Creek turning basin (BC TB) ranged from 0.9 to 4 m; increasing from the east and south shore to the creek center with a mean depth of 2.6 m. The mean depth from water surface to clay hardpan was 8 m. The estimated total sediment volume is 85,000 m^3 in the turning basin. The temperature of the sediment surface core samples varied from 10 to 16.5° C and the water temperature during sample collection was 16° C. Bulk analysis of a homogenized entire sediment core by the USACE *(264)* reported that gravel accounts for 2.3% of the solids by mass, with sand, silt and clay accounting for the remaining 32.5, 35.5 and 29.7% of mass, respectively.

An extensive characterization of the solid and moisture content, organic matter and organic carbon content and anion concentration (mainly nitrate and sulfate) was performed. The physical parameters, organic content and PAH results described here are for core samples collected at the four corners of the turning basin (cores 2, 5, 13 and 16). Cores 2, 13 and 16 (Figure 5.1) are mainly composed of silty mud in the top, transitioning to silty-clay at the bottom. Core 5 is mainly sandy mud at the top transitioning to silty-clay at the bottom. A pronounced naphthalene smell was observed in cores 5, 13 and 16.

Moisture, percent solids and porosity in the sediment cores are shown in Figure 5.2. The moisture content of the samples in general decreased with depth and varied from 42.9% to 66.7% (the mean moisture content was 55.4 ± 5.2%). Porosity reflected the same behavior, with a mean

value of 76.5 ± 4.0%. The wet and dry bulk density and particle density were 1.3 ± 0.1, 0.6 ± 0.1 and 2.4 ± 0.04 g mL^{-1}, respectively.

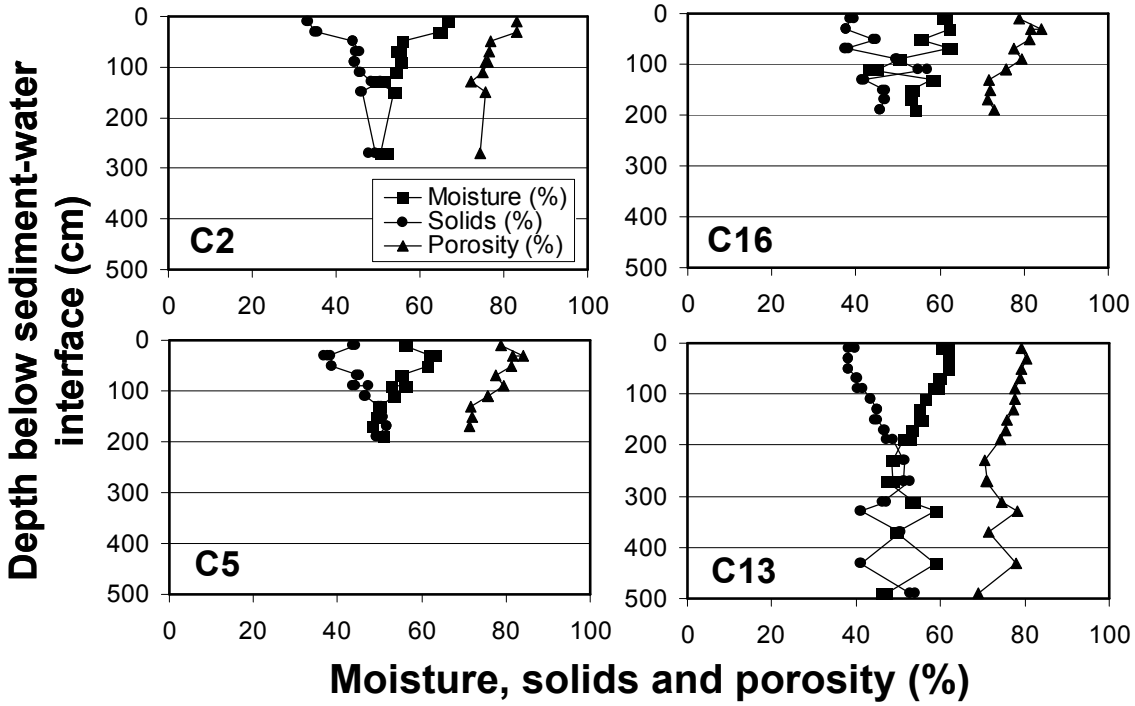

Figure 5.2. Percent solids, moisture and porosity versus depth below sediment-water interface for cores 2, 5, 16 and 13 sampled in the Bubbly Creek turning basin. Core locations are shown in Figure 5.1.

Sediment OM and OC for cores 2, 5, 13 and 16 are shown in Figure 5.3. OM varied from 10.4 to 22.0%, with a mean ± standard deviation of 15.3 ± 2.6%, while OC varied from 11.0 to 19.1% (mean ± standard deviation of 14.7 ± 1.7%). These results are typical for carbon-rich, highly reduced near shore sediments.

PAH data are shown in Figure 5.4. Seven of the 16 measured PAHs are classified as probable human carcinogens *(269)*: benz[a]anthracene (BaA), benzo[b]fluoranthene (BbF), benzo[k]fluoranthene (BkF), benzo[a]pyrene (BaP), chrysene (Chry), dibenz[a,h]anthracene

(DahA) and indeno[1,2,3-cd]pyrene (IcdP). Due to their much higher human health impacts (and concomitantly higher risk), we have focused on these compounds here.

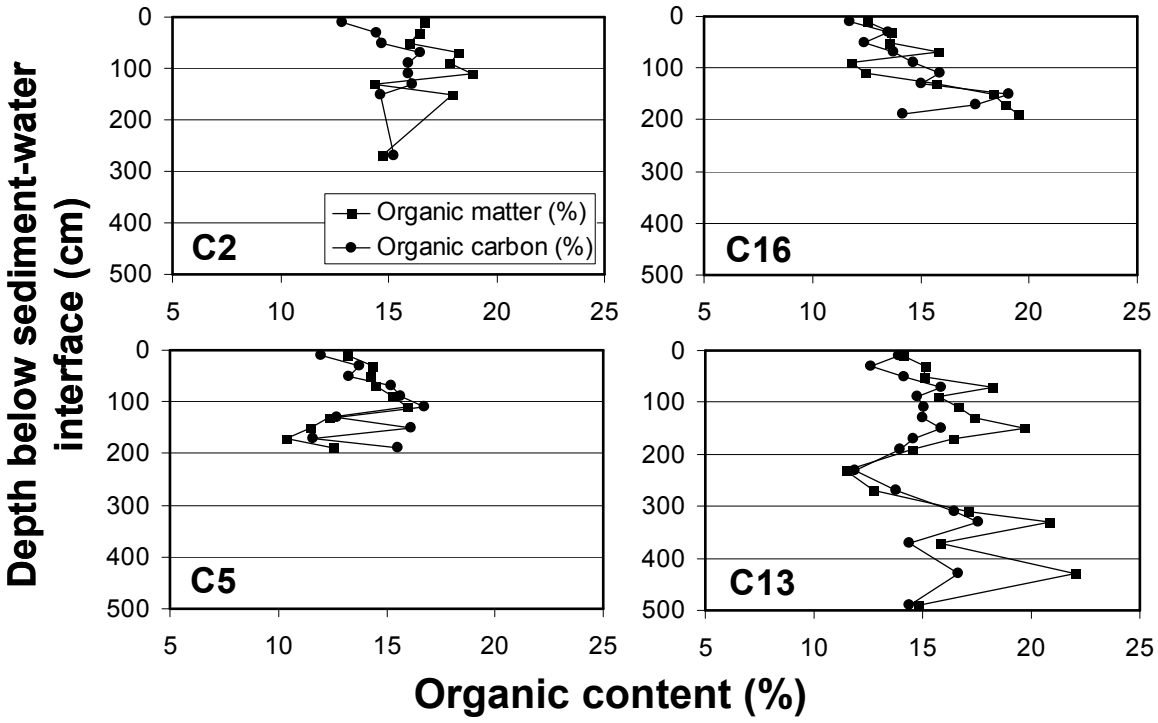

Figure 5.3. Organic matter and organic carbon versus depth below sediment-water interface for cores 2, 5, 13 and 16 in the Bubbly Creek turning basin. Core locations are shown in Figure 5.1.

Although surficial total PAH concentrations are typically below 100 mg kg^{-1}, deeper sediments have much higher PAH concentrations, even exceeding 1000 mg kg^{-1} near the clay/hardpan layer (Figure 5.4). The concentration profile clearly shows that older sediments deposited in the beginning of the last century were highly polluted with PAHs (the clay/hardpan layer represents the original construction of the turning basin in the late 1800's). The creek has received large amounts of organic and inorganic pollution from industrial waste runoff, as well as stormwater and CSO discharges *(264)*.

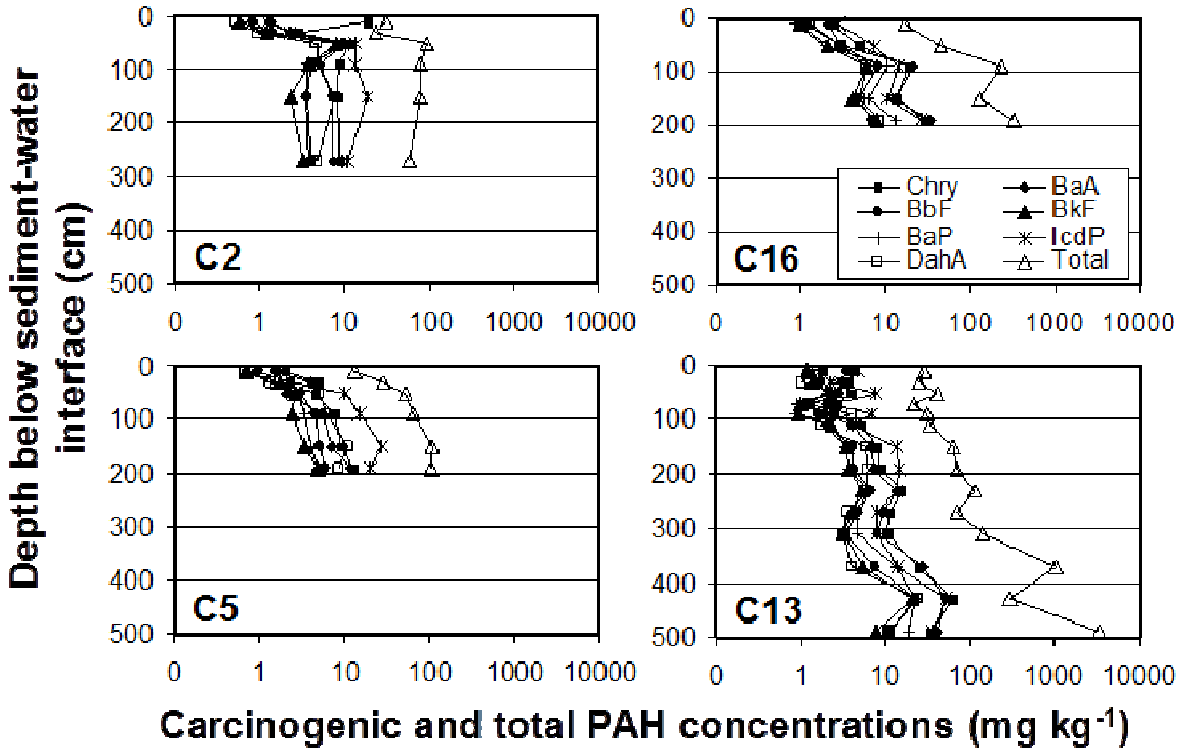

Figure 5.4. Carcinogenic and total PAH concentrations versus depth below sediment-water interface for cores 2, 5, 13 and 16 in the Bubbly Creek turning basin. Note the logarithmic scale. Core locations are shown in Figure 5.1.

Mean sediment PAH levels for all core samples were compared to National Oceanic and Atmosphere Administration (NOAA) guidelines for contaminated sediments *(270)*. NOAA guideline values are for preliminary screening purposes in freshwater sediment for upper effects threshold (UET), defined as the lowest concentration above which adverse biological impacts would always be expected due to exposure to that concentration alone. With the lone exception of benzo[k]fluoranthene, all other PAHs were present in turning basin sediments at much higher concentrations than the NOAA UET guidelines (Figure 5.5).

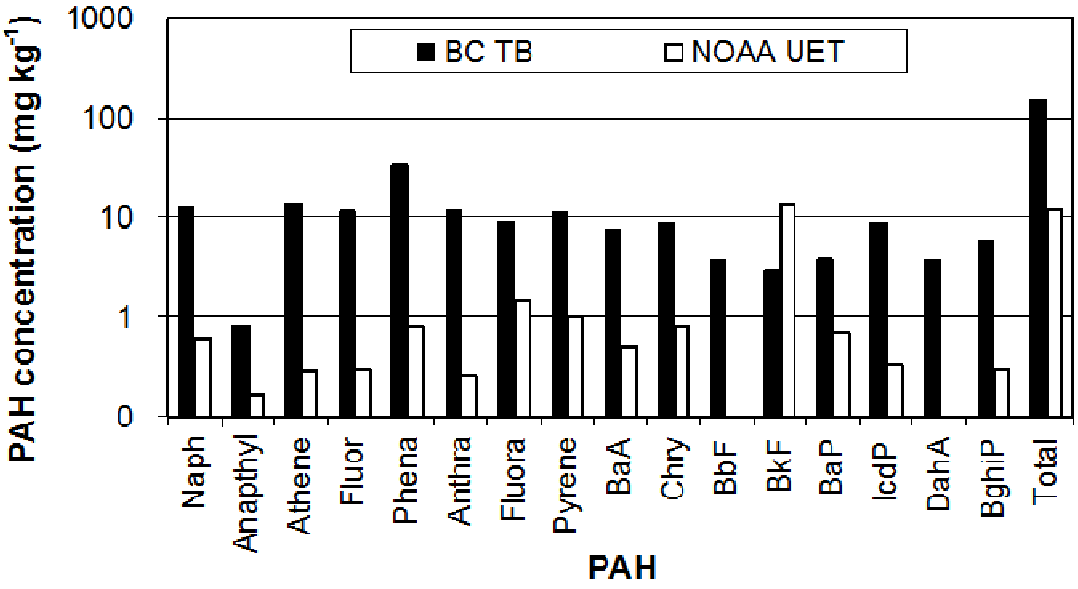

Figure 5.5. Mean PAH concentrations in all Bubbly Creek turning basin (BC TB) core samples compared with NOAA guidelines for upper effects threshold levels (UET) for freshwater sediments *(270)*. Note logarithmic scale on the y axis.

The total PAH mass in the turning basin sediment is estimated to be 6,600 kg. These elevated PAH levels suggest the necessity for active cap amendments with high organic sorption capacity. Granular activated carbon (GAC), organo-clay and coke have all been proposed as potentially good sequestration agents capable of reducing release and breakthrough of PAHs through the cap.

Total and specific aroclor concentrations are shown in Figure 5.6. Although the Illinois Environmental Protection Agency (IEPA) does not have criteria for specific aroclors, the total PCB levels in the turning basin exceed the "extreme elevated" (EE) criterion used by IEPA *(30)* (Figure 5.6).

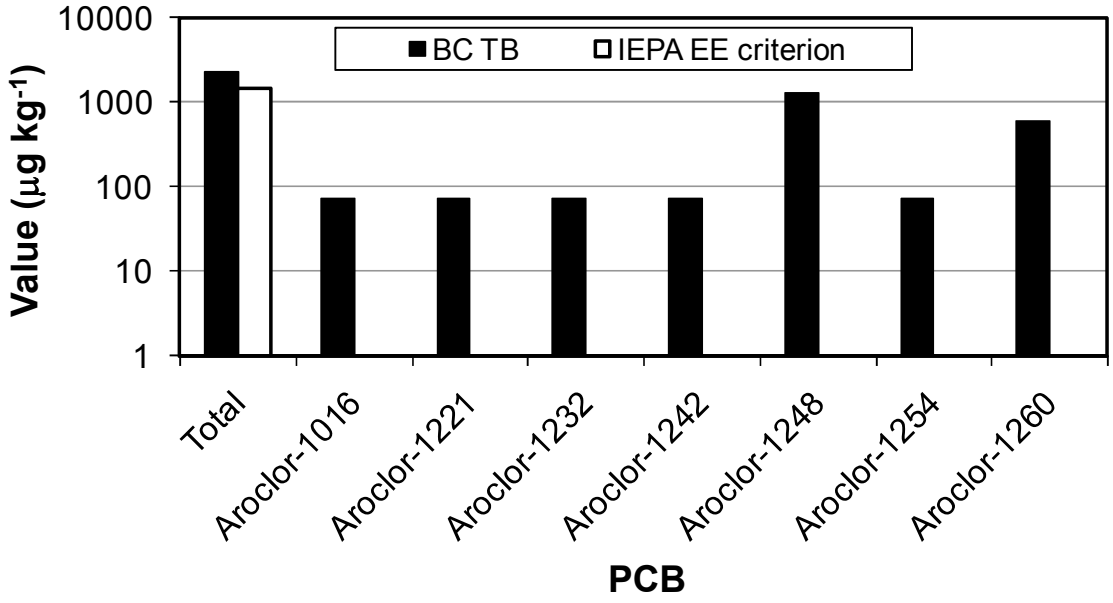

Figure5.6. Total and specific aroclor concentrations of a complete composited sediment core from USACE *(264)* compared to the IEPA criterion to classify stream sediments *(30)*. Note logarithmic scale on the y axis. Core location is shown in Figure 5.1.

Heavy metal levels in Bubbly Creek sediments are shown in Figure 5.7. Comparing pollutant levels with both toxic threshold limit concentrations (TTLC) provided by the State of California Assessment Manual (CAM) *(271)* and EE values used by IEPA *(30)*, demonstrate that heavy metal concentrations in the turning basin sediment may present a threat to ecological and/or human health. Although no metal exceeds CAM criteria, Cr, Cu, Pb, Zn and Hg are all well above IEPA EE criteria. These elevated metal concentrations suggest the necessity for active capping amendments able to bind metals into insoluble and/or non-bioavailable phases. Apatite would be an option as it sequesters metals by continuously supplying phosphate to solution to exceed the solubility limits of various metal-phosphate phases (e.g. pyromorphite and autunite for Pb).

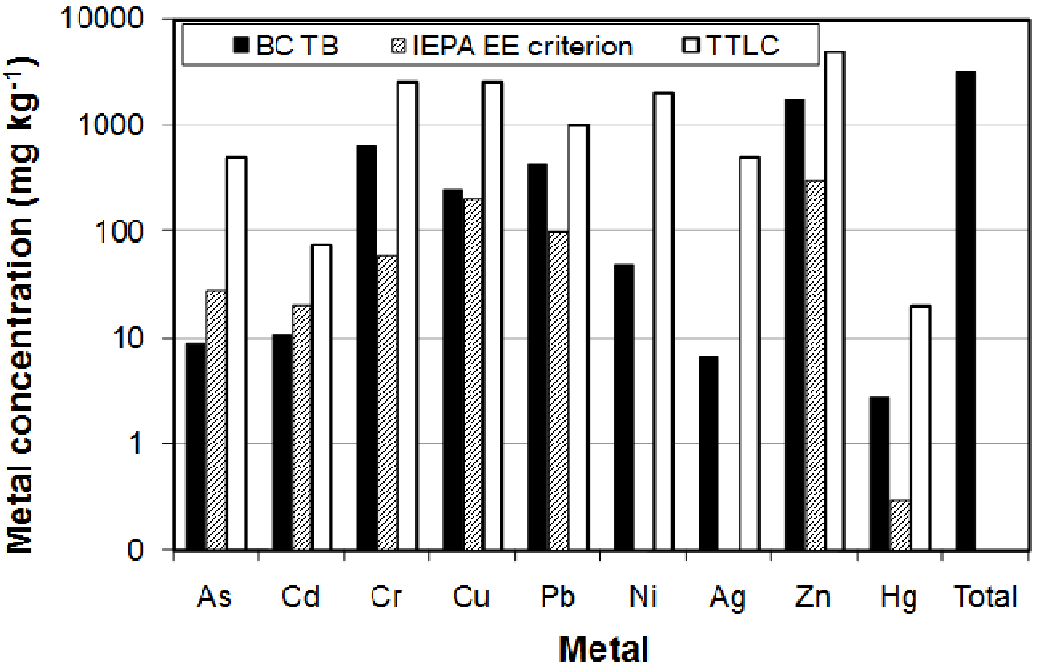

Figure 5.7. Total and specific metal content in Bubbly Creek turning basin sediments. Turning basin data compared to IEPA stream sediment classification *(30)* and CAM toxic threshold limit concentrations (TTLC) criteria *(271)*. Note logarithmic scale on the y axis. Locations of samples are shown in Figure 5.1.

The presence of both heavy metal and hydrophobic organic contaminants at levels of concern necessitate selection of capping materials effective at combined treatment of mixtures. Therefore, GAC, coke, shredded tires and organo-clay were investigated as possible cap materials. Although apatite is reported to be an effective amendment for metal sequestration, our preliminary simulations suggest it is less effective for organic contaminant sequestration than GAC is for metal sequestration. The time for breakthrough of over 20 different contaminants in different cap materials under different environment conditions was modeled as in Yin et al. *(129)*.

Figure 5.8 is an example of diffusive transport of phenanthrene, pyrene and Pb (at pH 4 and 9) in different cap materials. The effects of porewater pH on the breakthrough of the pH sensitive metals Pb, Cr and Cd were studied. It was observed that the time needed for breakthrough will be

longer for higher molecular weight PAHs like pyrene than for lower molecular weight PAHs like phenanthrene. Similar behavior was observed for more highly chlorinated PCBs. The results clearly demonstrate that cap thickness is the most important parameter determining breakthrough time for metals; even more than choice of cap material (Figure 5.8).

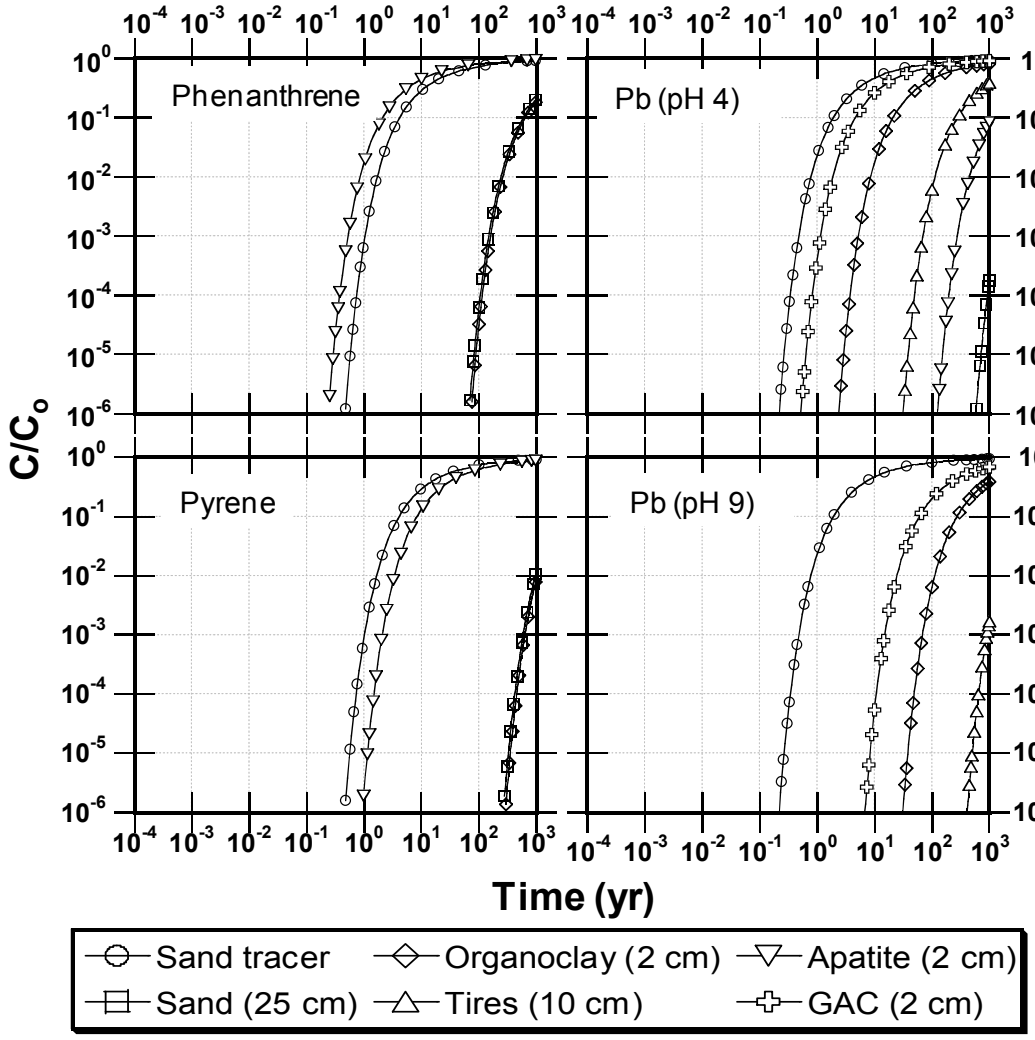

Figure 5.8. Breakthrough concentration of phenanthrene, pyrene and Pb (at pH 4 and 9) in different cap materials (25 cm sand, 2 cm organoclay, 10 cm shredded tire, 2 cm apatite and 2 cm GAC) under static conditions. Also shown is the transport of a conservative tracer in the sand cap for comparison. Note logarithmic scale on both axes.

As noted in the introduction, cap integrity is dependent upon cap scouring by hydraulic forces and gas ebullition due to methanogenic degradation of organic matter. Because Bubbly Creek has high surface water velocities during RAPS discharge events, we analyzed erosion effects considering a predicted maximal velocity of 2 m s^{-1}. With this value, the mean scour depth for a sand cap would be 1 m; and depths exceeding 2 m could be reached without sufficient armoring. Moreover, the critical velocity for initiation of suspension was 0.7 m s^{-1}; well below maximal velocities expected during a discharge event. These results indicate that armoring of the site must be considered; particularly in the main channel where the highest velocities were predicted to occur. More detailed data collection and modeling efforts are being undertaken to determine more precisely the erosion potential in the creek proper.

Experiments to measure gas production rates in two sites along the creek were performed as a function of temperature and modeled using the Arrhenius equation. The results show that gas production varied substantially as a function of temperature, but not with site location. The biogenic gas production reaction rate constant k was calculated for each site assuming a zero order rate law (other rate laws were considered but did not fit the kinetic data). Rate constants were plotted on an inverse temperature Arrhenius plot to obtain the activation energy for methanogenesis (E_a) as in Viana et al. *(272)*. The mean E_a of methanogenesis was 42.5 ± 8.1 kJ mol^{-1}. These results are comparable to methanogenic E_a values reported in the literature *(273-275)*, which range from 27 to 138 kJ mol^{-1}. The lowest observed E_a values were with simple defined substrates (phenol) and the higher values were reported with more complex organic compounds like fulvic acids and humic acids commonly found in peat soil.

Using these kinetic data, we were able to predict the amount of gas that could be produced during an entire year for the upper 1 m of sediment (the most active zone with the greatest

ebullition potential) and decide whether gas control systems would be necessary. Even though neither site produced gas in excess of its own volume on an annual basis, the amount of gas produced was still considerable (Figure 5.9). It is entirely possible that the sediment will be disturbed during cap placement and it may stimulate higher rates of gas production. Therefore, gas control will likely be adopted for this site to ensure cap integrity.

A further important consideration is the composition of the biogenic gas. The ratio of methane to carbon dioxide in biogenic gas produced from the BC TB sediments is also shown in Figure 5.9. The CH_4/CO_2 ratio was clearly affected by temperature. These results suggest strongly that changes in microbial community composition took place as a function of incubation temperature. Hydrogenotrophic methanogens produce only methane (while consuming CO_2 and H_2), while acetoclastic methanogens produce CH_4 and CO_2. The finding that lower CH_4/CO_2 ratios were observed in sediment incubated at lower temperatures suggests the dominance of acetoclastic methanogens at lower temperatures, while hydrogenotrophic methanogens become dominant at higher temperatures, thus increasing the CH_4/CO_2 ratio.

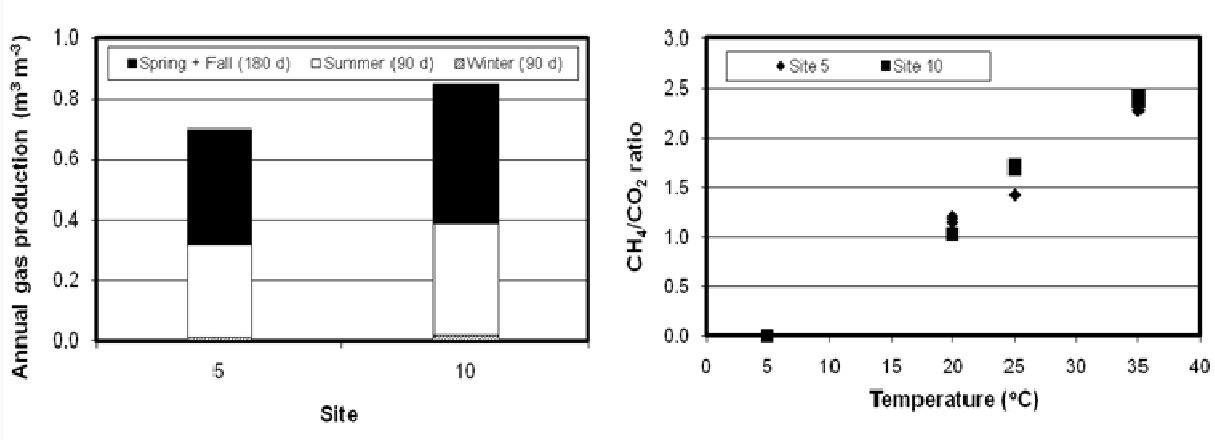

Figure 5.9. Estimated annual volumetric gas production (m^3 m^{-3} of sediment) and CH_4/CO_2 ratio of biogenic gas produced in Bubbly Creek turning basin surficial sediments. Site locations are shown in Figure 5.1.

The conceptual design for the Bubbly Creek active capping demonstration project is shown in Figure 5.10. The focus of the design is on the sequestration of both metal and organic pollutants. The impact of high flows on cap scouring will be determined by having both a sub-aqueous area exposed to high shear flows and an enclosed wetland covered area. Four capping strategies will be used in both the enclosed and open areas: sand, GAC/geotextile, apatite/clay and nitrate-salt amended. Each treatment will address different mechanisms for active capping; sand as the reference site, GAC for organic sequestration (our simulations suggest it will not work well in sequestering heavy metals), apatite/clay for metals and hydraulic barrier and nitrate to stimulate anaerobic biodegradation of organics and oxidation of sulfides. Dry active capping materials will be sandwiched between geotextile fabric layers overlain on the contaminated sediments. An overlying permeable sand layer will then be placed on top of the active capping material and covered with a highly permeable GeoNet layer to facilitate lateral gas transport. This will allow evolved biogenic gas to be captured and channeled to the side shoreline. On top of the GeoNet will be wetland fill in the shallow zones near shore (Figure 5.10). The purpose of the wetland is to provide habitat and nutrient removal for the Chicago River water diverted through the wetland. During construction, monitoring tubes will be placed on top of the sediment, on top of the active capping layer and on top of the permeable sand layer to provide long term continuous monitoring of contaminant release. A walkway will be developed on the separation between the wetland and sub-aqueous cap areas to allow public use and monitoring of the facility following construction.

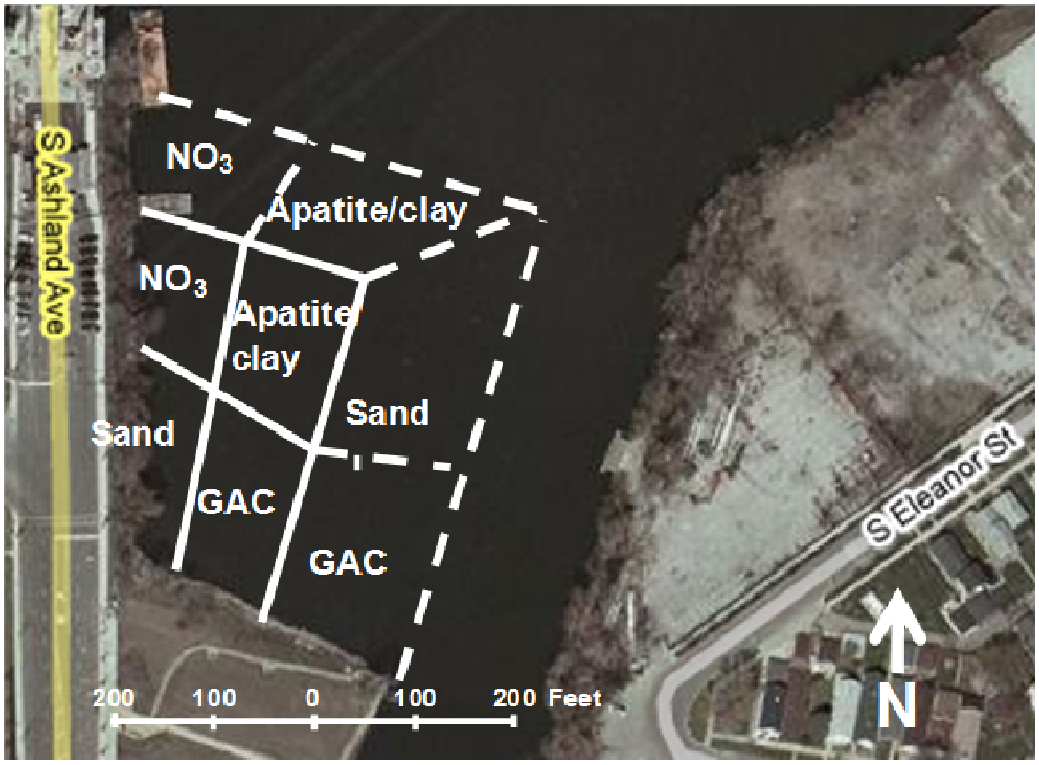

Figure 5.10. Capping demonstration project at the Bubbly Creek turning basin. Subaqueous cap is represented by dashed lines and wetland covered cap by solid lines in the shallow near shore zone. Base satellite photo from Google – Map data© 2007 NAVTEQ™.

5.5. Conclusion

Characterization of the sediments at the Bubbly Creek turning basin showed the presence of mixed heavy metal and organic contamination. Concentrations of Pb, PCBs and PAHs were as high as 900 mg kg^{-1}, 2.3 mg kg^{-1} and 3270 mg kg^{-1}, respectively. These concentrations exceed both IEPA criteria for stream sediments and NOAA guidelines for preliminary screening purposes in freshwater sediment. Four different active capping strategies will be employed (sand, GAC/geotextile, apatite/clay and nitrate-salt amended) in both a sub-aqueous area exposed to higher shear flows during RAPS discharge events and an enclosed wetlands covered area. Long term flux monitors will be employed in conjunction with cap construction to allow detailed examination of cap component effectiveness.

CHAPTER VI. FIELD MEASUREMENTS AND MODELING OF EBULLITION-FACILITATED FLUX OF HEAVY METAL AND PAH CONTAMINANTS FROM SEDIMENTS TO THE WATER COLUMN

I worked on this project with the student Ke Yin from the Environmental Engineering Laboratory of Professor Rockne at the University of Illinois at Chicago. The research included field work in 14 sites in the Chicago River, IL. Gas ebullition due to methanogenic activity and ebullition-facilitated contaminant transport were investigated. Models were also developed to predict ebullition-facilitated contaminant release and compare these predictions to literature values.

6.1. Abstract

Metal and polycyclic aromatic hydrocarbon (PAH) transport from the sediment to the water column due to gas ebullition was investigated in 14 urban waterway locations. Ebullition-facilitated fluxes were surprisingly large for both contaminant classes, with fluxes up to 18, 2.5, 5, 20 and 450 mg m^{-2} d^{-1} for Pb, Cr, Ba, Zn and Fe, respectively, and up to 11, 44, 3, 52 and 31 mg m^{-2} d^{-1} for anthracene, fluoranthene, naphthalene, phenanthrene and pyrene, respectively. The magnitude of the ebullition-facilitated measured fluxes indicates that gas ebullition is an important pathway for release of both PAHs and heavy metals from buried sediments in urban freshwater systems. Mechanistic and empirical models were developed to predict *in situ* gas ebullition flux and ebullition-facilitated contaminant flux. Results from both multivariate regression analyses and a mechanistic model suggest that metal transport likely is due to sediment particle re-suspension, while PAH transport is due to both contaminant partitioning to gas bubbles and to sediment re-suspension.

6.2. Introduction

Gas ebullition due primarily to methanogenic activity in sediments is an important mechanism of contaminant transport in sediments *(3-4, 17-19)*. Because gas bubbles are hydrophobic, hydrophobic contaminants from sediment porewater tend to partition into the gas phase and to sorb onto the bubble interface, leading to contaminant transport from the sediment to the water column and atmosphere. Gas bubbles also facilitate the transport of contaminants to the water column by causing sediment re-suspension. Ebullition-facilitated sediment re-suspension may be as or more significant a mechanism of contaminant transport than bubble-porewater contaminant partitioning *(3, 19)*. Although contaminant transport from sediments by diffusion and advection has been extensively investigated, comparatively less is known about contaminant transport due to gas ebullition. Understanding and quantifying this contaminant transport mechanism is key to enable prediction of the total contaminant transport from sediments to the water column.

Ebullition has also been investigated due to its negative impact on capping performance. Several capping projects have recently been implemented for remediation of contaminated sediments as an alternative to dredging, including the Anacostia River in Washington, DC *(10)*, the McCormick and Baxter Creosote Superfund Site in Portland, OR *(11)*, the Grasse River in Massena, NY *(12)*, and Stryker Bay in Duluth, MN *(13)*. Although it has been demonstrated that capping is effective at minimizing release of contaminants to the water column *(14-16)*, gas bubble migration may cause cap damage and a pathway for contaminant release *(10, 17)*.

Widely varying gas production fluxes have been reported in the field. Tanner et al. *(199)* observed methane fluxes varying from 0.07 to 0.67 L m^{-2} d^{-1} for a wetlands used to treat wastewater. Sovik et al. *(200)* measured gas production in ten constructed wetlands, with fluxes of methane and carbon dioxide up to 53 and 47 L m^{-2} d^{-1}, respectively. Ostrovski et al. *(201)* reported a flux of 0.23 L m^{-2} d^{-1} from hypolimnetic sediments and Hughes et al. *(202)* observed gas

production fluxes of 2.7 L m^{-2} d^{-1} on a laboratory study with sediment from the Anacostia River, Washington, DC.

There are comparatively few studies investigating organic contaminant transport due to gas ebullition *(3, 19-21)*. Hulls and Costello *(206)* observed that polycyclic aromatic hydrocarbons (PAHs) are transported to the water column due to groundwater advection and gas ebullition in bench tests with sediment from Stryker Bay. Fendinger et al. *(20)* reported that sediment organic contaminant transport is likely a function of gas ebullition rate, Henry's law constant, and porewater contaminant concentration. According to the authors, organic contaminant partitioning occurred mainly between sediment gas and porewater; whereas partitioning between the solid and gas phase was negligible due to the high water content of sediments. Particle re-suspension was not considered in this study. Re-suspension is potentially an important mechanism for sediment release of PAHs because organic-rich sediment particles are more readily suspended *(276)*; and these particles contain much higher levels of more toxic high molecular weight PAHs *(259, 277)*. More recent studies have included re-suspension by gas ebullition as a transport mechanism *(19)*.

In contrast to the case with organic contaminants, to our knowledge, almost no studies have investigated the role ebullition plays in facilitating metal release from sediments. The objective of this study was to quantify the magnitude of organic and metal contaminant facilitated transport due to gas ebullition at numerous urban waterway sites with wide variation in physical, chemical, and contamination characteristics. A second objective was to develop models to predict ebullition-facilitated contaminant release and compare these predictions to literature values *(3, 19, 278-279)*.

6.3. Materials and Methods

Sediment sampling and analysis. Sediment sampling of Collateral Channel (CC) off the Chicago Sanitary and Ship Canal, the South Fork of the South Branch of the Chicago River, colloquially known as "Bubbly Creek" (BC-CDM), and the Chicago River turning basin (BCTB) was conducted onboard the Metropolitan Water Reclamation District (MWRD) vessel *PC1* in September 2005, November 2005 and July 2008, respectively. There is a combined sewer Outfall (CSO) on the northern terminus of CC that released storm and wastewater in the channel for several decades *(280)*. BCTB is adjacent to the Canal Origins Park and is located in a newly developed residential housing area, which is changing from industrial to mixed-residential *(130)*. BC-CDM is impacted by CSO effluent on an approximately monthly basis from the Racine Avenue pumping station (RAPS). Detailed description and location of this sites can be found elsewhere *(130, 281)*. A total of five whole core samples from the sediment surface to the clay/hardpan layer (6-7 m below water surface at all sites) and five surface grab (SG) samples were collected at CC *(280)*, four whole cores and four SG samples at BCTB, and five whole core and five SG samples at Bubbly Creek *(130, 264)*.

Sediment wet bulk density, dry bulk density, percent solids, percent moisture, porosity, organic carbon (OC), organic matter (OM), and chemical oxygen demand (COD) were measured as described previously *(130)*. Sediment metals and PAHs were analyzed by a National Environmental Laboratory Accreditation Program (NELAP) certified laboratory. PAHs were extracted according to USEPA SW 3550B and analyzed by gas chromatography-mass spectrometry single ion mode by SW 8270C-SIM *(258)*. Samples were prepared for metals analysis by acid digestion according to USEPA method SW 3050B and analyzed by inductively coupled plasma-mass spectrometry using method SW 6020A *(258)*.

Gas collection and analysis. Gas collection systems were constructed as described in Viana et al. *(4)*. The system consisted of a funnel of known area that directs gas bubbles through a glass wool contaminant trap on the interior. A second glass wool trap was maintained on the exterior of the funnel, shielded from bubbles but exposed to the water column as a control. The system had a gas collection tube with valve assembly, and a weight was used to hold the entire unit in a vertical position suspended well below the surface from a large foam float. The depth was adjusted to approximately mid-water column to avoid any surface wave disturbance and maintain a vertical orientation. Total gas volume was measured by displacement of water in graduated cylinders from the collector in the field. Clean glass wool (GW), pre-combusted at 550 °C for 4 h, was placed inside the gas collectors to trap contaminants transported with gas bubbles. The difference between the contaminant mass in the exterior and interior traps thus represented contaminant flux due to gas ebullition as reported here. T-tests comparing these samples showed they were statistically significantly different at the 95% confidence interval (CI). GW metal and PAH analyses were performed as described above for the sediment characterization.

Ebullition flux modeling. Measured gas fluxes were compared to those predicted using a mechanistic model based on an expanded form of the Monod equation proposed by Goldman and Carpenter *(282)*, an empirical model using backward stepwise multivariate regression analysis of our data, as well as predictions from models proposed by Winterwerp and van Kesteren *(283)* and by Mogollon et al. *(284)* (complete model development is presented in this chapter's supporting information, *Section S1*). The mechanistic model utilizes a limiting substrate concentration term (S_{labile}) that represents the portion of the sediment organic matter that actively contributes to gas generation and is equal to the ratio SG COD/SG OC. The model is simplified as described in the

model development supplemental information to the following equation valid for 278K<T<303K and 2%<SG OC< 20%:

$$\log(\mu) = 23 - 1.6log(\rho_b) - 3{,}800\left(\frac{1}{T}\right) - 2{,}500\left(\frac{S_{labile}}{T}\right) + 2{,}600\left(\frac{{S_{labile}}^2}{T}\right) \quad (6.1)$$

$$+ 1.5\log(S_{labile}) + 0.28\log(\gamma_0 + \gamma_1 T + S_{labile})$$

Where μ is the specific gas ebullition rate (mmol m^{-3} d^{-1}); ρ_b is the wet bulk density (kg m^{-3}); T is the average temperature during the measurement period (K); and γ_0 and γ_1 are constants equal to (0.8083) and (-0.0026), respectively. For simplicity, we assumed that ρ_b and S_{labile} do not vary with time.

Gas fluxes are determined assuming that the top 1 m of sediment is ebullition active, which is supported by several studies *(4, 285)*. An empirical model (described in *Results and Discussion*) was then developed using stepwise multivariate regression analysis of this data set that identified temperature and sediment S_{labile} as the primary factors accounting for gas ebullition for comparison.

Ebullition-facilitated contaminant flux modeling. The measured metal and PAH fluxes were compared to both an empirical model based upon stepwise multivariate regression analysis (described in *Results and Discussion*), as well as predictions from a model of ebullition-facilitated contaminant flux *(279)* and literature values *(3, 278)*.

Data analysis and Quality Assurance. All statistical analyses and exploratory factor analysis was performed using principle components analysis with Varimax rotation using the computer program MYSTAT v.12. Sampling and analytical protocols complied with requirements for NELAP accreditation and included matrix spikes, field blanks, and method blanks. Uncertainties at

the 95% confidence interval ($U_{95\%} = \sqrt{2(\mathrm{RSD})^2 + \mathrm{B}^2}$) for sediment samples were 30.5% and 20.3% for PAHs and metals respectively; and 24.1%, and 6.6% for PAHs and metals in GW, respectively.

6.4. Results and Discussion

Large heterogeneities exist at the field sites. Sediment characteristics varied greatly in the study sites. SG OM and SG OC was 1.5 to 32% and 1.8 to 20%, respectively, and whole core OM and OC ranged from 5.5 to 46% and 0.6 to 17%, respectively. Concentrations of PAHs in the surficial sediment varied from 20 to 24,000 mg kg^{-1}, and whole core PAH concentrations from 60 to 1,230 mg kg^{-1}. In 11 of 14 sites, surficial PAH levels were similar to or higher than the whole core mean values, indicating that PAH-impacted sediments have not been buried by less polluted sediments at the sediment-water interface. A complete set of descriptive statistics for the sediment properties can be found in the supporting information (Tables S1, S3, and S5).

Gas ebullition varied substantially as a function of temperature and sediment composition. Measured field gas fluxes ranged from 0.05 up to 11 L m^{-2} d^{-1} (Figure 6.1); values that are consistent with other reports in the literature *(199-200)*. CH_4, N_2, and CO_2 comprised 55±20%, 42±20%, and 3±2% of the evolved gas by volume, respectively. These results are consistent with reported lake sediment values of 48-67% and 0.01-3%, for CH_4 and CO_2, respectively *(204-205)*. Methanogenic activation energy values determined from Arrhenius plots of inverse rate versus inverse temperature varied from 12 up to 146 kJ mol^{-1}; also consistent with literature-reported values for sediments from 27 to 138 kJ mol^{-1} *(273-274)*. These values were used to estimate the annual volume of gas released from the Arrhenius equation to correct the measured gas production rates based on the annual temperature variations observed on-site (Figure 6.2), with total volumes ranging from 1.0- 2.1 m^3 m^{-2} yr^{-1}.

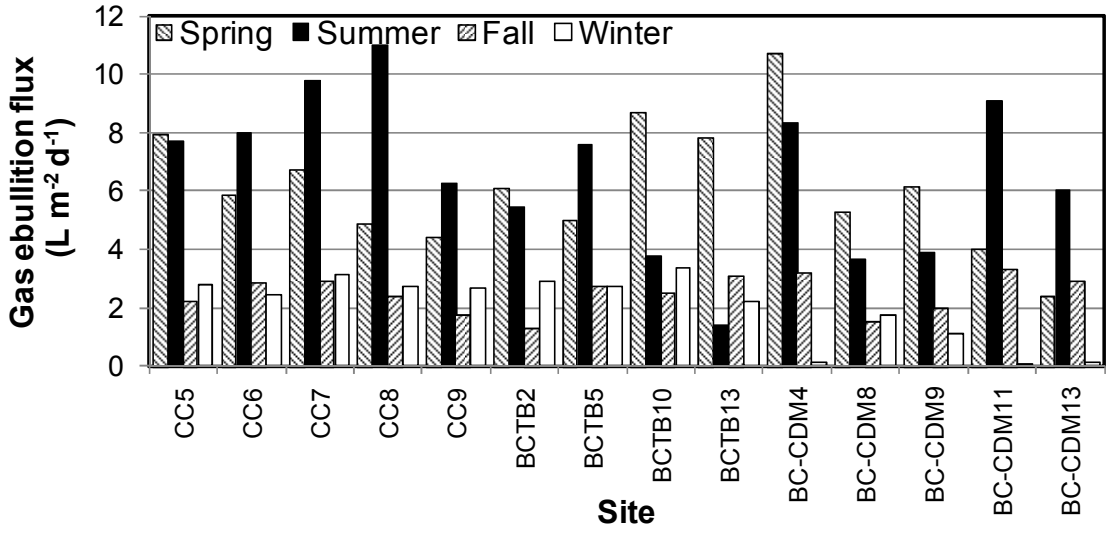

Figure 6.1. Measured total field gas fluxes in the 14 sampled sites by season. Overall, CH_4, N_2, and CO_2 comprised 55±20%, 42±20%, and 3±2% of the gas by volume, respectively.

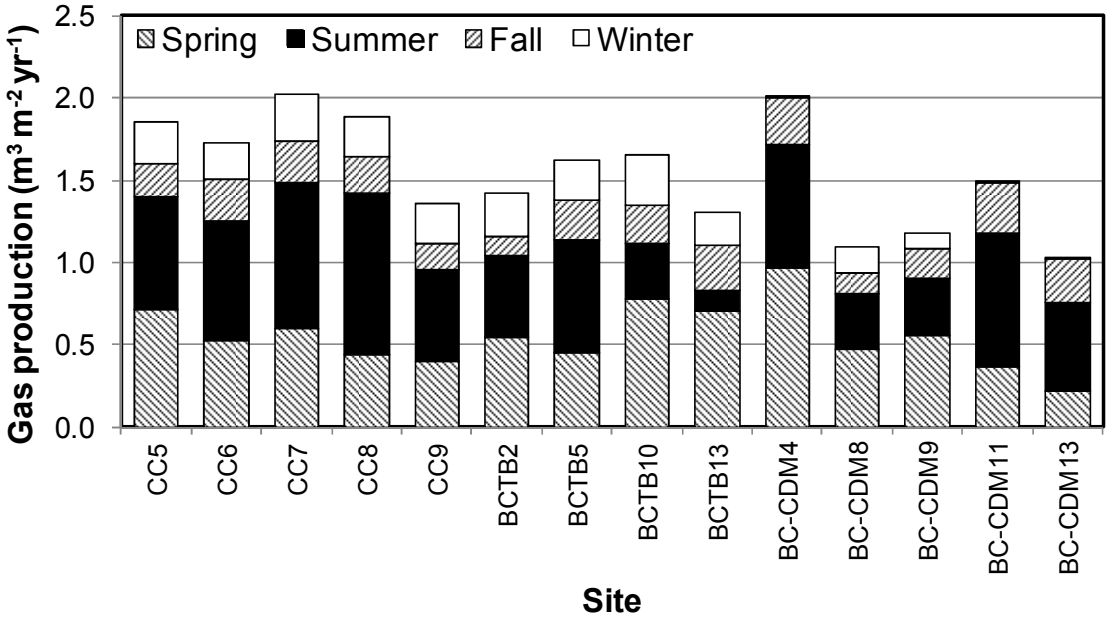

Figure 6.2. Estimated volumetric gas ebullition per square meter of sediment on an annual basis for the 14 sample sites based upon Arrhenius-corrected ebullition rates over the year.

Mechanistic and empirical models describe gas ebullition well. A mechanistic model was developed to predict biogenic gas production from substrate utilization following the Monod

kinetic regime *(4, 206)*. Comparison of the predictions to the observed results (Figure 6.3a) confirms that the model yields a good fit to the data (p-value=4E-06, R^2=0.56).

Although the mechanistic model resulted in a good fit to the observed results, we also found that linear relationships existed between gas flux and readily measurable parameters using the 56 sets of measurements in the 14 sites. Backward stepwise multivariate regression analysis of the data set indicated that sediment temperature and S_{labile} were able to predict field gas fluxes (GF_f) better than all the other measured parameters, explaining 63% of the variation:

$$GF(L\ m^{-2}\ d^{-1}) = -0.009 + 0.31T(℃) - 4.5S_{labile} \quad \text{(p-value=2E-10, } R^2\text{=0.63)} \qquad (6.2)$$

Exploratory factor analysis was also performed to assess the robustness of our model. Measured field gas flux and sediment temperature, physical and chemical properties produced a four factor solution with clearly demarcated predictive capabilities (Table S6). The results show high correlation within each factor and poor correlation across factors. Surficial sediment properties such as SG OC, SG OM, SG wet bulk density, SG % solids and S_{labile}, are highly loaded on factor 1 (loading factor, LF≥0.9). Gas flux and temperature are highly loaded into factor 2 (LF≥0.9). Site characteristics such as sediment depth and water depth are highly loaded on factor 3 (LF≥0.9), and core sediment properties such as core OC and core OM are highly loaded on factor 4 (LF≥0.9). The fact that both gas flux and temperature are highly loaded on the same factor agrees with the inclusion of temperature as a major predictive variable in both our mechanistic and predictive models. In addition, the finding that gas flux is also loaded onto factor 1 with surficial sediment parameters such as S_{labile} indicates that biogenic gas production is also a function of organic material lability, in agreement with both models and literature findings *(283)*.

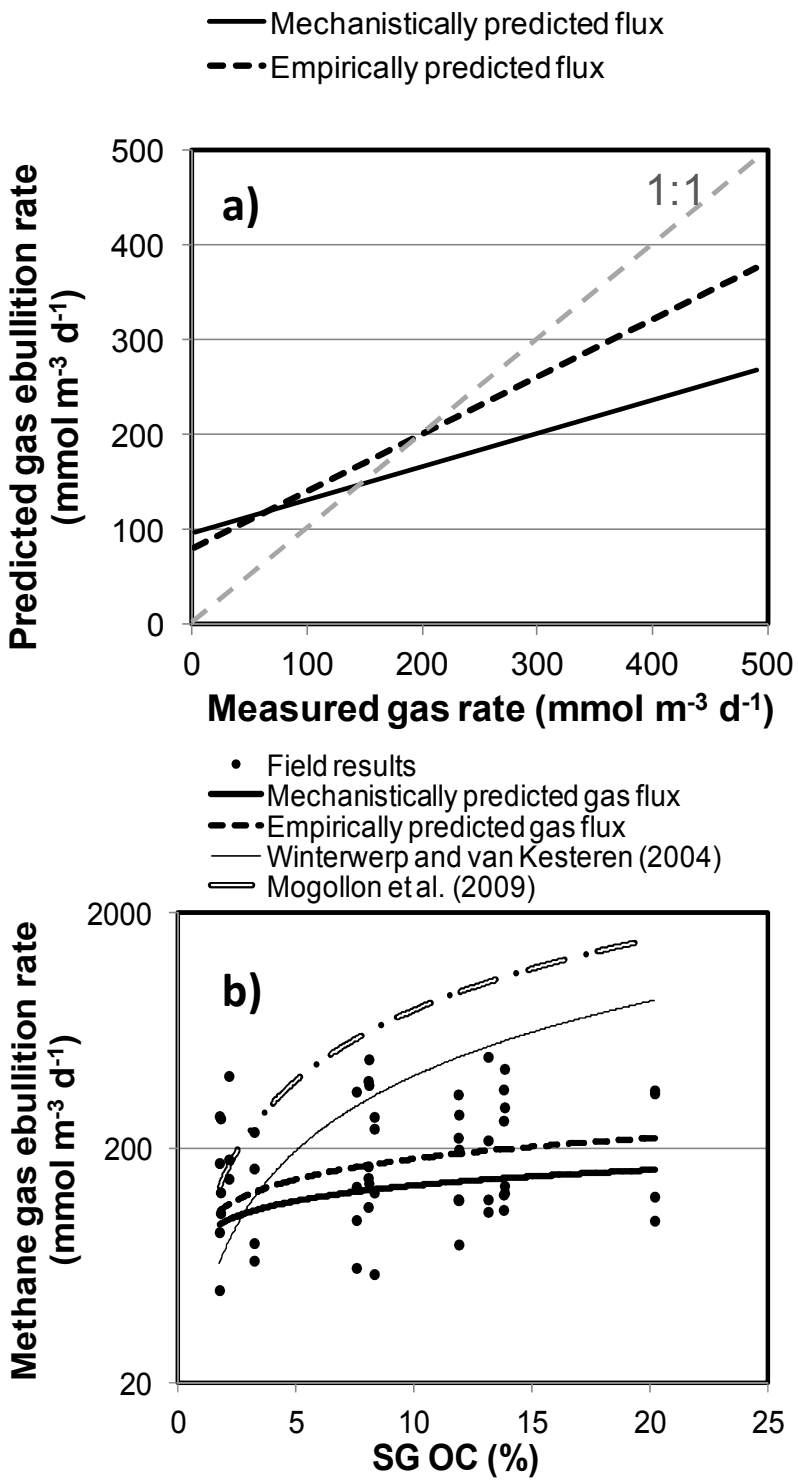

Figure 6.3. Comparison of measured and predicted gas ebullition rates in sediments. Shown are a) comparison of the measured values with the mechanistic and empirical models developed in the present study (dashed line represents 1:1 slope), and b) comparison of the measured values (bold dash) to the two models developed in the present study (bold and dotted lines), as well as two literature models (thin and dot/dashed lines). Note log scale on y axis in lower figure.

Our mechanistic and empirical gas ebullition model results were compared to models available in the literature *(283-284)*. The literature models predict gas ebullition rates substantially higher than the ones we observed in the field (Figure 6.3b); likely due to parameter uncertainty and system differences. Winterwerp and van Kesteren report the parameter *k(t)* can vary by a factor of 10 *(283)*; and the Mogollon et al. model *(284)* was developed for marine sediments, while our results are for an organic-rich urban freshwater river. The wide disparity in results suggests that the models developed here may be a more suitable predictive tool for quantification of gas ebullition rates in such systems.

Gas ebullition results in large sediment-to-water flux of contaminants. Particulate matter was found in the glass wool samples located inside the gas collection systems (in contrast to the control glass wool on the exterior of the collection system), resulting from gas bubbles transporting solid particulates into the trap. For most sites As, Ag, Be, Cd, Co, Mo and Se were below the detection limit (DL) in the glass wool, while Ba, Cr, Cu, Fe, Mn, Pb, Ni and Zn were all present above the DL for most samples. We thus confine our discussion here to the latter group of metals. Contaminant fluxes varied substantially with season. Higher temperatures in spring and summer led to higher gas ebullition fluxes compared to the fall, with concomitantly higher metal contaminant fluxes. Surprisingly, many sites had significant ebullition-facilitated metal contaminant fluxes during winter. Fe and Pb fluxes varied from 0-450 mg m^{-2} d^{-1} and 0-18 mg m^{-2} d^{-1}. Ba, Cr and Zn flux ranged from 0-5.2 mg m^{-2} d^{-1}, 0-2.4 mg m^{-2} d^{-1} and 0-20 mg m^{-2} d^{-1}, respectively (Figure S1, Table S2). Sediment metal concentrations at these sites ranged from 3.4-390 mg kg^{-1}, 2.6-730 mg kg^{-1}, 230-43000 mg kg^{-1}, 0.07-1.8 mg kg-1, 1.8-3400 mg kg^{-1}, and 6.0-1,800 mg kg^{-1} for Ba, Cr, Fe, Hg, Pb and Zn, respectively (Table S3).

Nearly all PAHs were present above the DL in the glass wool samples inside the gas collection systems, and thus had measurable fluxes. The effect of temperature and gas flux was less pronounced on ebullition-facilitated PAH fluxes compared to metals. This lack of variability was driven by the relatively high PAH fluxes observed during fall and winter compared to metals, particularly in the highly PAH-contaminated CC sites (Figure S2). Anthracene, benzo(a)pyrene, chrysene, fluoranthene and fluorene fluxes varied from 0-11 mg m^{-2} d^{-1}, 0-13 mg m^{-2} d^{-1}, 0-11 mg m^{-2} d^{-1}, 0-45 mg m^{-2} d^{-1} and 0-15 mg m^{-2} d^{-1}, respectively. Naphthalene, phenanthrene and pyrene fluxes ranged from 0-3 mg m^{-2} d^{-1}, 0-52 mg m^{-2} d^{-1} and 0-31 mg m^{-2} d^{-1}, respectively (Table S4). Sediment PAH concentrations at these sites ranged from 0.3-630 mg kg^{-1}, 1.2-240 mg kg^{-1}, 0.3-6,900 mg kg^{-1}, 2.3-5,100 mg $kg^{-}1$ and 3.5-2,000 mg kg^{-1} for anthracene, benzo(a)pyrene, naphthalene, phenanthrene and pyrene, respectively (Table S5). Interestingly, naphthalene was often observed in these sediments at concentrations similar to the PAHs phenanthrene or pyrene. In contrast, naphthalene flux was relatively lower than either PAH. We would not expect such an observation if partitioning to the gas phase were the only mechanism for ebullition-facilitated transport, because naphthalene is much more volatile than the PAHs. However, we would expect such results if hydrophobic partitioning to the hydrophobic gas bubble and/or re-suspension of organic-rich particles were the primary mechanism of enhanced flux because of the less hydrophobic nature of naphthalene compared to the PAHs. The latter interpretation is supported by the observation that increased ebullition-facilitated fluxes follow a slight positive trend with PAH hydrophobicity.

Empirical models describe total gas ebullition-facilitated contaminant fluxes. Ebullition-facilitated metal fluxes increased in a linear fashion with gas ebullition fluxes (p-values <0.05 for

most metals, Figure S3), but were not statistically significantly correlated with SG OC or S_{labile} (data not shown). Conversely, ebullition-facilitated PAH fluxes were not highly correlated with gas flux changes (Figures S4), but were statistically significantly correlated with sediment SG OC (Figure S5, seasonal dummy variables used as regressors).

Ebullition-facilitated summer metal contaminant fluxes had a statistically significant increase with metal contaminant concentrations in the sediments on a seasonal basis (p-value=1E-15, R^2=0.55) based on a linear function between the natural logarithms of all metal contaminant fluxes and all metal contaminant concentrations in sediments. The variation within a single contaminant was not sufficient to represent a significant metal contaminant concentration range; thus we confine our discussion to all metal contaminants considered together in the regression. A similar logarithmic trend between sediment concentration and ebullition-facilitated fluxes was observed for the PAHs (p-value=1E-14, R^2=0.51).

Backward stepwise multivariate regression analysis was carried out to predict ebullition-facilitated contaminant flux using gas flux and sediment physical and chemical variables (Figure 6.4a). The variables sediment-water partitioning coefficient, sediment contaminant concentration, gas flux, % solids, sediment depth, SG OC and S_{labile} are able to explain 68% of the variation of ebullition-facilitated metal contaminant flux (p-value=9E-16, R^2=0.68):

$$lnCF_{metal} = -1.3 * 10^{-5} kd + 0.31GF_f + 0.76lnC_{sed} - 0.096\phi - 0.23SG\ OC + 3.1S_{labile} - 0.26D_{sed} \quad (6.3)$$

Where CF_{metal} is the ebullition-facilitated metal contaminant flux (mg m^{-2} d^{-1}); K_d is the sediment-water partitioning coefficient (L kg^{-1}); C_{sed} is the metal concentration in the sediment (mg kg^{-1}); ϕ is the percent of solids in the sediment; and D_{sed} is the sediment depth (m).

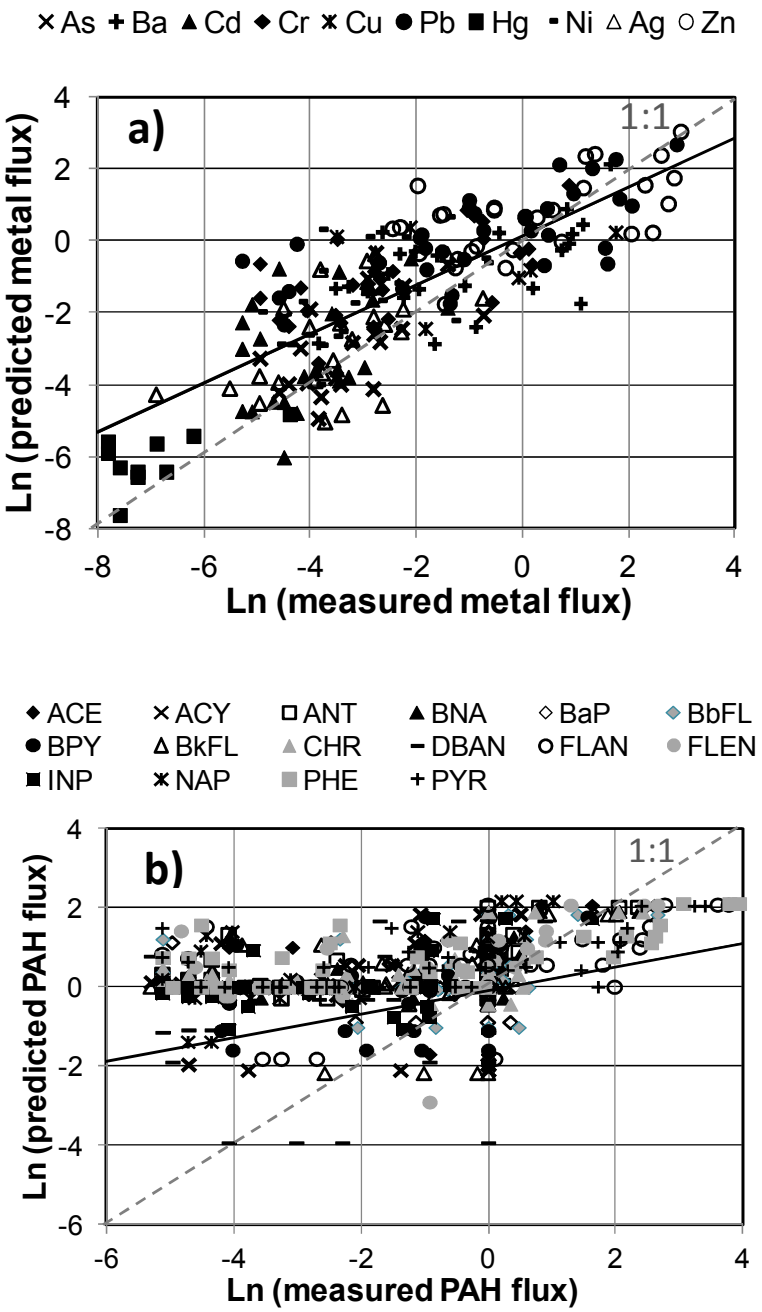

Figure 6.4. Comparison of empirically predicted ebullition-facilitated contaminant fluxes to measured values of a) individual metal fluxes (p-value=9E-16, R^2=0.68), and b) individual PAH fluxes (p-value=9E-16, R^2=0.27). Dashed line represents a 1:1 slope. ACE=acenaphthene, ACY=acenaphthylene, ANT=anthracene, BNA=benzo[a]anthracene, BaP=benzo[a]pyrene, BbFL=benzo[b]fluoranthene, BPY=benzo[g,h,i]perylene, BkFL=benzo[k]fluoranthene, CHR=chrysene, DBAN=dibenzo[a,h]anthracene, FLAN=fluoranthene, FLEN=fluorene, INP=indenopyrene, NAP=naphthalene, PHE=phenanthrene, PYR=pyrene.

A similar analysis was performed for the ebullition-facilitated PAH flux data (Figure 6.4b). Although the regression is statistically significant (p-value=9E-16), gas flux and sediment physical and chemical variables were able to explain only 27% of the variation for individual PAH fluxes (p-value=9E-16):

$$CF_{PAH} = 12 - 0.28logK_{OC} + 0.50lnC_{sed} - 0.028\rho_b + 0.39\emptyset + 0.19SG\ OM + 0.097Core\ OM - 0.59Core\ OC - 7.0S_{labile} + 2.2D_{sed} + 1.9D_w \quad (6.4)$$

Where CF_{PAH} is the ebullition-facilitated PAH flux (mg m^{-2} d^{-1}); k_{oc} is the organic carbon-water partitioning coefficient (L kg^{-1}); and D_w is the water depth (m).

In contrast, our empirical model was able to explain 59% of the variation on total PAH flux (p-value=1E-04, Figure 6.5b):

$$lnCF_{TPAH} = 13.1 - 0.674lnC_{sed} + 0.301GF_F - 0.017\rho_b + 0.744SG\ OC + 0.17Core\ OM - 0.51Core\ OC + 18.3S_{labile} \quad (6.5)$$

Where CF_{TPAH} is the ebullition-facilitated total PAH flux (mg m^{-2} d^{-1}); and C_{sed} is total PAH concentration in the sediment (mg kg^{-1}).

The difference in predictive ability between the metals and PAHs indicate that ebullition facilitated PAH flux may be a more complex process, and thus more difficult to predict than metal fluxes. This is consistent with a facilitated flux mechanism whereby metals are primarily particle bound and suspended by bubble ebullition, whereas PAHs are transported by both particle re-suspension and sorption into/onto gas bubbles. The nature of the sediment organic carbon and amount of organic content in the re-suspended particles, rather than in the bulk sediment as a whole, as well as the presence of NAPL formation, likely play an important role in PAH flux.

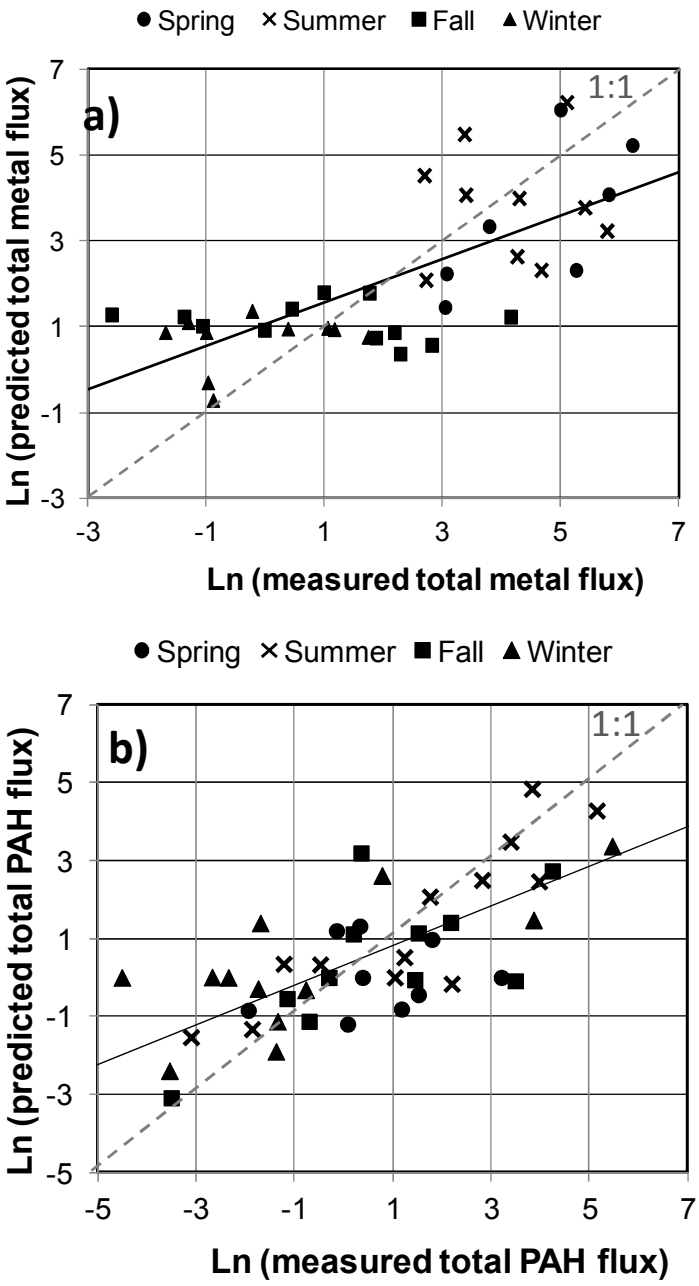

Figure 6.5. Comparison of empirically predicted ebullition-facilitated contaminant fluxes to measured values of a) total metals (p-value=3E-05, R^2=0.60), and b) total PAHs (p-value=1E-04, R^2=0.59). Dashed line represents a 1:1 slope.

The empirical model results for individual PAHs were compared to results obtained using a phase-partitioning correction *(279)*:

$$CF_{PAH} = HC_{pw}GF_f \text{ , and } C_{pw}\ assumed\ equal\ to\ \frac{C_{sed}}{K_{OC}f_{OC}} \quad (6.6)$$

Where: H is the Henry's law constant (dimensionless); C_{pw} is the porewater PAH concentration (mg L^{-1}); and f_{oc} is the fraction of organic carbon. Literature H and K_{oc} values *(286)* and measured C_{sed}, f_{oc} and GF_f values were used to calculate CF_{PAH}. The literature model substantially under-predicts ebullition-facilitated PAH fluxes compared to our observed values, which is likely because the model does not account for contaminant transport due to particle re-suspension (Figure S6). It should be noted that our system does not fall out of the range of reported PAH fluxes in the literature, which vary by several orders of magnitude from 1E-06 up to 169 mg m^{-2} d^{-1} under extreme gas flux conditions *(3, 19, 278)*.

6.5. Conclusions and Implications

Contaminant release due to gas ebullition was consistently observed in our 14 sampled sites (Figure 6.6). The magnitude of these fluxes indicates that gas ebullition is an important pathway for release of PAH and heavy metal pollutants buried in sediments to the water column in contaminated riverine freshwater systems. The results from this study also demonstrate that quantifying and predicting gas flux and ebullition-facilitated contaminant transport at sites within a relatively broad range of sediment organic content and contamination levels as the ones studied in this paper is feasible. In addition, we have presented both mechanistic and an empirical models for predicting gas fluxes at urban contaminated freshwater systems that are based on more easily measurable parameters such as temperature and S_{labile}. The heterogeneity in sediment chemical and physical parameters among all of the studied sites contributes to broad validity of these findings.

We have shown that both metal and organic contaminants are transported by gas ebullition and represent a significant contribution to the total contaminant flux from sediments to the water column. Multiple lines of evidence support the hypothesis that ebullition-facilitated transport is mechanistically different for PAHs compared to metals. These include the statistically significant

correlation between ebullition-facilitated metal flux and gas flux, contrasted with the statistically significant correlations between ebullition-facilitated PAH flux and both SG OC and concentration in the sediments (p-value<1E-05). These results are consistent with a PAH transport mechanism combining organic-rich particle re-suspension and sorption into/onto the gas bubbles from sediment porewater; while metal release is due mainly to particle re-suspension. Thus, the limiting factor for metal release is the amount of bubbles produced (and indirectly the lability of the sediment organic matter to biodegradation), whereas the amount of organic carbon (indirectly affecting partitioning), coupled with its lability to biodegradation limits PAH release.

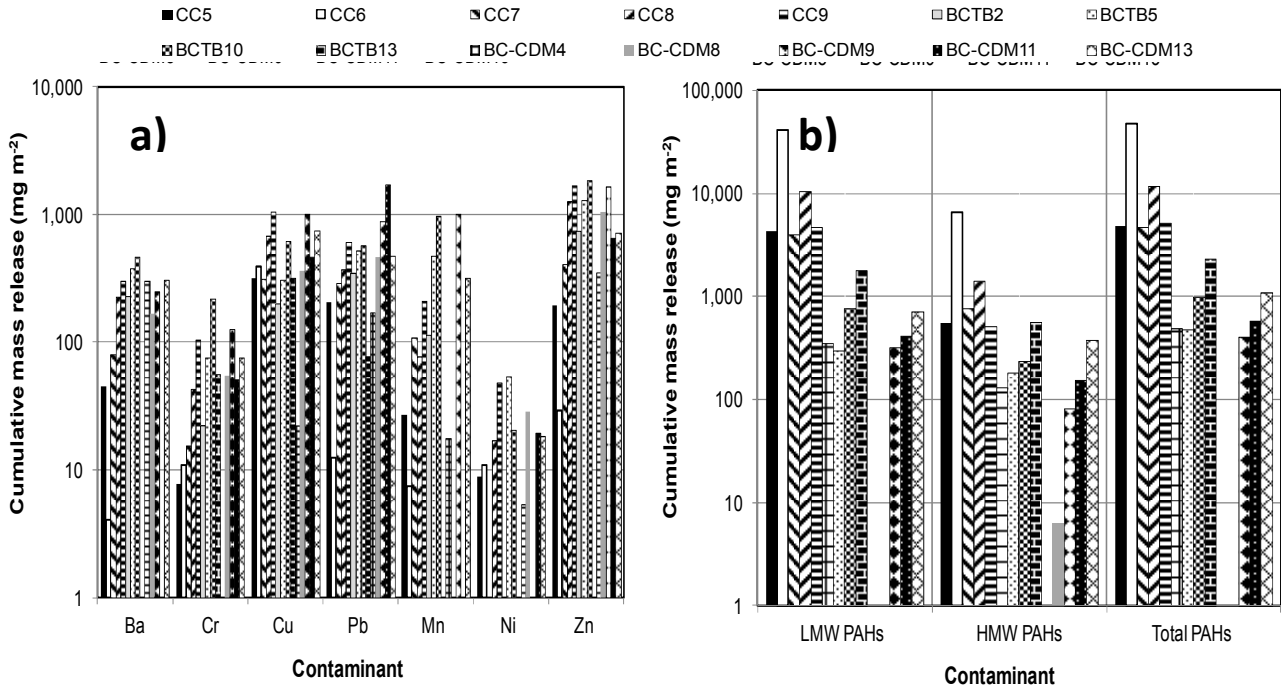

Figure 6.6. Cumulative annual metal (a) and PAH (b) release. Shown is mass release to the water column per m^2 of sediment on an annual basis by gas ebullition. Note different log scales on the y axis.

6.6. Supporting Information

Tables S1 to S6, Figures S1 to S5, and Section S1.

Table S1. Descriptive Statistics for Sediment Physical Parameters and Gas Ebullition Fluxes

	T (°C)	Gas flux (L m^{-2} d^{-1})	SG OM (%)	SG OC (%)	Core OM (%)	Core OC (%)	Sed depth (m)
N of Cases	56	56	14	14	14	14	14
Minimum	7	0.05	1.53	1.76	5.4	0.59	0.3
Maximum	26.5	11.0	32	20	46	17	6.46
Range	19.5	10.9	30.6	18.4	40.6	16.4	6.16
Median	18.5	3.3	13.6	8.20	14.1	12.0	3.08
Arithmetic Mean	17.7	4.3	14.4	8.98	16.0	10.6	3.27
Trimmed Mean (10%, 2 sided)	17.9	4.1	13.7	8.81	13.9	11.3	3.29
SEM	0.91	0.37	2.65	1.47	2.8	1.26	0.51
COV	0.39	0.64	0.69	0.61	0.66	0.44	0.59
Skewness(G1)	-0.21	0.72	0.45	0.27	1.92	-0.78	0.05
Kurtosis(G2)	-1.44	-0.30	-0.59	-0.38	4.52	-0.03	-0.87
Shapiro-Wilk Statistic	0.89	0.93	0.93	0.93	0.81	0.92	0.97
Anderson-Darling Statistic	-	1.55	0.34	0.40	0.93	0.52	0.17

Table S2. Descriptive Statistics for Metal Contaminant Fluxes due to Gas Ebullition

	Metal flux due to gas ebullition (mg m^{-2} d^{-1})													
	As	**Ba**	**Cd**	**Cr**	**Co**	**Cu**	**Fe**	**Pb**	**Mn**	**Hg**	**Ni**	**Se**	**Ag**	**Zn**
N of Cases	49	49	49	49	49	49	49	49	49	26	49	49	49	49
Minimum	0.00	0.00	0.00	0.00	0.00	0.00	0.00	0.00	0.00	0.00	0.00	0.00	0.00	0.00
Maximum	0.47	5.13	0.24	2.35	0.47	9.64	452	17.9	9.58	0.01	0.49	0.47	0.47	19.6
Range	0.47	5.13	0.24	2.35	0.47	9.65	452	17.9	9.58	0.01	0.49	0.47	0.47	19.6
Median	0.00	0.07	0.00	0.02	0.00	0.74	14	0.25	0.03	0.00	0.02	0.00	0.01	0.28
Arithmetic Mean	0.03	0.62	0.02	0.19	0.03	1.39	50	1.45	0.79	0.00	0.06	0.03	0.03	2.61
Trimmed Mean (10%, 2 sided)	0.01	0.36	0.01	0.08	0.01	0.95	26	0.73	0.34	0.00	0.03	0.01	0.02	1.29
SEM	0.01	0.16	0.01	0.06	0.01	0.28	13.0	0.43	0.26	0.00	0.02	0.01	0.01	0.71
COV	2.48	1.82	2.35	2.24	2.48	1.43	1.83	2.09	2.35	2.78	1.98	2.48	2.22	1.90
Skewness(G1)	4.61	2.18	4.44	3.49	4.61	2.36	2.79	3.83	3.71	4.63	2.87	4.61	4.41	2.21
Kurtosis(G2)	24.2	4.73	23.0	14.4	24.2	6.26	8.46	18.2	14.6	22.6	8.1	24.2	22.8	3.94
Shapiro-Wilk Statistic	0.43	0.62	0.46	0.51	0.43	0.71	0.60	0.52	0.47	0.37	0.55	0.43	0.48	0.59
Anderson-Darling Statistic	9.10	7.85	8.49	8.92	9.10	4.57	7.27	7.66	9.19	5.90	8.25	9.10	7.86	8.62

Table S3. Descriptive Statistics for Metal Concentration in the Sediments

	Metals in sediments (all mg kg^{-1} sed dry wt, except Fe in g kg^{-1} sed dry wt)													
	As	**Ba**	**Cd**	**Cr**	**Co**	**Cu**	**Fe**	**Pb**	**Mn**	**Hg**	**Ni**	**Se**	**Ag**	**Zn**
N of Cases	14	14	14	14	14	14	14	14	14	14	14	14	14	14
Minimum	2.60	3.40	0.82	2.60	1.30	6.50	0.23	1.80	6.70	0.07	2.60	0.55	2.60	6.00
Maximum	13.0	390	17.0	730	15.0	1000	43	3400	410	1.80	85.0	2.90	15.0	1800
Range	10.4	387	16.2	727	13.7	994	42.8	3398	403	1.74	82.4	2.35	12.4	1794
Median	7.28	236	8.06	125	7.41	404	21.5	677	255	1.05	44.5	1.69	7.03	985
Arithmetic Mean	7.13	244	7.89	85.1	7.29	380	21.4	497	259	1.10	45.1	1.69	6.47	993
Trimmed Mean (10%, 2 sided)	6.35	175	5.13	68.0	6.17	264	14.7	343	199	0.83	33.3	1.46	6.21	626
SEM	0.97	29.0	1.53	47.9	1.05	74.3	3.34	221	31.2	0.14	7.05	0.23	0.99	163
COV	3.63	108	5.72	179	3.94	278	12.5	827	117	0.51	26.4	0.86	3.69	610
Skewness(G1)	0.10	-0.55	-0.15	3.37	0.14	0.62	0.00	3.09	-0.40	-0.71	-0.13	-0.02	0.99	-0.03
Kurtosis(G2)	0.60	0.60	0.60	0.60	0.60	0.60	0.60	0.60	0.60	0.60	0.60	0.60	0.60	0.60
Shapiro-Wilk Statistic	1.15	1.15	1.15	1.15	1.15	1.15	1.15	1.15	1.15	1.15	1.15	1.15	1.15	1.15
Anderson-Darling Statistic	0.16	0.72	0.05	0.00	0.88	0.71	0.91	0.00	0.43	0.32	0.41	0.13	0.12	0.34

Table S4. Descriptive Statistics for PAH Contaminant Fluxes due to Gas Ebullition

	PAH flux due to gas ebullition (mg m^{-2} d^{-1})															
	ACE	**ACY**	**ANT**	**BNA**	**BaP**	**BfFL**	**BPY**	**BkFL**	**CHR**	**DBAN**	**FLAN**	**FLEN**	**INP**	**NAP**	**PHE**	**PYR**
N of Cases	49	49	49	49	49	49	49	49	49	49	49	49	49	49	49	49
Minimum	0	0	0	0	0	0	0	0	0	0	0	0	0	0	0	0
Maximum	13.6	1.7	10.6	12.1	12.8	14.3	4.8	7.5	11.4	2.4	44.1	14.3	5.1	2.8	51.5	30.5
Range	13.6	1.7	10.6	12.1	12.8	14.3	4.8	7.5	11.4	2.4	44.1	14.3	5.1	2.8	51.5	30.5
Median	0.03	0.02	0.04	0.07	0.07	0.08	0.04	0.07	0.07	0.02	0.12	0.02	0.04	0.02	0.07	0.10
Arithmetic Mean	0.60	0.12	0.61	0.94	0.65	0.68	0.23	0.54	0.72	0.12	3.51	0.85	0.25	0.23	3.84	2.46
SEM	0.30	0.04	0.27	0.33	0.28	0.30	0.10	0.21	0.28	0.05	1.23	0.38	0.11	0.08	1.47	0.86
COV	3.47	2.34	3.10	2.46	3.03	3.11	3.06	2.66	2.74	3.07	2.46	3.13	3.06	2.39	2.68	2.44
Skewness(G1)	5.51	4.39	4.47	3.88	5.41	5.83	6.13	4.10	4.47	5.95	3.61	4.31	6.02	3.26	3.61	3.57
Kurtosis(G2)	33.2	22.1	20.6	15.9	32.1	37.1	40.3	17.1	21.3	38.4	13.9	19.0	39.1	11.3	13.6	13.6
Shapiro-Wilk Statistic	0.31	0.46	0.35	0.44	0.34	0.32	0.31	0.40	0.39	0.32	0.46	0.36	0.32	0.48	0.43	0.47
Anderson-Darling Statistic	12.6	8.8	12.3	9.8	11.2	11.1	10.9	10.9	10.7	11.0	10.0	12.5	11.0	10.5	11.3	9.9

ACE=acenaphthene, ACY=acenaphthylene, ANT=anthracene, BNA=benzo[a]anthracene, BaP=benzo[a]pyrene, BbFL=benzo[b]fluoranthene, BPY=benzo[g,h,i]perylene, BkFL=benzo[k]fluoranthene, CHR=chrysene, DBAN=dibenzo[a,h]anthracene, FLAN=fluoranthene, FLEN=fluorene, INP=indenopyrene, NAP=naphthalene, PHE=phenanthrene, PYR=pyrene

Table S5. Descriptive Statistics for PAH Concentration in the Sediments

	PAHs in sediments (mg kg^{-1} sed dry wt)															
	ACE	**ACY**	**ANT**	**BNA**	**BaP**	**BfFL**	**BPY**	**BkFL**	**CHR**	**DBAN**	**FLAN**	**FLEN**	**INP**	**NAP**	**PHE**	**PYR**
N of Cases	14	14	14	14	14	14	14	14	14	14	14	14	14	14	14	14
Minimum	0.13	0.14	0.32	1.30	1.20	1.20	0.72	1.30	1.50	0.32	4.50	0.32	0.72	0.29	2.30	3.50
Maximum	2000	72.0	630	590	240	350	40.0	280	390	25.0	3100	2000	140	6900	5100	2000
Range	2000	71.9	630	589	239	349	39.3	279	389	24.7	3096	2000	139	6900	5098	1997
Median	3.05	0.98	8.60	23.0	14.5	14.0	6.45	12.5	21.0	2.95	60.0	3.35	6.60	0.88	39.5	46.5
Arithmetic Mean	175	6.91	60.3	62.5	31.9	40.4	9.97	31.9	47.3	4.63	302	177	16.8	580	469	202
SEM	141	5.04	44.1	40.9	16.4	24.1	2.92	19.3	26.7	1.70	217	141	9.61	488	358	139
COV	3.02	2.73	2.74	2.45	1.92	2.23	1.10	2.26	2.11	1.37	2.69	2.97	2.15	3.15	2.86	2.58
Skewness(G1)	3.67	3.67	3.65	3.65	3.47	3.61	1.83	3.63	3.58	2.86	3.66	3.66	3.57	3.68	3.66	3.64
Kurtosis(G2)	13.6	13.6	13.5	13.5	12.5	13.3	3.63	13.4	13.1	9.17	13.5	13.5	13.1	13.7	13.6	13.4
Shapiro-Wilk Statistic	0.37	0.38	0.39	0.40	0.48	0.42	0.80	0.42	0.44	0.64	0.39	0.38	0.44	0.36	0.38	0.40
Anderson-Darling Statistic	3.95	3.85	3.73	3.63	2.88	3.42	0.99	3.50	3.26	1.75	3.73	3.89	3.26	4.09	3.82	3.62

ACE=acenaphthene, ACY=acenaphthylene, ANT=anthracene, BNA=benzo[a]anthracene, BaP=benzo[a]pyrene, BbFL=benzo[b]fluoranthene, BPY=benzo[g,h,i]perylene, BkFL=benzo[k]fluoranthene, CHR=chrysene, DBAN=dibenzo[a,h]anthracene, FLAN=fluoranthene, FLEN=fluorene, INP=indenopyrene, NAP=naphthalene, PHE=phenanthrene, PYR=pyrene

Table S6. Rotated Loading Matrix

Variables	Factor 1	Factor 2	Factor 3	Factor 4
Gas Flux (L m^{-2} d^{-1})	0.18	0.07	0.92	0.05
Temperature (°C)	0.04	0.04	0.94	0.02
SG OM (%)	0.90	0.29	0.02	0.09
SG OC (SGOC)	0.92	0.27	0.06	0.10
Core OM (%)	0.27	0.03	0.01	0.92
Core OC (%)	0.12	0.23	0.04	0.93
Wet Bulk Density (kg m^{-3})	0.93	0.03	0.03	0.22
Solids (%)	0.90	0.06	0.05	0.25
COD/TOC	0.94	0.07	0.08	0.02
Sed Depth (m)	0.06	0.94	0.00	0.19
Water Depth (m)	0.14	0.90	0.03	0.06

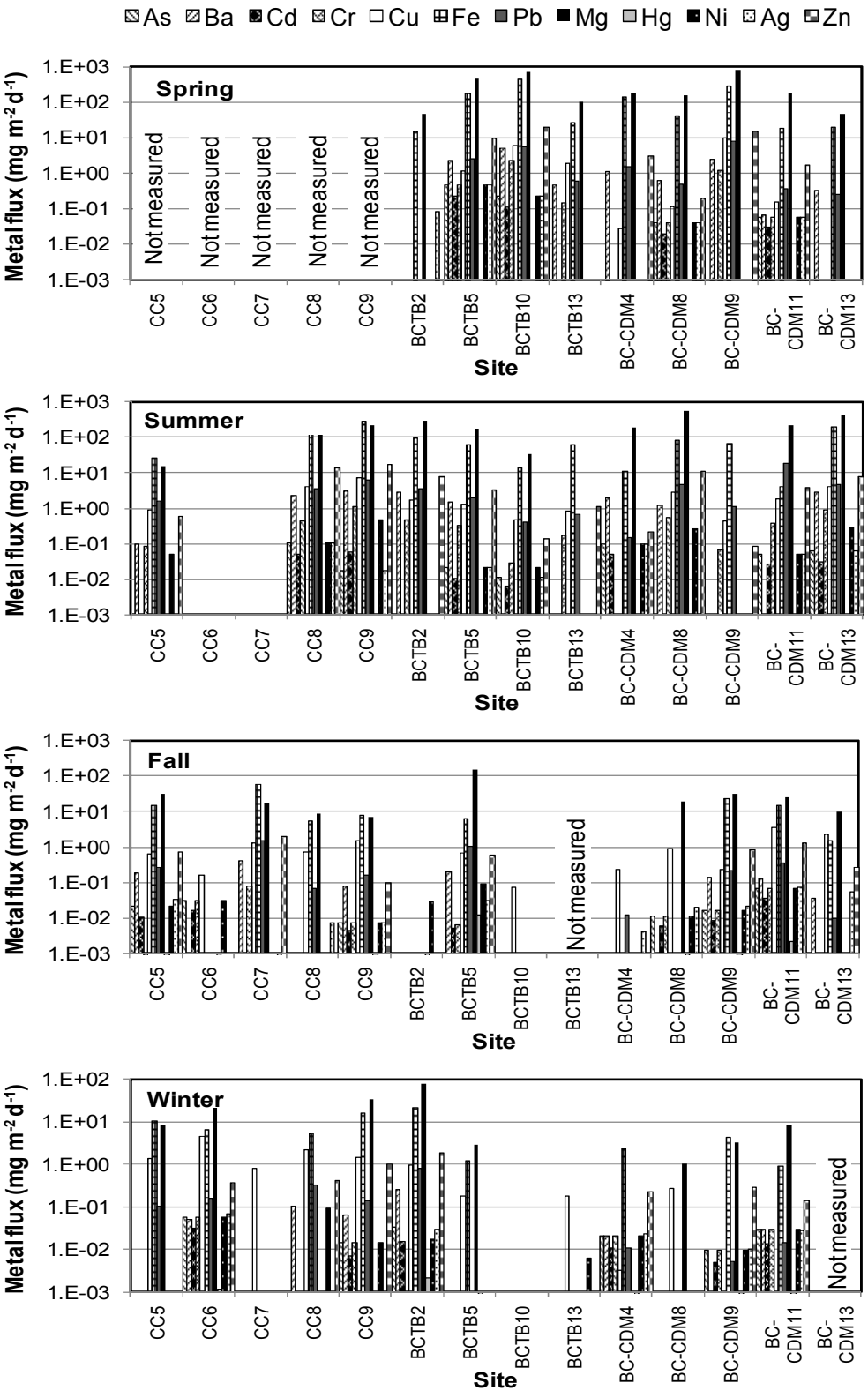

Figure S1. Ebullition-facilitated metal flux to the water column by season.

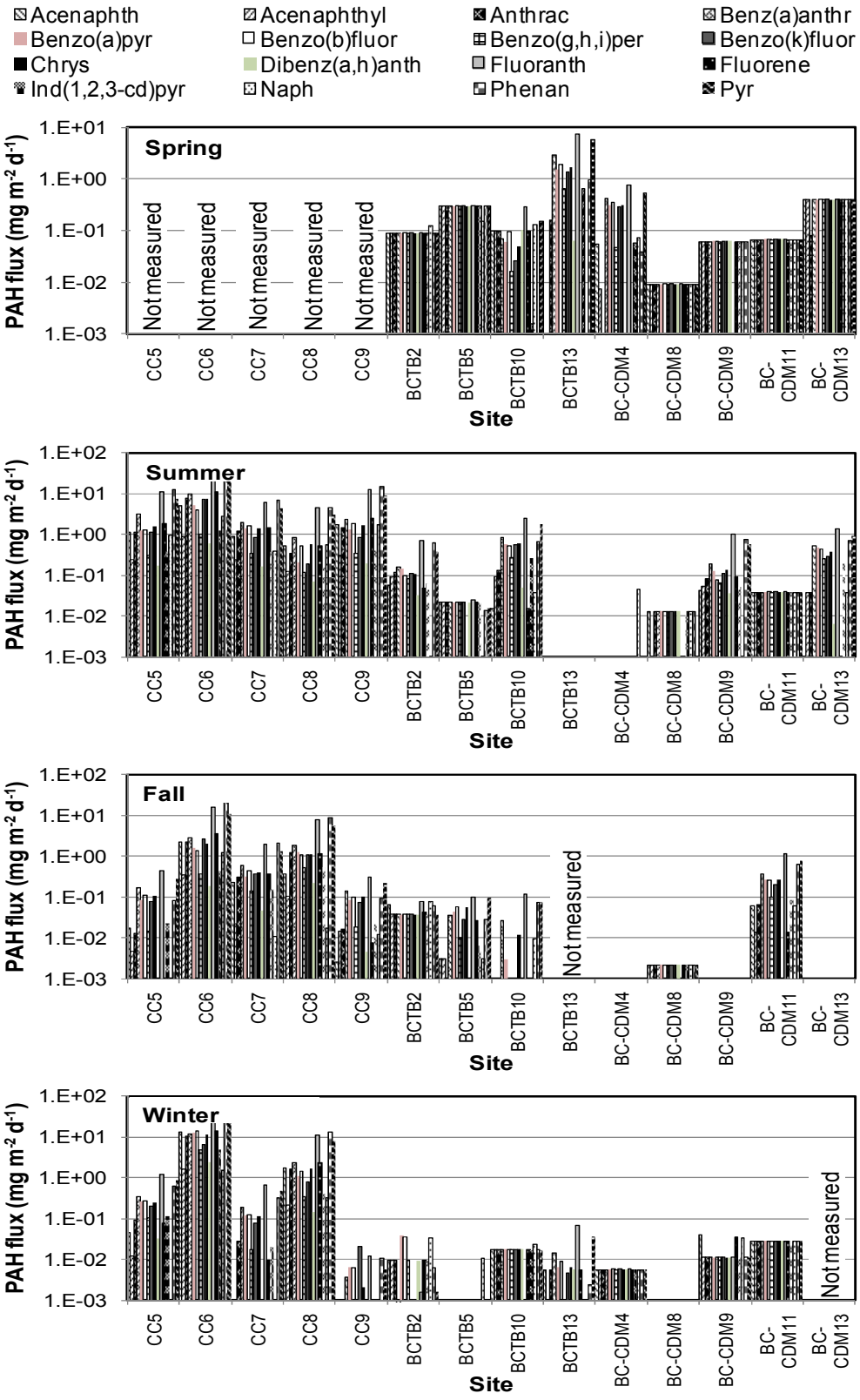

Figure S2. Ebullition-facilitated PAH flux to the water column by season. DL values are shown where PAHs were measured but not significantly different from exterior trap.

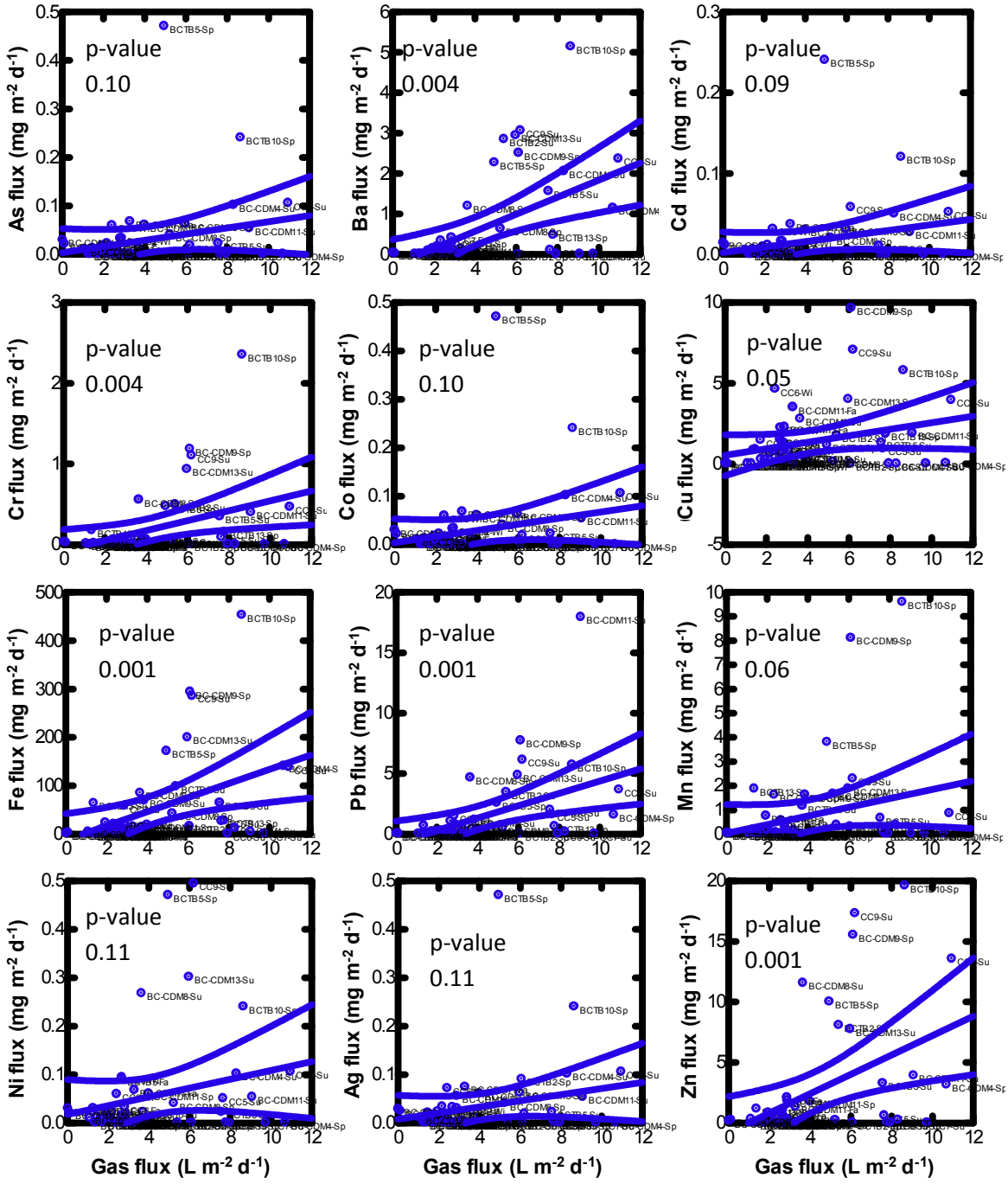

Figure S3. Correlation between gas flux and metal contaminant flux. Curved lines represent the 95% confidence interval of the least squares linear regressions. Hg and Se were not plotted due to low levels of both metals.

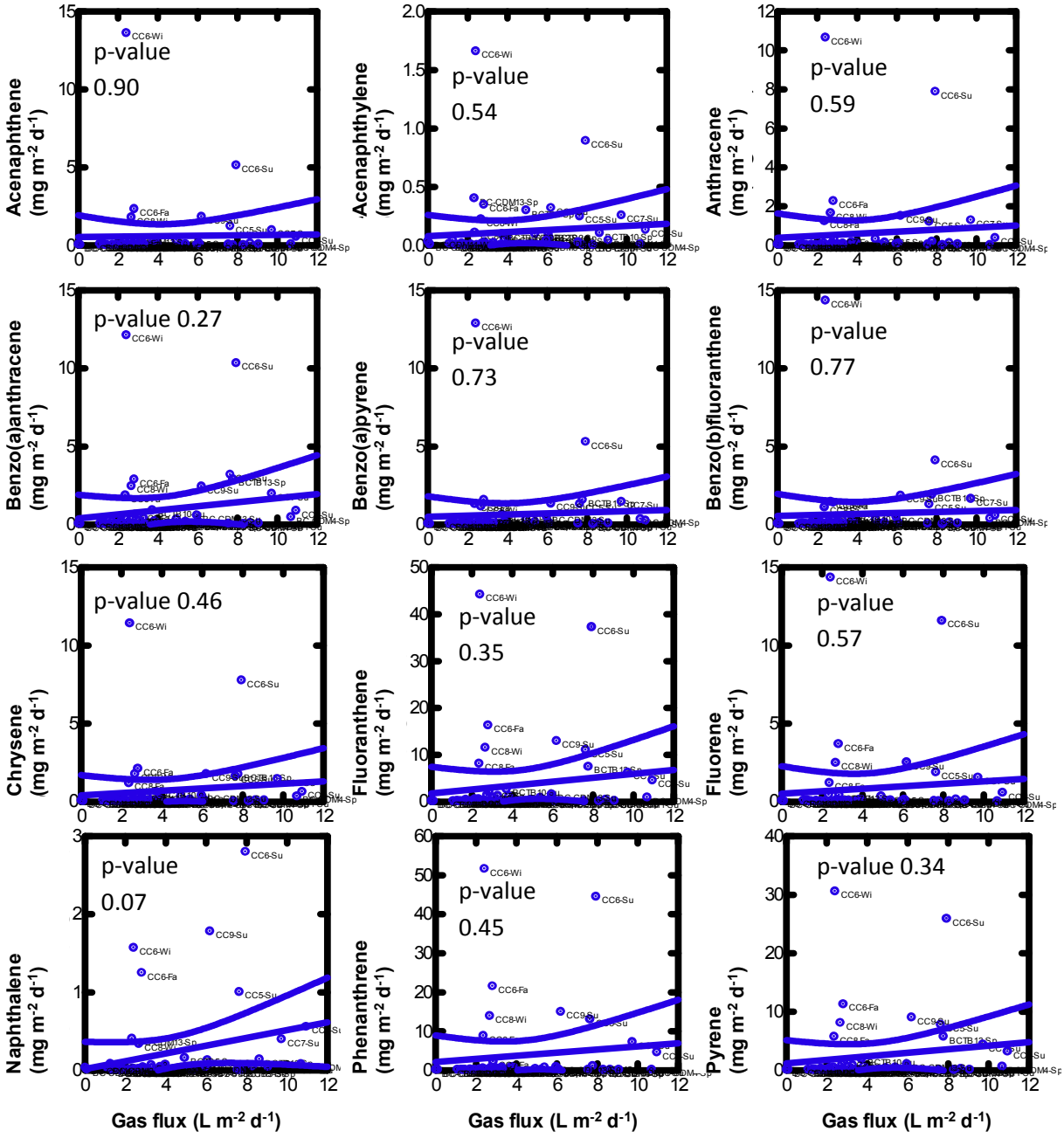

Figure S4. Correlation between gas flux and PAH flux. Curved lines represent the 95% confidence interval of the least squares linear regressions. Benzo[ghi]perylene, dibenzo[a,h]anthracene, and benzo[k]fluoranthene were not shown due to lack of correlation.

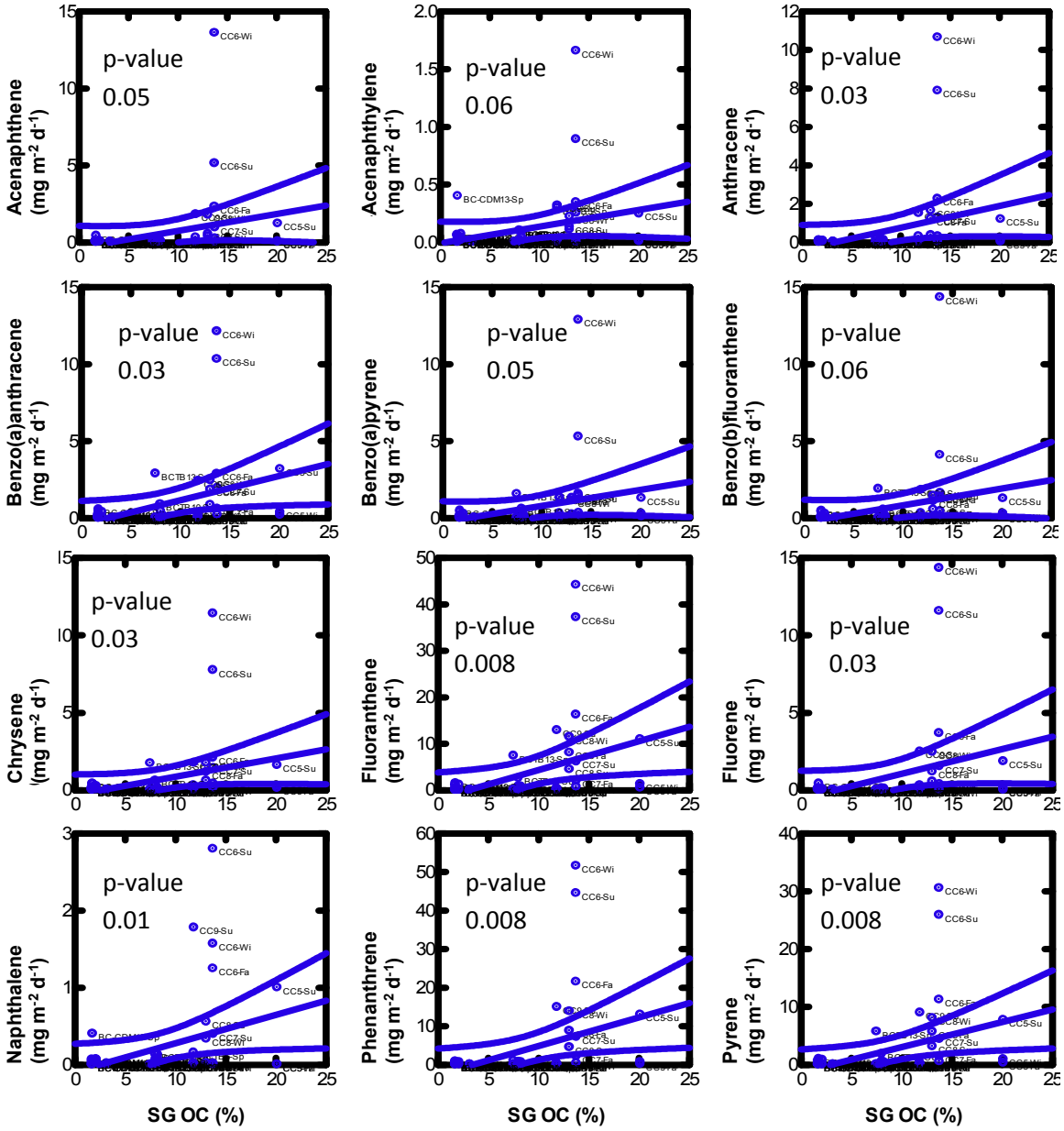

Figure S5. Correlation between SG OC and ebullition-facilitated PAH flux. Curved lines represent the 95% confidence interval of the least squares linear regressions. Benzo[ghi]perylene, dibenzo[a,h]anthracene, and benzo[k]fluoranthene were not shown due to lack of correlation.

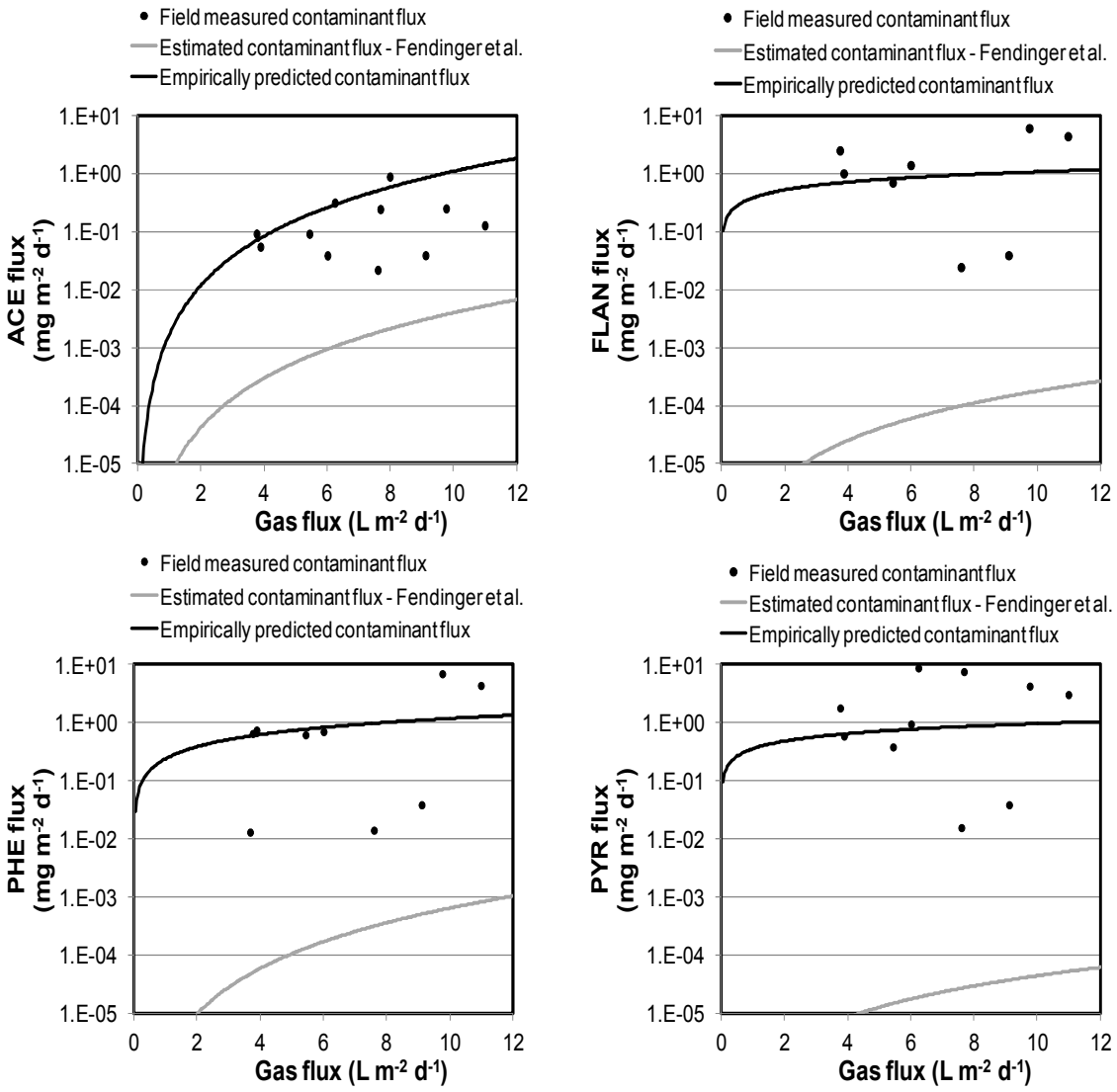

Figure S6. Ebullition-facilitated contaminant flux to the water column. Shown are acenaphthene (ACE), fluoranthene (FLAN), phenanthrene (PHE), and pyrene (PYR). Estimated and empirically predicted contaminant fluxes calculated from equations 7 and 4, respectively.

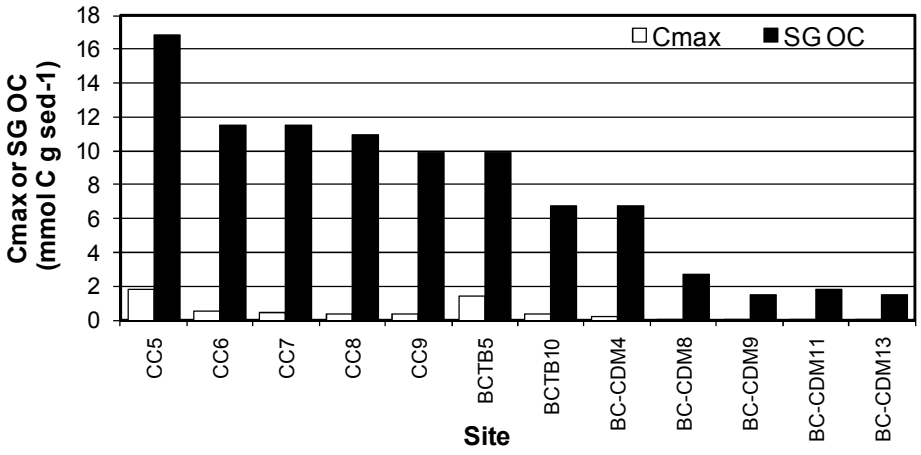

Figure S7. Calculated C_{max} and measured SG OC. C_{max} represents the maximum amount of biogenic gas production estimated assuming a first order reaction rate for samples incubated in serum bottles, sparged with nitrogen gas, sealed and incubated upside down quiescently at 35° C, with gas production monitored for more than one year.

Section S1: Gas ebullition models

Mechanistic gas flux model development. A mechanistic model was developed to predict biogenic gas production from biodegradation of sedimentary organic matter substrate as the sole limiting resource. Substrate utilization was assumed to follow Monod kinetics. The basic Monod equation does include a temperature dependence, which is clearly important in gas ebullition *(4, 206)*. Therefore, we used an expanded form of the Monod equation proposed by Goldman and Carpenter *(282)*, where the Arrhenius equation is used to describe the maximum specific gas ebullition rate μ_{max} (mmol kg^{-1} d^{-1}):

$$\mu = \rho_b \mu_{max} \left[\frac{S}{K_s+S}\right] \quad \text{with} \quad \mu_{max} = A e^{-E_a/RT} \tag{S1}$$

Where μ is the specific gas ebullition rate (mmol m^{-3} d^{-1}); ρ_b is the wet bulk density (kg m^{-3}); S is the limiting substrate concentration; A is a constant (mmol kg^{-1} d^{-1}); E_a is the activation energy (kJ mol^{-1}); R is the universal gas constant (8.3144E-3 kJ mol^{-1} K^{-1}); and T is the average temperature during the measurement period (K). Equating S with total SG OC is not warranted because laboratory experiments with sediment from the study sites confirm that only a small fraction of SG OC is actually labile to biodegradation by microorganisms (Figure S7). S is thus assumed to represent the labile portion of the sediment organic matter that more actively contributes to gas generation. We operationally define this parameter as equal to the SG COD/SG OC ratio because gas production is highly correlated with SG COD/SG OC (p-value = 2E-10, R^2=0.69, seasonal dummy variables used as regressors). For ease of representation, the parameter SG COD/SG OC is in this paper renamed as S_{labile}.

If we apply the logarithmic operator to equation S1, it yields:

$$log\mu = log\rho \quad + \log A - \frac{E_a}{RT} \quad + log\left[\frac{S}{K_s+S}\right] \tag{S2}$$

We calculated the maximum specific gas production rate μ_{max} (mmol kg^{-1} d^{-1}) for each site based on the data collected for temperature and field gas ebullition fluxes. We then plotted the data on an inverse temperature Arrhenius plot to obtain E_a. Physical and chemical sediment parameters were regressed with E_a values and the result demonstrates that E_a is highly correlated with sediment OC lability. Overall, 50% of the E_a variance can be explained by the S_{labile} parameter (p-value=0.012), and we thus use this parameter to estimate E_a using a Taylor expansion around zero:

$$\frac{E_a}{RT} \cong \frac{\beta_0}{R}\left(\frac{1}{T}\right) + \frac{\beta_1}{R}\left(\frac{S_{labile}}{T}\right) + \frac{\beta_2}{R}\left(\frac{{S_{labile}}^2}{T}\right) = \widetilde{\beta_0}\left(\frac{1}{T}\right) + \widetilde{\beta_1}\left(\frac{S_{labile}}{T}\right) + \widetilde{\beta_2}\left(\frac{{S_{labile}}^2}{T}\right) \quad \text{(S3)}$$

Where $\widetilde{\beta_J} = \frac{\beta_j}{R}, j \in \{0,1,2\}$; β_j are constants. Note that the terms (β_j, R) do not have a particular meaning in the equation. They are used to fit the equation for the maximum gas production term that arises from the mechanistic model of gas production (equation S1).

Assuming that K_s is related with temperature through a linear relationship ($K_s = \gamma_0 + \gamma_1 T$), we obtain:

$$\log(\mu) \cong log(\rho_b) + log(A) + \widetilde{\beta_0}\left(\frac{1}{T}\right) + \widetilde{\beta_1}\left(\frac{S_{labile}}{T}\right) + \widetilde{\beta_2}\left(\frac{{S_{labile}}^2}{T}\right) \quad \text{(S4)}$$

$$+ \log(S_{labile}) - \log(\gamma_0 + \gamma_1 T + S)$$

We estimate equation S4 through the following equation:

$$\log(\mu) \cong k + log(\rho_b) + \widetilde{\beta_0}\left(\frac{1}{T}\right) + \widetilde{\beta_1}\left(\frac{S_{labile}}{T}\right) + \widetilde{\beta_2}\left(\frac{{S_{labile}}^2}{T}\right) + \log(S_{labile}) \quad \text{(S5)}$$

$$- \log(\gamma_0 + \gamma_1 T + S_{labile}) + \varepsilon$$

Where $k = \log A$ is a constant.

Regression analysis confirmed that K_s *(287-289)* was a linear function of temperature in a statistically significant manner, as shown in the linear-in-parameters model with $\gamma_0 = 0.8083$ and

γ_1 = -0.0026 (p-value=0.007, R^2=0.86). We estimated our model through classical maximum likelihood estimation and we adopted the assumption of independent and identically distributed normal error terms ε:

$$\log(\mu) = 23 - 1.6log(\rho_b) - 3{,}800\left(\frac{1}{T}\right) - 2{,}500\left(\frac{S_{labile}}{T}\right) + 2{,}600\left(\frac{{S_{labile}}^2}{T}\right) \quad \text{(S6)}$$

$$+ 1.5\log(S_{labile}) + 0.28\log(\gamma_0 + \gamma_1 T + S_{labile})$$

Where μ is the specific gas ebullition rate (mmol m^{-3} d^{-1}); ρ_b is the wet bulk density (kg m^{-3}); T is the average temperature during the measurement period (K); and γ_0 and γ_1 are constants equal to (0.8083) and (-0.0026), respectively. For simplicity, we assumed that ρ_b and S_{labile} do not vary with time.

The estimated model yields a good fit to the data with a R^2 of 0.56, p-value of 4E-06.

Literature gas ebullition models. Measured fluxes and results from our gas flux model predictions were compared to predictions using two models previously developed for sediments *(283-284)*. The Winterwerp and van Kesteren (WvK) model predicts gas production from organic matter and temperature as follows:

$$GP\left(\text{kg kg}_{\text{sed}}^{-1}\,\text{yr}^{-1}\right) = k(t)OM, where\ k(t) = \frac{m^{T-T_c-1}}{m^{T_r-T_c-1}}k_1(t)^{k_2} \quad \text{(S7)}$$

Where *GP* is the biogenic gas production; *k(t)* is the time-dependent decomposition decay function; *m* is a dimensionless temperature scale equal to 1.1 for cohesive sediments; *T* is the temperature (°C); T_c is the lowest temperature at which decomposition of organic matter occurs; T_r is a reference temperature (25° C); k_1 and k_2 are coefficients determined as 0.178 and -0.95, respectively, for t (yr) equal to 1; and OC is the organic matter content (kg kg_{sed}^{-1}). A more detailed description of this model can be found elsewhere *(283)*. The Mogollon et al. model

(284) includes sediment porosity to account for the role sediment density plays on gas bubble formation, but does not include a temperature term:

$$GP\left(\text{kg kg}_{\text{sed}}^{-1}\,\text{yr}^{-1}\right) = \frac{1}{2} k_{POC} OM \rho_s \frac{(1-\varepsilon_0)}{\varphi_a} \quad \text{(S8)}$$

Where K_{POC} is the decay constant for particulate organic matter (yr^{-1}); ρ_s is the solid phase density (kg m^{-3}); ε_0 is the sediment porosity; and φ_a is the volume fraction of the aqueous phase.

A more complex mechanistic model that distinguishes between gas ebullition transport modes (fracturing versus pore perfusion) has recently been proposed for deep water sediments to predict the formation of gas hydrates *(290)*. This model includes extremely fine-grained sediments (<1 μm) that are not found in the test sites of the present study. While this model holds promise to predict gas ebullition, it may not be suitable for the shallow sediments in the present study.

CHAPTER VII. FIELD MEASUREMENT OF BENTHIC FLUXES AND COMPARISON WITH EBULLITION-FACILITATED FLUXES

I worked on this project with the student Ke Yin from the Environmental Engineering Laboratory of Professor Rockne at the University of Illinois at Chicago. The research included field work in nine sites in Bubbly Creek, Chicago River, IL. Benthic organic and metal contaminant fluxes at the sediment-water interface were measured using benthic chambers. The results were compared to the ebullition-facilitated organic and metal contaminant fluxes shown in chapter VI of this dissertation. Sulfide, ammonia, nitrate, dissolved organic carbon (DOC) and total filtered phosphorous (TFP) benthic fluxes were also measured.

7.1 Abstract

No studies to date have compared ebullition-facilitated organic and metal contaminant fluxes to direct benthic contaminant fluxes measured in the field. To this end, we measured benthic organic and metal contaminant fluxes at the sediment-water interface using benthic chambers and compared them to ebullition-facilitated contaminant fluxes at nine sites in the Chicago River, IL USA to determine the relative importance of each transport mechanisms to the total sediment release. Benthic metal fluxes ranged from -0.082 to 0.429, -0.379 to 2.22, -0.341 to 1.92, and -0.364 to 0.625 mg m^{-2} d^{-1} for Ba, Fe, Pb and Zn, respectively. In comparison, ebullition-facilitated metal fluxes were up to 5, 450, 18, 20 and mg m^{-2} d^{-1} for Ba, Fe, Pb and Zn, respectively. Maximal sum 16 polycyclic aromatic hydrocarbon (Σ_{16}PAH) sediment-to-water benthic flux was 0.07 mg m^{-2} d^{-1}, although direct benthic flux of PAHs at many sites was non-detectable over the flux study time period. In contrast, maximal ebullition-facilitated PAH fluxes were 0.3, 7.3, 0.4, 0.9 and 5.7 mg m^{-2} d^{-1} for anthracene, fluoranthene, naphthalene, phenanthrene

and pyrene, respectively in the study sites. While not all sites had higher ebullition-facilitated contaminant flux compared to direct benthic flux, these results do demonstrate that gas ebullition is frequently a dominant pathway for release of PAHs and heavy metal pollutants to the water column; as much as >10 times greater. The relative increase in sediment-to-water flux by ebullition compared to direct benthic release is not as great for metals as for PAHs, but ebullition facilitated release rates were frequently greater. Sulfide, ammonia, nitrate, dissolved organic carbon (DOC) and total filtered phosphorous (TFP) benthic fluxes were observed from both sediment-to-water and vice versa; and ranged from -0.696 to 1.78, 0.648 to 3.34, -2.95 to 0.336, -0.168 to 0.816 and -1.75 to 0.288 mg m^{-2} d^{-1}, respectively. Nitrate and ammonia fluxes were inversely correlated (95% confidence interval, CI), indicating that nitrate was consumed at a stoichiometrically proportional rate with ammonia release from the sediment. DOC and sulfide fluxes were positively correlated (95% CI). Sediment oxygen demand was higher in the turning basin compared to the creek proper (95% CI), with rates up to 5 mg m^2 d^{-1} at site BCTB13. These results are consistent with modeling studies of Bubbly creek that indicate the sediments are a sink for electron acceptors like oxygen and nitrate *(291)*, as well as with the observed high rates of biogenic gas production due to anaerobic microbial activity in the sediment.

7.2 Introduction

Contaminants like polycyclic aromatic hydrocarbons (PAHs) and heavy metals have accumulated on the bottom of rivers and lakes from current and past release. As water bodies become cleaner from tighter controls and regulation of waste release, these past activities frequently result in large concentration gradients at the sediment-water interface. Diffusive flux can then occur in response to such gradients, resulting in significant release of contaminants from the sediment to the overlying water. Advection and bioturbation can greatly increase this

process; typically by an order of magnitude or greater *(292-293)*. In addition, biogenic gas production by anaerobic microorganisms in sediments with high organic matter content can result in production of bubbles that we have shown can greatly increase the release contaminants to the water column *(3-4)*.

Gradient and benthic chambers are the two most commonly-used methods for measuring the benthic chemical fluxes to and from sediment to the overlying water column. Each has its strengths and limitations and neither method isolates the diffusive flux versus advective (or bioadvective) components of the benthic flux unless modifications are made. The gradient method uses multiple measurements of the compound of interest along a sediment transect at depth and across the sediment-water interface into the water column. These data are then used to predict the flux rates from diffusion models (typically Fickian 1D or 2D models are employed) *(294-296)*. While this technique can be quite sensitive, it is sometimes difficult to employ for compounds that can exist in the gas phase or have low detection limits. In addition, reactions that occur in the sediment column can convolute the data and make it difficult to extract the flux parameter from the profile data. Techniques have been developed that can extract consumption/production reactions from fluxes, they necessitate very detailed profiles *(294, 297)*. The second main technique involves the deployment of benthic chambers on the sediment to create an isolated water volume where consumption/release can be monitored over time *(298)*. Consumption will manifest itself by a decrease in concentration in the chamber over time, while release will result in an increase. The concentration versus time data can then be used to determine a flux rate. Careful design of the chamber and appropriate stirring rate is critical to avoid excessive shear stress and the development of pressure gradients that may result in porewater advection inside the chamber*(299)*.

Important parameters affecting benthic chamber flux measurements are sediment and porewater contaminant concentrations, length of chamber deployment, chamber size and stirring *(279, 300)*. The stirrer should mimic flow conditions in the natural environment *(301)*. In non-permeable sediments, as long as appropriate water mixing is maintained, the type of stirring mechanism and chamber design are not critical for the magnitude of the measured fluxes *(300)*. However, in permeable sediments, fluxes are likely to depend on stirrer-induced pressure gradients *(299)*. Knowledge of the *in situ* bottom flow conditions and sediment surface topography enable setting adequate stirrer rate to more closely match natural conditions. Deployment time is critical for redox-sensitive analytes. If the chamber is kept in place for too long, anoxia might develop from sediment oxygen consumption, particularly in organic-rich sediments. This will likely result in biological and/or chemical transformation of compounds (e.g. metals have greatly different solubility in their more reduced form) that will affect measurements of their transport *(302)*.

A few studies have utilized benthic chambers to measure benthic fluxes of metals, with the following results (all in mg m^{-2} d^{-1}): 0.002 to 0.022 for Cd, -0.028 to 4.08 for Fe, -1.08 to 0.576 for Pb, and -2.88 to 14.5 for Zn *(279, 303-304)*. Positive fluxes indicate sediment to water column flux and vice versa. Some selected reports of benthic fluxes for the nutrient elements dissolved oxygen (termed sediment oxygen demand, SOD), ammonium, and phosphate fluxes also show wide variation: -350 to -16, -7.92 to 22, and 0.192 to 5.2 mg m^{-2} d^{-1}, respectively *(300, 303-304)*. Relatively fewer studies have measured polycyclic aromatic hydrocarbon (PAH) fluxes. For example, pyrene benthic fluxes in the range of 0.00015 to 0.0015 mg m^{-2} d^{-1} was reported at the sediment-water interface *(278)*.

Although contaminant transport at the sediment-water interface has been investigated for decades, little is known about contaminant transport due to gas ebullition. As we have shown, the magnitude of this contaminant transport mechanism can be quite high *(3, 20-21)*. The question remains as to whether these fluxes are comparable to, lower than, or higher than the direct benthic release in the field. No studies to date have compared ebullition-facilitated organic and metal contaminant fluxes to direct benthic contaminant fluxes measured in the field. To this end, we measured benthic organic and metal contaminant fluxes at the sediment-water interface using benthic chambers and compared them to ebullition-facilitated contaminant fluxes at nine sites in the Chicago River, IL USA to determine the relative importance of each transport mechanisms to the total sediment release.

7.3 Materials and Methods

Sediment sampling and analysis. A total of nine sample locations were selected for the flux studies (Figure 7.1). Four sites are located in the Turning Basin of the south branch of the south fork of the Chicago River, known as Bubbly Creek (termed BCTB sites). An additional five sites are in the Creek itself (termed BC-CDM sites). Table 7.1 shows the coordinates for the sampling sites. Bubbly Creek connects with the main south branch of the Chicago River at the turning basin. In the early-1900's, Bubbly Creek was a sewer for industrial effluents and wastes from the adjacent stock yards *(263)*. Although direct wastewater discharge is prohibited now, the creek still is impacted by large combined sewer outflow (CSO) effluent (up to 175 $m^3 s^{-1}$); on average >13 times per year with an annual average discharge volume of 20,200,000 m^3 from the Racine Avenue pumping station (RAPS), the largest sewage pumping station in the world (Figure 7.2). During periods of no discharge, the water in Bubbly Creek is normally stagnant and the quiescent sediments are susceptible to gas ebullition events.

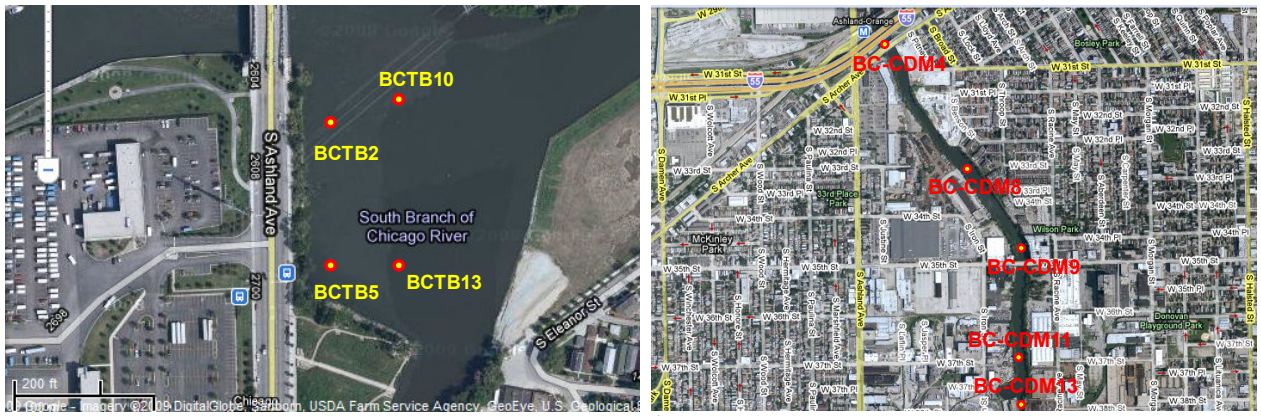

a) b)

Figure 7.1. Aerial view at the turning basin of Bubbly Creek (a) and at Bubbly Creek (b). The turning basin (a) lies immediately north of (b). Shown are site locations that were sampled for benthic gas ebullition and benthic flux studies. Bubbly Creek sites are at the exact location of sediment core sites from the USACE *(264)* (identical site numbering has been maintained).

Table 7.1. Sampling coordinates for BCTB and BC-CDM sample sites

Sample	Latitude (Decimal °N)	Longitude (Decimal °W)	Water depth (m)	Sed depth to clay/hardpan (m)
BCTB 2	41.844262	87.665200	2.2	5.7
BCTB 5	41.843447	87.665219	1.5	6.5
BCTB 10	41.844406	87.664667	3.2	4.8
BCTB 13	41.843417	87.664667	2.5	5.5
BC-CDM4	41.839481	87. 664440	3.5	3.2
BC-CDM8	41.832538	87.658447	2.1	2.5
BC-CDM9	41.830881	87.662924	3.1	3.0
BC-CDM11	41.827138	87.657503	1.2	3.6
BC-CDM13	41.825048	87.657362	4.6	2.1

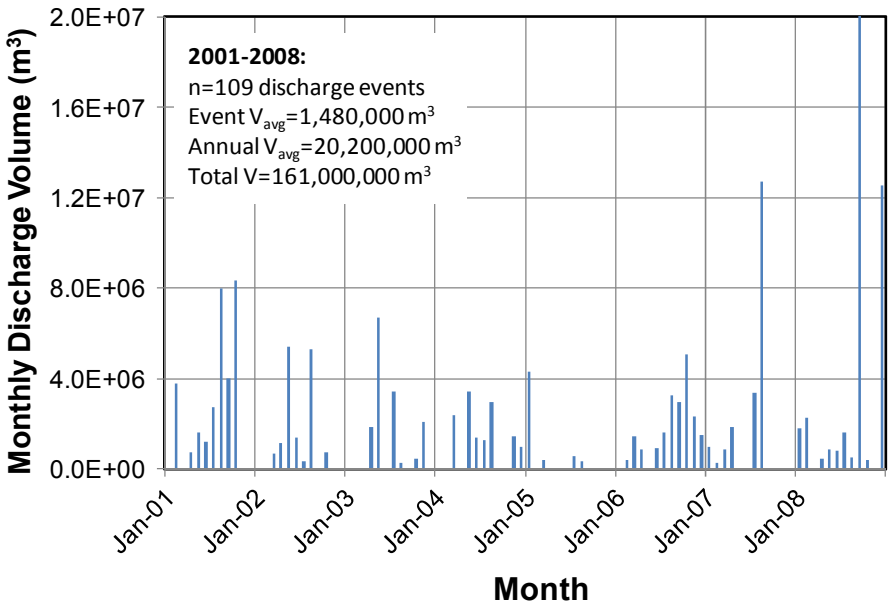

Figure 7.2. Data from the Metropolitan Water Reclamation District of Greater Chicago (MWRD) for discharge activities at the Racine Avenue Pumping Station (RAPS).

Sampling of core and surface grab (SG) samples in the BCTB was performed onboard the MWRD RV *PC1* in October and November 2005 as described in chapter VI. A total of 15 sediment cores and 13 SG samples were collected, but we present here only the results for the four sites chosen to perform the benthic and gas ebullition flux studies (Figure 7.1a). Additionally, five SG samples were collected in July 2008 for the BC-CDM sites (Figure 7.1b). These samples were collected in the same sites sampled by Camp, Dresser & McKee Engineering (CDM) consultants for the USACE *(264)*. Core samples were not collected in Bubbly Creek and results from USACE *(264)* were used for all core data for the BC-CDM sites reported in this work. Detailed sampling procedure can be found elsewhere *(130)*. Wet bulk density, percent moisture, dry bulk density, percent solids, organic carbon (OC) and organic matter (OM) were analyzed *(265)*. The 16 USEPA priority-pollutant Σ_{16}PAHs were extracted from the sediments and measured as described elsewhere *(130, 258)*.

Benthic chamber flux sampling and analysis. Two benthic chambers were built by Aquatic Research Instruments (Hope, ID) to measure *in situ* fluxes of PAHs, metals, sulfide, ammonia, nitrate, dissolved organic carbon (DOC), total filtered phosphorous (TFP), and dissolved oxygen (DO) flux to and from the sediments over time. Water pH and oxidation-reduction potential (ORP) were also monitored (Figure 7.3). The sampler consisted of a large polycarbonate funnel attached to polyvinyl chloride (PVC) pipes of various lengths to allow the autosampler to sit approximately 50 cm above the water surface (Figure 7.4 a). Strong threaded female/female couplers were placed between each pipe section for stability. The samplers had steel rod stabilizers (three total) connected from the cylinder to the PVC pipe. A toroidal-shaped weight was placed on the tubes to permit good penetration of the chambers into the sediments. Nylon ropes (approximately 12 m long) were attached to the top pipe section and tied to high density foam floats placed on the water surface. These floats were also tied to anchors to keep the samplers in place. A single stirrer was located inside each chamber. A DC motor for the stirrer was attached to the water-tight top of the sampling system (Figure 7.4 b) and connected to a battery installed on the float top. Batteries were replaced every 24 h during sampling and recharged (Figures 7.4 a-d).

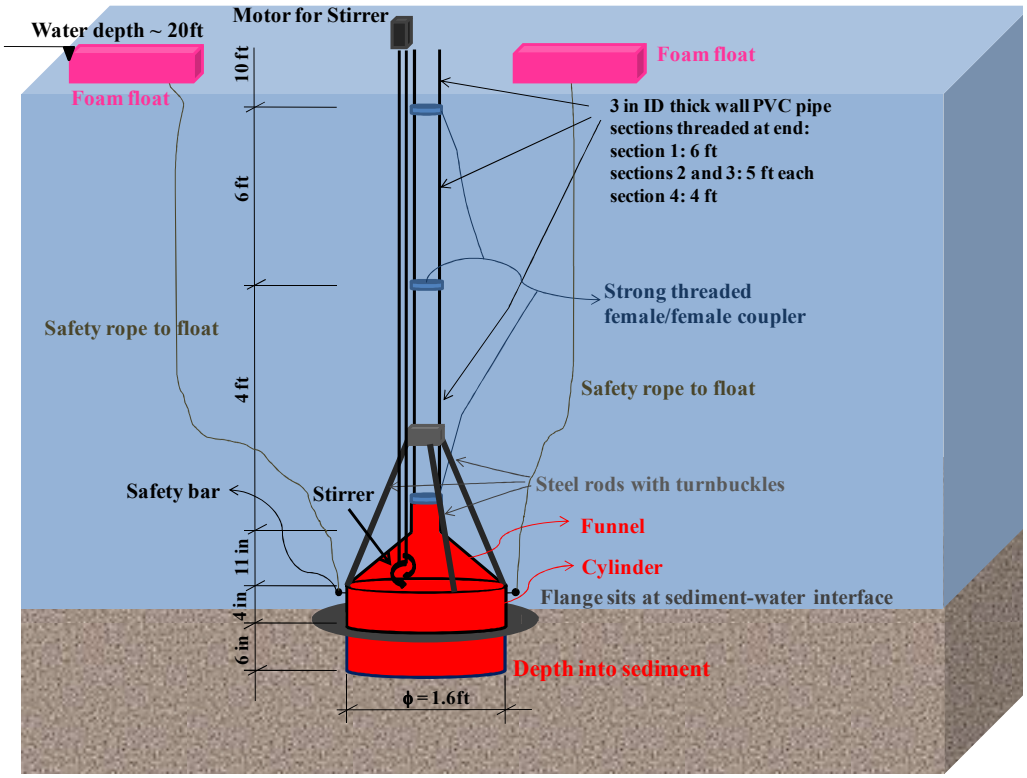

Figure 7.3. Benthic chamber build for the flux study in the nine sites at Bubbly Creek.

The stirrer performance was evaluated in the laboratory using the alabaster ($CaSO_4.2H_2O$) plate dissolution technique described by Buchholtz-ten Brink et al. *(305)*, which permits estimation of the diffusive boundary layer (DBL) thickness:

$$DBL = \frac{f D_{mol}(C_{sat} - C_0)At}{wt_{loss}} \quad (7.1)$$

Where f is the weight fraction of Ca^{2+} in alabaster and equal to 0.2328; D_{mol} is the Ca^{2+} molecular diffusivity; C_{sat} is the Ca^{2+} concentration at saturation; C_0 is the initial Ca^{2+} concentration; A is the area of exposed alabaster; t is the time allowed for dissolution; and wt_{loss} is the measured weight loss from the alabaster during mixing exposure. The molecular diffusivity values for calculation of the DBL was taken from Li and Gregory *(232)*. The same technique was used in the field to measure the natural riverine DBL thickness. From these results, the stirring

rates, blade diameter, and number of blades were adjusted to operate at the same magnitude of the field-measured DBL.

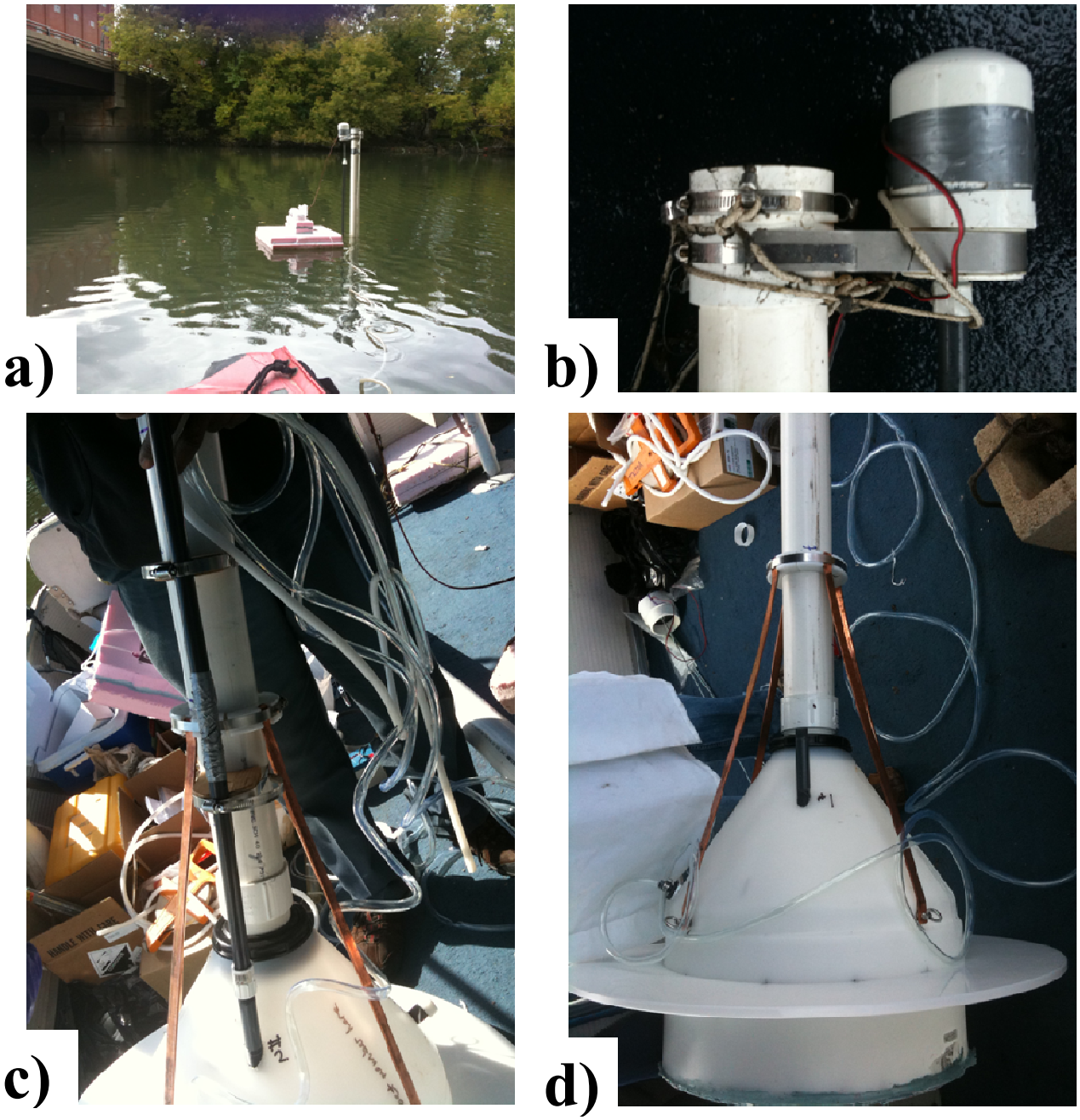

Figure 7.4. Photographs of a) sampler used to measure contaminant fluxes from and into the sediment, b) details of the top of the sampler with the motor for the stirrer covered by a PVC cap, c) funnel connected to PVC pipe and stirrer rod protection pipe, and d) funnel connected to steel rod stabilizers.

Chambers were thoroughly cleaned prior to each deployment. A Global Water SP200 peristaltic pump (Gold River, CA) was used for sample collection. Oakton PD 650 meter kit (Vernon Hills, IL) was used to measure pH, ORP and DO. A minimum of 5 samples were collected in amber glass bottles (1L) per site during the 48 to 270 h deployment period to determine heavy metal and nutrient fluxes. These samples were preserved at 4° C and sent to a NELAP-certified laboratory within 48 h of sample collection.

PAH samples were collected in amber glass bottles (4 L) at the end of the sampling campaign at each site. Sediment PAH flux was measured by comparing the PAH mass captured on Tenax® traps (a highly effective sorbent for removing hydrophobic organic compounds from aqueous solution) *(306)* inside the benthic flux chamber to the mass captured on traps placed outside the chamber. Water from inside and outside the chamber was passed through the trap using an Omnifit adjustable column from Fisher Scientific (Pittsburgh, PA) with diameter of 1.5 cm and length up to 10 cm. No PAH sample was collected for BCTB10 for the benthic chamber study due to high creek velocities that knocked the station over before a sample could be obtained, followed by a RAPS discharge event that changed sediment conditions. PAH sample analyses were performed by a NELAP-certified laboratory. MWRD boats and personnel assisted our group during sampling.

Ebullition-facilitated flux sampling and analysis. Gas collection systems were constructed as described in Viana et al. *(4)* All experimental sampling and analytical details are provided in chapter VI.

7.4. Results and Discussion

Sediment characterization. The sediments have widely varying core organic carbon contents from 0.59 to 17%, respectively. Concentrations of Pb in the surficial sediment layer varied from 1.8 to 3400 mg kg^{-1} and Pb mean core concentrations from 265 to 2800 mg kg^{-1}. Surprisingly, surficial concentrations of As, Ba, Cd, Cr, Pb, Hg and Zn were higher at the BCTB sites than at the BC-CDM sites. An opposite trend was observed for Σ_{16}PAHs. Concentrations of PAHs in the surficial sediment layer varied from 20 to 440 mg kg^{-1} and PAH mean core concentrations from 60 to 1230 mg kg^{-1} (Figure 7.6). In six of nine sites, surficial PAH levels were similar to or even higher than the whole core mean values, particularly in the non-turning basin sites. This indicates that PAH-impacted sediments exist at the sediment-water interface. Nitrate and sulfate SG concentrations varied from 0.05 to 0.5 and 11 to 28 mg kg^{-1}, respectively (Figure 7.5, sulfate only measured at BCTB sites).

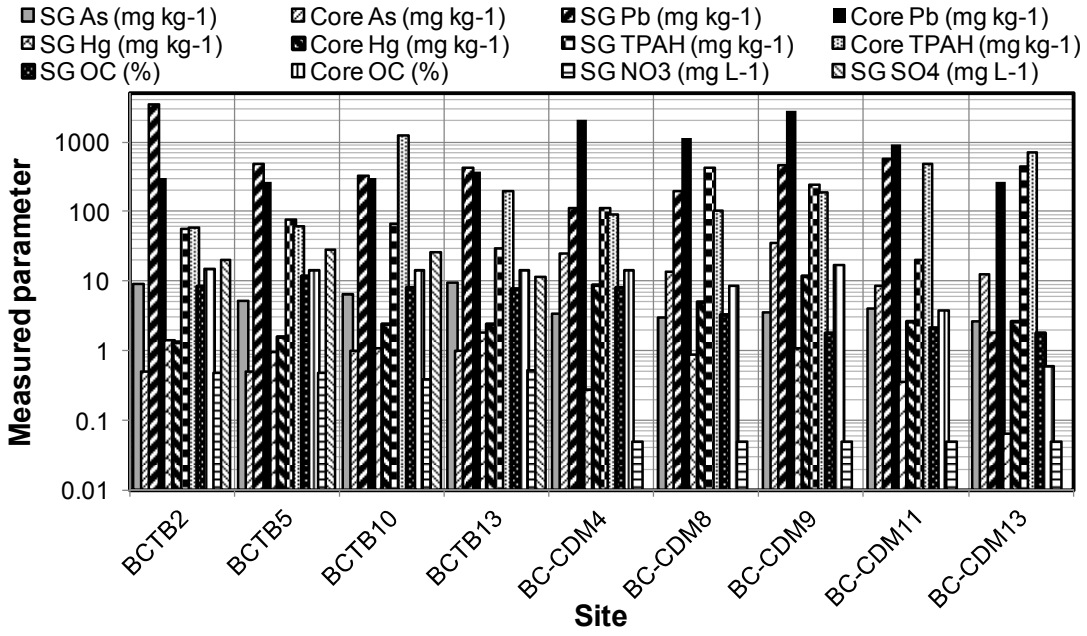

Figure 7.5. Metal and Σ_{16}PAH surficial and whole core concentrations, organic carbon content, nitrate and sulfate surficial concentrations in the nine sampled sites at Bubbly Creek and the turning basin of Bubbly Creek.

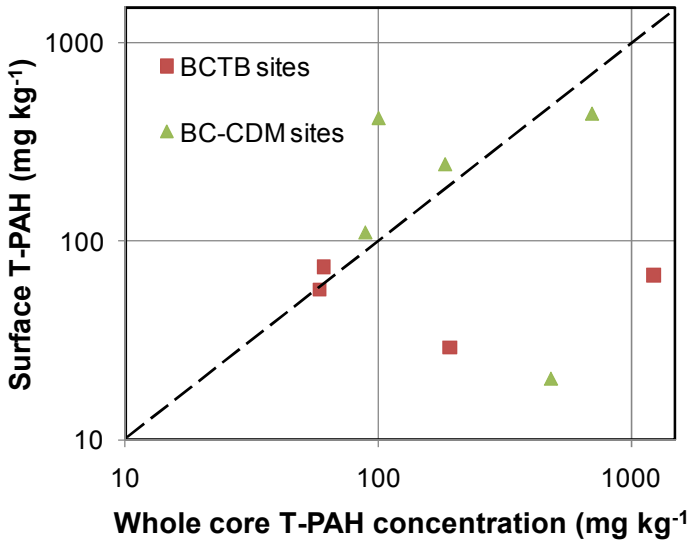

Figure 7.6. Surface Σ_{16}PAH concentration versus whole core Σ_{16}PAH concentration in the sediments of the nine sampled sites.

Chamber deployment and tracer study. Adequate chamber placement in an upright position was crucial for a successful chamber deployment to prevent excessive disturbance at the sediment-water interface in the measurement site. The first sample was collected approximately 1 h after deployment to ensure sediment resuspended by deployment did not contaminate the sample. A minimum of 5 samples were collected during the 48 to 270 h deployment period to determine heavy metal and nutrient fluxes. A tracer (NaBr) was added in two of the sampling sites and its concentration monitored with time to verify that significant chemical leaching from the chamber occurred during the measurements (Figure 7.7). The results demonstrate that no significant (95% CI) decreases of the conservative tracer were observed by 28 h.

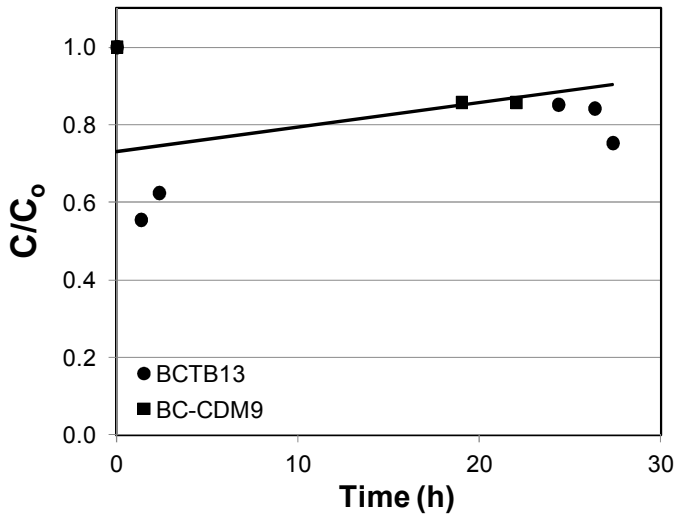

Figure 7.7. Br concentration in the benthic chamber as a function of time for sites BCTB13 and BC-CDM9.

Chamber stirring and alabaster method. Measured field DBL values ranged from a low of 58±16 at site BCTB10 to a high of 325±29 μm at site BC-CDM9. They are in agreement with literature values, which range from 75 μm for high energy coastal environments to 2,000 μm for quiescent lake bottoms.*(300, 305)* The lower value for site BCTB10 might have been affected by the high flow-induced disturbance of the system described in the *materials and methods*. The shear velocity u^* (cm s^{-1}) was estimated based on the measured DBL (μm) from the empirical relationship developed by Tengberg et al. *(300)*:

$$DBL = 76.18(u^*)^{-0.933}$$

Results varied from 0.5 to 1.2 cm s^{-1}. Again, these observed values in the field are consistent with literature-reported shear velocities, which vary from 0.1 to 0.7 cm s^{-1} *(300, 305)*.

Metal flux measurements. Metal fluxes measured in the benthic chamber varied between 0.082 to 0.429, -0.379 to 2.22, -0.341 to 1.92, and -0.364 to 0.625 mg m^{-2} d^{-1} for Ba, Fe, Pb and Zn, respectively (Figure 7.8). Negative values indicate flux into the sediment. For comparison,

measured benthic fluxes have been reported in the range of 0.002 to 0.022, -0.028 to 4.08, -1.08 to 0.576, and -2.88 to 14.5 mg m^{-2} d^{-1} for Cd, Fe, Pb and Zn, respectively *(279, 303-304)*. For comparison, *in situ* measured ebullition-facilitated fluxes of Fe and Pb varied from 0-450 mg m^{-2} d^{-1} and 0-18 mg m^{-2} d^{-1}, respectively. Ba, Cr and Zn ebullition-facilitated fluxes ranged from 0-5.2 mg m^{-2} d^{-1}, 0-2.4 mg m^{-2} d^{-1} and 0-20 mg m^{-2} d^{-1}, respectively. The higher Fe, Pb and Zn metal fluxes due to gas ebullition are consistent with their higher observed sediment concentrations, although this would also be expected to result in higher diffusive fluxes resulting from higher porewater concentrations in equilibrium with the solid phase. Interestingly, there is an observable trend of increasing metal fluxes from the creek terminus at the RAPS to the turning basin. This also mimics the trend of increasing surficial sediment metal concentration, organic matter and gas ebullition rates. It is possible that this results from the deposition of lighter, organic-rich sediment at the end of the creek and turning basin that were scoured/suspended upstream by RAPS discharge events. This is also supported by the higher bulk sediment density at sites closer to the RAPS.

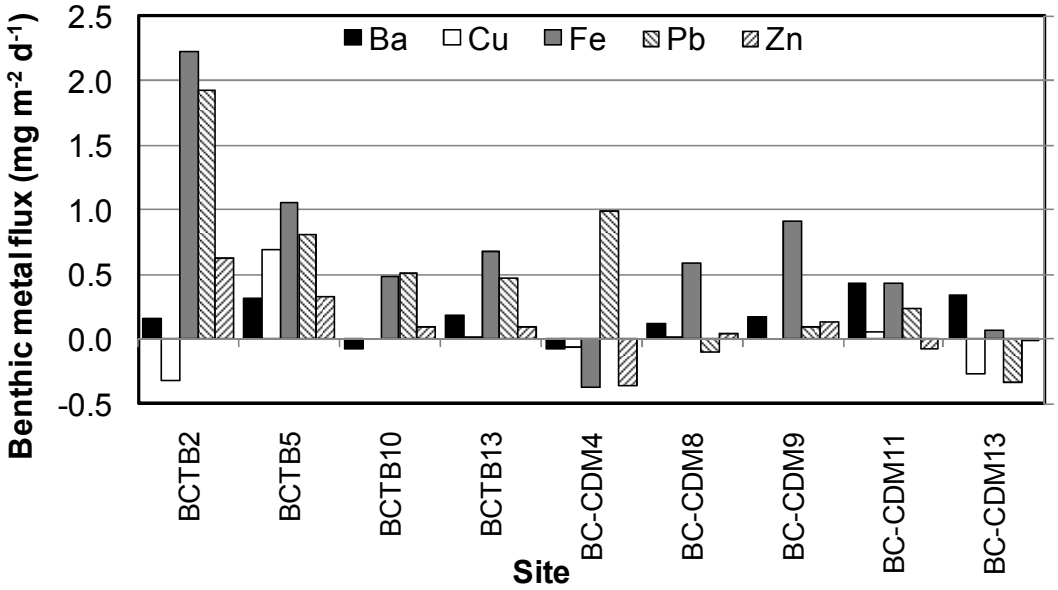

Figure 7.8. Metal flux to the water column measured during the benthic chamber study in the nine sampled sites at Bubbly Creek and the turning basin of Bubbly Creek.

PAH flux measurements. Benthic release of Σ_{16}PAHs was frequently below the detection limit; significant fluxes above the method detection limit were observed at only five sites. The observed Σ_{16}PAH fluxes from the sediment were equal to 0.05, 0.07 and 0.008 mg m^{-2} d^{-1} at sites BCTB5, BCTB13 and BC-CDM11, respectively (Figure 1.9). A negative flux of PAH (i.e. into the sediment) was observed at sites BC-CDM8 and BC-CDM13 (Figure 7.9). For sites BCTB5 and BCTB13 (which had the highest PAH fluxes), 2-3 ring PAH release was similar to that of 5-6 ring PAHs. These values were within the range of a literature values (0.00015 to 0.0015 mg m^{-2} d^{-1}) observed in a benthic chamber study of pyrene flux *(278)*. In contrast, our measured ebullition-facilitated PAH fluxes were typically much higher. Anthracene, benzo(a)pyrene, chrysene, fluoranthene and fluorene ebullition-facilitated fluxes varied from 0-0.3 mg m^{-2} d^{-1}, 0-1.6 mg m^{-2} d^{-1}, 0-1.7 mg m^{-2} d^{-1}, 0-7.3 mg m^{-2} d^{-1} and 0-0.4 mg m^{-2} d^{-1}, respectively. Naphthalene, phenanthrene and pyrene ebullition-facilitated fluxes ranged from 0-0.4 mg m^{-2} d^{-1}, 0-0.9 mg m^{-2} d^{-1} and 0-5.7 mg m^{-2} d^{-1}, respectively *(307)*.

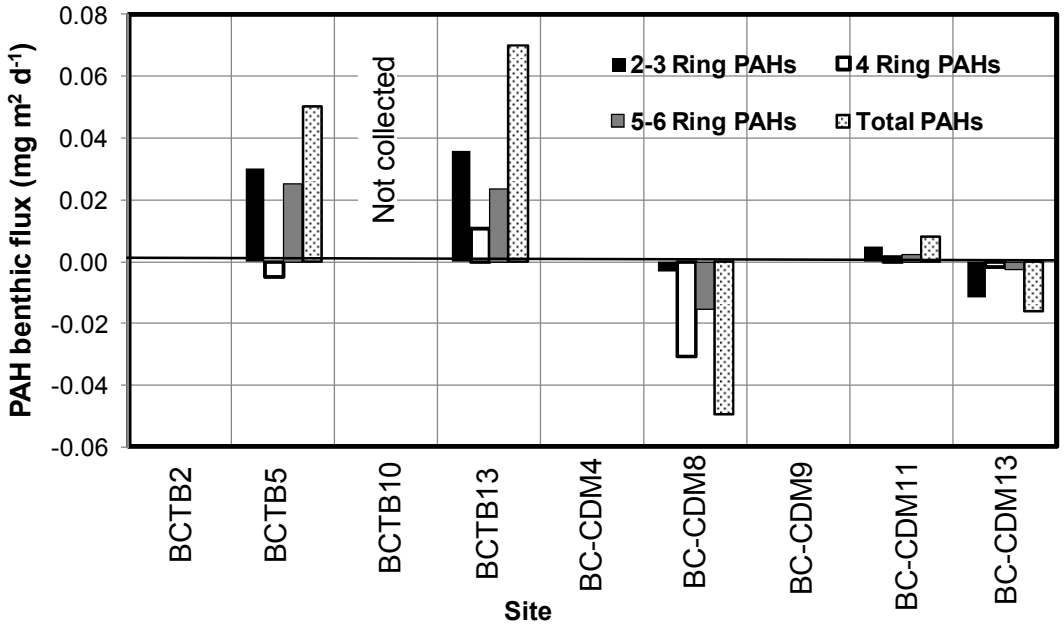

Figure 7.9. PAH fluxes to the water column measured during the benthic chamber study in the nine sampled sites at Bubbly Creek and the turning basin of Bubbly Creek. BCTB2, BC-CDM4, BC-CDM9 and BC-CDM13 all had non-detectable PAH fluxes.

Comparison between benthic and ebullition-facilitated contaminant fluxes. The benthic fluxes were compared on an annual basis to the magnitude of the ebullition facilitated fluxes (with some simplifying assumptions) to provide a point for comparison of each process magnitude. Although the benthic flux was measured only during one season (fall), the rate was extrapolated for the entire year to a first approximation if we assume that the release is due to a diffusive process (with no bioturbation). In Fickian diffusion, transport in response to a concentration gradient is controlled by the apparent diffusivity D_{app}. The D_{app} observed in the field incorporates both the physical diffusion process (effective diffusivity, D_{eff}) and any advective or bioadvective processes that facilitate flux. Although D_{eff} is affected by temperature, its magnitude is not as sensitive to changes of temperature as compared to biological processes. Bioadvection would clearly be sensitive to seasonal changes. However, the benthic flux measurements were done in relatively warmer conditions than the yearly average (12.3° C versus an annual average of 9.7° C), and thus we could assume to a first approximation that the benthic flux measured is largely representative of the average benthic flux observed throughout the year. Based on this assumption, we compute the total areal mass release to the water column per m^2 of sediment on an annual basis and compare it to the cumulative mass release by gas ebullition (assuming a constant rate for each season in the current study).

The results demonstrate that contaminant transport due to gas ebullition is as significant a source of pollutant release to the water column as direct benthic transport (Figures 7.10-7.11). In several sites, Σ_{16}PAHs and some metals were released from the sediments by gas ebullition at higher rates than released by direct benthic release. For example, total annual areal mass release of metals due to gas ebullition at site BCTB5 (Figure 7.10b) followed the trend of (mass release in mg m^2 yr^{-1}): Zn(1300) >> Pb(510) ~ Mn (470) > Ba(370) > Cu(300) >> Cr(75) > Ni(50). A

different trend was observed for direct benthic flux (Figure 7.10a): Pb(300) > Cu(250) ~ Mn (250) ~ Ni(240) > Cr(180) > Zn(120) ~ Ba(110). At the same site, the ebullition facilitated release of total PAHs on an annual basis is predicted to be 470 mg m^2 (Figure 7.11b). These levels were more than an order of magnitude greater than by direct benthic release (Figure 7.11a).

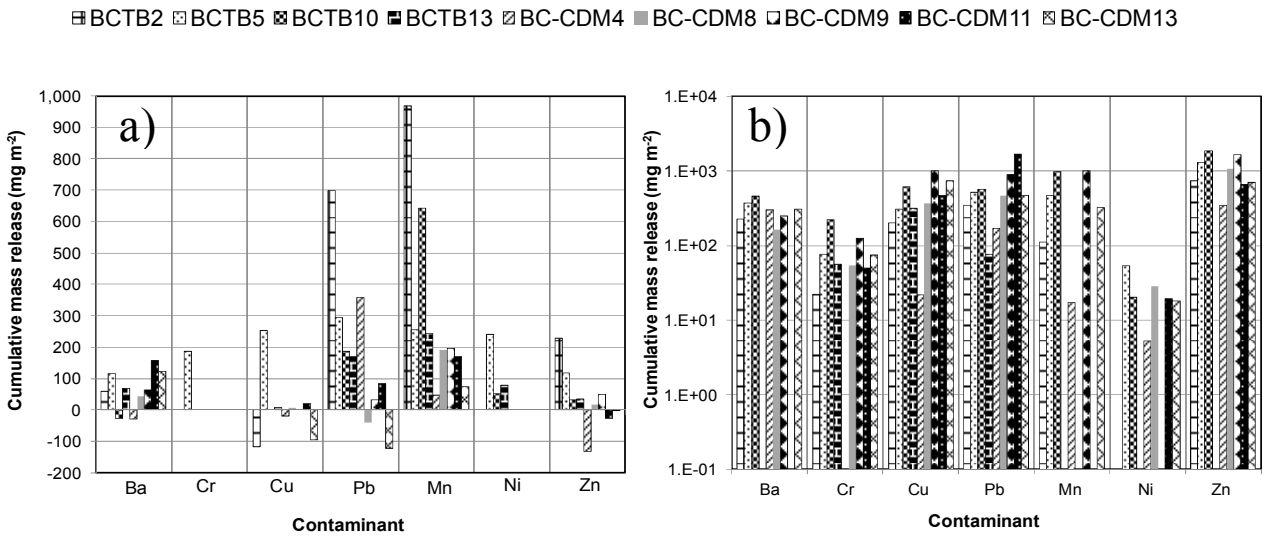

Figure 7.10. Cumulative annual metal release on an areal basis by a) direct release and b) ebullition. Shown are areal mass release rates to the water column per m^2 of sediment on an annual basis in nine sampled sites at the Chicago River. Note different y axis.

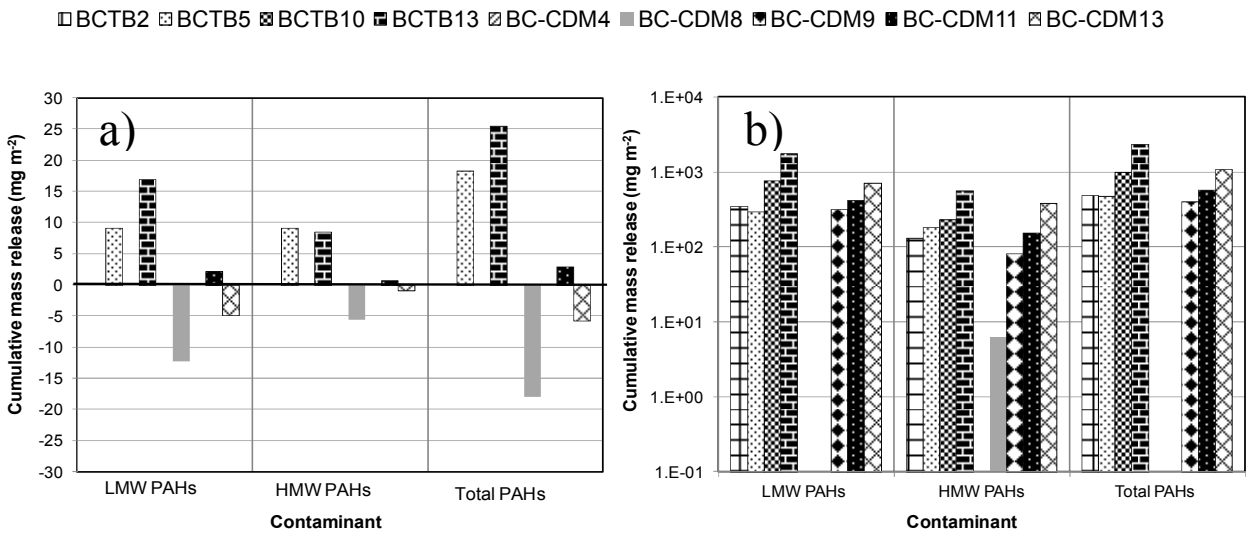

Figure 7.11. Cumulative annual PAH release on an areal basis by a) direct release and b) ebullition. Shown are areal mass release rates to the water column per m^2 of sediment on an annual basis in nine sampled sites at the Chicago River. LMW PAHs have 2-4 rings and HMW PAHs have 5-6 rings. Benthic flux mass release assumes constant rate of flux throughout year. Note different scale on the y axis.

In general, the fluxes due to gas ebullition are significantly higher than the fluxes from the benthic flux study (Figures 7.10-7.11). The difference between direct benthic flux release and ebullition-facilitated release of PAHs was much greater than for metals. As an example, the ebullition facilitated release of PAHs on an annual basis for BCTB5 is predicted to be ~180 mg m^2 for 5-6 ring PAHs and ~150 mg m^2 for 2-3 ring PAHs, with a Σ_{16}PAH mass release of 480 mg m^2 on an annual basis. These levels were more than an order of magnitude greater than by direct benthic release.

In addition to the relative magnitude of the mass fluxes between direct release and ebullition, there is also an observable inverse trend of PAH fluxes with location in the creek. As previously mentioned, ebullition-facilitated Σ16PAH fluxes increase with distance away from RAPS. This is clearly observed on an annual basis (Figure 7.11), and is also consistently

observed for both HMW and LMW PAHs. A similar trend was observed for direct release of Σ16PAHs.

Nutrient and electron acceptor/donor flux measurements. Sulfide, ammonia, nitrate, DOC and TFP fluxes varied from -0.70 to 1.8, 0.65 to 3.3, -2.9 to 0.34, -0.17 to 0.82 and -1.8 to 0.29 mg m^{-2} d^{-1}, respectively (Figure 7.12). Sediment oxygen demand (SOD) was statistically significantly higher (95% CI, Student's t-test) in the turning basin (2.7±1.7 mg m^{-2} d^{-1}) compared to the creek proper (0.65±0.38 mg m^{-2} d^{-1}). This is consistent with our observations of higher SOM in the turning basin sediments, as well as our conjecture that RAPS discharge events may be responsible for the deposition of organic-rich sediments in the turning basin as velocities drop when the creek widens. For comparison, literature measured benthic dissolved oxygen, ammonium, and phosphate fluxes vary from -350 to -16, -7.92 to 22, and 0.192 to 5.2 mg m^{-2} d^{-1}, respectively *(300, 303-304)*. Not surprisingly, higher SOD fluxes were observed at BCTB10 and BCTB13 than at BC-CDM9. The former sites have higher water flow because they are affected by the main stem Chicago river flow through the turning basin and thus also have decreased DBL thickness, which should result in higher SOD fluxes (all other factors been equal) *(308)*. The DBL constitutes a resistance layer for oxygen diffusion into the sediments *(308-309)*.

We observed positive sediment-to-water sulfide fluxes in eight of the nine sampled sites. The fluxes of sulfide were statistically significantly correlated with DOC fluxes out of the sediment. While these data are not sufficient to ascertain any mechanistic relationship between DOC and sulfide, they are consistent with high rates of sulfate-reducing bacteria activity forming sulfides, which was likely given the highly reducing sediments. DOC release from anaerobic sediments has been reported for other systems, frequently accompanied by phosphorus release

(310-311), as was observed in our benthic flux results. From a water quality standpoint, neither of these processes is desirable because they are well known to contribute or exacerbate eutrophication. From a toxicity standpoint, sulfide flux into the water column that exceeds the oxidizing capability of aerobic activity contributes to low DO and anoxia in the water column, as well as direct toxicity to sensitive species such as zooplankton *(310)*.

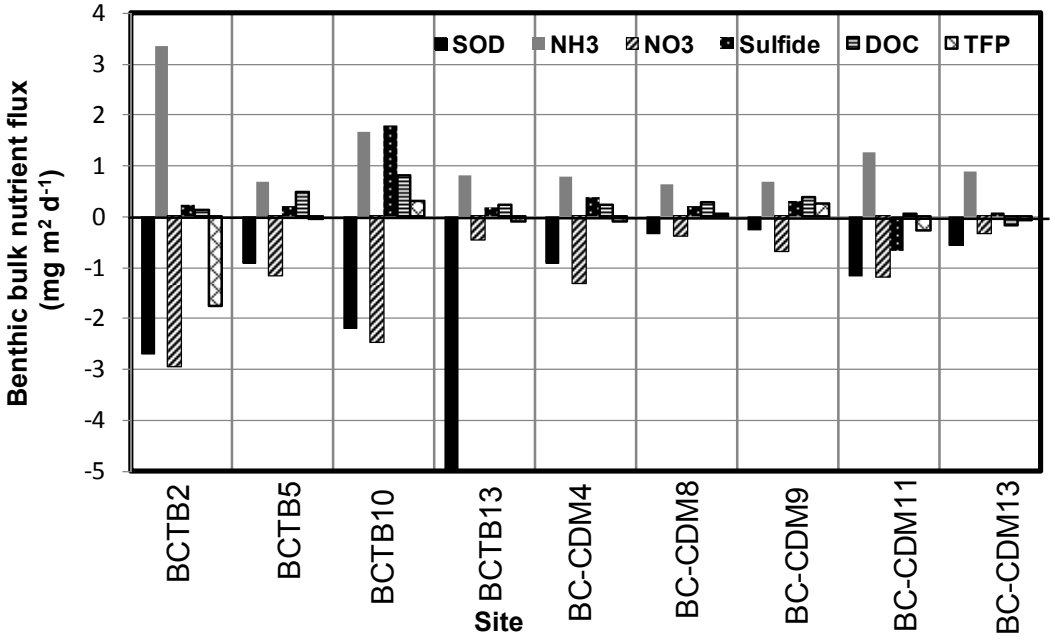

Figure 7.12. Sediment oxygen demand (SOD), ammonia, nitrate, sulfide, dissolved organic carbon (DOC) and total filtered phosphorous (TFP) fluxes to the water column measured in the benthic chamber study at nine sampled sites at Bubbly Creek and the turning basin of Bubbly Creek. Except for SOD, positive fluxes represent sediment-to-water transport and negative fluxes represent water-to-sediment flux. SOD is positive when consumption of water column DO occurs due to oxygen sinks in the sediment.

There was a strong, statistically significant (95% CI) negative correlation between ammonia fluxes from the sediments to the water column and nitrate fluxes (Figure 7.13). While these data are not sufficient to determine where nitrogen transformation processes such as denitrification, ammonification (release of ammonia from organic matter biodegradation) *(312)*, and nitrification occur in relation to the sediment-water interface, we can draw some conclusions about the

relative importance of these processes. The slope of the correlation is consistent with a stoichiometrically proportional rate of nitrate consumption with ammonia release from the sediment. This is consistent with a global balance between dissolved N species fluxes into and out of sediment. Under anaerobic conditions, nitrification, a strictly aerobic process, would be inhibited *(302, 313)*. Non-zero concentrations of DO and nitrate were always present in the chamber during the experiment, and mid-depth water column measurements were also non-zero, varying from 4.8-6.8 mg L^{-1} DO and 0.8-3.5 mg L^{-1} nitrate, respectively. Thus aerobic processes would likely occur in the water column rather than the highly reducing sediments. Neither nitrification of ammonia nor denitrification would be consistent with the high sediment-to-water fluxes of ammonia. If nitrification were the only process occurring in the benthic chamber, we would expect to see decreasing ammonia and increasing nitrate. Although significant denitrification occurs in all of these sediments, as demonstrated by the 44±10% N_2 content *(4)* in the evolved gas measured in the field (resulting in average N_2 fluxes out of the sediments 1772±441 mg N m^{-2} d^{-1}), we also would not expect to see increasing ammonia. The data are thus most consistent with ammonification of SOM being the dominant nitrogen transformation process relative to nitrification/denitrification.

Sediment oxygen demand was significantly higher in the turning basin compared to the creek proper (95% CI), with rates up to 5 mg m^2 d^{-1} at site BCTB13. These results are consistent with 1D modeling of quiescent periods and 2D modeling of Bubbly creek RAPS events *(291)* using the numerical model STREMR-HySedWq that indicate the sediments are a sink for electron acceptors like oxygen and nitrate, as well as with the observed high rates of biogenic gas production due to anaerobic microbial activity in the sediment.

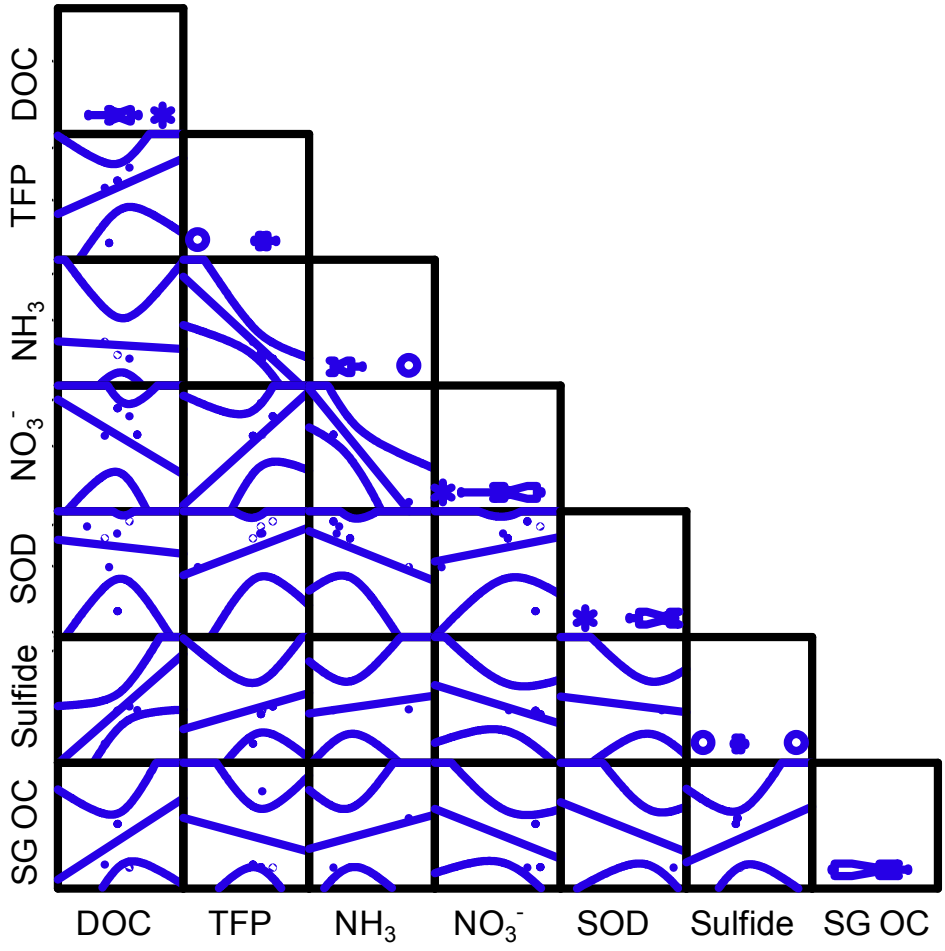

Figure 7.13. Scatterplot matrix of SG OC, sulfide, SOD, nitrate, ammonia, TFP and DOC. Curves represent the 95% confidence level.

7.5. Conclusions and Implications

Gas ebullition is an important pathway for release of PAHs and heavy metal pollutants to the water column. Comparison of the direct benthic release rates to ebullition facilitated rates suggest that Σ_{16}PAHs are released at significantly greater rates by biogenic gas production. Although the increase in release rate is not as great for metals, ebullition facilitated release rates are frequently much greater. On an annual basis, ebullition-facilitated fluxes for Σ_{16}PAHs for the entire creek are predicted to be 59 kg based on the annual fluxes for each site using the Thiessen

polygon method *(313-314)*. For the six metals Ba, Cr, Cu, Pb, Ni and Zn, the total annual ebullition-facilitated fluxes are predicted to be 26, 8, 50, 75, 2 and 106 kg using the same method. On an annual basis, benthic fluxes released from the sediments for Σ_{16}PAHs for the entire creek are predicted to be 0.4 kg based on the annual fluxes for each site. For the six metals Ba, Cr, Cu, Pb, Ni and Zn, the total annual fluxes are predicted to be 8, 1.5, 2.5, 21, 3 and 4.5 kg using the same method. While we do not have data to determine the current input to the creek from CSOs and other sources, we can estimate the concentration of these pollutants in the RAPS stormwater/wastewater discharges that would need to be present to exceed these values based on the average 0.64 m^3 s^{-1} flowrate of RAPS discharge events for the period 2000-2008. The metals Ba, Cr, Cu, Pb, Ni and Zn would need to be present on the order of only 2, 0.5, 3, 5, 0.2 and 6 μg L^{-1} and Σ_{16}PAHs would need to be present at 3 μg L^{-1}. Therefore, the contaminant release by the RAPS is likely an important source of contamination to the Creek compared to benthic and ebullition-facilitated contaminant release.

Based on these findings, it is clear that attempts to clean up Bubbly Creek must take into account controlling RAPS discharge as well as the continued release of contaminants from the sediments due to historical pollution; particularly in sediments with active gas ebullition. The RAPS is, however, the largest sewage pumping station in the world. Normal CSO inputs are substantially lower than the RAPS input. Thus, not taking sediment contaminant release in urban waterways into account will likely result in a re-contaminated sediment-water interface, and continuing releases into the water column.

CHAPTER VIII. CONCLUSIONS AND IMPLICATIONS

The results from simulations performed with measured K_d and cap parameters compared to literature-derived model simulations demonstrate the need for uncertainty analysis, which is driven primarily by sediment chemistry that greatly affects K_d and the variety of cap materials with different permeabilities. More K_d data under realistic field conditions are needed to reduce uncertainty to a level more acceptable in managing risk. The measured K_d values reported here contribute to reduce uncertainties in parameters to a level more acceptable in managing risk. Although none of the caps exhibited a high sorption capacity for As, OC and apatite performed clearly better than sand and GAC. The K_d results indicate close agreement between the experimental and literature K_d values with the exception of As and Cd with apatite. Surprisingly, OC exhibited a significantly higher sorption capacity than apatite for Cd based on the isotherm study results. On the other hand, based on the column study, apatite performed very well for Cd in the column study with full breakthrough after 12000 pore volumes, as expected. Sand did not exhibit such a poor sorption capacity as expected for Cd with full breakthrough after 4000 pore volumes. Based on the column experiment results, GAC performed poorly for both As and Cd.

Knowing site specific conditions would also contribute to decrease uncertainty in my simulations for a specific site, but the utility of a broader comparison is the ability to focus data-gathering efforts on the caps that are likely to be more effective and the contaminants that are driving risk. Further, the importance of k_h is clearly demonstrated by my simulations. These results may lead to modified cap formulations to decrease permeability and thus improve performance.

Based on the literature-derived simulations, cap thickness is clearly the most important factor under diffusion with sand caps performing best under diffusion. However, an inadequately armored sand cap layer alone may not work satisfactorily, even in sites that are only under diffusive transport conditions due to erosive losses of cap material over time. Under advection, decreased hydraulic conductivity may be as or more important than increased K_d. Apatite had the best performance for Cd, Cr and Pb and low hydraulic conductivity organoclay performed best for Ag, As, Ba, CH_3Hg and CN. In some cases, organoclay behaved similarly under diffusion and advection because this cap material is both a sorbent and a hydraulic barrier, while the thick sand cap effectiveness was completely different under advection because it is not a sorbent and is highly permeable.

Overall, no cap is predicted to be effective for Cr and CN under advection. Thicker caps could thus be applied to ensure effective performance, although this would result in increased cost. Sand and apatite are the most effective caps for Hg, but organoclay may be effective as well. Sand, organoclay and tires are predicted to be effective for CH_3Hg under diffusion only, but a thicker cap of organoclay would probably be more effective under advection. Sand is predicted to be effective for Ag and As under diffusion, but a thicker cap of organoclay would likely be the best alternative for these metals under advection. Sand and apatite are predicted to be effective for Cd and Pb at neutral pH, but only apatite is predicted to be effective under advection.

Cap combinations (e.g. apatite or organoclay followed by sand) may be the most economically efficient capping formulation. The apatite or organoclay mat providing effective advective sequestration and the sand layer contributing for both stability and as a thick diffusive pathway.

There are currently >100 contaminated sediment projects were capping is planned or has been implemented. However, capping tends to be "harder sell" for regulatory agencies and the public. I hope these experimental and modeling results from cap efficiency for different metal contaminants under a variety of environmental conditions and cap characteristics contribute to a better understanding of the effectiveness of capping and to focus efforts on future studies.

The results shown in chapters 6 and 7 demonstrate that both metal and organic contaminants are transported by gas ebullition and represent a significant contribution to the total contaminant flux from sediments to the water column in contaminated riverine freshwater systems. In addition, both the mechanistic and an empirical models for predicting gas fluxes at urban contaminated freshwater systems shown in chapter 6 may be used to predict field gas fluxes based on more easily measurable parameters such as temperature and S_{labile}. The heterogeneity in sediment chemical and physical parameters among all of the studied sites contributes to broad validity of these findings.

Multiple lines of evidence support the hypothesis that ebullition-facilitated transport is mechanistically different for PAHs compared to metals. These include the statistically significant correlation between ebullition-facilitated metal flux and gas flux, contrasted with the statistically significant correlations between ebullition-facilitated PAH flux and both SG OC and concentration in the sediments (p-value<1E-05). These results are consistent with a PAH transport mechanism combining organic-rich particle re-suspension and sorption into/onto the gas bubbles from sediment porewater; while metal release is due mainly to particle re-suspension. Thus, the limiting factor for metal release is the amount of bubbles produced (and indirectly the lability of the sediment organic matter to biodegradation), whereas the amount of

organic carbon (indirectly affecting partitioning), coupled with its lability to biodegradation limits PAH release.

Comparison of the direct benthic release rates to ebullition facilitated rates suggest that Σ_{16}PAHs are released at significantly greater rates by biogenic gas production. Although the increase in release rate is not as great for metals, ebullition facilitated release rates are frequently much greater.

On an annual basis, ebullition-facilitated fluxes for Σ_{16}PAHs for the entire Bubbly Creek are predicted to be 59 kg *(313-314)*. For the six metals Ba, Cr, Cu, Pb, Ni and Zn, the total annual ebullition-facilitated fluxes are predicted to be 26, 8, 50, 75, 1.9 and 106 kg. On an annual basis, benthic fluxes released from the sediments for Σ_{16}PAHs for the entire creek are predicted to be 0.39 kg. For the six metals Ba, Cr, Cu, Pb, Ni and Zn, the total annual fluxes are predicted to be 7.8, 1.4, 2.5, 21, 2.9 and 4.3 kg. The estimated concentration of these pollutants in the RAPS stormwater/wastewater discharges that would need to be present to exceed these values (based on the average 0.64 m^3 s^{-1} flowrate of RAPS discharge events for the period 2000-2010) are on the order of only 1.7, 0.45, 2.6, 4.7, 0.24 and 5.5 μg L^{-1} for Ba, Cr, Cu, Pb, Ni and Zn, respectively, and on the order of 2.9 μg $L^{-1}$for Σ_{16}PAHs. Therefore, the contaminant release by the RAPS is likely an important source of contamination to the Creek compared to benthic and ebullition-facilitated contaminant release. Based on these findings, it is clear that attempts to clean up Bubbly Creek must take into account controlling RAPS discharge as well as the continued release of contaminants from the sediments due to historical pollution; particularly in sediments with active gas ebullition. Note that the RAPS is one of the largest sewage pumping stations in the world. Normal CSO inputs are substantially lower than the RAPS input. Thus, not taking sediment contaminant release in urban waterways into account will likely result in a

contaminated sediment-water interface, and continuing releases into the water column as demonstrated by the measured values of contaminant release from the sediments to the water column shown in chapters 6 and 7.

APPENDICES

APPENDIX A: MODELING AND CONTROL OF GAS EBULLITION IN CAPPED SEDIMENTS

The following publication is a first-authored refereed conference proceeding based upon research I participated with two other graduate students from the Environmental Engineering Laboratory of Professor Rockne at University of Illinois at Chicago. My component of the research included field sampling and laboratory analysis of sediments for physical parameters. I was also responsible for performing the gas production study in the laboratory. The University of Illinois graduate college guidelines allow the inclusion of first-authored publications in the body of the PhD dissertation.

A.1. Abstract

A major concern in sediment capping effectiveness is gas ebullition from organic matter biodegradation in sediments. Gases may open advective channels that can result in substantial pollution release. The aim of this study was to determine the gas ebullition rate in sediments in preparation for construction of an active capping technology demonstration at the Collateral Channel site in the Chicago River. Sediment samples were collected from five sites along a transection of Collateral Channel from the combined sewer outfall at the Channel terminus. Biogenic gas production was measured in samples incubated at 5° to 35° C. Gas production followed a first order reaction trend and Arrhenius plots were obtained to determine the temperature dependence of the kinetic rate. These allowed us to predict gas ebullition for the

annual temperature variation in the sediments. CO_2/CH_4 ratios change with temperature, with lower ratios at lower temperatures suggesting dominance by acetoclastic methanogens. These data were used to select adequate active capping remedial alternatives for the Channel. We conclude that wide variations in gas production occur, necessitating gas capture/control during the elevated temperatures of summer. To achieve this, an innovative geo-mesh material with an overlying highly permeable layer will be employed.

A.2. Introduction

Gas ebullition due to methanogenic activity in sediment caps has yet to be fully investigated; even though it is known that methanogenic organic matter degradation facilitates contaminant transport through caps and gas accumulation may cause cap damage *(195)*. Gas bubbles generated due to methanogenic activity are hydrophobic and tend to accumulate hydrophobic contaminants and colloids on their surface. If the amount of gas produced is too high, the gas will evolve in a separate phase and the cap may burst, particularly in unconsolidated surface layers. The aim of this study is to estimate the amount of gas that may be produced at Collateral Channel (Chicago, IL, USA) on an annual basis and to evaluate the methanogenic activity due to acetoclasts and hydrogenotrophs in the surface grab samples.

Collateral Channel is a former navigation slip to the Chicago Sanitary Ship Canal (CSSC) located near Kedzie Avenue, Chicago, IL, USA. A large combined sewer overflow (CSO) is located at the head of the Channel. The CSSC is dominated by industrial and commercial land uses. However, there are plans for urban ecological restoration in the area. Through many decades contaminants were deposited in Collateral Channel with polycyclic aromatic

hydrocarbon (PAH) concentrations approaching 1500 mg/kg and lead concentrations up to 228 mg/kg *(8)*.

Methane and carbon dioxide are end products of the degradation of organic matter under anaerobic conditions. In the complex process of organic matter degradation, fermenters degrade the more complex organic matter producing monosaccharides, fatty acids/alcohols and hydrogen. Under low hydrogen concentrations, syntrophic bacteria consume those fatty acids and alcohols producing acetate, carbon dioxide and hydrogen that may be consumed by homoacetogens to produce acetate, and also by hydrogenotrophs to produce methane. Additionally, homoacetogens degrade monosaccharides producing acetate, which can then be converted to methane and carbon dioxide by acetoclastic methanogens *(197)*. The microbial community structure (and thus the volume and type of gas produced) is strongly affected by temperature changes. Hydrogenotrophic methanogens are stimulated by increased temperature to a greater extent than are acetoclastic methanogens *(198)*. Hydrogenotrophs produce only methane, consuming carbon dioxide and hydrogen, while acetoclasts produce methane and carbon dioxide as shown in equations A.1 and A.2.

Hydrogenotrophic methanogenesis

$$CO_2 + 4H_2 \rightarrow CH_4 + 2H_2O \qquad \Delta G_0 = \text{-131 kJ/mol} \qquad \text{(A.1)}$$

Acetoclastic methanogenesis

$$CH_3COO^- + H^+ \rightarrow CH_4 + CO_2 \qquad \Delta G_0 = \text{-76 kJ/mol} \qquad \text{(A.2)}$$

A.3. Materials and Methods

Sampling. Surface grab samples were collected along the east transect of Collateral Channel as described in Zhao et al. *(8)* (Figure A.1). Surface grab samples were chosen to represent the

likely “worst case” scenario with the most diagenetically young organic matter in the surface layers and thus the highest gas production potential.

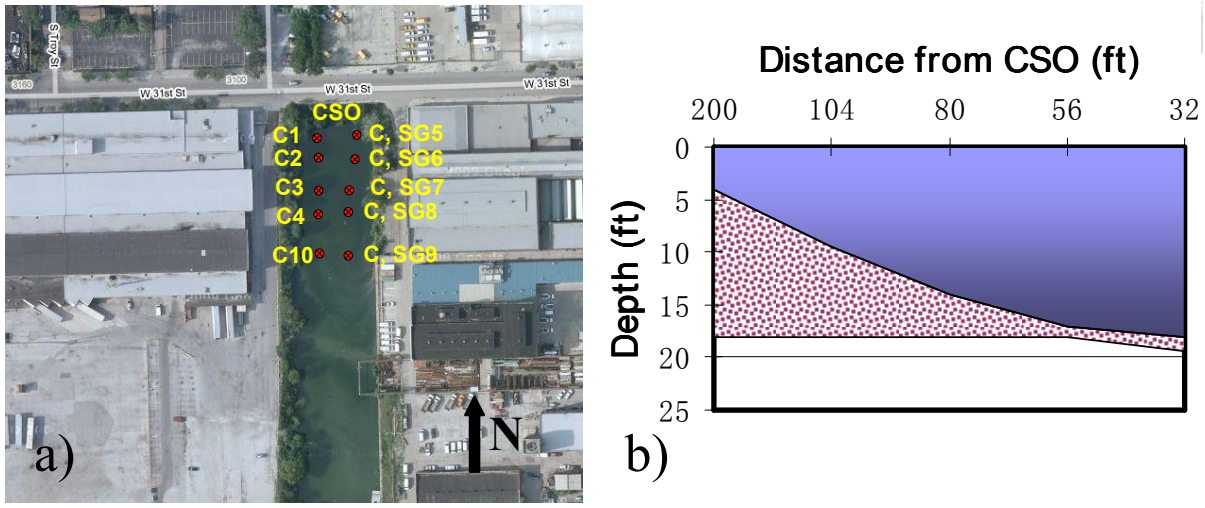

Figure A.1. Sampling sites at Collateral Channel: (a) Highlighted are selected core (C) and surface grab (SG) locations from the current study. A large combined sewer overflow (CSO) is located at the north head of the Channel (at the top of the figure); (b) Surface grab locations along eastern transect from the CSO at the northern terminus of the channel. Base satellite photo from Google – Map data© 2007 NAVTEQ™.

Physical/chemical analyses. Organic carbon content was determined by elemental analysis (FlashEA® 1112, Thermo Electron), nitrate and sulfate were determined by ion chromatography (Dionex IC25), organic matter content and percent solids were determined as described in Zhao et al. *(8)*. The samples from sites five to nine (see Figure A.1a) were homogenized and a 100 mL subsample was added to serum bottles, sparged with nitrogen gas, sealed and incubated upside down quiescently at 5°, 20°, 25° or 35° C. Volumetric gas production was monitored with a calibrated syringe in duplicates and killed controls. Methane and carbon dioxide were quantified by gas chromatography with thermal conductivity detection (9300B, SRI instruments).

A.4. Results and Discussion

The results for nitrate and sulfate concentration in porewater can be observed in Figure A.2a. The amount of nitrate was very low, but there was some sulfate present. Considering the immediate commencement of gas production, the very high ratio of methane production to carbon dioxide observed since the beginning of the incubation period and the total amount of methane produced during a one year period, it is clear that sulfate was rapidly consumed and methanogenesis was the predominant microbial activity at these sites. The organic matter content of the samples (Figure A.2b) was as high as 32%, while the solids content varied from 10 to 26%. Consumption of all sulfate at site 8 would at most account for oxidation of 34 mmol C/L, a small fraction (<1%) of the total organic carbon in the sediment.

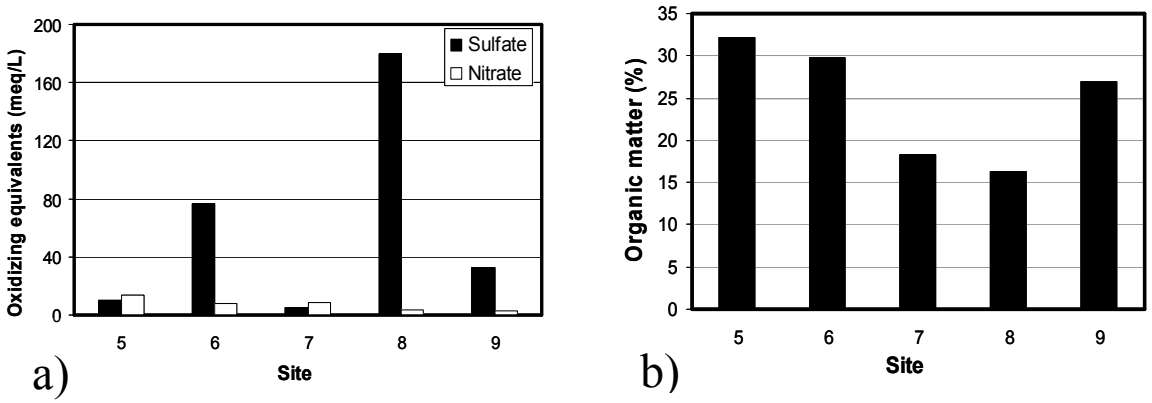

Figure A.2. Collateral Channel surface sediments: a) Sulfate and nitrate in porewater; b) Organic matter content.

Gas production varied substantially as a function of temperature and site location (Figures A.3a-b). The highest amount of gas production was observed at site 5 nearest the CSO (Figure A.3b). Gas production decreased as the distance from the CSO increased. We speculate that less diagenetically aged organic matter near the CSO probably stimulated these higher rates of gas

generation. Summer temperatures result in three times more gas production than winter temperatures.

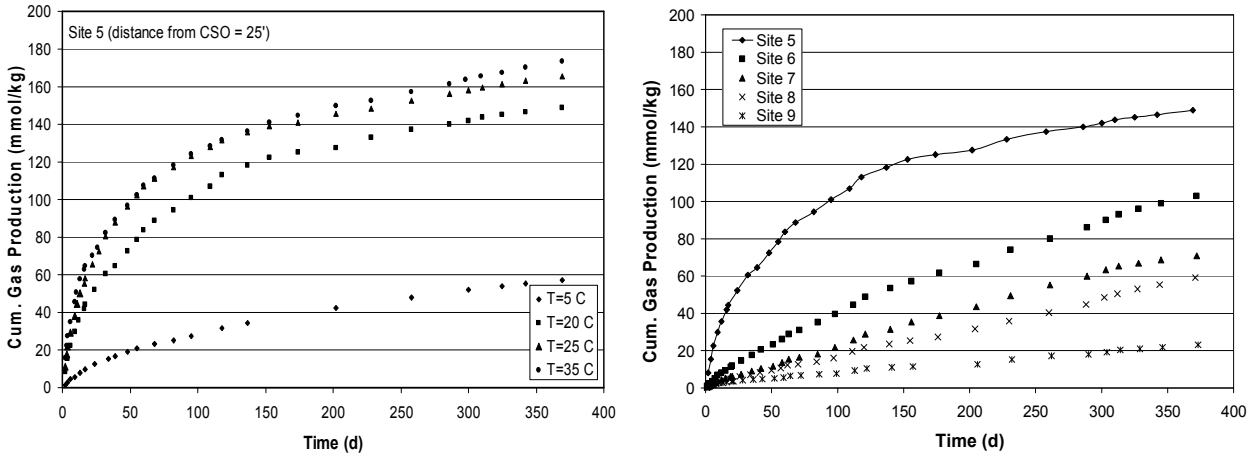

Figure A.3. (a) Gas production as a function of temperature for Collateral Channel sediment site 5; (b) Gas production at all Collateral Channel sediment sites at 20° C.

The biogenic gas production reaction rate constant k was calculated for each site using the Fujimoto method (Figure A.4a) assuming a first order depletion of available methanogenic substrate as shown in equation A.3:

$$C(t) = C_{\max}(1 - e^{-kt}) \tag{A.3}$$

It can be observed that the rate constant values decrease as the distance from the CSO increases, showing the impact of the wastewater and storm water discharges in the past. Rate constants were plotted on an inverse temperature Arrhenius plot to obtain the activation energy for methanogenesis (E_a). The mean activation energy of methanogenesis for all sediments was 43 ± 17 kJ/mol (Figure A.4b). Site 5 (near the CSO) had material that was more biodegradable, while site 7 likely had a more complex substrate, as shown by its higher activation energy.

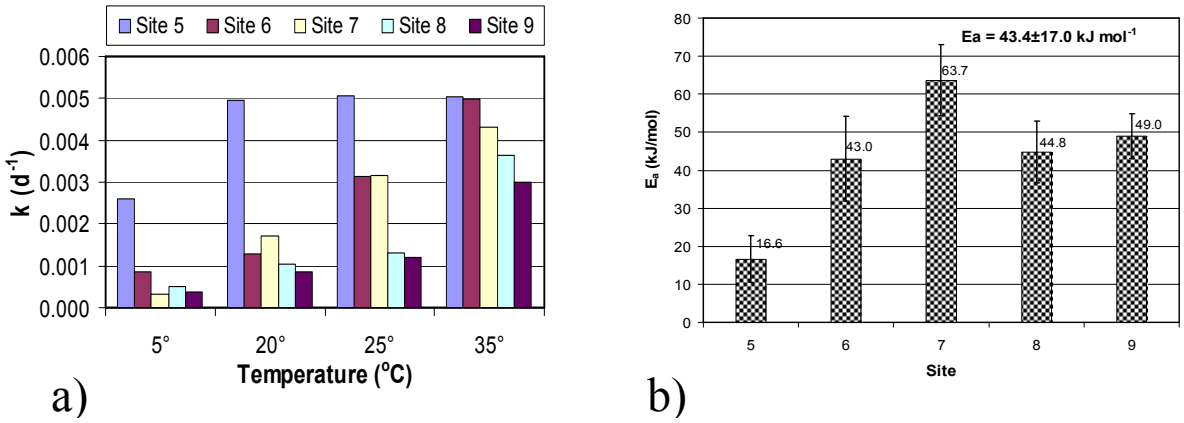

Figure A.4. (a) First order methanogenic rate constants for surfacial Collateral Channel sediments as a function of temperature; (b) Methanogenic activation energy for Collateral Channel surfacial sediments.

Our results agree with methanogenic E_a values reported in the literature (Table A.1). Values ranged from 27 – 138 kJ/mol; the lowest observed with simple substrates (phenol) and higher values were observed with more complex organic compounds like fulvic acids and humic acids commonly found in peat soil.

Table A.1. Activation energy values from literature.

Matrix	*Ea* (kJ/mol)	Reference
Wetlands (fen soil)	138±17 (unsaturated) 84±6 (saturated)	*(274)*
Wetlands	74.3 – 79.5	*(315)*
Wetlands	29 – 50 at 51 d	*(316)*
Primary sludge	50	*(317)*
UASB reactor (phenol)	27.2	*(273)*
Paddy soil	59.7	*(318)*
Paddy soil	91.0	*(198)*
Wetland rice soil	48 - 65	*(319)*
120 mL serum bottles (45 mL mineral medium, 2 mL amorphous cellulose)	121±1	*(320)*
Peat soil	123 - 271	*(321)*
Alder swamp	92 - 110	*(322)*
Lake sediment	76	*(275)*

The volume of gas that may be produced at each site per cubic meter of sediment was estimated for the whole year (Figure A.5). Gas production at site 5 (nearest the CSO) may exceed 4 m^3 gas/ m^3 sediment. Sites 6, 7 and 8 all exceed 2 m^3 gas/m^3 sediment. Site 9, most distant from the CSO, was the only site containing sediment that would not produce gas in excess of its own volume on an annual basis. Although these sediments were disturbed during experimental set up (and therefore may represent a higher value than in undisturbed sediments *in situ*) we argue that it still may represent a realistic prediction under capping scenarios because the sediment will be disturbed during cap placement.

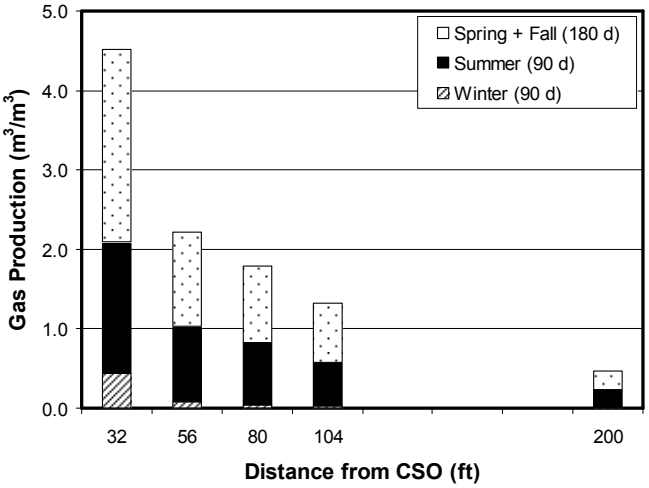

Figure A.5. Estimated volumetric gas production (m^3 /m^3 of sediment) in Collateral Channel surfacial sediments as a function of distance from the CSO.

The maximum amount of methanogenic substrate (C_{max}) was estimated for each sediment from the first order depletion kinetic model (Equation A.3). Comparing the total organic carbon content value at each site (Figure A.6a) with the C_{max} value (Figure A.6b) indicates that the amount of substrate available to methanogenesis is very low. Well less than 10% of the total organic carbon could be accounted for as methanogenic substrate, even after more than a year of

incubation. It is likely that the organic matter that could serve as methanogenic substrate was depleted, leaving behind more complex organic matter.

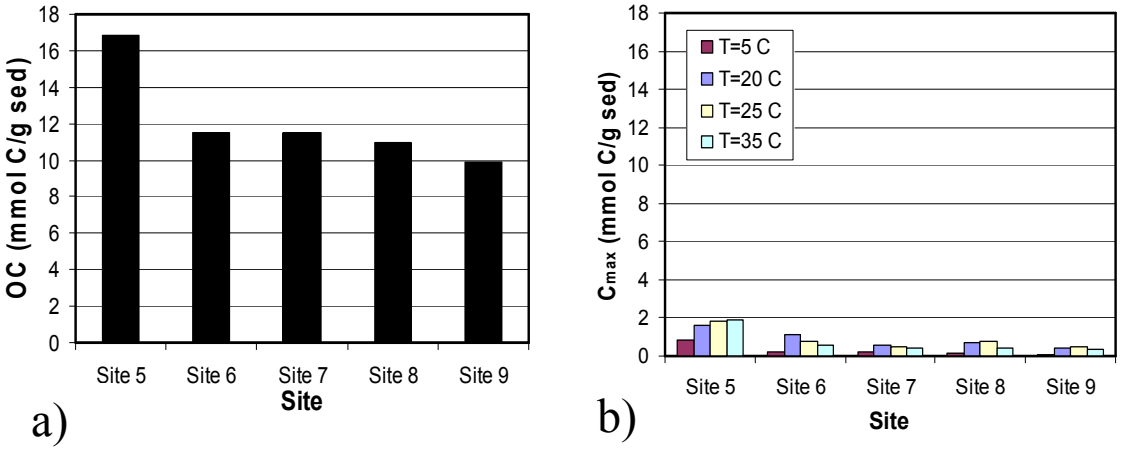

Figure A.6. (a) Organic carbon content of surficial Collateral Channel sediments as a function of distance from the CSO and (b) C_{max} at each site as a function of temperature.

The CH_4/CO_2 ratio of biogenic gas was affected by temperature (Figure A.7). Lower ratios were observed at lower temperatures, suggesting dominance by acetoclastic methanogens. Higher gas production and higher CH_4/CO_2 ratios were observed at sites 5 and 6 at low temperatures than for the other sites, suggesting a greater prevalence of hydrogenotrophic methanogens.

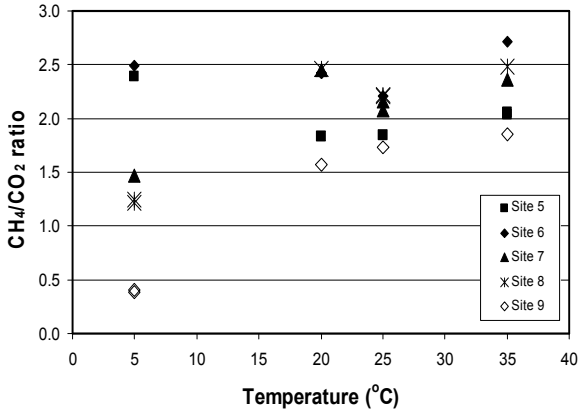

Figure A.7. CH_4/CO_2 ratio of biogenic gas produced from Collateral Channel surfacial sediments as a function of temperature.

A.5. Conclusions and Implications

Due to the high amount of gas produced, particularly at site 5, gas control will likely be needed for this site to ensure cap integrity. To achieve this, the design team will employ a geonet layer with overlying high permeability sand between the contaminated sediment and the cap material to collect the gas at the sides of the Channel. This will prevent the cap from potential breach by gas ebullition. Monitoring of gas production for an entire year was important to better predict the amount of gas produced. This can be seen by comparing the predicted gas ebullition from a short term (30 d) data set. Gas production would be overestimated by a factor of 2 – 3. The activation energy of methanogenesis in Collateral Channel sediments is 43.4 ± 17.0 kJ/mol. The amount of organic carbon available as substrate for methanogenic activity is very low, suggesting that sedimentary organic carbon is a poor predictor of methanogenic activity.

APPENDIX B. EBULLITION-FACILITATED TRANSPORT OF HEAVY METAL CONTAMINANTS TO THE WATER COLUMN

The following publication is a first-authored refereed conference proceeding based upon research I participated with other graduate student from the Environmental Engineering Laboratory of Professor Rockne at University of Illinois at Chicago. My component of the research included field sampling and laboratory analysis of sediments for physical parameters. I was also responsible for performing the gas ebullition study. The University of Illinois graduate college guidelines allow the inclusion of first-authored publications in the body of the PhD dissertation.

B.1. Abstract

Our study aims to quantify metal contaminant transport from the sediment to the water column due to gas ebullition. Sediment surface grab (SG) and core samples were collected in 14 contaminated sediment locations in three different sites in the Chicago River. We investigated correlations between *in situ* gas ebullition rates and laboratory gas production rates, sediment organic carbon (OC), organic matter, chemical oxygen demand and sediment composition. Biogenic gas production was measured in laboratory incubations over the temperature range 5° to 35° C. Gas ebullition was measured in the field (GF_f) with gas collector systems placed at the 14 sample sites. Glass wool traps were placed in each gas collector system to collect bubble-entrained particulates and non aqueous phase liquids to measure the ebullition-facilitated contaminant transport. Principle component and multivariate analysis demonstrates that the

correlation between laboratory gas production and SG OC content is statistically significant (p-value 0.08). SG OC combined with laboratory gas production rate predicted GF_f best (p-value 0.02). Interestingly, both increased sediment depth and increased whole core OC levels were inversely proportional to GF_f, indicating that biogenic gas ebullition may be localized to upper sediment layers, which explains that SG OC is better correlated with field gas ebullition than core OC. Ebullition-facilitated metal fluxes were surprisingly large, with resultant fluxes of 10, 2, 6, 30 and 490 mg m^{-2} d^{-1} for Pb, Cr, Ba, Zn and Fe, respectively. These fluxes were 10-1000 times higher than predicted to occur by porewater diffusion from uncapped sediments, and on the order of advective porewater metal flux under a large hydraulic gradient of 0.05 m/m.

B.2. Introduction

Gas ebullition due to methanogenic activity is an important factor that needs to be understood and accounted for in a cap design. As observed by Reible and others *(10)*, gas bubbles may damage the cap layer. Because gas bubbles are hydrophobic and tend to accumulate hydrophobic contaminants and sediment particles on their surface, they may transport contaminants by enhancing sediment resuspension *(3)*.

There have been some studies measuring gas production in the field, with very different gas production fluxes due to site characteristics. Tanner et al. *(199)* observed a methane flux varying from 0.07 to 0.67 L m^{-2} d^{-1} for a wetlands that had treated wastewater. Sovik et al. *(200)* measured methane and carbon dioxide fluxes in ten constructed wetlands in Europe, which were up to 53 and 47 L m^{-2} d^{-1}, respectively. Hughes et al. *(202)* obtained, based on a laboratory study, gas production fluxes of up to 2.7 L m^{-2} d^{-1} in the Anacostia River, Washington, D.C. However, the researchers commented that the amount of bubbles released naturally is probably about only 10% of the obtained in a laboratory experiment because both trapped and bubble gas are

measured in laboratory due to overpressure in serum bottles. The authors also mentioned the effect of water tide in field gas ebullition. During low tide, overlying hydrostatic pressure is decreased and the gas flux increases. The opposite would occur for higher tides. Fendinger et al. *(20)* stated that sediment composition, redox potential, microbial population of the sediments (methanogenesis and denitrification activity) and water depth are some of the factors affecting gas ebullition. Thus, field gas fluxes can vary a lot and better understanding the factors influencing gas fluxes can help in predicting more accurate field gas flux values.

Knowing the composition of gas produced is also important as three of the most important greenhouse gases worldwide may be produced through methanogenic and denitrification activity. Carbon dioxide and methane are the common products of methanogenic degradation, but N_2O can also be produced as an intermediate of the denitrification process. According to Stadmark and Leonardson *(203)*, experiments have shown seasonal variation in the emission of greenhouse gases due to temperature and to varying composition and bioavailability of organic bacterial substrates in aquatic sediments. Huttunen et al. *(204)* observed bubble gas content of CH_4 and CO_2 equal to 48-67% and 0.01-1.1%, respectively, while Casper et al. *(205)* observed mean gas content of CH_4, CO_2 and N_2 equal to 66, 3 and 36%, respectively. Both studies were performed *in situ* with lake sediment.

There are a limited number of studies investigating the amount of contaminants transported to the water surface due to gas ebullition. Yuan et al. *(3)* found that significant amounts of both solid particulate matter and contaminant can be transported from the sediment to the water column by gas movement. The authors observed that the amount of contaminant and solid particulate transported is related to the volume of gas released. Hulls and Costello *(206)* observed in their bench tests with sediment from Stryker Bay, Duluth Minnesota, that PAH are

transported to the water column due to groundwater advection and gas ebullition. The authors concluded that a sand cap can be effective to minimize contaminant release and to prevent gas from forming due to sediment insulation. Fendinger et al. *(20)* noted that sediment contaminant transport may be a function of gas ebullition rates, Henry's law constant and porewater contaminant concentration. According to the researchers, organic contaminant partitioning occurs mainly between sediment gas and porewater, which is determined by gas/water partition coefficients of each compound in the sediment pore water. The process of organic contaminant partition between sediment solid material and gas bubbles is probably negligible due to the high liquid water content of many sediments.

The objectives of this study were to A) compare gas production in the laboratory with field production under summer temperature to investigate correlations between easily measured parameters and field gas flux with the goal of eliminating the necessity to perform field measurements and B) quantify metal flux in gas collectors to quantify the magnitude of metal facilitated transport due to gas ebullition.

B.3. Materials and Methods

Sampling of Collateral Channel, the Turning Basin near Bubbly Creek and Bubbly Creek was conducted onboard the Metropolitan Water Reclamation District (MWRD) RV *PC1* in September 2005, November 2005 and July 2008, respectively. A combined sewer Outfall (CSO) exists on the northern terminus of Collateral channel that released wastewater for decades but is no longer in use. Five core samples and five surface grabs (SG) were analyzed at Collateral Channel, four core samples and four SG at the Turning Basin, and five core samples and five SG at Bubbly Creek. Bubbly Creek is impacted by CSO effluent on an approximately monthly basis

from the Racine Avenue pumping station (RAPS), the largest sewage pumping station in the world. Detailed description and location of this sites can be found elsewhere *(323)*.

Gas production assays in serum bottle, wet bulk density, dry bulk density, percent solids, percent moisture, porosity (φ_e), organic carbon (OC) and organic matter (OM) were analyzed in the laboratory as described by Viana et al. *(130)*.

Gas collection systems (Figure B.1) were based upon a design by Huttunen et al. *(204)* that was modified to provide a more robust sampler valve system with most parts available from a hardware store. The collector consists of an inverted funnel (25 cm external diameter), connected to a 1" PVC tube (75 cm long). The tube length was shortened when necessary to prevent the funnel from touching the sediment in shallow areas. A steel flange was placed on the tube to help the system sink while remaining in a vertical position. A PVC connection with a rubber stopper was used to facilitate collection of gas samples. Each collector was attached to a float and anchor. MWRD boats and personnel assisted our group during sampling.

Glass wool was placed inside the funnel to trap contaminants transported with gas bubbles and outside the funnels as controls. The difference between these two values is the metal flux due to gas ebullition reported in this paper. T-tests comparing these samples showed that they were statistically significant different at the 95%. Metal analyses were performed by ICP-MS using standard methods by Stat Analysis (Chicago, IL). Gas sampling was conducted every day to minimize gas leakage. Samples of gas were collected with 1 mL syringes for gas composition characterization by GC-TCD (SRI instruments 9300B, Torrance, CA). Glass wool samples were brought to the laboratory intact and gas volume was measured by displacement of water in graduated cylinders.

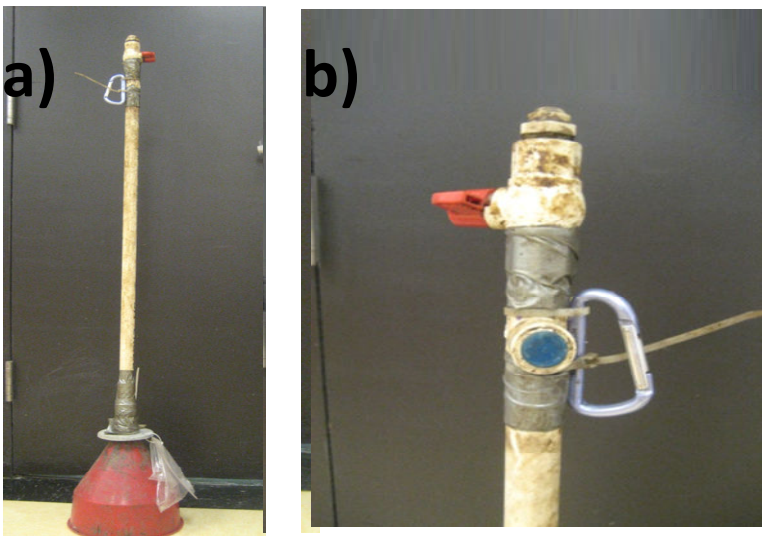

Figure B.1. Gas collector system. Shown are a) complete collectors and b) detail of the collector valve.

B.4. Results and Discussion

The sediments are very heterogeneous, with SG OM content varying from 1.5 to 32%, core OM from 5.4 to 26%, SG OC from 1.8 to 20%, core OC from 0.6 to 15%, and SG porewater nitrate concentrations from 0.4 to 1.8 mg/L. Field sediment temperature varied from 23.5 to 27° C. Laboratory gas production data was best fit as a zero order rate law for the turning basin (TB) and for Bubbly Creek (BC), and as a first order rate law for Collateral Channel (CC). Mean field gas flux (GF_f) and laboratory volumetric gas rate ($VGPR_l$) can be observed in Table B.1, as well as the activation energy (E_a) per site.

Table B.1. Laboratory gas production rates, field gas flux, sediment depth and activation energy.

Site	GF_f (L m^{-2} d^{-1})	CH_4 GF_f (L m^{-2} d^{-1})	$VGPR_l$ (L m^{-3} d^{-1})	Water depth (m)	Sed depth (m)	E_a (kJ mol^{-1})
CC5	7.7	4.6	18	5.5	0.5	16.6 ± 6.1
CC6	8.0	0.8	11	5.2	0.3	43.0 ± 11.1
CC7	9.8	6.7	8.7	4.3	1.2	63.7 ± 9.4
CC8	11	4.9	6.0	2.9	2.6	44.8 ± 8.1
CC9	6.2	1.4	2.4	1.2	4.3	49.0 ± 5.9
TB2	5.4	3.6	3.7	2.2	5.7	
TB5	7.6	3.9	3.4	1.5	6.5	48.3 ± 7.4
TB10	3.8	1.8	4.1	3.2	4.8	36.8 ± 11.9
TB13	1.4	0.9	3.9	2.5	5.5	
BC13	6.0	2.6	2.2	4.6	2.1	61.7 ± 11.8
BC11	9.1	3.6	1.8	1.2	3.6	41.0 ± 13.1
BC9	3.9	2.4	10	3.1	3.0	21.2 ± 8.9
BC8	3.7	2.5	7.5	2.1	2.5	29.8 ± 7.7
BC4	8.3	5.4	14	3.5	3.2	32.1 ± 8.2

CC5 had the highest $VGPR_l$ of all sites. We attribute this to its location as the site nearest to a CSO coupled with its very high SG OC (20%) and OM (32%). Further, the OM was diagenetically very young, as suggested by the copious prevalence of vascular plant debris and the lowest E_a for methanogenesis among all the sites. Sites BC13 and 11 had very low $VGPR_l$, likely due to the low SG OC and SG OM content (<2.4%). Site BC11 had an anomalously high GF_f, which may have been due to a recent storm resulting in new deposition of debris from a RAPS release event within 1 week prior to sampling. Site CC7 and BC13 were likely composed by a more diagenetically aged OM, as shown by their higher E_a values. Further, although site BC13 was nearest to RAPS, it had the lowest OM and OC levels and its sediment depth was among the shallowest. We attribute this to scouring of lower density OM-laden sediment particles during RAPS release events (flows from the RAPS can reach up to 175 m^3 s^{-1}), which is supported by the fact that sand comprised >80% of the sediment mass.

Our results show that GF_l does not necessarily overestimate GF_f, as reported by Hughes et al. *(202)*, even when considering the entire sediment depth to hardpan (hereafter referred to as

"sediment depth") to calculate GF_l. If we consider only the top 1m of sediment as ebullition active, eight of our 14 sites actually had higher GF_f than GF_l. The measured CH_4 GF_f are consistent with values reported in the literature, which range from 0.07 up to 53 L m^{-2} d^{-1} *(199-200)*. Our GF_f are higher than those observed by Hughes et al. *(202)*, which is not surprising as their study site (Anacostia River) had OC levels <6% *(324)*. Our methanogenic E_a values are also consistent with literature-reported values, which range from 27 to 138 kJ mol^{-1} *(273-274)*; lower values were observed with simple substrates and higher values were observed with complex organic compounds like fulvic and humic acids in peat soil.

The yearly volume of gas that may evolve at each site was estimated based on the annual temperature variations on site corrected by the Arrhenius equation and laboratory gas production results (Figure B.2). Although these sediments were disturbed during experimental set up, we believe these results are a realistic prediction under a capping scenario as the sediment will also be disturbed and field gas ebullition rates were consistent with laboratory results (discussed in detail below). These results were used to estimate the total amount of CH_4 and CO_2 emitted to the atmosphere from the sediments based upon the field gas composition (51±9%, 5±1% and 44±10% for CH_4, CO_2 and N_2, respectively), assuming that summer gas composition was similar year round. Thus we estimate that 371,000 m^3 of CH_4 and 23,000 m^3 of CO_2 would be emitted per year by 325,000 m^3 of sediment with a surficial area of 102,212 m^2 for Bubbly Creek, the Turning Basin and Collateral Channel.

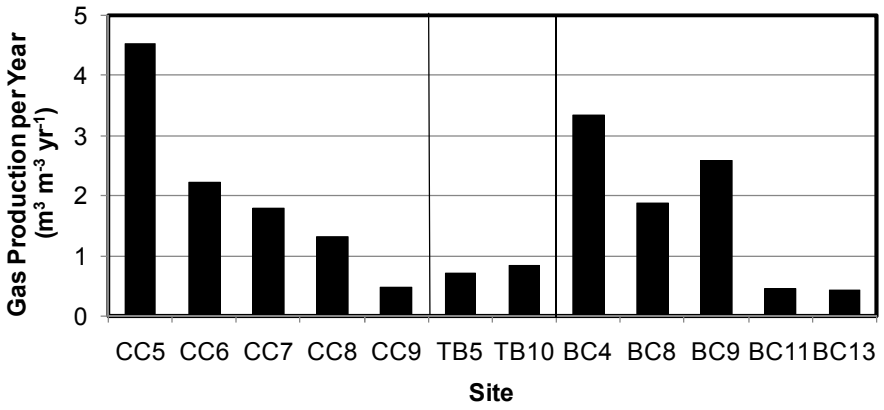

Figure B.2. Estimated volumetric gas production per m^3 of sediment in field sites shown in roughly a north to south transect.

We estimated the GF_l and $VGPR_f$ based on a 1 m deep active ebullition zone. This depth was chosen based on Costello and Talsma *(285)* and on the changes observed in φ_e and bulk density below 1 m depth. $VGPR_f$ based upon 1 m deep active zone were more correlated with SG OM and OC than $VGPR_f$ assuming the entire sediment depth was active. This suggests that using the entire sediment depth overestimates $VGPR_f$.

Surprisingly, GF_l calculated from $VGPR_l$ were not correlated with any sediment parameter. This is likely because very shallow or very deep sediments include atypical biogenic gas production. OM and OC were more closely correlated with gas production. Chemical oxygen demand values are not well correlated with gas production; thus this variable was not considered for further correlations. Two data points were considered outliers and not used in the correlations: site CC5, which had very high SG OM and OC, and site BC11, which had very high GF_f, which we attribute to a RAPS release event as described above.

Principle component analysis indicates that of all the sediment physical and chemical properties, SG OC was best able to predict GF_f (Figure B.3). Multi-variate correlations show that core OC is negatively correlated with GF_f, even though core OC is bigger than SG OC for most

cores, suggesting that part of the buried carbon is recalcitrant to methanogenesis and thus resistant to diagenetic alteration. These findings suggest that it may not be necessary to analyze the entire sediment core to predict field gas fluxes. Further, $VGPR_l$ does not successfully predict GF_f as a sole variable (p-value 0.36). However, $VGPR_l$ together with SG OC is highly correlated to GF_f for summer temperatures (p-value 0.04). The variables SG OC, SG OM and $VGPR_l$ may also be used to predict GF_f. However, the combination of these variables does not increase the ability to predict GF_f (Table B.2). Although the high correlation between $VGPR_l$ and SG OC which is predicted by: $VGPR_l$=0.43SG OC+3.02 (p-value 0.08) is expected, the goodness of fit suggests this equation may be used in lieu of performing laboratory experiments.

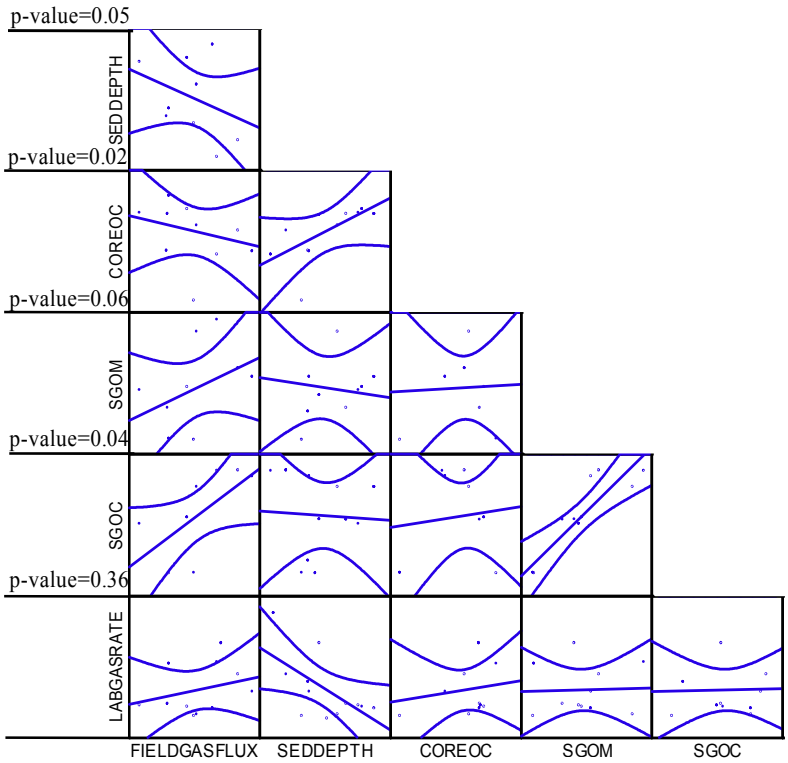

Figure B.3. Scatterplot matrix of GF_f with $VGPR_l$, SG OC, SG OM, core OC and sediment depth. Curves represent the 95% CL. P-values represent correlation of GF_f and corresponding variable.

Table B.2. Best correlations found between GF_f, $VGPR_l$, SG OC, SG OM and core OC.

Correlations (summer temperature)	p-value
GF_f=0.41SGOC+2.7	0.02
GF_f=0.73SGOC-0.19SGOM+2.6	0.04
GF_f=0.41SGOC+0.20$VGPR_l$+1.5	0.04
GF_f=0.73SGOC-0.20SGOM+0.21$VGPR_l$+1.3	0.06
GF_f=0.44SGOC+0.26$VGPR_l$-0.26coreOC+3.8	0.02

As expected, high levels of particulate matter were found in the glass wool samples located inside the gas collector systems (in contrast to the control gas wool on the exterior of the collector). This resulted from gas bubbles transporting solid particulates, as observed by Yuan et al. *(3)*. ICP-MS analysis demonstrated that As, Ag, Be, Cd, Co, Mo, Ni and Se were below the detection limit (DL) in the glass wool. Ba, Cr, Cu, Fe, Mg, Mn, Na and Zn were all present above the DL, and we confine our discussion to these metals. Fe and Pb fluxes varied by less than an order of magnitude: 70-500 mg m^{-2} d^{-1} and 2-10 mg m^{-2} d^{-1}, respectively (Figure B.4). Cr, Ba and Zn flux were more variable by location, ranging from 0.1-2 mg m^{-2} $d^{-}1$, 0.5-6 mg m^{-2} d^{-1} and 2-30 mg m^{-2} d^{-1}, respectively. Sediment metal concentrations were measured for most sites and they ranged from 260-2,800 mg kg^{-1}, 45-540 mg kg^{-1}, 110-660 mg kg^{-1}, 210-6,600 mg kg^{-1}, and 10,000-18,000 mg kg^{-1} for Pb, Cr, Ba, Zn and Fe, respectively. The higher Pb, Zn and Fe metal fluxes due to gas ebullition are thus likely due to the higher metal sediment concentration. However, sediment Cr levels were not high at these sites, and they did not co-vary with ebullition-enhanced Cr flux.

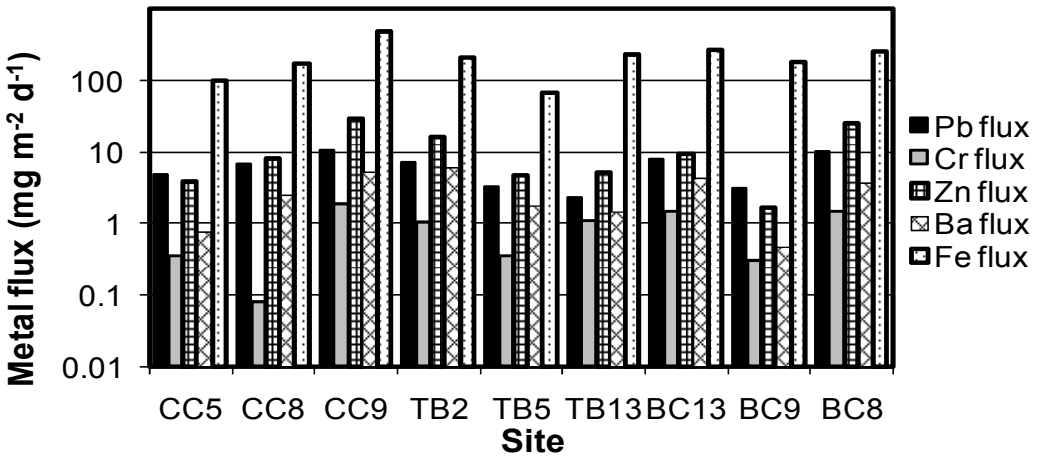

Figure B.4. Metal flux to the water column due to gas ebullition.

We compared the measured Pb, Cr and Ba fluxes due to gas ebullition to simulated mass fluxes released via sediment porewater from uncapped sediment under diffusive and advective conditions (Table B.3) based on parameters from Viana et al. *(15)*. This analysis conservatively assumes that the porewater is saturated with the respective metal, which may not have been the case in our test sediments. In all cases, the ebullition-enhanced flux was one to three orders of magnitude higher than diffusive release, and comparable to advective flux under a high hydraulic gradient of 0.05 m/m. These results clearly indicate that the elevated metal concentrations in particulate matter brought to the water column by ebullition greatly enhanced flux for metals like Pb that have limited solubility in sediment porewater.

Table B.3. Comparison of simulated mean Pb, Cr and Ba mass flux released from uncapped sediment under different hydraulic gradients (assuming C=0 in overlying water) to measured ebullition-facilitated fluxes.

	Pb pH7 ($mg\ m^{-2}\ d^{-1}$)	**Cr pH7 ($mg\ m^{-2}\ d^{-1}$)**	**Ba pH7 ($mg\ m^{-2}\ d^{-1}$)**
Uncapped sediment, no gradient	0.005	0.07	0.04
Uncapped sediment, 0.005 m/m	0.01	1	2
Uncapped sediment, 0.05 m/m	0.13	14	17
Field measurement	**2-10**	**0.1-2**	**0.5-6**

B.5. Conclusions and Implications

We present two main findings from this research. First, as measurement of GF_f is time consuming and potentially costly, we provide equations that may be used to predict field gas fluxes under summer temperatures based on more easily measurable parameters. Our results indicate that laboratory studies do not necessarily overestimate field results and that SG OC content is a reliable predictor of GF_f. In contrast, whole core OC content and sediment depth may not necessarily contribute to increased GF_f. The heterogeneity in sediment OM, OC and other parameters among all of the study sites contributes to validity of these findings. Second, ebullition-facilitated metal fluxes were surprisingly large, with resultant fluxes of 10, 2, 6, 30 and 490 mg m^{-2} d^{-1} for Pb, Cr, Ba, Zn and Fe, respectively. These fluxes were 10-1000 times higher than predicted to occur by porewater diffusion from uncapped sediments, and on the order of advective porewater metal flux under a large hydraulic gradient of 0.05 m/m.

CITED LITERATURE

(1) Donald, C. M.; Bruce, B. M.; Donald, W. B.; Usha, V.; Margaret, M. K.; Mark, S. M.; Sin-Lam, C. Sediment-associated contaminants and liver diseases in bottom-dwelling fish. *Hydrobiologia* **1987,** *149* (1), 67.

(2) USEPA. *EPA's contaminated sediment management strategy*; EPA-823-R-98-001; US Environmental Protection Agency: Washington, D.C., 1998; p 105.

(3) Yuan, Q.; Valsaraj, K. T.; Reible, D. D.; Willson, C. S. A laboratory study of sediment and contaminant release during gas ebullition. *J Air Waste Manag. Assoc.* **2007,** *57* (9), 1103-1111.

(4) Viana, P. Z.; Yin, K.; Zhao, X.; Rockne, K. *Contaminant-facilitated transport due to sediment gas production: Laboratory and field studies*. In Fifth International Conference on Remediation of Contaminated Sediments, Jacksonville, FL, Feb 2-5, 2009; Jacksonville, FL, 2009.

(5) Bergen, B. J.; Nelson, W. G.; Mackay, J.; Dickerson, D.; Jayaraman, S. Environmental monitoring of remedial dredging at the New Bedford Harbor, MA, Superfund Site. *Environ. Monit. Assess.* **2005,** *111* (1-3), 257-275.

(6) Mohan, R. K.; Brown, M. P.; Barnes, C. R. Design criteria and theoretical basis for capping contaminated marine sediments. *Appl. Ocean Res.* **2000,** *22* (2), 85-93.

(7) Simpson, S. L.; Pryor, I. D.; Mewburn, B. R.; Batley, G. E.; Jolley, D. Considerations for capping metal-contaminated sediments in dynamic estuarine environments. *Environ. Sci. Technol.* **2002,** *36*, 3772-3778.

(8) Zhao, X.; Viana, P. Z.; Yin, K.; Rockne, K. J. *Combined active capping/wetland demonstration in the Chicago River. Paper D-019* In Conference Chairs, Remediation of Contaminated Sediments-2007. Proceedings of the Fourth International Conference on Remediation of Contaminated Sediments. ISBN 978-1-57477-159-6, Battele Press, Columbus, OH, January 22-25; Columbus, OH, 2007.

(9) Viana, P. Z.; Yin, K.; Zhao, X.; Rockne, K. J. *Active capping: A low cost technology to contain and reduce the exposure risk of contaminated sediments*. In 7th Regional Conference of USA Inter-American Association of Sanitary Engineering and Environmental Sciences, Chicago, USA, Chicago, USA, 2006.

(10) Reible, D.; Lampert, D.; Constant, D.; Mutch-Jr., R. D.; Zhu, Y. Active capping demonstration in the Anacostia River, Washington, D.C. *Remediation J.* **2006,** *17* (1), 39-53.

(11) DEQ. *McCormick and Baxter creosoting company superfund site*; ORD009020603; Oregon Department of Environmental: Portland, Multnomah County, OR, 2006.

(12) Quadrini, J. D.; VanDewalker, H. M.; Mihm, J. E.; McShea, L. J. Pilot-scale demonstration of in situ capping of PCB-containing sediments in the lower Grasse River. *Remediation J.* **2003,** *14* (1), 33-53.

(13) Olsta, J. T.; Hornaday, C. *Installation of an in-situ cap at a superfund site. paper D-025*. In Fourth International Conference on Remediation of Contaminated Sediments, Savannah, GA, Battelle Press: Savannah, GA, 2007.

(14) Murphy, P.; Marquette, A.; Reible, D.; Lowry, G. V. Predicting the performance of activated carbon-, coke-, and soil-amended thin layer sediment caps. *J. Environ. Eng.-ASCE* **2006,** *132* (7), 787-794.

(15) Viana, P. Z.; Yin, K.; Rockne, K. J. Modeling active capping efficacy. 1. Metal and organometal contaminated sediment remediation *Environ. Sci. Technol.* **2008,** *42* (23), 8922-8929.

(16) Yin, K.; Viana, P. Z.; Rockne, K. J. *Verification of active cap contaminant breakthrough simulations via laboratory column studies*. In Fifth International Conference on Remediation of Contaminated Sediments, Jacksonville, FL, Feb 2-5, 2009; Jacksonville, FL, 2009.

(17) McLinn, E. L.; Stolzenburg, T. R. Investigation of NAPL transport through a model sand cap during ebullition. *Remediation J.* **2009,** *19* (2), 63-69.

(18) Huls, H. H.; Costello, M.; Sheets, R. *Gas, NAPL and PAH flux assessment in sediments*. In Second International Conference on Remediation of Chlorinated and Recalcitrant Compounds, Monterey, CA, Monterey, CA, 2002.

(19) Yuan, Q.; Valsaraj, K. T.; Reible, D. D. A model for contaminant and sediment transport via gas ebullition through a sediment cap. *Environ. Eng. Sci.* **2009,** *26* (9), 1381-1391.

(20) Fendinger, N. J.; Adams, D. D.; Glotfelty, D. E. The role of gas ebullition in the transport of organic contaminants from sediments. *Sci. Total Environ.* **1992,** *112* (2-3), 189.

(21) McLinn, E. L.; Stolzenburg, T. R. Ebullition-Facilitated Transport of Manufactured Gas Plant Tar from Contaminated Sediment. *Environmental Toxicology and Chemistry* **2009,** *28* (11), 2298-2306.

(22) Stumm, W.; Morgan, J. J. *Aquatic chemistry, chemical equilibria and rates in natural waters*. 3rd ed. ed.; John Wiley & Sons, Inc.: New York, NY, 1996.

(23) Salomon, W.; Forstner, U. *Metals in the hydrocycle*. Springer, Berlin: 1984.

(24) Snoeyink, V. L.; Jenkins, D. *Water Chemistry*. John Wiley & Sons, Inc.: 1980.

(25) Hinga, K. R. Effects of pH on coastal marine phytoplankton. *Mar. Ecol. Prog. Ser.* **2002,** *238*, 281-300.

(26) Potapova, M.; Charles, D. F. Distribution of benthic diatoms in U.S. rivers in relation to conductivity and ionic composition. *Freshw. Biol.* **2003,** *48* (8), 1311-1328.

(27) Vega, M.; Pardo, R.; Herguedas, M. M.; Barrado, E.; Castrillejo, Y. Pseudopolarographic determination of stability constants of labile zinc complexes in fresh water. *Analytica Chimica Acta* **1995,** *310* (1), 131.

(28) Chubarenko, B. *Assessment of the fate and effects of toxic agents on water resources: Monitoring physical processes*. Springer Netherlands: 2007; p 109.

(29) USEPA. *National recommended water quality criteria*; U. S. Environmental Protection Agency 2006; p 25.

(30) Kelly, M. H.; Hite, R. L. *Evaluation of Illinois stream sediment data, 1974-1 980*; IEPA/WPC/84-004; IEPA.: Springfield, Illinois, 1984.

(31) NOAA. *Screening quick reference tables* National Oceanic and Atmospheric Administration: Seattle, WA, 2008.

(32) Hunter, K. A.; Kim, J. P.; Reid, M. R. Factors influencing the inorganic speciation of trace metal cations in freshwater. *Mar. Freshwater Res.* **1999,** *50*, 367-372.

(33) Wang, W.-X.; Rainbow, P. S. Comparative approaches to understand metal bioaccumulation in aquatic animals. *Comp. Biochem. Physiol. Part C: Toxicol. Pharmacol.* **2008,** *148* (4), 315.

(34) Hubbard, A. T. *Encyclopedia of surface and colloid science: 2004 update supplement*. CRC Press: 2004.

(35) Rockne, K. J. Kinetic hindrance of Fe(II) oxidation at alkaline pH and in the presence of nitrate and oxygen in a facultative wastewater stabilization pond. *J. Environ. Sci. Health Part A Toxic-Hazard. Subst. Environ. Eng.* **2007,** *42* (3), 265-275.

(36) Himmelheber, D. W.; Taillefert, M.; Pennell, K. D.; Hughes, J. B. Spatial and temporal evolution of biogeochemical processes following in situ capping of contaminated sediments. *Environ. Sci. Technol.* **2008,** *42* (11), 4113-4120.

(37) Bodegom, P. M. v.; Stams, A. J. M. Effects of alternative electron acceptors and temperature on methanogenesis in rice paddy soils. *Chemosphere* **1999,** *39* (2), 167.

(38) Rockne, K. J. Alternative electron acceptors for polycyclic aromatic hydrocarbons biodegradation. University of Washington, Seattle, WA, USA, 1997.

(39) Sawyer, C. N.; McCarty, P. L.; Parkin, G. F. *Chemistry for environmental engineering* 4th ed.; McGraw-Hill 1994.

(40) Wang, F.; Chapman, P. M. Biological implications of sulfide in sediment—A review focusing on sediment toxicity. *Environ. Toxicol. Chem.* **1999**.

(41) Canavan, R. W.; Van Cappellen, P.; Zwolsman, J. J. G.; van den Berg, G. A.; Slomp, C. P. Geochemistry of trace metals in a fresh water sediment: Field results and diagenetic modeling. *Science of The Total Environment* **2007,** *381* (1-3), 263.

(42) Barnhart, J. Occurrences, Uses, and Properties of Chromium. *Regulatory Toxicology and Pharmacology* **1997,** *26* (1), S3.

(43) Huerta-Diaz, M. A.; Tessier, A.; Carignan, R. Geochemistry of trace metals associated with reduced sulfur in freshwater sediments. *Applied Geochemistry* **1998,** *13* (2), 213.

(44) USEPA. *Procedures for the derivation of equilibrium partitioning sediment benchmarks (ESBs) for the protection of benthic organisms: Metal mixtures (Cadmium, Copper, Lead, Nickel, Silver and Zinc)*; EPA-600-R-02-011; U. S. Environmental Protection Agency: Washington, DC, 2005.

(45) Wang, L.; Govind, R.; Dobbs, R. A. Sorption of toxic organic compounds on wastewater solids: mechanism and modeling. *Environmental Science & Technology* **1993,** *27* (1), 152-158.

(46) Klobes, P.; Meyer, K.; Munro, R. G. *Porosity and Specific Surface Area Measurements for Solid Materials*; National Institute of Standards and Technology - NIST: 2006.

(47) Alvarez, P. J. J.; Illman, W. A. *Bioremediation and natural attenuation: process fundemental and mathematical models*. John Wiley & Sons, Inc.: Hoboken, NJ, 2006.

(48) Karickhoff, S. W.; Brown, D. S.; Scott, T. A. Sorption of hydrophobic pollutants on natural sediments. *Water Res.* **1979,** *13*, 241–248.

(49) USEPA. *Partition coefficients for metals in surface water, soil, and waste*; EPA/600/R-05/074; U. S. Environmental Protection Agency: Washington, DC, 2005; p 93.

(50) Knox, A. S.; Paller, M. H.; Reible, D. D.; Ma, X.; Petrisor, I. G. Sequestering agents for active caps - Remediation of metals and organics. *Soil Sediment Contam* **2008,** *17* (5), 516 - 532.

(51) USEPA. *Understanding variation in partition coefficient, Kd, values*; EPA 402-R-99-004B; U. S. Environmental Protection Agency: Washington, DC, 1999.

(52) Buergisser, C. S.; Cernik, M.; Borkovec, M.; Sticher, H. Determination of nonlinear adsorption isotherms from column experiments: an alternative to batch studies. *Environ. Sci. Technol.* **1993,** *27* (5), 943-948.

(53) Campbell, P. G. C. *Interactions between trace metals and aquatic organisms: A critique of the free-ion activity model. Metal Speciation and Bioavailability in Aquatic Systems*. J. Wiley & Sons: New York, NY, 1995.

(54) Doig, L. E.; Liber, K. Nickel partitioning in formulated and natural freshwater sediments. *Chemosphere* **2006,** *62* (6), 968.

(55) IETEG. *Chromium (VI) handbook. Independent Environmental Technical Evaluation Group*. CRC Press: 2004.

(56) Santore, R. C.; Di Toro, D. M.; Paquin, P. R.; Allen, H. E.; Meyer, J. S. Biotic ligand model of the acute toxicity of metals. 2. Application to acute copper toxicity in freshwater fish and Daphnia. *Environ. Toxicol. Chem.* **2001,** *20* (10), 2397-2402.

(57) Heijerick, D. G.; Janssen, C. R.; Coen, W. M. D. The combined effects of hardness, pH, and dissolved organic carbon on the chronic toxicity of Zn to D. magna : Development of a surface response model. *Arch. Environ. Contam. Toxicol.* **2003,** *44* (2), 0210.

(58) ATSDR. *Toxicological profile for mercury*; US Department of Health and Human Services, Public Health Services (Agency for Toxic Substances and Disease Registry): Atlanta, GA, 1999.

(59) ATSDR. *Toxicological profile for chromium*; US Department of Health and Human Services, Public Health Services (Agency for Toxic Substances and Disease Registry): Atlanta, GA, 2000.

(60) ATSDR. *Toxicological profile for arsenic*; US Department of Health and Human Services, Public Health Services (Agency for Toxic Substances and Disease Registry): Atlanta, GA, 2007.

(61) Hutchinson, T. C.; Meema, K. M. *Lead, mercury, cadmium, and arsenic in the environment* John Wiley & Sons: Great Britain, 1987.

(62) USEPA. *Fish physiology, toxicology, and water quality*; EPA/600/R-02/097; U.S. Envrionmental Protection Agency: Washington, D.C., 2002.

(63) Graham, A. M.; Wadhawan, A. R.; Bouwer, E. J. Chromium occurrence and speciation in Baltimore Harbor sediments and porewater, Baltimore, Maryland, USA. *Environ. Toxicol. Chem.* **2009,** *28* (3), 471-480.

(64) ATSDR. *Toxicological profile for cadmium*; US Department of Health and Human Services, Public Health Services (Agency for Toxic Substances and Disease Registry): Atlanta, GA, 1999.

(65) Baird, C. *Environmental Chemistry*. W. H. Freeman and Company: New York, NY, USA, 1999.

(66) Kong, I. C.; Liu, S. M. Determination of heavy metals distribution in the anoxic sediment slurries by chemical sequential fractionation. *Ecotoxicol. Environ. Safety* **1995,** *32* (1), 34.

(67) Pardo, R.; Barrado, E.; Lourdes, P.; Vega, M. Determination and speciation of heavy metals in sediments of the Pisuerga river. *Water Res.* **1990,** *24* (3), 373.

(68) Adhikari, S.; Ghosh, L.; Ayyappan, S. Combined effects of water pH and alkalinity on the accumulation of lead, cadmium and chromium to Labeo rohita (Hamilton). *Intern. J. Environ. Sci. Technol.* **2006,** *3* (3), 289-296.

(69) Daskalakls, K. D.; Helz, G. R. Solubility of CdS (greenockite) in sulfidic waters at 25 °C. *Environ. Sci. Technol.* **1992,** *26*, 2462-2468.

(70) Stephen, H.; Stephen, T. *Solubilities of inorganic and organic compounds*. Pergamon Press: New York, NY, 1963.

(71) IUPAC. *Solubility data series* Pergamon Press: Oxford, UK, 1986; Vol. 23 and 26.

(72) Orem, W. H.; Lerch, H. E.; Rawlik, P. *Geochemistry of surface and porewater at USGS coring sites in wetlands of south Florida: 1994 and 1995*; 97-454; U.S. Geological Survey: West Palm Beach, FL, 1997.

(73) Leonard, E.; Mattson, V.; Benoit, D.; Hoke, R.; Ankley, G. Seasonal variation of acid volatile sulfide concentration in sediment cores from three northeastern Minnesota lakes. *Hydrobiologia* **1993,** *271* (2), 87.

(74) Bruland, K. W. Complexation of cadmium by natural organic ligands in the central North Pacific. *Limnol. Oceanogr.* **1992,** *37* (5), 1008-1017

(75) OEHHA. *Water - public health goals (PHGs)*; Office of Environmental Health Hazard Assessment: California, 2003.

(76) ATSDR. *Toxicological profile for lead*; US Department of Health and Human Services, Public Health Services (Agency for Toxic Substances and Disease Registry): Atlanta, GA, 2007.

(77) NRCB. *Measuring lead exposure in infants, children, and other sensitive populations*; National Research Council Board on Environmental Studies and Toxicology National Academy Press, Washington, D.C., 1993.

(78) Renberg, I.; Brännvall, M. L.; Bindler, R.; Emteryd, O. Stable lead isotopes and lake sediments--a useful combination for the study of atmospheric lead pollution history. *Sci. Total Environ.* **2002,** *292* (1-2), 45.

(79) Brannvall, M.-L.; Bindler, R.; Renberg, I.; Emteryd, O.; Bartnicki, J.; Billstrom, K. The Medieval Metal Industry Was the Cradle of Modern Large-Scale Atmospheric Lead Pollution in Northern Europe. *Environmental Science & Technology* **1999,** *33* (24), 4391-4395.

(80) Bränvall, M. L.; Bindler, R.; Emteryd, O.; Renberg, I. Four thousand years of atmospheric lead pollution in northern Europe: a summary from Swedish lake sediments. *Journal of Paleolimnology* **2001,** *25* (4), 421.

(81) Lacerda, L. D.; Ribeiro, M. G. Changes in lead and mercury atmospheric deposition due to industrial emissions in Southeastern Brazil. *J. Braz. Chem. Soc.* **2004,** *15* (6), 931-937.

(82) Bollhöfer, A.; Rosman, K. J. R. Isotopic source signatures for atmospheric lead: the Southern Hemisphere. *Geochimica et Cosmochimica Acta* **2000,** *64* (19), 3251.

(83) Smolyakov, B. S.; Zhigula, M. V.; Ishchenko, A. V. Effect of the lead speciation on a natural freshwater ecosystem. *Mendeleev Communications* **2000,** *10* (4), 164.

(84) Tessier, A.; Campbell, P. G. C.; Bisson, M. Sequential extraction procedure for the speciation of particulate trace metals. *Anal. Chem.* **1979,** *51* (7), 844-851.

(85) Trimble, S. W. *Encyclopedia of water science*. 2nd ed.; CRC Press: 2007.

(86) Schlautman, M. A.; Han, I. Effects of pH and dissolved oxygen on the reduction of hexavalent chromium by dissolved ferrous iron in poorly buffered aqueous systems. *Water Res.* **2001,** *35* (6), 1534.

(87) Eary, L. E.; Rai, D. Kinetics of chromium(III) oxidation to chromium(VI) by reaction with manganese dioxide. *Environ. Sci. Technol.* **1987,** *21* (12), 1187-1193.

(88) Patterson, R. R.; Fendorf, S.; Fendorf, M. Reduction of hexavalent chromium by amorphous iron sulfide. *Environ. Sci. Technol.* **1997,** *31* (7), 2039-2044.

(89) ATSDR. *Toxicological profile for silver*; Agency for Toxic Substances and Disease Registry, U.S. Public Health Service: 1990.

(90) Janes, N.; Playle, R. C. Modeling silver binding to gills of rainbow trout (Oncorhynchus mykiss). *Environ. toxicol. chem.* **1995,** *14* (11), 1847-1858.

(91) Hogstrand, C.; Wood, C. M. Toward a better understanding of the bioavailability, physiology, and toxicity of silver in fish : Implications for water quality criteria *Environmental Toxicology and Chemistry* **1998,** *17* (4), 547-561.

(92) Rodgers, J. H.; Deaver, E.; Rogers, P. L. Partitioning and effects of silver in amended freshwater sediments. *Ecotoxicol. Environ. Safety* **1997,** *37* (1), 1.

(93) Howe, P. D.; Dobson, S. *Silver and silver compounds: environmental aspects*; World Health Organization: Geneva, 2002.

(94) Miller, L. A.; Bruland, K. W. Organic speciation of silver in marine waters. *Environ. Sci. Technol.* **1995,** *29* (10), 2616-2621.

(95) Masscheleyn, P. H.; Delaune, R. D.; Patrick, W. H. Effect of redox potential and pH on arsenic speciation and solubility in a contaminated soil. *Environmental Science & Technology* **1991,** *25* (8), 1414-1419.

(96) Campbell, K. Biogeochemical mechanisms of arsenic mobilization in Haiwee reservoir sediments. California Institute of Technology, Pasadena, CA, 2007.

(97) Sarkar, B. *Heavy metals in the environment*. CRC Press: 2002.

(98) Wang, S.; Mulligan, C. N. Occurrence of arsenic contamination in Canada: Sources, behavior and distribution. *Sci. Total Environ.* **2006,** *366* (2-3), 701.

(99) Jay, J. A.; Blute, N. K.; Lin, K.; Senn, D.; Hemond, H. F.; Durant, J. L. Controls on arsenic speciation and solid-phase partitioning in the sediments of a two-basin lake. *Environ. Sci. Technol.* **2005,** *39* (23), 9174-9181.

(100) Floroiu, R. M.; Davis, A. P.; Torrents, A. Kinetics and Mechanism of As2S3(am) Dissolution under N2. *Environmental Science & Technology* **2004,** *38* (4), 1031-1037.

(101) Sigel, H.; Sigel, A. *Metal ions in biological systems*. CRC: 1997; Vol. 34.

(102) Gilmour, C. C.; Henry, E. A. Mercury methylation in aquatic systems affected by acid deposition. *Environ. Pollut.* **1991,** *71*, 131-169.

(103) Benoit, J. M.; Gilmour, C. C.; Mason, R. P. Aspects of bioavailability of mercury for methylation in pure cultures of Desulfobulbus propionicus (1pr3) *Appl. Environ. Microbiol.* **2001,** *67* (1), 51-58.

(104) Weber, J. H.; Evans, R.; Jones, S. H.; Hines, M. E. Conversion of mercury(II) into mercury(0), monomethylmercury cation, and dimethylmercury in saltmarsh sediment slurries. *Chemosphere* **1998,** *36* (7), 1669.

(105) Sadiq, M. *Toxic metal chemistry in marine environments*. CRC Press: 1992.

(106) Boszke, L.; Kowalski, A.; Gosiska, G.; Szarek, R.; Siepak, J. Environmental factors affecting the speciation of mercury in the bottom sediments; an overview. *Polish J. Environ. Studies* **2003,** *12*, 5-13.

(107) Kannan, K.; Falandysz, J. Speciation and concentrations of mercury in certain coastal marine sediments. *Water Air Soil Pollut.* **1998,** *103* (1), 129.

(108) Stoichev, T.; Amouroux, D.; Wasserman, J. C.; Point, D.; De Diego, A.; Bareille, G.; Donard, O. F. X. Dynamics of mercury species in surface sediments of a macrotidal estuarine-coastal system (Adour River, Bay of Biscay). *Estuar. Coast. Shelf Sci.* **2004,** *59* (3), 511.

(109) Eagleson, M. *Concise encyclopedia chemistry* 1994.

(110) NRC. *Toxicological effects of methylmercury*. National Research Council. National Academy Press: Washington, D.C., 2000.

(111) ATSDR. *Toxicological profile for cyanide*; US Department of Health and Human Services, Public Health Services (Agency for Toxic Substances and Disease Registry): Atlanta, GA, 2006.

(112) Dzombak, D. A.; Ghosh, R. S.; Wong-Chong, G. M. *Cyanide in water and soil: chemistry, risk and management*. CRC Press: 2006.

(113) Meeussen, J. C. L.; Keizer, M. G.; Van Riemsdijk, W. H.; De Haan, F. A. M. Dissolution behavior of iron cyanide (Prussian blue) in contaminated soils. *Environ. Sci. Technol.* **1992,** *26* (9), 1832-1838.

(114) Rennert, T.; Mansfeldt, T. Mobility of iron-cyanide complexes in a humic topsoil under varying redox conditions. *Appl. Environ. Soil Sci.* **2009**.

(115) Luque-Almagro, V. M.; Huertas, M.-J.; Martinez-Luque, M.; Moreno-Vivian, C.; Roldan, M. D.; Garcia-Gil, L. J.; Castillo, F.; Blasco, R. Bacterial degradation of cyanide and its metal complexes under alkaline conditions. *Appl. Environ. Microbiol.* **2005,** *71* (2), 940-947.

(116) Fuller, W. H. *Cyanides in the environment with particular attention to the soil*. In Cyanide and the environment Tucson, Arizona, Dec. 11-14, 1984; Geotechnical Engineering Program - Colorado State University - Fort CoIlins, Colorado: Tucson, Arizona, 1984; pp 19-46.

(117) Eisler, B. R. Handbook of chemical risk assessment: Health hazards to humans, plants, and animals. **2000**.

(118) Liao, V. H.-C.; Chien, M.-T.; Tseng, Y.-Y.; Ou, K.-L. Assessment of heavy metal bioavailability in contaminated sediments and soils using green fluorescent protein-based bacterial biosensors. *Environ. Pollut.* **2006,** *142* (1), 17.

(119) Hansen, D. J.; Berry, W. J.; Mahony, J. D.; Boothman, W. S.; Di Toro, D. M.; Robson, D. L.; Ankley, G. T.; Ma, D.; Yan, Q.; Pesch, C. E. Predicting the toxicity of metal-contaminated field sediments using interstitial concentration of concentration metals and acid-volatile sulfide normalizations. *Environ. Toxicol. Chem.* **1996,** *15* (12), 2080-2094.

(120) Lebo, J. A.; Huckins, J. N.; Petty, J. D.; Cranor, W. L.; Ho, K. T. Comparisons of coarse and fine versions of two carbons for reducing the bioavailabilities of sediment-bound hydrophobic organic contaminants. *Chemosphere* **2003,** *50* (10), 1309-1317.

(121) Ankley, G. T.; Di Toro, D. M.; Hansen, D. J.; Berry, W. J. Technical basis and proposal for deriving sediment quality criteria for metals. *Environ. Toxicol. Chem.* **1996,** *15* (12), 2056-2066.

(122) Singh, S. P.; Ma, L. Q.; Harris, W. G. Heavy metal interactions with phosphatic clay: Sorption and desorption behavior. *J. Environ. Qual.* **2001,** *30* (6), 1961-1968.

(123) Adriaens, P.; Li, M.-Y.; Michalak, A. M. Scaling methods of sediment bioremediation processes and applications. *Eng. Life Sci.* **2006,** *6* (3), 217-227.

(124) Zhao, X.; Drumm, L.; Yin, K.; Rockne, K. J. Segregation of PAH contaminated sediments during hydraulic dredging and dewatering *J. Environ. Eng.-ASCE* **2007**, In review.

(125) Kaplan, D. I.; Knox, A. S. Enhanced contaminant desorption induced by phosphate mineral additions to sediment. *Environ. Sci. Technol.* **2004,** *38*, 3153-3160.

(126) Ruiz, C. E. *Contaminated sediments remediation* In EPA Forum, 2001.

(127) USEPA. *Contaminated sediment remediation: Guidance for hazardous waste*; EPA-540-R-05-012; U. S. Environmental Protection Agency: 2005.

(128) Johnson, K. M.; Smith, M. L.; Lowry, G. V. *Sediment management in the Anacostia and Grasse river: Applying Fe(0)-based reactive sediment caps for in situ PCB destruction*; Progress Report 9/1/02; Carnegie Mellon University: Pittsburgh, PA, 2002; p 11.

(129) Yin, K.; Viana, P. Z.; Zhao, X. H.; Rockne, K. J. *A Monte Carlo simulation approach for active caps in mixed contaminant environments*. In Proceedings of the Fourth International Conference on Remediation of Contaminated Sediments, Savannah, GA, 2007.

(130) Viana, P. Z.; Yin, K.; Zhao, X.; Rockne, K. J. Active sediment capping for pollutant mixtures: Control of biogenic gas production under highly intermittent flows. *Land Contam. Reclamation* **2007,** *15* (4), 413-425.

(131) Dong, Y.; Liang, X.; Krumholz, L. R.; Philp, R. P.; Butler, E. C. The relative contributions of abiotic and microbial processes to the transformation of tetrachloroethylene and trichloroethylene in anaerobic microcosms. *Environ. Sci. Technol.* **2009,** *43* (3), 690-697.

(132) Lendvay, J. M.; Loffler, F. E.; Dollhopf, M.; Aiello, M. R.; Daniels, G.; Fathepure, B. Z.; Gebhard, M.; Heine, R.; Helton, R.; Shi, J.; Krajmalnik-Brown, R.; Major, C. L.; Barcelona, M. J.; Petrovskis, E.; Hickey, R.; Tiedje, J. M.; Adriaens, P. Bioreactive barriers: A comparison of bioaugmentation and biostimulation for chlorinated solvent remediation. *Environ. Sci. Technol.* **2003,** *37* (7), 1422-1431.

(133) Major, D. W.; McMaster, M. L.; Cox, E. E.; Edwards, E. A.; Dworatzek, S. M.; Hendrickson, E. R.; Starr, M. G.; Payne, J. A.; Buonamici, L. W. Field demonstration of successful bioaugmentation to achieve dechlorination of tetrachloroethene to ethene. *Environ. Sci. Technol.* **2002,** *36* (23), 5106-5116.

(134) Mikszewski, A. *Emerging technologies for the in situ remediation of PCB-contaminated soils and sediments: Bioremediation and nanoscale zero-valent iron*; U. S. Environmental Protection Agency: Washington, D. C., 2004.

(135) Pignatello, J. J. *Issues of biostimulation, bioaugmentation and bioavailability in the remediation of PAHs in a coal tar soil*. In The Annual Conference on Soils, Sediments, Water and Energy, University of Massachusetts at Amherst, University of Massachusetts at Amherst, 2005.

(136) Tabak, H. H.; Hazen, T. C. *Developments in bioremediation of soils and sediments polluted with metals and radionuclides: 2. Field research on bioremediation of metals and radionuclides*. In The Annual Conference on Soils, Sediments, Water and Energy, University of Massachusetts at Amherst, University of Massachusetts at Amherst, 2005.

(137) Löffler, F. E.; Edwards, E. A. Harnessing microbial activities for environmental cleanup. *Current Opinion Biotechnol.* **2006,** *17* (3), 274.

(138) Crannell, B. S.; Eighmy, T. T.; Willson, C.; Reible, D. D.; Yin, M. *Pilot-scale reactive barrier technologies for containment of metal-contaminated sediments and dredged materials*; Submitted to NOAA/UNH Cooperative Institute for Coastal and Estuarine Environmental Technology (CICEET): 2004.

(139) Lampert, D. J.; Reible, D.; Constant, D.; Zhu, Y. W. *Evaluation of active capping of contaminated sediments in the Anacostia River; Paper D-020.* In Proceedings of the Fourth International Conference on Remediation of Contaminated Sediments, Columbus, OH, Battele Press: Columbus, OH, 2007.

(140) Chen, X.; Wright, J. V.; Conca, J. L.; Peurrung, L. M. Effects of pH on heavy metal sorption on mineral apatite. *Environ. Sci. Technol.* **1997,** *31* (3), 624-631.

(141) McDonough, K. M.; Murphy, P.; Olsta, J.; Zhu, Y.; Reible, D.; Lowry, G. V. Development and placement of a sorbent-amended thin layer sediment cap in the Anacostia River. *Soil Sediment Contam.: Int. J.* **2007,** *16* (3), 313 - 322.

(142) USEPA. *Demonstration of the AquaBlok® sediment capping technology innovative technology evaluation report*; U. S. Environmental Protection Agency: Cincinnati, OH, 2007.

(143) Truitt, C. L. *The Duwamish waterway capping demonstration project: Engineering analysis and results of physical monitoring*; D-86-2; U.S. Army Engineer Waterways Experiment Station: Vicksburg, MS, 1986.

(144) Keeley, K.; Wakeman, J. *Planning for cap design and construction during the RI/FS. Case Studies from Region 10*.

(145) Brenner, R. C.; Magar, V. S.; Ickes, J. A.; Abbott, J. E.; Stout, S. A.; Crecelius, E. A.; Bingler, L. S. Characterization and fATE of PAH-contaminated sediments at the Wyckoff/Eagle Harbor superfund site. *Environ. Sci. Technol.* **2002,** *36* (12), 2605-2613.

(146) USEPA. *Record of decision amendment. Operable unit 1: Lower Fox River and Green Bay superfund site*; U.S. Environmental Protection Agency: 2008.

(147) USEPA. *Five-year review report Marathon Battery Company superfund site, village of Cold Spring, Putnam County, New York*; U.S. Environmental Protection Agency: New York, NY, 2008.

(148) Zeller, C. *Five year review report. Second five year review for the Koppers Co., Inc (Charleston Plant) NPL site*; U.S. Environmental Protection Agency: Charleston, SC, 2008.

(149) Perrone, J.; Fourest, B.; Giffaut, E. Sorption of nickel on carbonate fluoroapatites. *J. Colloid Interface Sci.* **2001,** *239* (2), 303.

(150) Bostick, W. D.; Stevenson, R. J.; Harris, L. A.; Peery, D.; Hall, J. R.; Shoemaker, J. L.; Jarabek, R. J.; Munday, E. B. *Use of apatite for chemical stabilization of subsurface contaminants*; DE-AD26-01NT41306; Materials and Chemistry Laboratory, Inc.: Oak Ridge, TN, 2003.

(151) Kanel, S. R.; Manning, B.; Charlet, L.; Choi, H. Removal of Arsenic(III) from Groundwater by Nanoscale Zero-Valent Iron. *Environ. Sci. Technol.* **2005,** *39* (5), 1291-1298.

(152) Alther, G. R.; Tillman-Jr., F. D.; Smith, J. A. *Contaminated soils, sediments and water - Chapter 29: Evaluation of two organoclays, clinoptilolite, and hydroxy-apatite as sorbents for heavy metal removal from water* 2006; p 457-468.

(153) Matusik, J.; Bajda, T.; Manecki, M. Immobilization of aqueous cadmium by addition of phosphates. *J. Hazard. Mater.* **2008,** *152* (3), 1332.

(154) Lang, F.; Kaupenjohann, M. Effect of dissolved organic matter on the precipitation and mobility of the lead compound chloropyromorphite in solution. *European J. Soil Sci.* **2003,** *54* (1), 139-148.

(155) Nriagu, J. O. Lead orthophosphates-II. Stability of chloro-pyromorphite at 25° C. *Geochim. Cosmochim. Acta 37*, 367-377.

(156) Manecki, M.; Maurice, P.; Traina, S. J. Kinetics of aqueous Pb reaction with apatites. *Soil Sci.* **2000,** *165* (12), 920-933.

(157) Scheckel, K. G.; Ryan, J. A. Spectroscopic speciation and quantification of lead in phosphate-amended soils. *J. Environ. Qual.* **2004,** *33* (4), 1288-1295.

(158) Seaman, J. C.; Hutchison, J. M.; Jackson, B. P.; Vulava, V. M. In situ treatment of metals in contaminated soils with phytate. *J. Environ. Qual.* **2003,** *32*, 153-161.

(159) Roberts, K. L. Modeling of river hydrodynamics and active cap effectiveness in the Anacostia River. Louisiana State University, 2004.

(160) Alther, G. R. *Organoclays remove organic and metals from water*. In The Annual International Conference on Soils, Sediments, Water and Energy, University of Massachusetts at Amherst, University of Massachusetts at Amherst, 2001.

(161) Smith, J. A.; Jaffe, P. R.; Chiou, C. T. Effect of ten quaternary ammonium cations on tetrachloromethane sorption to clay from water. *Environ. Sci. Technol.* **1990,** *24* (8), 1167-1172.

(162) Groisman, L.; Rav-Acha, C.; Gerstl, Z.; Mingelgrin, U. Sorption of organic compounds of varying hydrophobicities from water and industrial wastewater by long- and short-chain organoclays. *Appl. Clay Sci.* **2004,** *24* (3-4), 159.

(163) Pernyeszi, T.; Kasteel, R.; Witthuhn, B.; Klahre, P.; Vereecken, H.; Klumpp, E. Organoclays for soil remediation: Adsorption of 2,4-dichlorophenol on organoclay/aquifer material mixtures studied under static and flow conditions. *Appl. Clay Sci.* **2006,** *32* (3-4), 179.

(164) Witthuhn, B.; Pernyeszi, T.; Klauth, P.; Vereecken, H.; Klumpp, E. Sorption study of 2,4-dichlorophenol on organoclays constructed for soil bioremediation. *Colloid Surface A* **2005,** *265*, 81-87.

(165) Varma, R. S. Clay and clay-supported reagents in organic synthesis. *Tetrahedron* **2002,** *58* (7), 1235.

(166) Ho, Y. S.; McKay, G. The sorption of lead(II) ions on peat. *Water Research* **1999,** *33* (2), 578.

(167) Kaufhold, S.; Dohrmann, R.; Koch, D.; Houben, G. The pH of aqueous bentonite suspensions. *Clays Clay Miner.* **2008,** *56* (3), 338-343.

(168) Sen Gupta, S.; Bhattacharyya, K. G. Immobilization of Pb(II), Cd(II) and Ni(II) ions on kaolinite and montmorillonite surfaces from aqueous medium. *J. Environ. Manag.* **2008,** *87* (1), 46.

(169) Reible, D.; Lu, X.; Moretti, L.; Galjour, J.; Ma, X. *Organoclays for the capping of contaminated sediments*. In AIChE Annual Meeting, Salt Lake City, UT, Salt Lake City, UT, 2007.

(170) ASTM. *Standard D5158 - 98(2005) Standard Test Method for Determination of Particle Size of Powdered Activated Carbon by Air Jet Sieving*; American Society for Testing and Materials: 2005.

(171) ASTM. *Standard D2862 - 10 Standard Test Method for Particle Size Distribution of Granular Activated Carbon*; American Society for Testing and Standards: 2010.

(172) Mohan, D.; Pittman-Jr., C. U. Arsenic removal from water/wastewater using adsorbents - A critical review. *J. Hazard. Mater.* **2007,** *142* (1-2), 1.

(173) Lozano-Castelló, D.; Cazorla-Amorós, D.; Linares-Solano, A. Can highly activated carbons be prepared with a homogeneous micropore size distribution? *Fuel Processing Technol.* **2002,** *77-78*, 325.

(174) Wilson, K.; Yang, H.; Seo, C. W.; Marshall, W. E. Select metal adsorption by activated carbon made from peanut shells. *Bioresour. Technol.* **2006,** *97* (18), 2266.

(175) Sellers, K.; Alsop, W. R.; Clough, S. R.; Hoyt, M.; Pugh, B.; Robb, J. *Perchlorate: environmental problems and solutions*. CRC Press: 2006.

(176) Yin, C. Y.; Aroua, M. K.; Daud, W. M. A. W. Review of modifications of activated carbon for enhancing contaminant uptakes from aqueous solutions. *Sep. Purif. Technol.* **2007,** *52* (3), 403.

(177) Ahn, C. K.; Park, D.; Woo, S. H.; Park, J. M. Removal of cationic heavy metal from aqueous solution by activated carbon impregnated with anionic surfactants. *J. Hazard. Mater.* **2009,** *164* (2-3), 1130.

(178) Lorenzen, L.; van Deventer, J. S. J.; Landi, W. M. Factors affecting the mechanism of the adsorption of arsenic species on activated carbon. *Minerals Eng. 8* (4-5), 557.

(179) Lowry, G.; Murphy, P. J.; Marquette, A.; Reible, D., Sorbent-amended “active” sediment caps for in-place management of PCB-contaminated sediments. In *Contaminated Soils, Sediments and Water*, Springer: 2006; pp 379-391.

(180) McLeod, P. B.; vandenHeuvel-Greve, M. J.; Allen-King, R. M.; Luoma, S. N.; Luthy, R. G. Effects of particulate carbonaceous matter on the bioavailability of benzo[a]pyrene and 2,2',5,5'-tetrachlorobiphenyl to the clam, Macoma balthica. *Environ. Sci. Technol.* **2004,** *38* (17), 4549-4556.

(181) McDonough, K. M.; Fairey, J. L.; Lowry, G. V. Adsorption of polychlorinated biphenyls to activated carbon: Equilibrium isotherms and a preliminary assessment of the effect of dissolved organic matter and biofilm loadings. *Water Res.* **2008,** *42* (3), 575.

(182) Zimmerman, J. R.; Ghosh, U.; Millward, R. N.; Bridges, T. S.; Luthy, R. G. Addition of carbon sorbents to reduce PCB and PAH bioavailability in marine sediments: Physicochemical tests. *Environ. Sci. Technol.* **2004,** *38* (20), 5458-5464.

(183) Millward, R. N.; Bridges, T. S.; Ghosh, U.; Zimmerman, J. R.; Luthy, R. G. Addition of activated carbon to sediments to reduce PCB bioaccumulation by a polychaete (Neanthes arenaceodentata) and an amphipod (Leptocheirus plumulosus). *Environ. Sci. Technol.* **2005,** *39* (8), 2880-2887.

(184) Kadirvelu, K.; Namasivayam, C. Activated carbon from coconut coirpith as metal adsorbent: adsorption of Cd(II) from aqueous solution. *Adv. Environ. Res.* **2003,** *7* (2), 471.

(185) Namasivayam, C.; Kadirvelu, K. Uptake of mercury (II) from wastewater by activated carbon from an unwanted agricultural solid by-product: coirpith. *Carbon* **1999,** *37* (1), 79.

(186) Jusoh, A.; Su Shiung, L.; Ali, N. a.; Noor, M. J. M. M. A simulation study of the removal efficiency of granular activated carbon on cadmium and lead. *Desalination* **2007,** *206* (1-3), 9.

(187) Aggarwal, D.; Goyal, M.; Bansal, R. C. Adsorption of chromium by activated carbon from aqueous solution. *Carbon* **1999,** *37* (12), 1989.

(188) Weber, W. J. Comment on "Addition of carbon sorbents to reduce PCB and PAH bioavailability in marine sediments: Physicochemical Tests". *Environ. Sci. Technol.* **2005,** *39* (4), 1197-1198.

(189) Palermo, M.; Maynord, S.; Miller, J.; Reible, D. *Guidance for in-situ subaqueous capping of contaminated sediments*; EPA 905-B96-004; U.S. EPA Great Lakes National Program Office: Chicago, IL, 1998.

(190) Jacobs, P. H.; Förstner, U. Concept of subaqueous capping of contaminated sediments with active barrier systems (ABS) using natural and modified zeolites. *Water Res.* **1999,** *33* (9), 2083.

(191) Yang, T. C.; Zall, R. R. Absorption of metals by natural polymers generated from seafood processing wastes. *Ind. Eng. Chem. Prod. Res. Dev.* **1984,** *23* (1), 168-172.

(192) Wang, X.; Cook, R.; Tao, S.; Xing, B. Sorption of organic contaminants by biopolymers: Role of polarity, structure and domain spatial arrangement. *Chemosphere* **2007,** *66* (8), 1476.

(193) Srivastava, P. Analysis of in-situ bioremediation of PAH contaminated sediments using hollow fiber membranes. University of Cincinnati, 2005.

(194) Charbeneau, R. J. *Groundwater hydraulics and pollutant transport*. Prentice Hall: Upper Saddle River, NJ, 2000.

(195) Reible, D. *In situ sediment remediation through capping: status and research needs*; 2005; p 20.

(196) Reible, D.; Lampert, D.; Constant, D.; Jr., R. D. M.; Zhu, Y. Active capping demonstration in the Anacostia River, Washington, D.C. *Remediation J.* **2006,** *17* (1), 39-53.

(197) Conrad, R. Contribution of hydrogen to methane production and control of hydrogen concentrations in methanogenic soils and sediments. *FEMS Microbiol. Ecol.* **1999,** *28* (3), 193-202.

(198) Conrad, R.; Schütz, H.; Babbel, M. Temperature limitation of hydrogen turnover and methanogenesis in anoxic paddy soil *FEMS Microbiol. Ecol.* **1987,** *45*, 281-289.

(199) Tanner, C. C.; Adams, D. D.; Downes, M. T. Methane emissions from constructed wetlands treating agricultural wastewaters. *J Environ Qual* **1997,** *26* (4), 1056-1062.

(200) Sovik, A. K.; Augustin, J.; Heikkinen, K.; Huttunen, J. T.; Necki, J. M.; Karjalainen, S. M.; Klove, B.; Liikanen, A.; Mander, U.; Puustinen, M.; Teiter, S.; Wachniew, P. Emission of the greenhouse gases nitrous oxide and methane from constructed wetlands in Europe. *J Environ Qual* **2006,** *35* (6), 2360-2373.

(201) Ostrovsky, I.; McGinnis, D. F.; Lapidus, L.; Eckert, W. Quantifying gas ebullition with echosounder: the role of methane transport by bubbles in a medium-sized lake. *Limnol. Oceanogr. Methods* **2008,** *6*, 105-118.

(202) Hughes, J. B.; Valsaraj, K. T.; Willson, C. S. *In-situ containment and treatment: Engineering cap integrity and reactivity*; HSRC/S&SW, Georgia Institute of Technology and Louisiana State University: 2005.

(203) Stadmark, J.; Leonardson, L. Greenhouse gas production in a pond sediment: Effects of temperature, nitrate, acetate and season. *Sci. Total Environ.* **2007,** *387* (1-3), 194.

(204) Huttunen, J. T.; Lappalainen, K. M.; Saarijärvi, E.; Väisänen, T.; Martikainen, P. J. A novel sediment gas sampler and a subsurface gas collector used for measurement of the ebullition of methane and carbon dioxide from a eutrophied lake. *Sci. Total Environ.* **2001,** *266* (1-3), 153.

(205) Casper, P.; Maberly, S. C.; Hall, G. H.; Finlay, B. J. Fluxes of methane and carbon dioxide from a small productive lake to the atmosphere. *Biogeochemistry* **2000,** *49* (1), 1.

(206) Huls, H. H.; Costello, M. *Designing assessments for decision making for remediation of contaminated sediments*; Service Engineering Group: St. Paul, MN, 2005.

(207) Palermo, M.; Schroeder, P.; Rivera, Y.; Ruiz, C.; Clarke, D.; Gailani, J.; Clausner, J.; Hynes, M.; Fredette, T.; Tardy, B.; Peyman-Dove, L.; Risko, A. *Options for in situ capping of Palos Verdes Shelf contaminated sediments*; EL-99-2; U.S. Army Corps of Engineers: 1999.

(208) Tsinker, G. P. *Port Engineering: Planning, construction, maintenance, and security* John Wiley & Sons, Inc.: 2004.

(209) Thoma, G. J.; Reible, D. D.; Valsaraj, K. T.; Thibodeaux, L. J. Efficiency of capping contaminated sediments in-situ: 2. Mathematics of diffusion-adsorption in the capping layer. *Environ. Sci. Technol.* **1993,** *27* (12), 2412-2419.

(210) Reible, D.; Mohanty, S. A levy flight-random walk model for bioturbation. *Environ. Toxicol. Chem.* **2002,** *21* (4), 875-881.

(211) Simpson, S. L.; Apte, S. C.; Batley, G. E. Effect of short-term resuspension events on trace metal speciation in polluted anoxic sediments. *Environ. Sci. Technol.* **1998,** *32* (5), 620-625.

(212) Thibodeaux, L. J.; Valsaraj, K. T.; Reible., D. D. Bioturbation-driven transport of hydrophobic organic contaminants from bed sediment. *Environ. Eng. Sci.* **2001,** *18* (4), 215-223.

(213) Reible, D. D. *Guidance for in-situ subaqueous capping of contaminated sediments. Appendix B: Model for chemical containment by a cap*; U.S. Environmental Protection Agency: 1998.

(214) Wheatcroft, R. A.; Martin, W. R. *Predictive modeling of the natural recovery of the contaminated effluent-affected sediment, Palos Verdes Margin, Southern California: Appendix E: Solid phase bioturbation processes on the Palos Verdes Shelf*; Woods Hole Oceanographic Institution: Woods Hole, MA., 1994.

(215) ERDC. *Subaqueous cap design: Selection of bioturbation profiles, depths, and process rates. Engineer Research and Development Center*; ERDC TN-DOER-C21; U.S. Army Corps of Engineers: 2001.

(216) Alshawabkeh, A. N.; Rahbar, N.; Sheahan, T. A model for contaminant mass flux in capped sediment under consolidation. *Journal of Contaminant Hydrology* **2005,** *78* (3), 147.

(217) Stark, T. D. *Program documentation and user's guide: PSDDF, Primary Consolidation, Secondary Compression, and Desiccation of Dredged Fill*

EL-96-XX; EL-96-XX; U.S. Army Corps of Engineers: Washington, D.C., 1996.

(218) Moo-Young, H.; Myers, T.; Tardy, B.; Ledbetter, R.; Vanadit-Ellis, W.; Kim, T.-H. Centrifuge simulation of the consolidation characteristics of capped marine sediment beds. *Engin. Geol.* **2003,** *70* (3-4), 249.

(219) Terzaghi, K. *Theoretical soil mechanics*. Wiley: New York, NY, 1943.

(220) ASTM. *Annual book of ASTM standards - ASTM D2435*. West Conshohocken, PA, 1998; Vol. 04.08.

(221) HES. *Basis of design for comparative validation of innovative 'active capping' technologies, Anacostia River, Washington, DC (Revised draft)*. R137983; Horne Engineering Services: 2003.

(222) GW-Partners. *OU1 design supplement Lower Fox River operable unit 1*; 07G017; Neenah, Wisconsin, 2007.

(223) Blodgett, J. C.; McConaughy, C. E. *Rock riprap design for protection of stream channels near highway structures, vol. 2 – Evaluation of riprap design procedures*; 86-4127; Sacramento, CA, 1986.

(224) Van Rijn, L. C. *Principles of sediment transport in rivers, estuaries and coastal seas.* . Aqua Publications: Amsterdam, The Netherlands, 1993.

(225) Wolanski, E. *Estuarine ecohydrology*. Elsevier: 2007; p 157.

(226) Dueri, S.; Therrien, R.; Locat, J. Simulation of the migration of dissolved contaminants through a subaqueous capping layer: model development and application for As migration. *Journal of Environmental Engineering and Science* **2003,** *2*, 213.

(227) Ruiz, C. E.; Aziz, N. M.; Schroeder, P. R. RECOVERY: A contaminated sediment-water interaction model. *Environ. Modeling Assess.* **2001,** *6* (3), 151.

(228) USEPA. *EPA's composite model for leachate migration with transformation products (EPACMTP). Technical background document*; EPA530-R-03-006; U. S. Environmental Protection Agency: Washington, D.C., 2003.

(229) Liu, C.; Jay, J. A.; Ika, R.; Shine, J. P.; Ford, T. E. Capping efficiency for metal-contaminated marine sediment under conditions of submarine groundwater discharge. *Environ. Sci. Technol.* **2001,** *35*, 2334-2340.

(230) Lee, K. Y. Modeling long-term transport of contaminants resulting from dissolution of a coal tar pool in saturated porous media. *J. Environ. Eng.-ASCE* **2004**, 1507-1513.

(231) IUPAC. *Solubility data series* Pergamon Press: Oxford, UK, 1986; Vol. 23 and 26.

(232) Li, Y.; Gregory, S. Diffusion of ions in sea water and in deep-sea sediments. *Geochim. Cosmochim. Ac.* **1974,** *38*, 703-714.

(233) USEPA. *Industrial waste air model technical background document*; EPA 530-R-02-010; U. S. Environmental Protection Agency: Washington, DC, 2002.

(234) Alther, G. R. Organoclays trap incalcitrant metals and organic compounds in sediments simultaneously. In *The Seventeenth Annual AEHS Meeting and West Coast Conference on Soils, Sediments and Water*, San Diego, CA, 2007; p 12.

(235) Areerachakul, N.; Vigneswaran, S.; Ngo, H. H.; Kandasamy, J. Granular activated carbon (GAC) adsorption-photocatalysis hybrid system in the removal of herbicide from water. *Sep. Purif. Technol.* **2007,** *55* (2), 206.

(236) Chapuis, R. P. Predicting the saturated hydraulic conductivity of sand and gravel using effective diameter and void ratio. *Can. Geotech. J.* **2004,** *41*, 787–795.

(237) Drescher, A.; Newcomb, D.; Heimdahl, T. *Deformability of shredded tires*; MN/RC-1999-13; Minnesota Department of Transportation: St. Paul, MN, 1999.

(238) Gu, R. R. Beneficial reuses of scrap tires in hydraulic engineering. *Handb. Environ. Chem.* **2005,** *5* (F, 1), 183-215.

(239) Lo, I. M. C.; Liljestrand, H. M. Laboratory sorption and hydraulic conductivity tests: evaluation of modified-clay materials. *Waste Manage. Res.* **1996,** *14*, 297–310.

(240) Lu, Q.; Sorial, G. A. Adsorption of phenolics on activated carbon - impact of pore size and molecular oxygen. *Chemosphere* **2004,** *55* (5), 671-9.

(241) McIsaac, R.; Rowe, R. K. Change in leachate chemistry and porosity as leachate permeates through tire shreds and gravel. *Can. Geotech. J.* **2005,** *42* (4), 1173-1188.

(242) Moazed, H.; Viraraghavan, T. Coalescence/filtration of an oil-in-water emulsion in a granular organo-clay/anthracite mixture bed. *Water Air Soil Poll.* **2002,** *138*, 253-270.

(243) Moody, T. E.; Conca, J. *Permeable barrier materials for strontium immobilization: UFA determination of hydraulic conductivity, column sorption experiments*; BHI-00857 Rev.0; CH2M HILL Hanford, U.S. Department of Energy Office of Environmental Restoration and Waste Management: 1996; p 40.

(244) Warith, M. A.; Evgin, E.; Benson, P. A. S. Suitability of shredded tires for use in landfill leachate collection systems. *Waste Manage.* **2004,** *24* (10), 967.

(245) Aktas, O.; Cecen, F. Adsorption, desorption and bioregeneration in the treatment of 2-chlorophenol with activated carbon. *J. Hazard. Mater.* **2007,** *141* (3), 769.

(246) Bosscher, P. J.; Edil, T. B. Design of highway embankments using tire chips. *J. Geotech. Geoenviron.* **1997,** *123* (4), 295-304.

(247) Lee, J.; Rao, P. S. C.; Poyer, I. C.; Toole, R. M.; Annable, M. D.; Hatfield, K. Oxyanion flux characterization using passive flux meters: Development and field testing of surfactant-modified granular activated carbon. *J. Contam. Hydrol.* **2007,** *92*, 208–229.

(248) Lowry, G. V.; Dzombak, D. A.; VanBriesen, J. *Predicting and validating the field performance of novel sorbent-amended sediment caps*; CICEET Progress Report 9/16/06 through 3/15/07; 2007.

(249) Moo-Young, H.; Sellasie, K.; Zeroka, D.; Sabnis, G. Physical and chemical properties of recycled tire shreds for use in construction. *J. Environ. Eng.-ASCE* **2003,** *129* (10), 921.

(250) Sperry, J. M.; Peirce, J. A model for estimating the hydraulic conductivity of granular material based on grain shape, grain size, and porosity *Ground Water* **1995,** *33* (6), 892-898.

(251) Zhao, H.; Jaynes, W. F.; Vance, G. F. Sorption of the ionizable organic compound, dicamba (3,6-dichloro-2-methoxy benzoic acid), by organo-clays. *Chemosphere* **1996,** *33*, 2089-2100.

(252) CETCO. Sediment remediation technology technical data. **2005**.

(253) Lo, I. M. C.; Mak, R. K. M. Transport of phenolic compounds through a compacted organoclay liner. *Water Sci. Technol.* **1998,** *38* (2), 143-150.

(254) Reible, D. Summary of contaminated sediment capping projects. **2006**.

(255) Zeller, C.; Cushing, B. Panel discussion: Remedy effectiveness: What works, what doesn't? I. *Integr. Environ. Assess. Manag.* **2006,** *2*, 75–79.

(256) De Schamphelaere, K. A. C.; Bossuyt, B. T. A.; Janssen, C. R. Variability of the protective effect of sodium on the acute toxicity of copper to freshwater cladocerans. *Environ. Toxicol. Chem.* **2007,** *26* (3), 535-542.

(257) Taillefert, M.; Bono, A. B.; Luther, G. W. Reactivity of freshly formed Fe(III) in synthetic solutions and (pore)waters: Voltammetric evidence of an aging process. *Environ. Sci. Technol.* **2000,** *34* (11), 2169-2177.

(258) USEPA. *Test Methods for Evaluating Solid Waste Physical/Chemical Analysis (SW-846)*; U.S. Environmental Protection Agency: 2008.

(259) Mittal, M.; Rockne, K. J. Naphthalene and phenanthrene sorption to very low organic content diatomaceous earth: modeling implications for microbial bioavailability. *Chemosphere* **2009,** *74* (8), 1134-1144.

(260) Gregg, S. J.; Sing, S. W. *Adsorption, Surface Area, and Porosity*. Academic Press: London, 1982.

(261) Rockne, K. J.; Taghon, G. L.; Kosson, D. S. Pore structure of soot deposits from several combustion sources. *Chemosphere* **2000,** *41*, 1125-1135.

(262) Kirkham, M. B. *Principles of soil and plant water relation*. Elsevier Inc.: 2005.

(263) Sinclair, U. B. *The jungle*. Doubleday, Page & Company: New York, NY, 1906.

(264) USACE. *Collection and analysis of sediment samples from the South Fork South Branch, Chicago River*; Prepared for U.S. Army Corps of Engineers - Chicago District, prepared by CDM Federal Programs Corporation: Chicago, IL, 2005.

(265) Buckley, D. R.; Rockne, K. J.; Li, A.; Millers, W. J. Soot deposition in the Great Lakes: Implications for semi-volatile hydrophobic organic pollutant deposition. *Environ. Sci. Technol.* **2004,** *38* (6), 1732-1739.

(266) Rockne, K. J.; Brezonik, P. L. Nutrient removal in a cold-region wastewater stabilization pond: Importance of ammonia volatilization. *J. Environ. Eng.-ASCE* **2006,** *132* (4), 451-459.

(267) Song, W. L.; Ford, J.; Li, A.; Mills, W. J.; Buckley, D. R.; Rockne, K. J. Polybrominated diphenyl ethers in the sediment of the Great Lakes. 1 - Lake Superior. *Environ. Sci. Technol.* **2004,** *38* (12), 38(12):3286-3293.

(268) USEPA. *Test methods for evaluating solid waste, physical/chemical methods (Method 6010B)*; EPA/SW-846; US Environmental Protection Agency: 1996.

(269) USEPA. *Provisional guidance for quantitative risk assessment of polycyclic aromatic hydrocarbons*; EPA/600/R-93/089; US Environmental Protection Agency: 1993.

(270) NOAA. *Screening quick reference tables* National Oceanic and Atmospheric Administration: Seattle, WA, 1999.

(271) CDHS. *California assessment manual for hazardous wastes*; California Department of Human Services: Sacramento, CA., 1981.

(272) Viana, P. Z.; Yin, K.; Zhao, X.; Rockne, K. J. *Modeling and control of gas ebullition in capped sediments*. In Proceedings of the Fourth International Conference on Remediation of Contaminated Sediments, Savannah, GA, 2007.

(273) Chou, H.-H.; Huang, J.-S.; Hong, W.-F. Temperature dependency of granule characteristics and kinetic behavior in UASB reactors. *J Chem. Technol. Biotechnol.* **2004,** *79*, 797–808.

(274) Prieme, A. Production and emission of methane in a brackish and a freshwater wetland *Soil Biol. and Biochem.* **1994,** *26* (1), 7-18.

(275) Thebrath, B.; Rothfuss, F.; Whiticar, M. J.; Conrad, R. Methane production in littoral sediment of Lake Constance. *FEMS Microbiol. Ecol.* **1993,** *102*, 279-289.

(276) Zhao, X.; Drumm, L.; Yin, k.; Rockne, K. J. Segregation of PAH Contaminated Sediments during Hydraulic Dredging and Disposal. *ASCE J. Environ. Eng.* **2009,** *135*, 291-298.

(277) Shor, L. M.; Kosson, D. S.; Rockne, K. J.; Young, L. Y.; Taghon, G. L. Combined effects of contaminant desorption and toxicity on risk from PAH contaminated sediments. *Risk Analysis* **2004,** *24* (5), 1109-1120.

(278) Eek, E.; Pettersen, A.; Cornelissen, G.; Breedveld, G. D. Field measurements of sediment to water fluxes of PAHs and PCBs for in situ quantification of capping effectiveness. In *Fifth International Conference on Remediation of Contaminated Sediments* Jacksonville, FL, 2009.

(279) Ciceri, G.; Maran, C.; Martinotti, W.; Queirazza, G. Geochemical cycling of heavy metals in a marine coastal area: benthic flux determination from pore water profiles and in situ measurements using benthic chambers. *Hydrobiol.* **1992,** *235-236* (1), 501.

(280) Yin, K.; Viana, P.; Zhao, X.; Rockne, K. Characterization, performance modeling, and design of an active capping remediation project in a heavily polluted urban channel. *Sci. Total Environ.* **2010,** *408*, 3454-3463.

(281) Zhao, X.; Viana, P. Z.; Yin, K.; Rockne, K. J.; Hey, D.; Schuh, J.; Lanyon, R. *Combined active capping/wetland demonstration in the Chicago River*. In Fourth International Conference on Remediation of Contaminated Sediments, Savannah, GA, Jan 22-25, 2007.

(282) Goldman, J. C.; Carpenter, E. J. A Kinetic Approach to the Effect of Temperature on Algal Growth. *Limnology and Oceanography* **1974,** *19* (5), 756.

(283) Winterwerp, J. C.; Van Kesteren, W. G. M. *Introduction to the Physics of Cohesive Sediment in the Marine Environment*. Elsevier: 2004.

(284) Mogollon, J. M.; L'Heureux, I.; Dale, A. W.; Regnier, P. Methane gas-phase dynamics in marine sediments: A model study. *American Journal of Science* **2009,** *309* (3), 189.

(285) Costello, M.; Talsma, D. *Remedial design modeling at a superfund sediment site*; http://www.serviceenv.com/Web2005/Docs/Paper42byCostello.pdf: 2005.

(286) USEPA. *Soil screening guidance: Technical background document*; U.S. Environmental Protection Agency: Office of solid waste and emergency response, Washington, DC, 1996.

(287) Amos, R. T.; Mayer, K. U. Investigating ebullition in a sand column using dissolved gas analysis and reactive transport modeling. *Environ. Sci. Technol.* **2006,** *40* (17), 5361.

(288) Lokshina, L. Y.; Vavilin, V. A.; Kettunen, R. H.; Rintala, J. A.; Holliger, C.; Nozhevnikova, A. N. Evaluation of kinetic coefficients using integrated monod and haldane models for low-temperature acetoclastic methanogenesis. *Water Research* **2001,** *35* (12), 2913.

(289) Robinson, J. A.; Tiedje, J. M. Competition between sulfate-reducing and methanogenic bacteria for H2 under resting and growing conditions. *Archives of Microbiology* **1984,** *137* (1), 26.

(290) Jain, A. K.; Juanes, R. Preferential Mode of gas invasion in sediments: Grain-scale mechanistic model of coupled multiphase fluid flow and sediment mechanics. *J. Geophys. Res.* **2009,** *114* (B8), B08101.

(291) Motta, D.; Abad, J. D.; García, M. H. Modeling Framework for Organic Sediment Resuspension and Oxygen Demand: Case of Bubbly Creek in Chicago *ASCE J. Environ. Eng.* **2010,** *136* (9), 952-964.

(292) Bosworth, W. S.; Thibodeaux, L. J. Bioturbation: A facilitator of contaminant transport in bed sediment. *Environmental Progress* **1990,** *9* (4), 211-217.

(293) Cook, P. L. M.; Wenzhofer, F.; Glud, R. N.; Janssen, F.; Huettel, M. Benthic solute exchange and carbon mineralization in two shallow subtidal sandy sediments: Effect of advective pore-water exchange. *Limnol. Oceanogr.* **2007,** *52* (5), 1943–1963.

(294) Meyer, R. L.; Kjær, T.; Revsbech, N. P. Use of NOx- microsensors to estimate the activity of sediment nitrification and NOx- consumption along an estuarine salinity, nitrate, and light gradient. *Anglais* **2001,** *26* (2), 181-193.

(295) Deflandre, B.; Duchêne, J.-C. PRO2FLUX – A software program for profile quantification and diffusive O2 flux calculations. *Environmental Modelling & Software* **2010,** *25* (9), 1059-1061.

(296) Bryant, L. D.; McGinnis, D. F.; Lorrai, C.; Brand, A.; Little, J. C.; Wüest, A. Evaluating oxygen fluxes using microprofiles from both sides of the sediment–water interface. *Limnol. Oceanogr.: Methods* **2010,** *8*, 610–627.

(297) Nielsen, M.; Gieseke, A.; de Beer, D.; Revsbech, N. P. Nitrate, nitrite, and nitrous oxide transformations in sediments along a salinity gradient in the Weser Estuary. *Anglais* **2009,** *55* (1), 39-52.

(298) Viollier, E.; Rabouille, C.; Apitz, S. E.; Breuer, E.; Chaillou, G.; Dedieu, K.; Furukawa, Y.; Grenz, C.; Hall, P.; Janssen, F.; Morford, J. L.; Poggiale, J. C.; Roberts, S.; Shimmield, T.; Taillefert, M.; Tengberg, A.; Wenzhöfer, F.; Witte, U. Benthic biogeochemistry: state of the art technologies and guidelines for the future of in situ survey. *Journal of Experimental Marine Biology and Ecology* **2003,** *285-286* (0), 5-31.

(299) Janssen, F.; Faerber, P.; Huettel, M.; Meyer, V.; Witte, U. Pore-water advection and solute fluxes in permeable marine sediments (I): Calibration and performance of the novel benthic chamber system Sandy. *Limnol. Oceanogr.* **2005,** *50* (3), 768–778.

(300) Tengberg, A.; Stahl, H.; Gust, G.; Müller, V.; Arning, U.; Andersson, H.; Hall, P. O. J. Intercalibration of benthic flux chambers I. Accuracy of flux measurements and influence of chamber hydrodynamics. *Progress In Oceanography* **2004,** *60* (1), 1.

(301) Tengberg, A.; De Bovee, F.; Hall, P.; Berelson, W.; Chadwick, D.; Ciceri, G.; Crassous, P.; Devol, A.; Emerson, S.; Gage, J.; Glud, R.; Graziottini, F.; Gundersen, J.; Hammond, D.; Helder, W.; Hinga, K.; Holby, O.; Jahnke, R.; Khripounoff, A.; Lieberman, S.; Nuppenau, V.; Pfannkuche, O.; Reimers, C.; Rowe, G.; Sahamir, A.; Sayles, F.; Schurter, M.; Smallman, D.; Wehrli, B.; De Wilde, P. Benthic chamber and profiling landers in oceanography. A review of design, technical solutions and functioning. *Progress In Oceanography* **1995,** *35* (3), 253-294.

(302) Beutel, M. W.; Leonard, T. M.; Dent, S. R.; Moore, B. C. Effects of aerobic and anaerobic conditions on P, N, Fe, Mn, and Hg accumulation in waters overlaying profundal sediments of an oligo-mesotrophic lake. *Water Research* **2008,** *42* (8-9), 1953-1962.

(303) Kuwabara, J. S.; Woods, P. F.; Berelson, W. M.; Balistrieri, L. S.; Carter, J. L.; Topping, B. R.; Fend, S. V. Importance of sediment–water interactions in Coeur d'Alene Lake, Idaho, USA: Management implications. *Environ. Manag.* **2003,** *32* (3), 348.

(304) HUETTEL, M.; ZIEBIS, W.; FORSTER, S.; LUTHER, G. W. Advective transport affecting metal and nutrient distributions and interfacial fluxes in permeable sediments. *Geochimica et Cosmochimica Acta* **1998,** *62* (4), 613–631.

(305) Buchholtz-ten Brink, M. R.; Gust, G.; Chavis, D. Calibration and performance of a stirred benthic chamber. *Deep Sea Res. Part A Oceanogr. Res. Pap.* **1989,** *36* (7), 1083.

(306) Rockne, K. J.; Shor, L. M.; Young, L. Y.; Taghon, G. L.; Kosson, D. S. Distributed Sequestration and Release of PAHs in Weathered Sediment: The Role of Sediment Structure and Organic Carbon Properties *Environ. Sci. Technol.* **2002,** *36* (12), 2636–2644.

(307) Viana, P. Z.; Rockne, K. J.; Thai, L. *Sediment gas ebullition and flux studies in Bubbly Creek, South Fork South Branch, Chicago River*. In Proceedings of the Sixth International Conference on Remediation of Contaminated Sediments, New Orleans, LA, Feb 7-10, 2011.

(308) Forster, S.; Glud, R. N.; Gundersen, J. K.; Huettel, M. In situ Study of Bromide Tracer and Oxygen Flux in Coastal Sediments. *Estuarine, Coastal and Shelf Science* **1999,** *49*, 813–827.

(309) Jogensen, B. B.; Revsbech, N. P. Diffusive boundary layers and the oxygen uptake of sediments and detritus. *Limnol. Oceanogr.* **1985,** *30* (I).

(310) Smolders, A. J. P.; Lamers, L. P. M.; Lucassen, E. C. H. E. T.; Velde, G. V. D.; Roelofs, J. G. M. Internal eutrophication: How it works and what to do about it - a review. *Chemistry and Ecology* **2006,** *22* (2), 93-111.

(311) Hickey, C. W.; Gibbs, M. M. Lake sediment phosphorus release management—Decision support and risk assessment framework. *New Zealand Journal of Marine and Freshwater Research* **2009,** *43* (3), 819-856.

(312) Francis, C. A.; Beman, J. M.; Kuypers, M. M. M. New processes and players in the nitrogen cycle: the microbial ecology of anaerobic and archaeal ammonia oxidation. *ISME J* **2007,** *1* (1), 19-27.

(313) Rockne, K. J.; Brezonik, P. L. Nutrient Removal in a Cold-Region Wastewater Stabilization Pond: Importance of Ammonia Volatilization. *ASCE J. Environ. Eng.* **2006,** *132* (4), 451-459.

(314) Brassel, K. E.; Reif, D. A Procedure to Generate Thiessen Polygons. *Geographical Analysis* **1979,** *11* (3), 289–303.

(315) MacDonald, J. A.; Fowler, D.; HARGREAVES, K. J.; U., S.; D., L. I.; B., M. M. Methane emission rates from a Northern Wetland; response to temperature, water table and transport. *Atmos. Environ.* **1998,** *32* (19), 3219-3227.

(316) Westermann, P. Temperature regulation of methanogenesis in wetlands. *Chemosphere* **1993,** *26* (1-4), 321-328.

(317) Mahmoud, N.; Zeeman, G.; Gijzen H; G., L. Anaerobic stabilisation and conversion of biopolymers in primary sludge--effect of temperature and sludge retention time. *Water Res.* **2004,** *38* (4), 983-991.

(318) Cai, Z. C.; Yan., X. Y. Kinetic model for methane oxidation by paddy soil as affected by temperature, moisture and N addition. *Soil Biol. Biochem.* **1999,** *31* (5), 715-725.

(319) Yao, H.; Conrad, R. .Effect of temperature on reduction of iron and production of carbon dioxide and methane in anoxic wetland rice soils. *Biol. Fertil. Soils* **2000,** *32*, 135-141.

(320) Chin, K.-J.; Lukow, T.; Stubner, S.; Conrad., R. Structure and function of the methanogenic archaeal community in stable cellulose-degrading enrichment cultures at two different temperatures (15°C and 30°C). *FEMS Microbiol. Ecol.* **1999,** *30*, 313-326.

(321) Dunfield, P.; Knowles, R.; R., D.; T., M. Methane production and consumption in temperate and subarctic peat soils: response to temperature and pH. *Soil Biol. and Biochem.* **1993,** *25* (3), 321-326.

(322) Westermann, P.; Ahring, B. K. Dynamics of methane production, sulfate reduction, and denitrification in a permanently waterlogged alder swamp. *Appl. Environ. Microbiol.* **1987,** *53*, 2554-2559.

(323) Zhao, X.; Viana, P. Z.; Yin, K.; Rockne, K.; Hey, D.; Schuh, J.; Lanyon, R. *Combined active capping/wetland demonstration in the Chicago River*. In Fourth International Conference on Remediation of Contaminated Sediments, Savannah, Georgia, 2007.

(324) Velinsky, D.; Wade, T.; Schlekat, C.; McGee, B.; Presley, B. Tidal river sediments in the Washington, D.C. area. I. Distribution and sources of trace metals. *Estuaries and Coasts* **1994,** *17* (2), 305.

VITA

Priscilla Zuconi Viana
priviana2@gmail.com, https://sites.google.com/site/priscillazviana

Education

1. **Ph.D. Student in Environmental Engineering (GPA 4.0)**, University of Illinois at Chicago (**UIC**) (2005–2011)
   - *Dissertation title*: Contaminant flux through capped and uncapped sediments
   - *Dissertation Adviser*: Karl Rockne
2. **M.S. in Environmental Engineering,** Federal University of Rio de Janeiro (**UFRJ**), **Brazil** (2002–2004)
   - *Dissertation title*: Membrane bioreactor applied to the treatment of domestic wastewater
   - *Dissertation Advisers*: Ronaldo Nobrega (Chemical Engineering) and Eduardo Jordão (Civil Engineering)
3. **B.S. in Civil Engineering,** State University of Campinas (**UNICAMP**), **Brazil** (1996–2001)

Research, Teaching and Professional Experience

1. **National Science Foundation (NSF),** Arlington, VA (2011)

   a) Science Assistant (2011)
   - Facilitated grant proposal review and management of the Ecology of Infectious Disease (EID) Program ($12 million/year);
   - Assisted the Federal interagency efforts with development of the: (a) Ocean Acidification Strategic Research Plan (OA-SRP); (b) Resiliency and Adaptation to Climate Change and Ocean Acidification Strategic Action Plan (SAP); and (c) Regional Ecosystem Protection and Restoration SAP.

   b) NOAA Sea Grant Knauss Marine Policy Internship (2010–2011)
   - Facilitated grant proposal review and management of the EID and OA programs ($12 and $15 million/year);
   - Assisted the Federal efforts with development of the OA-SRP (http://www.st.nmfs.noaa.gov/iwgoa/);
   - Facilitated coordination of two scientific conferences.
2. **Research Assistant, UIC,** Chicago, IL (2005–2010)
   - Research focusing on improving water quality through environmental restoration and remediation of contaminated sediments with a focus on reactive capping and on ebullition-facilitated contaminant transport;
   - Laboratory, field and modeling experience;
   - Work performed with The Wetlands Initiative, Metropolitan Reclamation District of Greater Chicago (MWRD-GC) and Army Corps of Engineers.
3. **Teaching Assistant, UIC,** Chicago, IL (2007–2008)
   - Prepared and taught laboratory classes, assisted students with assignments and evaluated their work;

- Occasionally instructed for undergraduate and PhD level courses, such as Wastewater Treatment, Applied Environmental Biotechnology and Environmental Microbiology.

4. **Researcher, COPPETEC Foundation,** Rio de Janeiro, RJ, **Brazil** (2004)
   - Research sponsored by Petrobras (Brazilian Petroleum Company) focusing in membrane bioreactors for wastewater treatment.

Technical Areas of Interest

- Stewardship of aquatic resources through remediation of contaminated sediments, wastewater treatment and environmental restoration. Long term goal: develop extensive experience on how environmental systems work to successfully protect human health and the environment;
- Experience on: (a) laboratory experiments, (b) field sampling, (c) data analysis, (d) model development, (e) report writing, (f) grant reviewing, (g) interagency work, and (h) meeting coordination.

Honors, Awards, Fellowships and Scholarships

1. **John Knauss Marine Policy Internship, NOAA** National Sea Grant Program (2010)
2. **American Association of University Women (AAUW)** International **Fellowship**. 36 fellowships awarded among 1,194 eligible applicants (2009-2010)
3. **Fulbright Scholarship** (2005-2009)
4. **Student Award** of the Illinois Section American Society of Civil Engineers (**ASCE**), Environmental Engineering and Water Resources Division (2009)
5. **Graduate Student Award** "in recognition of outstanding potential for future contributions to the field of environmental chemistry." American Chemical Society (**ACS**), Environmental Chemistry (2009)
6. **Chicago Consular Corps Scholarship** (2009-2010)
7. Student Travel Award, Graduate Student Council (GSC) and Graduate College, UIC, IL (2009)
8. Student Travel Award, Graduate Student Council (GSC) and Graduate College, UIC, IL (2007)
9. **Best paper** in XV **Brazilian Congress of Chemical Engineering** (COBEQ, 2004)
10. **Head of Class Award, UFRJ**, Brazil (2003-2004)
11. Rio de Janeiro State Research Support Foundation (**FAPERJ**) **Scholarship**, Brazil (2003–2004)
12. National Council for Scientific and Technology Development (**CNPq**) **Scholarship**, Brazil (2002-2003)
13. São Paulo State Research Support Foundation (**FAPESP**) **Scholarship**, Brazil (2000–2001)
14. Student Support Service (**SAE/UNICAMP**) **Scholarship**, Brazil (1998-2000)

Journal Publications

1. **Viana, P. Z.**, K. Yin and K. Rockne (2011) Field measurements and modeling of ebullition-facilitated flux of heavy metal and PAH contaminants from sediments to the water column. *In review.*
2. Yin, K., **P. Z. Viana,** and K. Rockne (2011) Modeling active capping efficacy. 2. Organic contaminated sediments remediation combined with an isotherm study and column study verification. *In review.*

3. Yin, K., **P. Z. Viana,** X. Zhao and K. Rockne (2010) Characterization, performance modeling, and design of an active capping remediation project in a heavily polluted urban channel. *Sci. Total Environ.* **408**(16):3454-3463.
4. **Viana, P. Z.**, K. Yin and K. Rockne (2008) Modeling active capping efficacy. 1. Metal and organometal contaminated sediment remediation. *Environ. Sci. Technol.* **42**(23):8922-8929.
5. **Viana, P. Z.**, K. Yin, X. Zhao and K. Rockne (2007) Active sediment capping for pollutant mixtures: Control of biogenic gas production under highly intermittent flows. *Land Contam. Reclam.* **15**(4):413-425.
6. **Viana, P. Z.**, R. Nobrega, E. P. Jordão and J. P. Azevedo (2005) Study of the best operational conditions of a membrane bioreactor used for domestic wastewater treatment. *Braz. Arch. Biol. Technol.* **48**:119-126.

Technical Reports

1. Rockne, K., **P. Z. Viana** and K. Yin (2011) Sediment gas ebullition and flux studies in Bubbly Creek, South Fork South Branch, Chicago River. USACE-Chicago District, Vol. 1 and 2.
2. Interagency Working Group on OA, Subcommittee on Ocean Science and Technology, Committee on Environment, Natural Resources, and Sustainability, National Science and Technology Council (2011) Initial report on Federally funded Ocean Acidification Research and Monitoring Activities and Progress in Developing a Strategic Plan.

Refereed Conference Proceedings

1. **Viana, P. Z.**, K. Rockne and L. Thai (2011) Sediment gas ebullition and flux studies in Bubbly Creek, South Fork South Branch, Chicago River. *In: Proceedings of the Sixth International Conference on Remediation of Contaminated Sediments*. New Orleans, LA. 8 pp.
2. Yin, K., **P. Z. Viana** and K. Rockne (2011) Verification of Aromatic Contaminant Transport in Amended Caps via Isotherm Adsorption and Column Studies. *In: Proceedings of the Sixth International Conference on Remediation of Contaminated Sediments*. New Orleans, LA. 8 pp.
3. **Viana, P. Z.**, K. Yin and K. Rockne (2009) Contaminant-facilitated transport due to sediment gas production: Laboratory and field studies. *In: Proceedings of the Fifth International Conference on Remediation of Contaminated Sediments*. Jacksonville, FL. 8 pp.
4. Yin, K., **P. Z. Viana** and K. Rockne (2009) Verification of active cap contaminant breakthrough simulations via laboratory column studies. *In: Proceedings of the Fifth International Conference on Remediation of Contaminated Sediments*. Jacksonville, FL. 8 pp.
5. **Viana, P. Z.**, K. Yin, X. Zhao and K. Rockne (2007) Modeling and control of gas ebullition in capped sediments. Paper D-027. *In: Proceedings of the Fourth International Conference on Remediation of Contaminated Sediments*. Savannah, GA. 7 pp.
6. Yin, K., **P. Z. Viana**, X. Zhao and K. Rockne (2007) A Monte Carlo simulation approach for active caps in mixed contaminant environments. Paper D-018. *In: Proceedings of the Fourth International Conference on Remediation of Contaminated Sediments*. Savannah, GA. 8 pp.
7. Zhao, X., **P. Z. Viana**, K. Yin, K. Rockne, D. Hey, J. Schuh and R. Lanyon (2007) Combined active capping/wetland demonstration in the Chicago River. Paper D-019. *In: Proceedings of the Fourth International Conference on Remediation of Contaminated Sediment*s. Savannah, GA. 8 pp.

8. **Viana, P. Z.**, R. Nobrega and J. P. Azevedo (2004) Study of the best operational conditions of a membrane bioreactor used for domestic wastewater treatment. *In: Proceedings of the XV Brazilian Congress of Chemical Engineering (COBEQ)*. Curitiba, Brazil. 8 pp.
9. Jordão, E. P., I. Volschan Jr. and **P. Z. Viana** (2003) Updated cost indicators for implementation of wastewater treatment plants. *In: Proceedings of the 4th Regional Conference of the Inter-American Association of Sanitary and Environmental Engineering (AIDIS)*. São Paulo, Brazil. 13 pp.
10. Volschan Jr., I., E. P. Jordão, **P. Z. Viana**, A. F. Barroso, R. P. Espíndola, M. A. Salek and A. Bonis (2003) Evaluation of the water quality in the Guandu River Basin (RJ) and the validity of application of the Water Quality Index. *In: Proceedings of the 22nd Brazilian Congress of Sanitary and Environmental Engineering (ABES)*. Joinville, Brazil. 12 pp.
11. Bueno-Bartholomei, C. L., L. C. Labaki and **P. Z. Viana** (2001) Behavior of different tree species in the attenuation of the solar radiation. *In: Proceedings of the VI National and III Latin American Meeting on Comfort in the Constructed Environment (ENCAC)*. São Pedro, Brazil. 9 pp.

Presentations

1. **Viana, P. Z.**, R. Kaliappan and K. Rockne (2011) The importance of sediment gas ebullition in sediment-to-water contaminant flux. *In: 242nd ACS National Meeting & Exposition.* Denver, CO, August 28.
2. **Viana, P. Z.**, K. Yin and K. Rockne (2011) Sediment gas ebullition and flux studies in the Chicago River. *In: RemTEC Summit 2011*. Chicago, IL, May 18.
3. **Viana, P. Z.**, K. Rockne and L. Thai (2011) Sediment gas ebullition and flux studies in Bubbly Creek, South Fork South Branch, Chicago River. *In: Sixth International Conference on Remediation of Contaminated Sediments*. New Orleans, LA, February 10.
4. **Viana, P.Z.** (2010) Transport of contaminants from sediments to the water column and environmental remediation strategies. *In: NOAA Sea Grant Knauss Fellowship Brown Bag Series*. Silver Spring, MD, Dec. 8.
5. **Viana, P. Z.** (2010) Reasons, rewards and challenges of career choices. Invited Panelist *In: IX Ecological Dissertations in the Aquatic Sciences Symposium (Eco-DAS)*. Honolulu, HI, October 15.
6. **Viana, P. Z.** (2010) Effects of environmental stressors on aquatic ecosystems and potential mitigation strategies. *In: IX Ecological Dissertations in Aquatic Sciences Symposium (Eco-DAS)*. Honolulu, HI, Oct. 12.
7. **Viana, P. Z.**, K. Yin and K. Rockne (2010) Remediation of heavy metal contaminated sediments: Active capping efficacy and transport of contaminants to the water column. *In: Civil and Materials Engineering - UIC Seminar Series*. Chicago, IL, February 10.
8. **Viana, P. Z.**, K. Yin and K. Rockne (2009) Contaminant-facilitated transport due to sediment gas production: Laboratory and field studies. *In: Fifth International Conference on Remediation of Contaminated Sediments*. Jacksonville, FL, February 05.
9. **Viana, P. Z.**, K. Yin and K. Rockne (2009) Active capping and contaminant-facilitated transport due to sediment gas production. *In: LEAP - University of Illinois at Chicago Seminar Series*. Chicago, IL, January 30.
10. **Viana, P. Z.**, K. Yin, X. Zhao and K. Rockne (2008) Remediation of contaminated sediments: Gas ebullition in capped sediments. *In: UIC-Student Research Forum*. Chicago, IL, April 18.

11. **Viana, P. Z**., K. Yin, X. Zhao and K. Rockne (2007) Active capping project in the Chicago River. *In: 233rd American Chemical Society (ACS) National Meeting & Exposition*. Chicago, IL, March 25-29.
12. **Viana, P. Z.**, K. Yin, X. Zhao and K. Rockne (2007) Modeling and control of gas ebullition in capped sediments. *In: Fourth International Conference on Remediation of Contaminated Sediments*. Savannah, GA, January 24.
13. **Viana, P. Z.**, K. Yin, X. Zhao and K. Rockne (2006) Active capping: A low cost technology to contain and reduce the exposure risk of contaminated sediments. *In: 7th Regional Conference of the Inter-American Association of Sanitary and Environmental Engineering (AIDIS)*. Chicago, IL, March 30.
14. **Viana, P. Z.**, K. Yin and K. Rockne (2006) Active capping and gas ebullition. *In: Civil and Materials Engineering - University of Illinois at Chicago Seminar Series*. Chicago, IL, October 24.
15. **Viana, P. Z.**, K. Yin, X. Zhao and K. Rockne (2005) Modeling sediment gas ebullition along a gradient from a combined sewer outfall. *In: 28th Midwest Environmental Chemistry Workshop*. Evanston, IL, October 16.
16. **Viana, P. Z.**, R. Nobrega and J. P. Azevedo (2004) Study of the best operational conditions of a membrane bioreactor used for domestic wastewater treatment. *In: XV Brazilian Congress of Chemical Engineering (COBEQ)*. Curitiba, Brazil, September 29.
17. **Viana, P. Z.**, R. Nobrega, E. P. Jordão and J. P. Azevedo (2003) Study of the best operational conditions of a membrane bioreactor used for domestic wastewater treatment. *In: Annual Chemical Engineering Colloquium*. Rio de Janeiro, Brazil, December 05.
18. Volschan Jr., I., E. P. Jordão, **P. Z. Viana**, A. F. Barroso, R. P. Espíndola, M. A. Salek and A. Bonis (2003) Evaluation of the water quality in the Guandu River Basin (RJ) and the validity of application of the Water Quality Index. *In: 22nd Brazilian Congress of Sanitary and Environmental Engineering (ABES)*. Joinville, Brazil, September 18.
19. Jordão, E. P., I. Volschan Jr. and **P. Z. Viana** (2003) Updated cost indicators for implementation of wastewater treatment plants. *In: 4th Regional Conference of the Inter-American Association of Sanitary and Environmental Engineering (AIDIS)*. São Paulo, Brazil, June 5.
20. **Viana, P. Z.** and B. Coraucci Filho (2001) Evaluation of filtration ditches as a method for anaerobic wastewater post-treatment. *In: IX UNICAMP Internal Congress for Scientific Initiation*. Campinas, Brazil, September 27.
21. **Viana, P. Z.** and L. C. Labaki (1999) Assessment of the cooling capacity of planting trees in urban environments. *In: VII UNICAMP Internal Congress for Scientific Initiation*. Campinas, Brazil, September 20.

Professional Memberships

Member of the Association of Environmental Engineering and Science Professors (**AEESP**), American Chemical Society (**ACS**), American Society of Civil Engineers (**ASCE**), Water Environment federation (**WEF**), Inter-American Association of Sanitary and Environmental Engineering (**AIDIS**), **Fulbright** Association, and UIC Women in Science and Engineering Association (**WISE**).

Professional Development, Mentorship and Extracurricular Activities

1. **Coordination of the Deepwater Horizon (DWH) Oil Spill Principal Investigator (PI) Conference**. Coordinated by NSF, NOAA, USGS, BOEMRE and NIH. 150 participants.

Objectives: Bring together PIs from academia, private research institutes and agencies conducting research in response to the DWH oil spill to explore the state of the science and propose recommendations (http://www.marine.usf.edu/conferences/fio/NSTC-JSOST-PI/index.shtml).

2. **Coordination of the Ecology of Marine Infectious Diseases (EMID) Workshop**. 60 participants. Objectives: (1) Foster new collaborations, (2) discuss about innovative projects, and (3) propose recommendations for research directions (https://sites.google.com/site/emidworkshop/).
3. Participant in the IX Ecological Dissertations in Aquatic Sciences Symposium (**Eco-DAS**). Honolulu, HI, October 11-16, 2010. Symposium aimed to **foster sustained, cross-disciplinary interactions among the top new researchers in ecological oceanography and limnology** to increase likelihood of career success.
4. Participant in the **Public Issues and Conflict Management Workshop**. Silver Spring, MD. August 23-24, 2010. Workshop developed to increase the participant's ability to **plan and facilitate effective meetings**.
5. **Chemical and Hygiene Officer** of the Environmental Biotechnology Laboratory (EBL) at UIC (2006–2010). Certified to liaison with the Environmental Health and Safety Office to provide laboratory safety and oversight.
6. **Trainee** in civil engineering at **Skanska Teknik, Malmö, Sweden**. Work abroad program (2000).
7. **English course in New York**, NY, USA (1999).
8. **Volunteer work**: Science Fair Judge, Montgomery, MD (2010), Ambassador for the Women in Science and Engineering Association (WISE) at UIC (2009), volunteer in the Chicago Brain Bee competition and Chicago Cares programs (2009), organizer of UIC Environmental Biotechnology Laboratory meetings (2006–2009), volunteer in the Brazilian Association of Support to Children with Cancer (ABRACE, 2000–2003) and as a teacher in Brazil (1993–1996).

Language Skills

Fluent in English and Portuguese (oral and written); Basic knowledge in Spanish.